



Design of polysaccharide-based conductive inks and hydrogels for the development of controllably biodegradable bioelectronics devices

Maxime Leprince

► To cite this version:

Maxime Leprince. Design of polysaccharide-based conductive inks and hydrogels for the development of controllably biodegradable bioelectronics devices. Polymers. Université Grenoble Alpes [2020-..], 2021. English. NNT : 2021GRALV040 . tel-03934656

HAL Id: tel-03934656

<https://theses.hal.science/tel-03934656>

Submitted on 11 Jan 2023

HAL is a multi-disciplinary open access archive for the deposit and dissemination of scientific research documents, whether they are published or not. The documents may come from teaching and research institutions in France or abroad, or from public or private research centers.

L'archive ouverte pluridisciplinaire **HAL**, est destinée au dépôt et à la diffusion de documents scientifiques de niveau recherche, publiés ou non, émanant des établissements d'enseignement et de recherche français ou étrangers, des laboratoires publics ou privés.

THÈSE

Pour obtenir le grade de

DOCTEUR DE L'UNIVERSITE GRENOBLE ALPES

Spécialité : **Science des polymères**

Arrêté ministériel : 25 mai 2016

Présentée par

Maxime LEPRINCE

Thèse dirigée par **Isabelle TEXIER-NOGUES**, docteur,
L2CB/DTBS/CEA

et co-dirigée par **Rachel AUZELY-VELTY**, professeur, **CERMAV**

préparée au sein du **CERMAV** et du **L2CB/DTBS/LETI/CEA**
dans l'**École Doctorale Chimie et Sciences du Vivant**

Design of polysaccharide-based conductive inks and hydrogels for the development of controllably biodegradable bioelectronics devices

Thèse soutenue publiquement le **24 septembre 2021**
devant le jury composé de :

Monsieur Saïd SADKI

Professeur CNRS, Université Grenoble Alpes, Grenoble, président

Monsieur Cyril BROCHON

Professeur à l'Université de Bordeaux, Bordeaux, rapporteur

Monsieur David MECERREYES

Professeur à l'Université des Pays basque, Espagne, rapporteur

Madame Maria ASPLUND

Chercheur à l'Université Technique de Freiburg, Allemagne, membre

Monsieur Vincent NOËL

Professeur à l'Université Paris Diderot, Paris, membre

Madame Isabelle TEXIER-NOGUES

Ingénieur chercheur CEA, Grenoble, directrice de thèse

Madame Rachel AUZELY-VELTY

Professeur CNRS, CERMAV, Grenoble, co-directrice de thèse



Acknowledgements

Those three years of Ph.D. in Grenoble gave me the opportunity to meet many researchers, students and friends. All of them have contributed more or less directly to the realization of this project, and I would like to thank them all.

First of all, I would like to thank my two supervisors, Rachel and Isabelle for their trust and advices along all my thesis. Your respective fields of competence were complementary and crucial for the realization of this project. I would like to thank you especially for the great autonomy you gave me during all those years, which enabled me to experiment various research paths, and work wherever I needed. And a special thanks to Isabelle who kept correcting my manuscript while recovering from an important surgery during spring 2021.

I would like to thank the CEA for funding my Ph.D. scholarship, but also Séverine Vignoud, Anne Imberty and Laurent Heux for letting me work in their respective team and laboratory. Thank you very much for setting up such a nice working atmosphere in your labs !

Then, I would like to thank Pr. David Mecerreyes and Pr. Cyril Ponchon for their time and interest in my work and their thorough reading of this manuscript, and Pr Maria Asplund, Pr. Saïd Sadki and Pr. Vincent Noël for accepting to evaluate my work, and deem if I am worthy of the title of Doctor of Science.

I also would like to thank specially Pr. Alice Nicolas, Pr. Saïd Sadki and Dr. Guillaume Nonglaton, members of my individual thesis committee, for their interest and advices all along my Ph.D.

Finally comes the long list of acknowledgments of all the people who have helped and/or advised me during this project, and God knows I have asked and disturbed many people. Thank you to Pierre Sailler, Patrick Perez and Laurent Chausse of CERMAV for their help and support in the design of all the home-made devices and experimental set-up. Thank you to Isabelle Jeacomine for your advice in NMR, Sonia Ortega for the SEC and TGA characterizations, Anna Szarpak for optical microscopy, Caroline Fontelaye and Guillaume Nonglaton for surface modification, Catherine Pudda for SEM analysis, Denis Mariolle for AFM characterization, Yannic Nedellec of the DCM and Denis Rouchon for Raman spectroscopy and Mathilde Menneteau for cytotoxicity experiments. A special thanks to Luc Choisnard for his

help in the design of the experimental design, and the treatment of data. It was unfortunate that this work could not be further exploited.

I would like to thank especially the members of the *eleetroccool* team of L2CB, which I solicited the most: thank you to Pascal Mailley, Maxime Gougis, Ayman Chmayssen, Frédéric Revol, Mélanie Alias, Charles Chatard, Michael Spann and Natalie Perreault for your help and support. Thank you for putting up with me when I came to your lab after months of silence, just for a few days, and asking you endless questions, changing a “do you have a few minutes for a quick question?” into a “could you give me a whole lesson about such aspect of electrochemistry, and oh by the way could you help me with this experimental setup?”

Lastly, this Ph.D. could not have succeeded with all my colleagues and friends, who helped me in tough times, and laughed with me in happy times. At CERMAV, thank you Claire, Simon, Mous, Vanina, Raphaël, Aude, Robin, Marlène, Tamiris, Raouf, Estelle, Maxime, Michel, Samuel and Mr Ficcus. Thank you Jean-Michel Rota for your great listening capacity, and your ceaseless help. At CEA, thank you Antoine, Michael, Juliette, Sacha, Natacha, Emilie, Mathilde, Prisca, Natalie, Mersha, Bilal, Thibault, Paul, Amelia and Mehrsa, and all those I may have forgotten. I apologize for having spent too little time at CEA. I really would have liked to spend more time with you to know you more.

Thank you to my successive roommates for listening to my complains and supporting me: thank you Pierre, Marco, Adrien, Tim, Thomas, Anne and Louis. And above all, thank you to my mountain co-hikers without whom it would have been impossible to keep my physical and mental sanity during those three years of Ph.D.: thank you Cécile, Lucie, Mélanie and Matthieu !!

This Ph.D. came after long years of study where I have been inspired and taught by great teachers, who transmitted me the love of science and curiosity. Thank you to all my teachers and supervisors for their help to improve myself and learn always more. Thank you Jérôme Claverie of UdeS for showing me how a great team spirit can uplift the whole scientific level of a lab. And thank you Luca Albertin for showing me the complexity of the scientific world, and that it was possible to conciliate a scientific career with a family life.

Finally, thank you to my parents, brothers and sister, without whom I could not have received such a wonderful education, general culture, and mind set.

Hic sunt dracones

Résumé en français

Le développement de matériaux conducteurs biocompatibles et souples a connu cette dernière décennie un engouement majeur en raison du grand nombre d'applications potentielles dans le domaine de la bioélectronique. Le matériau le plus rencontré dans la littérature est le PEDOT:PSS (3,4-poly(éthylènedioxythiophène : poly(styrène) sulfonate), où le PEDOT est un polymère conducteur dopé par du PSS. Ce matériau est utilisé aussi bien pour fabriquer des pistes conductrices, que pour concevoir des hydrogels conducteurs à l'interface électronique/tissus biologiques. Cependant, ce matériau n'est pas biodégradable, ce qui limite le développement de dispositifs médicaux implantés dégradables par le corps ne nécessitant pas de chirurgie explantatoire. De plus, le PEDOT :PSS étant entièrement composé de polymères synthétiques, sa biocompatibilité reste limitée.

Dans cette thèse, un nouveau dopant du PEDOT a été développé à partir d'un polysaccharide naturel, l'acide hyaluronique (HA). Ce dernier a été modifié afin d'obtenir un nouveau matériau, PEDOT :HA_{modifié} conducteur, hautement biocompatible, réticulable et dégradable en conditions physiologiques.

La première étape a consisté en la fonctionnalisation du HA par des fonctions chimiques d'intérêt pour imiter la structure du PSS, afin d'en faire un dopant du PEDOT adéquat. Le HA a d'abord été sulfaté selon un nouveau protocole plus efficace et moins agressif pour le HA que ceux décrits dans la littérature. Puis un groupe acide aminophényl-boronique (PBA) a été greffé sur la fonction carboxyle du HA. Une étude systématique a permis de mettre en évidence la synergie entre les sulfates et le groupe aromatique pour doper efficacement le PEDOT. La molécule finale, abrégée HAS-PBA, cytocompatible et dégradable par auto-hydrolyse, a permis d'obtenir une encre PEDOT :HAS-PBA dispersable en phase aqueuse, et conduisant à des films plus conducteurs en conditions physiologiques que ceux dérivés du PEDOT :PSS (conductivité de $1,5 \pm 0,3$ S/cm vs 0,1-0,5 S/cm). La synthèse de cette encre ainsi que ses propriétés physico chimiques (viscosité et tension de surface) ont ensuite pu être ajustées pour l'imprimer par jet d'encre.

Cette encre a par la suite été fonctionnalisée pour la rendre réticulable en milieu aqueux. Des études préliminaires ont montré l'encombrement stérique de la chaîne principale du HAS-PBA par les sulfates, et l'inaccessibilité des domaines de PEDOT comme points de

réticulation. Afin de réticuler l'encre par réaction thiol-ène photo-induite, une fonction alcène a été greffée sur le HAS-PBA, via un espaceur oligo-PEG. La molécule résultante HAS-PBA-PEGene, réticulable au moyen d'un PEG-bisthiol en présence d'un photo-initiateur, a permis d'obtenir des films conducteurs PEDOT :HAS-PBA-PEGene réticulés non solubles avec une conductivité initiale de $0,7 \pm 0,2$ S/cm en conditions physiologiques, et restant conducteurs après plusieurs jours d'immersion. La conductivité a par ailleurs pu être augmentée jusqu'à 4,9 S/cm par immersion dans l'eau puis séchage du dépôt réticulé. Cela est attribué à une restructuration du film, et une concentration des domaines de PEDOT conducteurs suite à un lavage du film.

Finalement, différentes stratégies ont été mises en œuvre pour tenter d'obtenir un hydrogel conducteur à base de PEDOT dopé par du HAS-PBA. Pour minimiser l'introduction de matériaux non conducteurs, le HAS-PBA a été réticulé par de l'acide adipique dihydrazide pour former la matrice de l'hydrogel. Pour contrôler les paramètres physico- et électrochimiques de l'hydrogel, un protocole où la réticulation de l'hydrogel et la polymérisation du PEDOT se déroulent simultanément a été développé. Finalement, un hydrogel avec un module de stockage G' de $1,5 \pm 0,2$ kPa, et des propriétés électrochimiques (capacité de stockage de charge, capacité d'injection de charge et impédance à 1 kHz) compatibles pour une utilisation en stimulation/suivi des tissus biologiques a pu être développé.

Table of contents

General introduction	1
Table of abbreviations	4
 Chapter 1. Towards PEDOT: hyaluronic acid inks for bioelectronics.....	5
I. Conductive polymers in bioelectronics.....	8
I.1. Bioelectronics: definition and applications.....	8
I.2. Design of conductive stretchable devices: Engineering approach.....	8
I.3. Design of conductive stretchable devices: Chemical approach	10
II. Chemistry of poly(3,4-ethylenedioxythiophene (PEDOT).....	12
II.1. PEDOT polymerization.....	12
II.2. PEDOT conduction mechanisms.....	13
II.3. Measurement of PEDOT doping degree.....	19
II.4. Influence of PEDOT dopant	21
III. Conductive hydrogels	25
III.1. Interest of hydrogels at the electronic tissue/interface	25
III.2. Conductive hydrogels	31
III.3. Conductive PEDOT hydrogels	32
III.4. Biocompatibility and applications of conductive hydrogels	41
III.5. Degradability	43
IV. Focus on PEDOT:biomolecules inks	46
IV.1. PEDOT:biomolecule inks	46
IV.2. PEDOT:glycosaminoglycans (GAGs) inks	47
V. Conclusion.....	51
VI. Bibliography	53
 Chapter 2. Development of a new conductive, biocompatible and degradable PEDOT-based ink ..	61
I. Introduction	64
II. HAS-PBA synthesis	68
II.1. Sulfation of hyaluronic acid.....	68
II.2. Grafting of phenylboronic moieties	77
II.3. Conclusion	79
III. Synthesis and characterization of PEDOT:HA _{derivative} inks.....	80
III.1. Synthesis of PEDOT: HA _{derivative} inks	80
III.2. Influence of HAd _{erivative} on electric and spectroscopic properties of PEDOT:HA inks.....	81

Table of contents

III.3. Optimization of the synthesis of PEDOT:HAS ₄ -PBA _{0.3} ink.....	83
III.4. Cytotoxicity using WST-1 assay	88
III.5. Extension of sulfate/PBA synergy to other GAGs.....	89
III.6. Conclusion	90
IV. Ink processing using inkjet printing.....	92
IV.1. Introduction	92
IV. 2. Optimization of Ink physico-chemical properties	95
IV.3. Inkjet printing with Dimatix DMP 2800 inkjet printer.....	99
IV.4. Characterization of film structure	102
IV.5. Conclusion	103
V. Discussion	104
V.1. HA sulfation.....	104
V.2. Enzymatic biodegradability	106
V.3. Development of highly conductive PEDOT:HAS-PBA ink	108
V.4. Optimization of the polymerization process.....	109
VI. Conclusion.....	112
VII. Materials and methods.....	113
VII.1. Synthesis	113
VII.2. Characterizations	119
VII.3. Experimental design procedure	125
VIII. Bibliography	129
Chapter 3. Ink cross-linking.....	133
I. Introduction	136
II. First cross-linking assays	139
II.1. Dynamic cross-linking of PEDOT: HAS ₄ -PBA _{0.3}	139
II.2. First assays for cross-linking the ink via thiol-ene chemistry	140
III. Development of alkene-functionalized HAS-PBA	152
III.1. Synthesis of HAS ₄ -PBA _{0.3} -PEGene _{0.22}	152
III. 2. Polymerization of EDOT in the presence of HAS ₄ -PBA _{0.3} -PEGene _{0.22} and cross-linking	157
III.3. Stability of PEDOT:HAS ₄ -PBA _{0.3} -PEGene _{0.22} cross-linked films.....	159
IV. Inkjet printing of PEDOT: HAS ₄ -PBA _{0.3} -PEGene _{0.22}	162
IV.1. Ink formulation.....	162
IV.2. Inkjet printing with Dimatix DMP-2800 printer	163
V. Discussion	168
V.I. Inclusion of a conductive ink inside a cross-linked matrix.	168

Table of contents

VI.2. Cross-linking PEDOT:HAS ₄ -PBA _{0.3} from PEDOT chains	169
VI.3. Cross-linking PEDOT:HAS ₄ -PBA _{0.3} from HAS ₄ -PBA _{0.3} chains	171
VI.4. Inkjet printing of cross-linkable PEDOT:HAS ₄ -PBA _{0.3} -PEGene _{0.22} ink.....	173
VI. Conclusion.....	175
VII. Materials and methods.....	176
VII.1. Synthesis	176
VII.2. Characterizations	185
VIII. Bibliography	190
 Chapter 4. Development of pure conductive PEDOT-based hydrogel doped by HAS₄-PBA_{0.3}	193
I. Introduction	196
II. Synthesis of conductive hydrogels in two steps	197
II.1. Development of HAS-ArEne	197
II.2. EDOT polymerization in a preformed hydrogel	201
III. Synthesis of conductive hydrogels in one step.....	205
III.1. Cross-linking of HAS ₄ -PBA _{0.3} by adipic acid dihydrazide without EDOT	205
III.2. Simultaneous hydrogel cross-linking and EDOT polymerization.....	210
IV. Electrochemical properties PEDOT:HAS ₄ -PBA _{0.3} / ADH hydrogels.....	217
IV.1. Properties of interest and experimental setup.....	217
IV.2. Charge storage capacity (CSC).....	218
IV.3. Charge injection capacity	220
IV.4. Electrical impedance spectroscopy	222
IV.5. Application: stimulation of mice hippocampus	224
V. Discussion	227
V.1. Synthesis of HAS ₄ -ArEne _{0.5}	227
V.2. Two-steps pure conductive hydrogels	227
V.3. One-step pure conductive hydrogel	228
VI. Conclusion.....	233
VII. Materials and methods.....	234
VII.1. Synthesis	234
VII.2. Characterization	238
VIII. Bibliography	244
 General conclusion	247
 Abstract	252

Table of contents

General introduction

This Ph.D. work was funded by the CEA (CFR scholarship), and was linked to the STRETCH ANR project (ANR-18-CE19-0018)^[1] which intends to develop a biocompatible, transient, flexible and stretchable electronic device for stimulating or monitoring biological tissues. The STRETCH device aims to be functional for a few months, and then to be degraded by the body without explantation surgery and side effects due to the degradation side products. Intracranial electrodes for electrical stimulation treatments such as these used in brain epileptic areas could be a first demonstrator. Such a device should include conductive tracks embedded in a flexible biopolymer matrix, linked at one extremity to electronic connectors, and on the other extremity to an electrode in contact with the brain tissues (Figure 1).

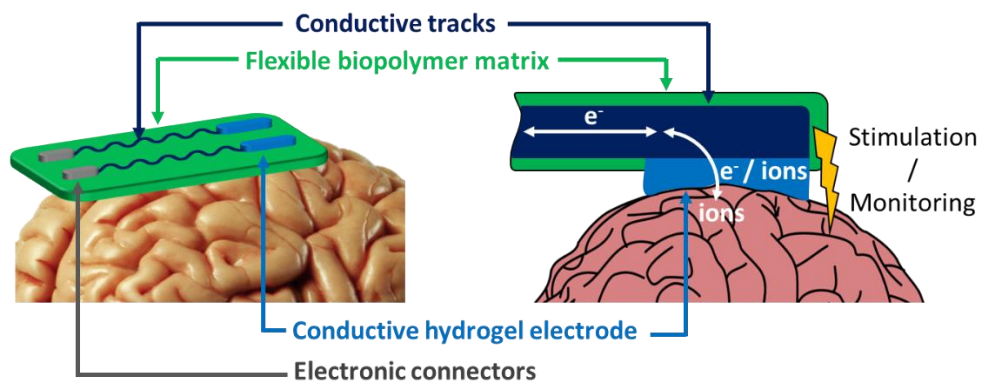


Figure 1. Structure of the intracranial electronic device for tissue stimulation or monitoring.

This Ph.D. work focused on the development of the conductive components of this bioelectronic device, namely the conductive tracks, and the conductive contact electrode. Both of them had to be flexible, biocompatible and disintegrable. Furthermore, the contact electrode should satisfy the requirements for tissue contact, namely match of mechanical properties and biocompatibility^[2]. Among conducting polymers, poly(3,4-ethylenedioxythiophene) (PEDOT) coupled with polystyrene sulfonate (PSS) has been widely used for designing bioelectronics devices, due to its high conductivity, easy processing, and commercial availability^[3,4]. PEDOT:PSS is commercialized as an aqueous dispersion which can be processed in the form of thin films by spin-coating and solvent-casting methods. Yet, PEDOT:PSS presents some limitations, mostly due to its low biofunctionality and biocompatibility. It is indeed known that progressive decrease in signal detection occurs in the weeks following implantation^[5], due to suboptimal biocompatibility and suboptimal

integration with surrounding tissue, resulting in neuronal degeneration and glial scar formation near the implants.

Therefore, our strategy to design the conductive components relied on the use of hyaluronic acid (HA) derivatives as a dopant of PEDOT, taking advantage of the biocompatibility and biodegradability of this natural polysaccharide as well as the existence of various functional groups that are accessible for chemical modification. In this PhD work, HA was thus suitably modified and cross-linked to not only optimize its properties as a doping agent of PEDOT, but also to prepare biocompatible insoluble conductive hydrogels as contact electrodes, and water-resistant tracks. Although PEDOT is not inherently biodegradable, we hypothesized that the biodegradability of the HA derivatives would enable disintegration of the conductive materials which is sufficient to alleviate the need for invasive device removal^[6]. Herein, the term disintegration refers to a partial chemical breakdown of polymer materials^[6] (Figure 2).

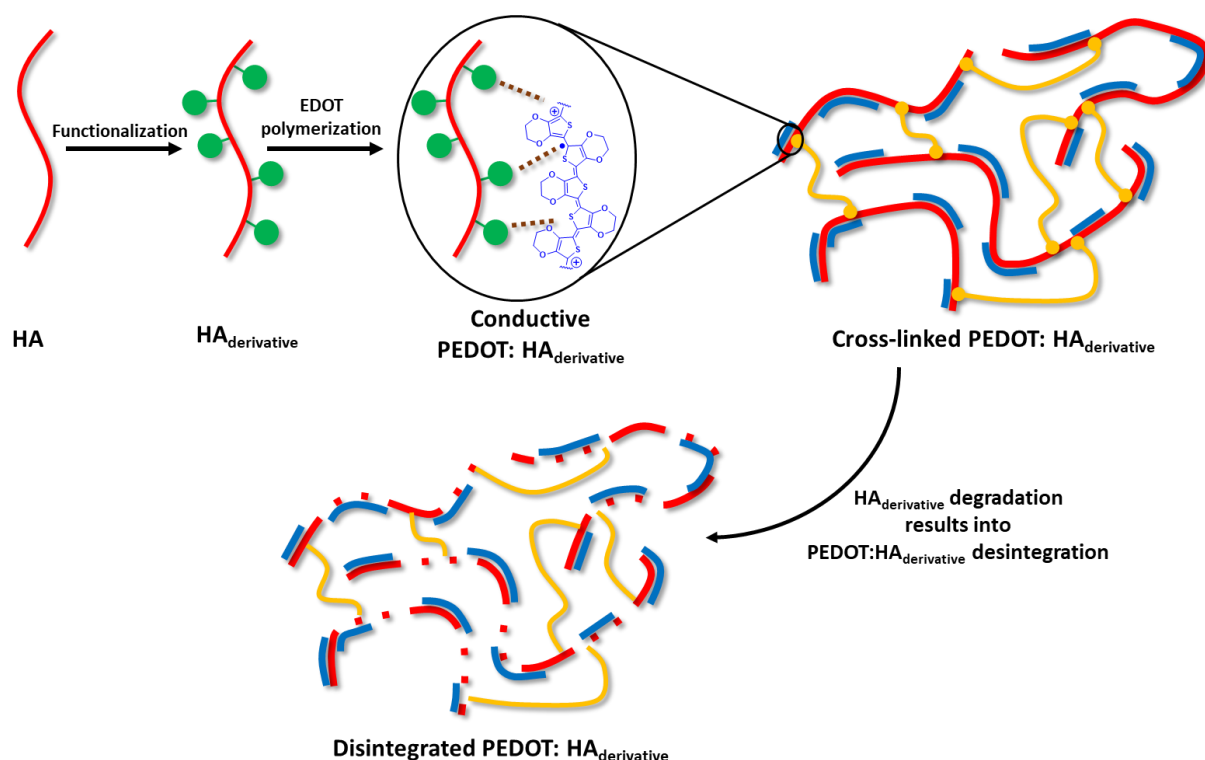


Figure 2. Design of disintegrable conductive materials based on PEDOT doped by degradable HA derivatives.

Table of abbreviations

(P)EDOT	(Poly)(3,4-ethylenedioxy)thiophene
PSS	Polys(styrenesulfonate)
PANI	Polyaniline
PPy	Polypyrrole
DMSO	Dimethylsulfoxyde
PEG	Polyethylene Glycol
GelMa	Gelatin methacryloyle
GAG	Glycosaminoglycan
DexS	Dextran sulfate
Hep	Heparin
Alg	Alginate
DexS	Dextran sulfate
ChS	Chondroitin sulfate
HA	Hyaluronic acid
HAS	Sulfated hyaluronic acid
3APBA	3-aminophenylboronic acid
ECM	Extra cellular matrix
CIC	Charge injection capacity
CSC	Charge storage capacity
CV	Cyclic voltammetry
EIS	Electrochemical impedance spectroscopy
IPN	Interpenetrating network
EDC	1-Ethyl-3-(3-dimethylaminopropyl)carbodiimide
DMTMM	4-(4,6-Dimethoxy-1,3,5-triazin-2-yl)-4-methylmorpholinium chloride
ADH	Adipic acid dihydrazide
APS	Ammonium persulfate
CEA	Commissariat à l'Energie Atomique
CERMAV	Centre d'Etude et de Recherche sur les MAcromolécules Végétales
GIN	Grenoble Institute of neuroscience

Chapter 1.

Towards PEDOT: hyaluronic acid inks for bioelectronics

I. Conductive polymers in bioelectronics	8
I.1. Bioelectronics: definition and applications	8
I.2. Design of conductive stretchable devices: Engineering approach.....	8
I.3. Design of conductive stretchable devices: chemical approach.....	10
II. Chemistry of poly(3,4-ethylenedioxythiophene) (PEDOT)	12
II.1. PEDOT polymerization.....	12
II.2. PEDOT conduction mechanisms.....	13
II.2.a. Band diagram of PEDOT	13
II.2.b. PEDOT primary doping: formation of polaron and bipolaron.....	14
II.2.c. PEDOT secondary doping: modification of microstructure	17
II.2.d. Conduction mechanisms at a higher scale	17
II.3. Measurement of PEDOT doping degree.....	19
II.3.a. Ultraviolet visible-near infrared absorbance spectroscopy	19
II.3.b. Raman spectroscopy	20
II.3.c. X-ray photoelectron spectroscopy	21
II.4. Influence of PEDOT dopant	21
II.4.a. Advantages of polyanions versus anions.....	22
II.4.b. Poly(3,4-ethylenedioxythiophene): poly(styrenesulfonate) (PEDOT:PSS)	22
III. Conductive hydrogels.....	25
III.1. Interest of hydrogels at the electronic tissue/interface	25
III.1.a. Hydrogels as biomechanical enhancers	25
III.1.b. Description of the electronic/tissue interface	26
III.2. Conductive hydrogels.....	31
III.2.a. Ionically conductive hydrogels	31
III.2.b. Composite hydrogels.....	31
III.3. Conductive PEDOT hydrogels	32
III.3.a. Interpenetrating networks	32
III.3.b. Pure conductive hydrogels	37
III.4. Biocompatibility and applications of conductive hydrogels	41
III.4.a. Biocompatibility.....	41
III.4.b. strain sensors.....	41
III.4.c. In-vivo stimulation/recording.....	42
III.5. Degradability	43
IV. Focus on PEDOT:biomolecules inks	46
IV.1. PEDOT:biomolecule inks	46

Chapter 1. Towards PEDOT: hyaluronic acid inks for bioelectronics

IV.2. PEDOT:glycosaminoglycans (GAGs) inks	47
IV.2.a. Generality on GAGs and PEDOT:GAGs inks	47
IV.2.b. Hyaluronic acid (HA) and PEDOT:HA inks.....	49
V. Conclusion	51
VI. Bibliography	53

This first chapter is devoted to the description of the stakes of transient bioelectronics, and the choice of materials and strategies to achieve transient degradable soft conductive hydrogels. The first part will describe the rise of bioelectronics and the following development of flexible electronics using PEDOT polymer as a conductive material. Then PEDOT chemistry and conduction mechanisms will be detailed, leading to the description of PEDOT-based conductive hydrogels and their wide range of applications at the electronic/tissue interface. Finally, the use of biomolecules to increase PEDOT-based conductive material biocompatibility and degradability will be described.

I. Conductive polymers in bioelectronics

I.1. Bioelectronics: definition and applications

Bioelectronics can be defined as the research field at the interface between living tissues, and inert electronics. The motivation to develop this field relies on the vast promises enabled by the possibility to monitor or stimulate tissues, in terms of health monitoring, movement detection, on-demand drug delivery, or development of scaffolds for electro-sensitive cell culture.

The current rise of bioelectronics relies on the development of **soft flexible electronics**^[7,8], as living tissues are much softer and more flexible than traditional electronic materials^[9,10]. For instance, tissue Young modulus can range from 10^3 Pa for cerebral tissue to 10^4 Pa for muscles or 10^5 Pa for the skin, far below the values of traditional electronic materials^[11] such as metals or plastics, ranging from 10^6 to 10^9 Pa.

I.2. Design of conductive stretchable devices: Engineering approach

One way to create flexible electronics is to engineer traditional conductive materials in order to undergo the mechanical deformation without rupture of the electronic circuit. Different strategies can be found in the literature^[11–13]:

- Design of the material so as the conductive parts buckle at a microscopic scale to deform under stress without rupture. Using this strategy, Sun *et al.*^[14] designed buckle-shape silicon nanoribbons (Figure 3a).

- Utilization of ultrathin substrate to take advantage of the natural ductility of some metals like gold.
- Use of origami or kirigami patterns which unfold when under strain, as described in the work of Shyu et al.^[15] (Figure 3b).
- Design of rigid islands on soft substrates, eventually bridged by serpentine-shape tracks embedded in, or printed on, the soft substrate. Sehng el al.^[16] designed rigid aluminium electrode islands connected by serpentine low modulus silicone paths (Figure 3c).
- Finally, utilization of a core-shell packaging, integrating the electronic circuitry inside a low modulus solid, or liquid, embedded in a low modulus solid in contact with tissues (Figure 3d).

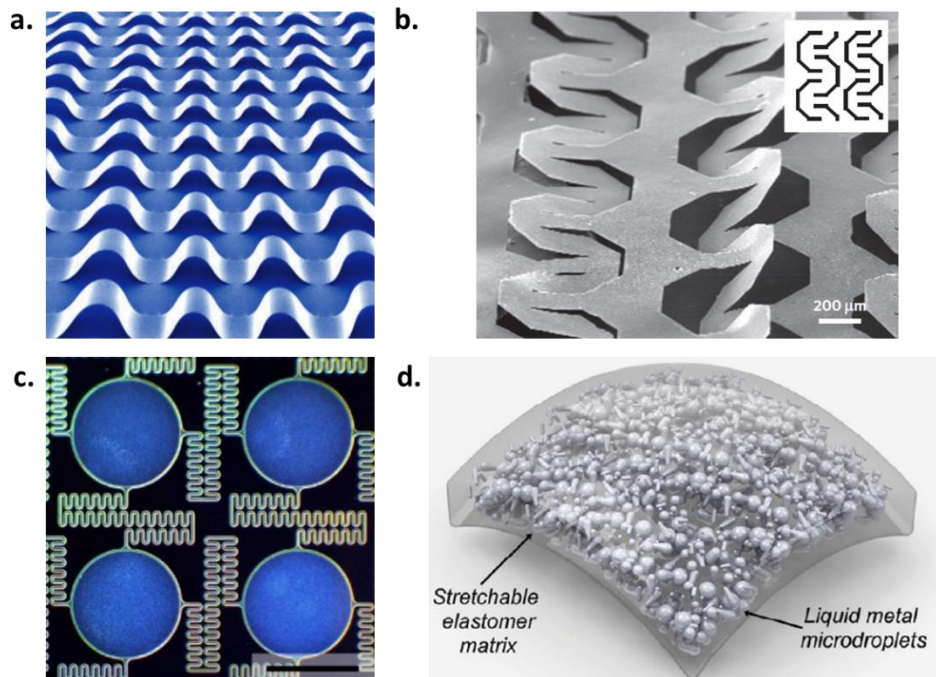


Figure 3. a. Buckle-shape silicon nanoribbons, adapted from Sun et al.^[14]. b. Microscaled kirigami patterns for stretchable electronics, adapted from Shyu et al.^[15]. c. Rigid aluminium electrode islands connected by serpentine low modulus silicone paths, adapted from Sehng el al.^[16]. d. Stretchable dielectric composed of liquid metal drops dispersed in a stretchable elastomer matrix, adapted from Barlett et al.^[17].

However, strategies based on the engineering of classically used conductive materials can be expensive and time-consuming, and often only answer to the need of flexibility, ignoring other important properties when dealing with living tissues, namely biocompatibility

and resorbability. They can be replaced by less conductive materials, but softer and more adapted to bioelectronics: conductive polymers.

I.3. Design of conductive stretchable devices: chemical approach

Conductive polymers are more promising candidates for the development of flexible bioelectronics, as their molecular design enables a fine-tuning of mechanical, electrical, electrochemical, and biological properties^[18]. Besides, their mixed ionic/electronic conductivity^[19] is interesting for the use at the electronic/tissue interface as electrical currents in tissues are supported by ionic flows, contrary to electronic for which it is electron flows.

Conductive polymers constitute a class of polymers whose backbone is conjugated, meaning that it is formed by a series of alternating single and double bonds. The overlapping of π -orbitals creates a π -delocalized system along which electrons can propagate. Three major families of conductive polymers are used in bioelectronics: derivatives of polypyrrole (PPy), polyaniline (PANI) and polythiophene^[18,20] (Figure 4).

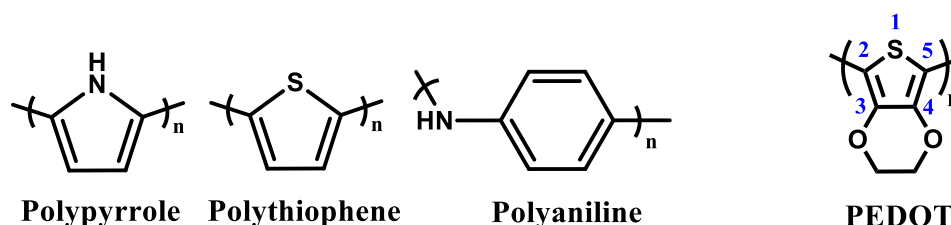


Figure 4. Main families of conductive polymers, and structure of PEDOT.

- Polypyrrole (PPy) has been widely studied as it displays good in vitro and in vivo biocompatibility^[21,22], good stability in air and water^[23,24], and a correct conductivity in physiological conditions^[25–27]. It can be synthesized in different solvents, including water, and is stimulus-responsive^[24,28,29]. However, it is difficult to process as it is insoluble in water^[30], brittle and mechanically rigid^[21,24,31].
- Polyaniline (PANI) exists in various forms according to the oxidation level of its backbone: pernigraniline when fully oxidized, emeraldine when half-oxidized, and leucoemeraldine when reduced. Emeraldine is the most stable and conductive form^[32,33]. Polyaniline is easy to synthesize, cheap and has a good environmental stability^[34–38]. But it has a limited use in bioelectronics as it is quite rigid, brittle, and

can cause chronic inflammation once implanted^[38,39]. Nonetheless, polyaniline oligomers (pentamers and tetramers) can be used as they present good biocompatibility properties, in addition to good conductivity and resorbability^[40–43].

- Pristine polythiophene is not very studied due to a lack of chemical stability and low biocompatibility^[20]. But **poly(3,4-ethylenedioxy)thiophene (PEDOT)**, a thiophene derivative has attracted a considerable attention over the past few years^[44] (Figure 5). It has been first synthesized in 1988 by Bayer researchers with the objective to achieve a more stable and conductive material than pristine polythiophene^[45]. Its monomer, EDOT, is a thiophene with an additional dioxyethylene side ring across the 3rd and 4th positions (Figure 4).

Considering all research fields, PEDOT and PANI appear to have been equally investigated, while PPy has aroused a greater interest (Figure 5a). However, in bioelectronics, the conductive material specifications are more constrained than in other fields, especially concerning biocompatibility, long-term stability, processability and inclusion with other (bio) materials. For instance, PANI has been scarcely used in bioelectronic studies in spite of its versatility and high conductivity, since it displays a low processability and is not very adapted to interface^[40–42,46]. Concerning PPy and PEDOT, they present similar conductivity, and compatibility with other materials, but PEDOT appeared to be more biocompatible^[47] and adapted for biosensor interfaces^[48], accounting for the increasing use of PEDOT in the bioelectronic field (Figure 5b).

PEDOT was therefore selected as the conductive polymer of choice for this study.

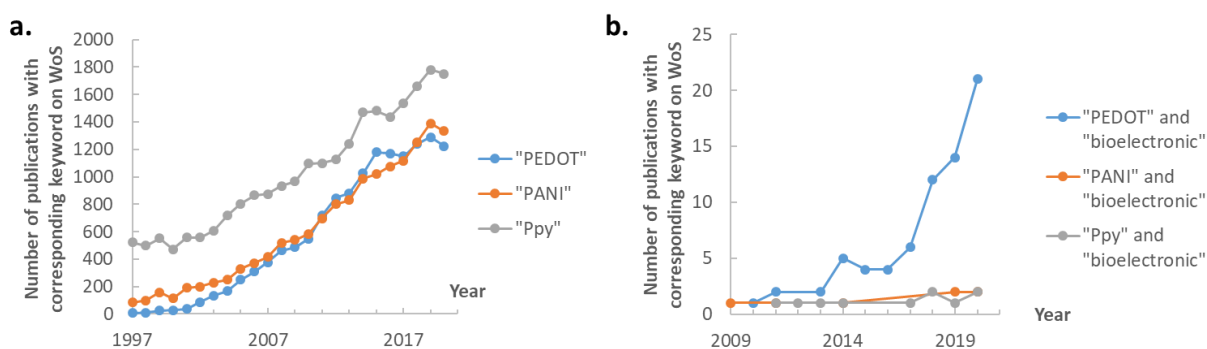


Figure 5. Number of publications per year for given search keyword, on Web of Science (WoS) research site.

II. Chemistry of poly(3,4-ethylenedioxythiophene) (PEDOT)

II.1. PEDOT polymerization

PEDOT is synthesized by **oxidative polymerization** of EDOT. As EDOT monomers are oxidized, they associate between each other, releasing two protons for each added monomer to the growing chain (Figure 6). PEDOT can be polymerized alone, but it is often synthesized in the presence of another molecule which plays the role of counter anion, as PEDOT chains are thermodynamically charged at the end of polymerization^[49]. In the literature, the counter anion is referred to as a “**dopant**”. This denomination will be explained further (Section II.4.).

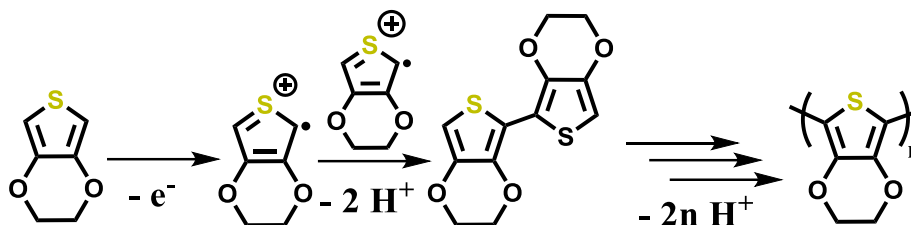


Figure 6. Electro-oxidative polymerization reaction of EDOT into PEDOT.

Two major polymerization methods are practically used to obtain PEDOT:

- Electro-polymerization consists in oxidizing the EDOT monomer (alone or with a dopant) on the surface of an electrode. The polymerization and deposition occur simultaneously, enabling complex patterning on a conductive substrate. The PEDOT film deposited on the electrode is generally insoluble and stuck to the electrode. A three-electrode cell is usually used with a reference electrode, a counter electrode, and a working electrode on which PEDOT is deposited. The polymerization can be done at constant potential (potentiosatic), constant current (galvanostatic), or varying potential (potentiodynamic)^[44]. The electrochemical deposition method influences PEDOT film morphology and its physicochemical properties.
- Chemical polymerization consists in polymerizing EDOT using an oxidizing agent in a solvent, and in the presence of a dopant. This method yields a suspension of **PEDOT:dopant particles, which will be referred to as PEDOT “inks” in the rest of this manuscript**. In contrast to electro-polymerization, chemical polymerization enables to

get PEDOT inks instead of electropolymerised film struck to an electrode, which enables further modification or processability.

The chemical polymerization of EDOT with or without a dopant yields to a conductive material whose electro-chemical properties are highly dependent on the polymerization parameters. Protocols reported in the literature differ from one publication to another, but three main steps can be distinguished:

1. The suspension of EDOT with a dopant in a solvent. The main solvent used in the literature is water, but others have been investigated such as methanol^[50] or formic acid^[51] for instance.
2. The addition of an oxidizer and eventually a catalyst. Main oxidizing agents are salts (iron (III) chloride or tosylate) and ammonium or potassium peroxodisulfates. Mainly used catalyzts are Fe^{III} salts. But for PEDOT:dopant materials dedicated to biological applications, Fe^{II} salts in tandem with ammonium persulfate can also be found in the litterature^[52,53], as Fe^{3+} is known to form with polyelectrolyte salts that may precipitate during reaction^[45].
3. The quenching of the polymerization reaction and purification of the final conductive PEDOT material to remove polymerization by-products and eventually increase pH after polymerization. Main purification methods are dialysis against water with a final removal of water (by freeze-drying or evaporation at low temperature under low pressure) and successive cycles of centrifugation, discard of supernatant and re-addition of water.

II.2. PEDOT conduction mechanisms

II.2.a. Band diagram of PEDOT

During the polymerization of EDOT monomers into PEDOT, the band diagram of the growing conductive polymer changes: as the number of associated EDOT monomers increases, the number of authorized electronic energetic levels increases, while the energy gap between the HOMO and the LUMO decreases (Figure 7). For a long enough PEDOT chain, it is considered that all those energetic levels form two continuous energetic bands within

which electrons can have any energy (Figure 7). Electrons in the **valence band** are tied to atoms, while electrons with high enough energy in the **conduction band** can move freely along the conjugated backbone. The energy gap between the valence band and the conduction band (known as E_{gap}), is around 1.7 eV^[54,55] for PEDOT. Noticeably, this energy gap depends on PEDOT environment, such as PEDOT chains conformation, its dopant, or PEDOT degree of crystallinity for instance.

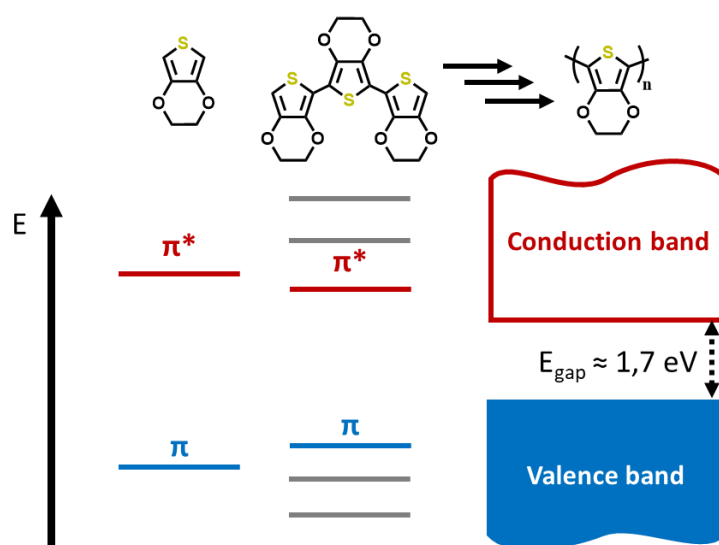


Figure 7. Evolution of the HOMO and LUMO levels as well as band gap E_{gap} with increasing number of thiophene repeating units, resulting in valence and conduction bands for PEDOT.

II.2.b. PEDOT primary doping: formation of polaron and bipolaron

Primary doping of PEDOT corresponds to any process modifying the oxidation degree of the backbone. Indeed, to be conductive, a conjugated polymer must be doped, namely to have either electrons in the conduction band, or to have electronic holes in the valence band. For PEDOT, the most common solution is to introduce electronic holes, namely positive charges, through oxidation. As the charge carriers in PEDOT are electronic holes, PEDOT is qualified as a “**p-doped polymer**”.

PEDOT conformation change and polaron/bipolaron propagation

When PEDOT is oxidized, an electron is removed from the backbone, yielding a positive charge associated with a radical: thiophene rings switch **from benzoid conformation, to quinoid conformation** (Figure 8). In the benzoid conformation, $C_{\alpha}=C_{\beta}$ double bonds, $C_{\alpha}-C_{\alpha}$ and

C_{β} - C_{β} simple bonds are prevalent, whereas in the quinoid conformation, $C_{\alpha}=C_{\alpha}$ and $C_{\beta}=C_{\beta}$ double bonds are more prevalent. Since double bonds are more rigid and shorter than simple bonds, this change of configuration triggers a distortion in PEDOT chains on few PEDOT repeating units. This distortion is accentuated by the electrostatic interactions between the positive charge of PEDOT and the surrounding lattice of counter anions (small molecules, or whole polyanions).

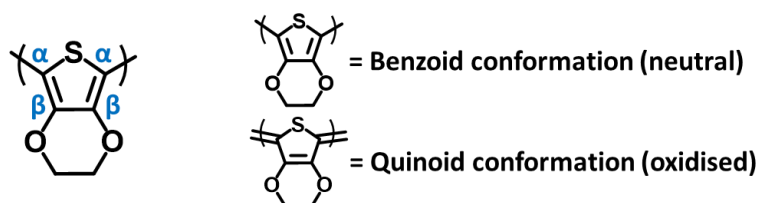


Figure 8. EDOT benzoid and quinoid conformations.

The association of the radical cation with this whole lattice deformation is called a **polaron**^[20,56]. If further oxidized, a dication is formed. Similarly, its association with the induced lattice deformation is called a **bipolaron** (Figure 9a and Figure 9c). Polaron and bipolaron can be considered as quasiparticles which propagate along the PEDOT backbone (Figure 9c): in doped PEDOT, polaron and bipolaron are considered as the charge carriers. PEDOT conductivity will be greater as their propagation along the backbone is eased^[57,58].

A recent study made by Zozoulenko *et al.*^[58], using density functional theory (DFT) calculations, showed that polarons and bipolarons are delocalized over 6-7 monomer units, with a bond length alternation characteristic of quinoid conformation. Gribkova *et al.*^[59-61] demonstrated that increasing the quinoid conformation prevalence on different PEDOT complex films resulted in an increase of conductivity, as can be expected by the more planar conjugated structure. Reciprocally, Yi *et al.*^[62] showed that chemical treatments which alleviate steric constraints of doped PEDOT chains can enable them to change conformation, getting a more linear structure, resulting in an increase of the quinoid conformation prevalence, an increase of charge delocalization, and thus, a higher conductivity.

More planar PEDOT domains (prevalence of quinoid conformation) enable a better polaron and bipolaron propagation, and also better interactions between PEDOT chains that

can organize themselves more easily (via π -stacking interaction), favoring electron hopping between PEDOT chains^[49].

Polaron and bipolaron energetic levels

Energetically speaking, the stabilization of PEDOT positive charges induces the appearance of new authorized energetic levels in the energetic gap: the polaronic and bipolaronic bands. The bipolaronic bands are slightly higher in energy than polaronic ones (Figure 9b). These new authorized bands lower the energetic gap for electrons to leave the valence band, enhancing PEDOT conductivity, which is directly correlated to polaron and bipolaron concentration. Noticeably, It has been shown that forming a bipolaron costs less energy than forming two polarons^[56].

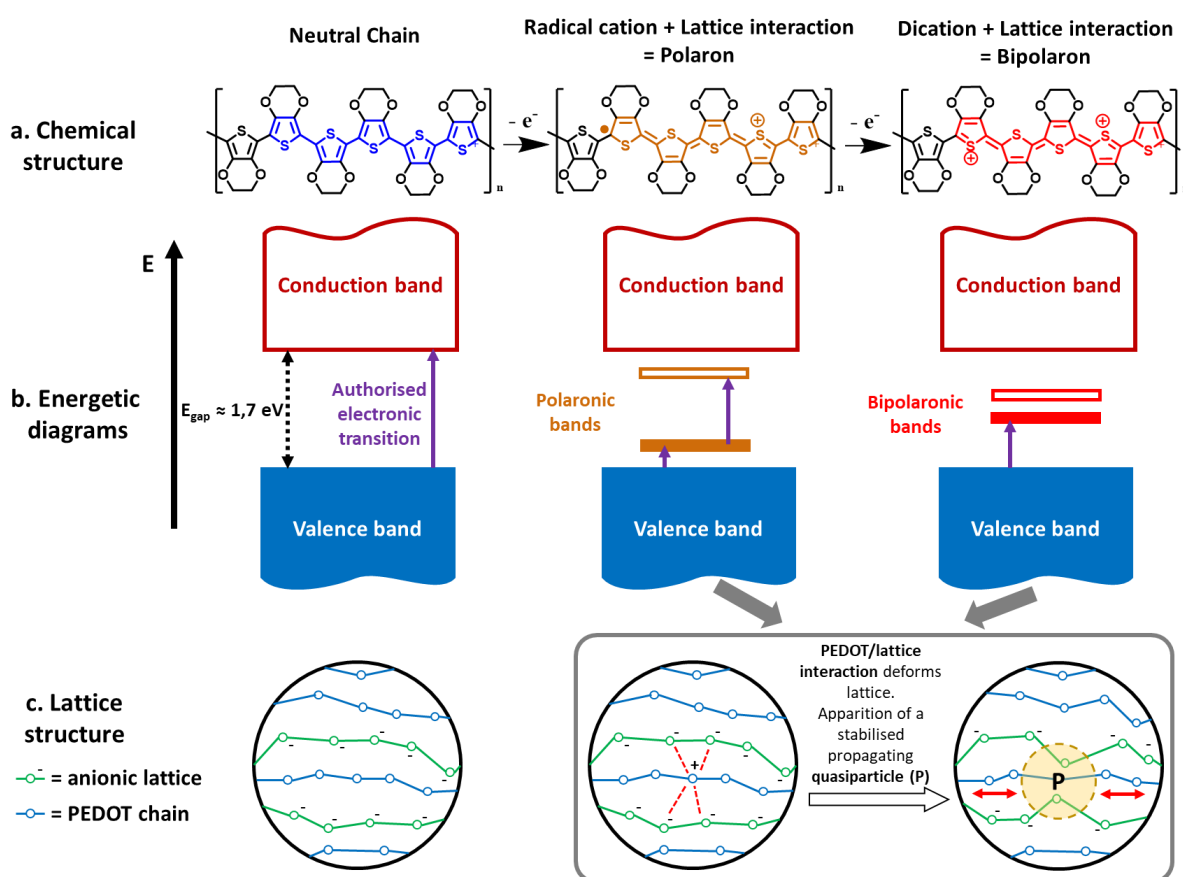


Figure 9. Chemical structure, band diagrams and lattice structure of a PEDOT-based conductive material, when doped via oxidation.

After EDOT polymerization, PEDOT chain doping degree is thermodynamically comprised between 25 and 33%, which means that the level of oxidation per monomer is between 1 charge per 3 EDOT units and 1 charge per 4 EDOT units. **Primary dopants** which

enable to adjust PEDOT doping degree can be the oxidant introduced during EDOT polymerization, a strong acid that can protonate PEDOT chains, or weak bases, such as imidazole^[63,64], that slow down EDOT polymerization, resulting in longer conductive PEDOT domains. Besides, PEDOT doping degree can be modified by electrochemical ways imposing a potential to the material.

II.2.c. PEDOT secondary doping: modification of microstructure

Secondary doping of PEDOT refers to any process that increases PEDOT conductivity without modifying its backbone oxidation degree, namely the concentration of charge carriers. Secondary dopants are inert molecules that do not react with PEDOT, but alter the film solid-state microstructure.

Secondary dopants can be high boiling point polar solvents (such as ethylene glycol, dimethylsulfoxide (DMSO), glycerol^[65] or sorbitol), various acids including formic and sulfuric acid, methanol, ionic liquids or surfactants (such as Zonyl[®] fluorosurfactant, dodecylbenzenesulfonic acid (DBSA^[66]) or Triton X-100)^[67,68]. Secondary dopants could favor a conformation change of PEDOT chains from benzoid to quinoid, resulting in more linear conductive domains that can organize themselves.

For the case of PEDOT doped by polystyrene sulfonate (PEDOT:PSS), the most investigated PEDOT material, the precise mechanisms of secondary doping that lead to an increase of conductivity are under study, and several propositions have been made^[49,67]. Polar and high boiling point solvents can screen charges and lower interaction between PEDOT and PSS chains, resulting in a concentration and partial crystallization of PEDOT domains enhancing the conductivity. Those solvents could also partially dissolve and remove PSS, increasing the ratio PEDOT/PSS, increasing the conductivity as PSS is an insulator.

II.2.d. Conduction mechanisms at a higher scale

At a macroscopic scale, conductive polymers are disordered materials, with various conjugation lengths and defects within the chains (Figure 10). Weak Van der Waals forces between chains, π - π and hydrophobic interactions yield to the apparition of small crystalline

domains. Charge transport is fast along the chains but moderate between the chains^[69,70] (red lines on Figure 10). To optimize conductive properties at the macroscopic scale, both charge carrier mobility and intra/interchain charge transport should be taken into account.

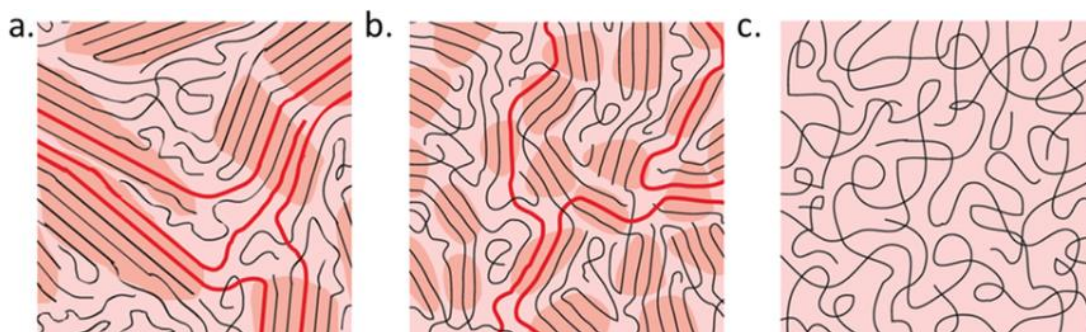


Figure 10. Schematic structure of a conductive polymer lattice with different organisation level: a. Very ordered. b. Lightly ordered. c. Disordered. Adapted from Noriega et al.^[70] The red lines in a. and b. represent the optimal charge propagating paths.

For conductive polymers, differently from metals, the density of charge carriers is independent from temperature. But as temperature rises, the mobility of charge carriers increases due to thermal motion. To describe the conductivity of highly disordered semiconductor material, **Mott's variable range hopping theory** considers that the charge carriers (polaron, bipolaron) hops from one site to another^[71,72] (Figure 11). This hopping is favored if there is a set charge nearby (the counter-ion), if there is no charge in the terminal site, and if as there is a strong coupling between the mobile and set charges. This model is relevant for conductive polymers with low conductivity, below 10 S/cm.

However for more conductive polymers which display high conductivity and quasi-metallic behavior, Mott's variable range hopping theory is not totally satisfactory. **Charging-energy-limited tunneling theory** developed by Sheng in 1980 is more relevant in that case^[73]. This theory proposes that charge transport is dominated by charge transfers between large conducting segments rather than hopping between localized states. In this theory, electrons pass from one neutral grain to another one via tunneling. In complement of this theory, Zuppiroli *et al.*^[74] demonstrated in 1994 via calculations that charge transport does not occur solely from hopping between single polarons and bipolarons along the chains, but also from the charge tunneling between polaron or bipolaron clusters (Figure 11). In addition this study highlighted that PEDOT dopants are the source of both polaronic cluster stability and of charges tunneling.

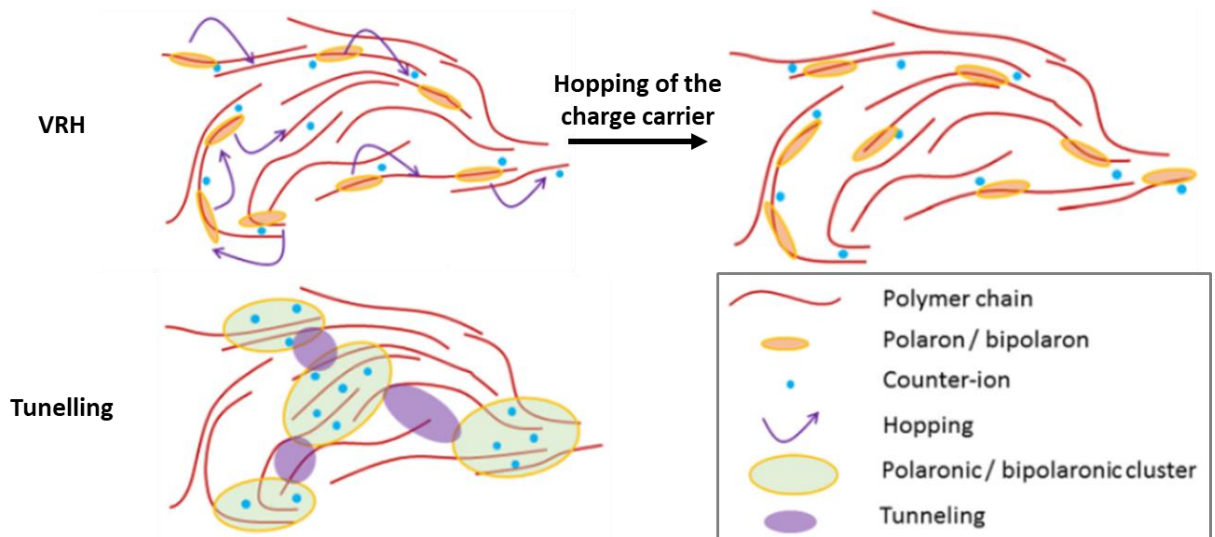


Figure 11. Schematic representation of the variable range hopping (VRH) model, and of the tunneling model. Adapted from Gueye et al.^[49].

II.3. Measurement of PEDOT doping degree

To quantify the intrinsic doping degree of PEDOT chains, namely their oxidation degree, three main techniques can be implemented.

II.3.a. Ultraviolet visible-near infrared absorbance spectroscopy

When PEDOT is doped, new energetic levels appear in the gap, authorizing new electron transitions. Those electronic transitions are associated with specific absorption bands. Henceforth quantification of PEDOT doping degree can be done using its absorption spectra as polaron and bipolaron display characteristic absorption bands in the red and near infrared domains (Figure 12).

Three zones can be distinguished^[49] (Figure 12): a first absorption band around 600 nm corresponding to the electronic transition from the valence band to the conduction bands (Transition **a** on Figure 12, $\Delta E \approx 1.7 - 2 \text{ eV}$), corresponding to the contribution of neutral PEDOT chains. A second absorption band around 850 nm corresponds to the electronic transitions from the valence band to the occupied polaronic band (Transition **b**, $\Delta E \approx 1.5 \text{ eV}$). Then in the near infrared (NIR), doped PEDOT displays a large absorption band corresponding to electronic transitions from the valence band to the occupied bipolaronic band, and to electronic transitions from the occupied to the unoccupied polaronic band (Transitions **c** and

d, $\Delta E \approx 1 \text{ eV}$). Intrachain or interchain polaron networks can broaden the polaronic bands, enabling electronic transitions of even lower energy, corresponding to the high absorption beyond 1500 nm. The more intrinsically doped a PEDOT chain is, the higher its absorbance in the NIR is.

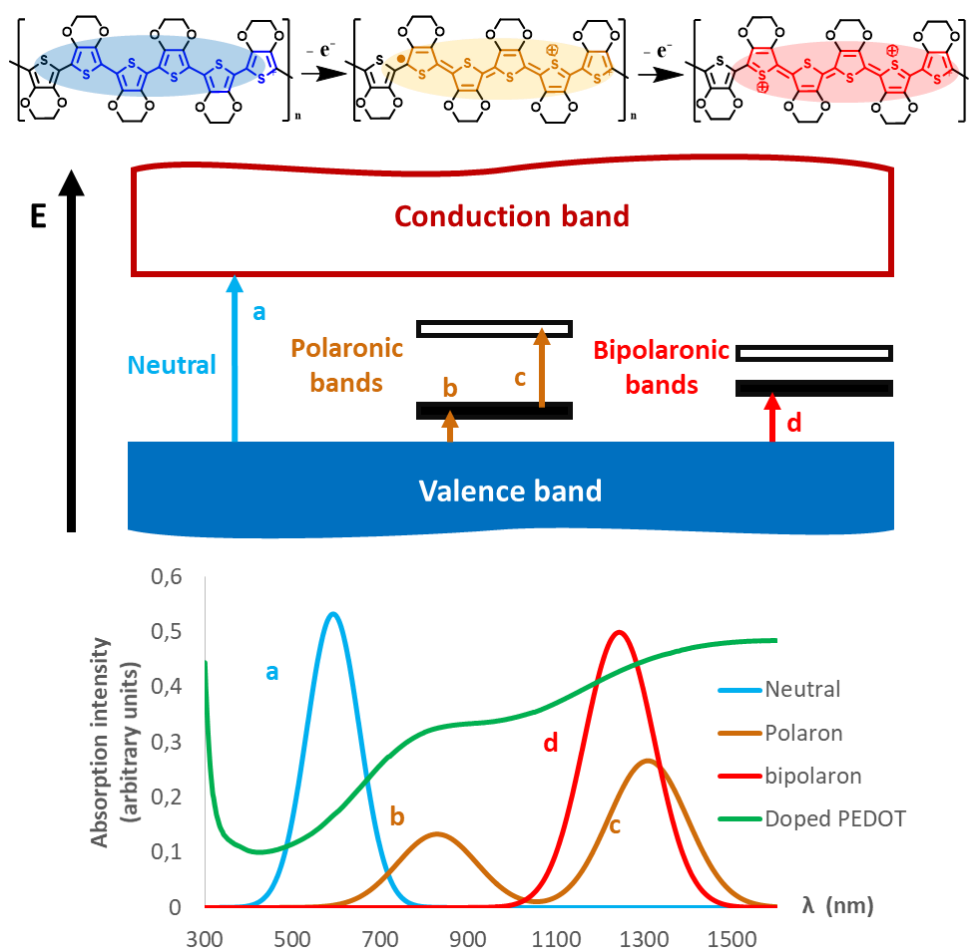


Figure 12. Evolution of the electronic characteristic of PEDOT at different doping levels and corresponding UV-vis-NIR absorption bands.

II.3.b. Raman spectroscopy

Raman spectroscopy is a spectroscopic technique which is used to investigate the vibrational modes of molecules. It relies on the inelastic scattering of photons by molecular bonds. In this technique, a laser is focalized on a sample, incident photons excite molecules or polymers, before being re-emitted with a higher or a lower energy. The energy shift between scattered and incident photons gives information about the molecule vibrational modes, and therefore allows the identification of the chemical bonds, as each molecular or intramolecular

bonds possess specific vibrational frequencies. Raman spectroscopy provides a fingerprint to identify molecules, or evolution of molecule conformation.

Raman spectroscopy can be used to quantify the intrinsic doping state of PEDOT chains as we have seen that the doped state of PEDOT is characterized by the prevalence of the quinoid conformation of the thiophene rings, whereas in neutral form the benzoid conformation is more preponderant (Figure 8).

However, as bonds vibrational frequencies are highly dependent on the matrix of the sample and the surrounding lattice, PEDOT bonds Raman shifts can vary depending on PEDOT dopant. For instance, the Raman shift of $C_{\alpha}=C_{\alpha}$ or $C_{\beta}=C_{\beta}$ double bonds of thiophene rings (Figure 8) will be slightly different whether PEDOT is doped by PSS or by another polyanion^[59].

Furthermore, Raman shift is expected to differ with PEDOT doping state. Using Raman spectroscopy, it is possible to assess quantitatively the doping degree of a sample, as demonstrated by Chiu *et al.*^[75] using Raman spectra deconvolution and fitting. Similarly, Gribkova *et al.*^[59] investigated the effect of PEDOT dopant on its doping degree using *in-situ* Raman spectroscopy during the electro-polymerization of PEDOT films.

II.3.c. X-ray photoelectron spectroscopy

X-ray photoelectron spectroscopy (XPS) measures the binding energy of electrons extracted from atoms at the surface of a sample (< 10 nm). For PEDOT:PSS for instance, XPS enables to evaluate PEDOT intrinsic doping state by analyzing the signal corresponding to sulfur atoms in Sp_2 configurations (thiophene sulfur), and comparing it to the signal of Sp_3 sulfur atoms (sulfate sulphur groups of PSS).

II.4. Influence of PEDOT dopant

To be conductive, PEDOT chains must present positive charges that need to propagate and be stabilized, as detailed in section II.2.b. Counter anions are thus needed. They act as dopants as they enhance PEDOT conductivity. They can affect both primary doping and secondary doping.

II.4.a. Advantages of polyanions versus anions

To increase the stability and solubility of PEDOT:dopant particles in water, **polyanions** were suggested in 1989 as they can serve as structural agents for conductive PEDOT domains, increasing the stability, processability and solubility of PEDOT:polyanion complexes^[45]. Polyanions serve different roles in addition to counterbalancing positive charges that propagate into PEDOT conductive domains^[76]. First they increase the low solubility of EDOT in water (2.1 mg/mL at 20 °C)^[45], due to their negative charges, and possibly their hydrophobic part that can interact with the apolar aromatic cycle of EDOT. Then polyanions serve as a polymerization template for EDOT monomers, which can bind along their chains before polymerization^[76], resulting into structured conductive domains along polyanion chains (Figure 13).

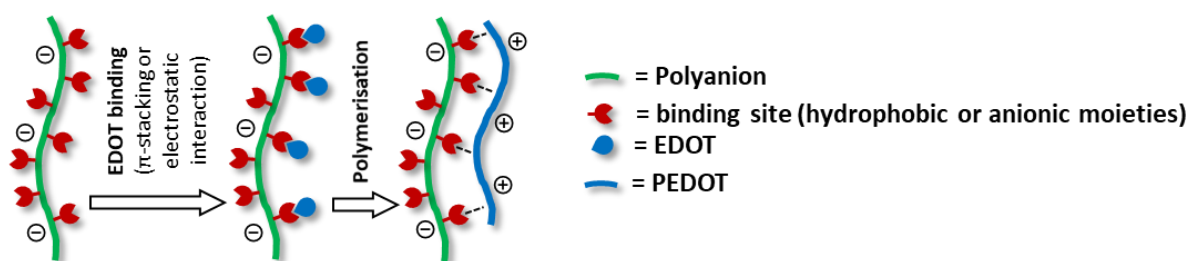


Figure 13. Structuration of EDOT monomers along polyelectrolyte chains and resulting structured PEDOT domains after polymerization.

II.4.b. Poly(3,4-ethylenedioxythiophene): poly(styrenesulfonate) (PEDOT:PSS)

Poly(3,4-ethylenedioxythiophene): poly(styrenesulfonate), or **PEDOT:PSS** is the most widely studied PEDOT:dopant material. It was the first to be described in 1989, product of a cooperation between Bayer and Agfa-Gevaert^[45]. Colloidal stable suspensions of PEDOT:PSS are commercialized by Heraeus (among others) under the name Clevios™ with a wide range of conductivity. Their commercial availability at reasonable cost in addition to tunable conductivity, thermal and chemical stability, processability, cytocompatibility and possible chemical modifications make these inks one of the most promising candidates to design soft, flexible conductive materials for bioelectronics^[67,77,78]. Surface tension, viscosity and wettability of the inks can be finely tuned to adapt to several processes: they can be modified

by adjusting PEDOT:PSS concentration, dispersion pH or ionic force, addition of surfactants, cross-linkers or co-solvent^[79–81].

Using bright field transmission electron microscopy (TEM) and high angle annular dark field scanning TEM, Lang *et al.*^[82] have demonstrated that PEDOT:PSS suspension after polymerization is constituted of particles from 30 to 50 nm, resulting from the aggregation of several tangles, where each tangle is composed of a single PSS chain with several PEDOT domains attached to it (Figure 14). As PEDOT is hydrophobic and PSS hydrophilic, tangles richer in PEDOT are in the center of each particle, while tangles richer in PSS constitute the outer layer of the particle. Inside each tangle, oligomers of PEDOT between 6 and 18 repeating units^[45] are physically attached along PSS chains via electrostatic interactions and π -stacking.

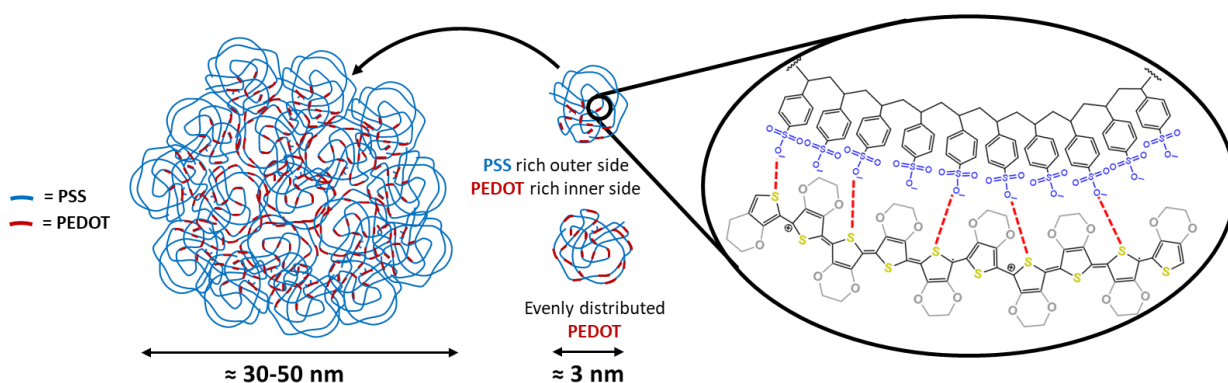


Figure 14. Structure of a PEDOT:PSS particles, with a core rich in hydrophobic PEDOT domains.

PEDOT:PSS films can be obtained by several methods: spin coating^[83], doctor blading^[79], spray coating^[84], inkjet printing^[81], roll-to-roll printing^[63], lithography or electrospinning^[85]. The nature and surface modification of the substrate, the conditions of drying (temperature and humidity) and annealing temperature all affect the final conductivity and stability of the dried PEDOT:PSS material^[86]. Nardes *et al.*^[69] have demonstrated via scanning tunneling microscopy and atomic force microscopy measurements that PEDOT:PSS thin films exhibited a structure composed of PEDOT-rich clusters of 20 to 25 nm long and 5 to 6 nm high, separated by PSS lamellae (Figure 15).

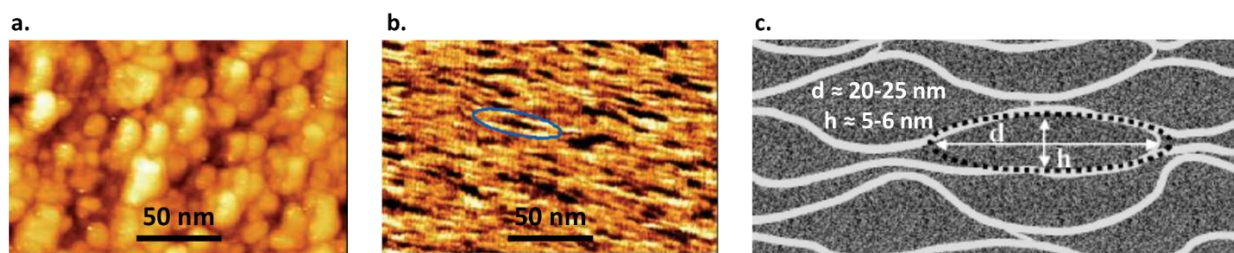


Figure 15. Microstructure of PEDOT:PSS films on different substrates. a. Scanning tunneling microscopy top view of a PEDOT:PSS film on ITO. b. Cross-sectional atomic force microscopy phase image of a cleaved PEDOT:PSS film on glass. c. Schematic morphological model for PEDOT:PSS thin films: pancake-like PEDOT rich clusters (grey dark) are separated by lamellae of PSS (white). Pictures adapted from Nardes *et al.*^[69].

Pristine PEDOT domains are essentially amorphous but secondary treatments can increase the crystallinity, as reported by Takano *et al.*^[87] using small- and wide-angle X-ray scatterings. The high hydrophilicity of PSS makes PEDOT:PSS film morphology and conductivity sensitive to moisture. At low humidity, hydrogen bonds in the PSS shell are strong, but at higher humidity, PSS shell absorbs water, resulting in an increase of particle shell inter-distance, diminishing hydrogen bonding and so decreasing film mechanical strength and conductivity^[82,88].

PEDOT:PSS appears to be cytocompatible^[48,89] and has been suggested for numerous applications in bioelectronic^[90,90]: it is used in strain sensors^[91–93], humidity sensors, drug delivery^[94], tissue engineering^[95–97], in organic electrochemical transistors, as electrode coating for intracranial micro electrode arrays (MEAs) and electrocorticography (ECOG)^[98,99], or just to improve cytocompatibility and decrease impedance at the interface with tissues^[100]. However, as PEDOT:PSS ink is soluble in water, it is in those applications either electropolymerized on a conductive rigid surface, or sandwiched between waterproof membranes. This can be a drawbacks for biological application, as the mechanical mismatch of the surface of the encapsulant with biological tissue could induce inflammation reactions.

To overcome this, it is possible to combine PEDOT:PSS with other soft materials such as hydrogels, to form new hybrid materials promising for the electronic tissue interface.

III. Conductive hydrogels

Hydrogels are highly hydrated networks designed from hydrophilic polymers. Their high water content, permeability to small molecules and mechanical resemblance with natural tissues make these soft materials promising candidates for tissue engineering^[101]. Hydrogels are composed of cross-linked hydrophilic polymer chains, forming a 3-dimensional matrix. If chains are covalently cross-linked, the hydrogel is classified as “chemical”. If the cross-linking network is due to physical interactions (electrostatic, hydrogen bonds, π -stacking or hydrophobic interaction) or chain entanglement, the gel is classified as “physical gel”.

III.1. Interest of hydrogels at the electronic tissue/interface

III.1.a. Hydrogels as biomechanical enhancers

Materials traditionally used in bioelectronics such as metal (for Michigan-type probe^[102], Utah arrays^[103] or deep brain stimulation probes^[104]), various plastics or elastomers^[105] are too hard for long term implanted medical devices (Figure 16a). The mechanical mismatch between electronic devices and tissues can trigger inflammation reactions, resulting in encapsulation of the foreign body by a glial scar and degradation of interface electrical properties^[106–108] (Figure 16b).

As hydrogels can display elastic moduli (G') ranging from 10^2 Pa to 10^5 Pa, there are suitable candidates for electronic/tissue interfacing. They can minimize the mechanical mismatch between electronic devices and tissues^[109–111] and enhance the interface quality with a more intimate contact than harder materials. They can be used as **biomechanical enhancers**.

Besides, the use of hydrogels at the tissue device/interface enables to keep tissues hydrated, improving interfacial contact. It also enhances biocompatibility by imitating the extracellular matrix allowing to promote cell adhesion, proliferation and tissue in-growth^[112,113]. Finally, hydrogels appear to increase the electrical quality of the tissue/electronic interface as their use enables to decrease interfacial impedance^[114].

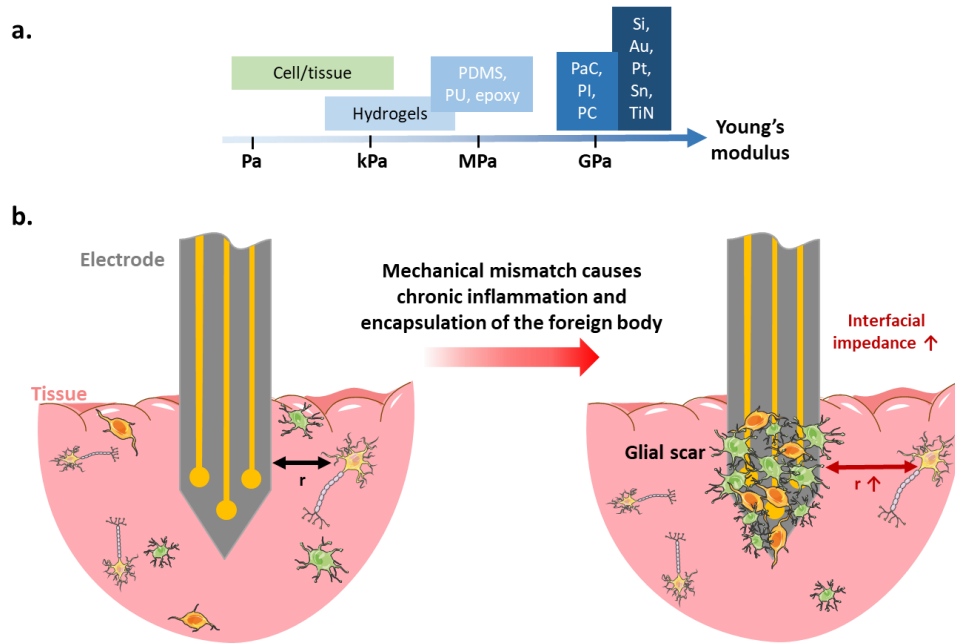


Figure 16. a. Young's modulus of materials used for intracranial monitoring or stimulation of tissues (polydimethylsiloxane (PDMS), polyurethane (PU), parylene C (PaC), polyimide (PI), polycarbonate (PC), titanium nitride (TiN)), in comparison to brain tissue mechanical properties, adapted from Yuk et al.^[101]. b. Scheme of glial scar formation: the scar increases the distance between the electrode and the neurons, as well as the interfacial impedance.

III.1.b. Description of the electronic/tissue interface

To better understand how hydrogels are expected to enhance the electric “quality” of the electronic/tissue interface, it is important to describe the electro-chemical phenomena occurring there. The physiological mechanisms for neurons are detailed below. Those mechanisms can be extrapolated to other electro-active tissues or electro-sensitive cells.

Ionic and electronic flows in tissues and electrode

Brain tissue has a conductivity around $4 \cdot 10^{-3} \text{ S/cm}$ ^[115], supported by ionic flows between neurons, contrary to electronic systems, for which conductivity is supported by electron flows.

At the cellular scale, the ionic flows are generated by the neurons, via spikes of ionic current, or **action potentials**^[101]. Neuronal cells maintain a negative resting transmembrane potential value (between -60 and -75 mV), via an ionic imbalance between intracellular K^+ and extracellular Na^+ cations (Figure 17a left). Environment modifications due to inputs from other neurons or from an electrode can modify the transmembrane potential (polarization of the membrane if the potential decreases, depolarization inversely), and when it reaches around - 50 mV, voltage-gated Na^+ channels open allowing a rapid influx of Na^+ ions into the cells,

which generates a spike of depolarization (Figure 17b). Upon reaching a potential around + 30 to + 40 mV, the transmembrane potential repolarizes to the resting potential via slow efflux of K^+ ions. Action potentials generate an **extracellular potential** which decays rapidly as the distance from the neuron increases (Figure 17a middle).

At a microscopic scale (10 to 100 μm), the superposition of all cell action potentials creates a **local field potential**, whose spatial and temporal variations and oscillations rely on ionic flows at different length scale (Figure 17a right).

Those variations of ionic flows can elicit electronic currents in an electrode. The closer the electrode will be from electro active cells, the more specific and sensitive the communication will be. Tissues and electrodes can communicate in both directions:

- Electrodes can stimulate neurons by triggering the firing of action potentials via delivering electrical inputs to the surrounding extracellular medium (Figure 17c).
- Reciprocally neurons can create ionic flows that drive electron flows in the electrode via modification of the electrolyte/electrode interface potential (Figure 17d).

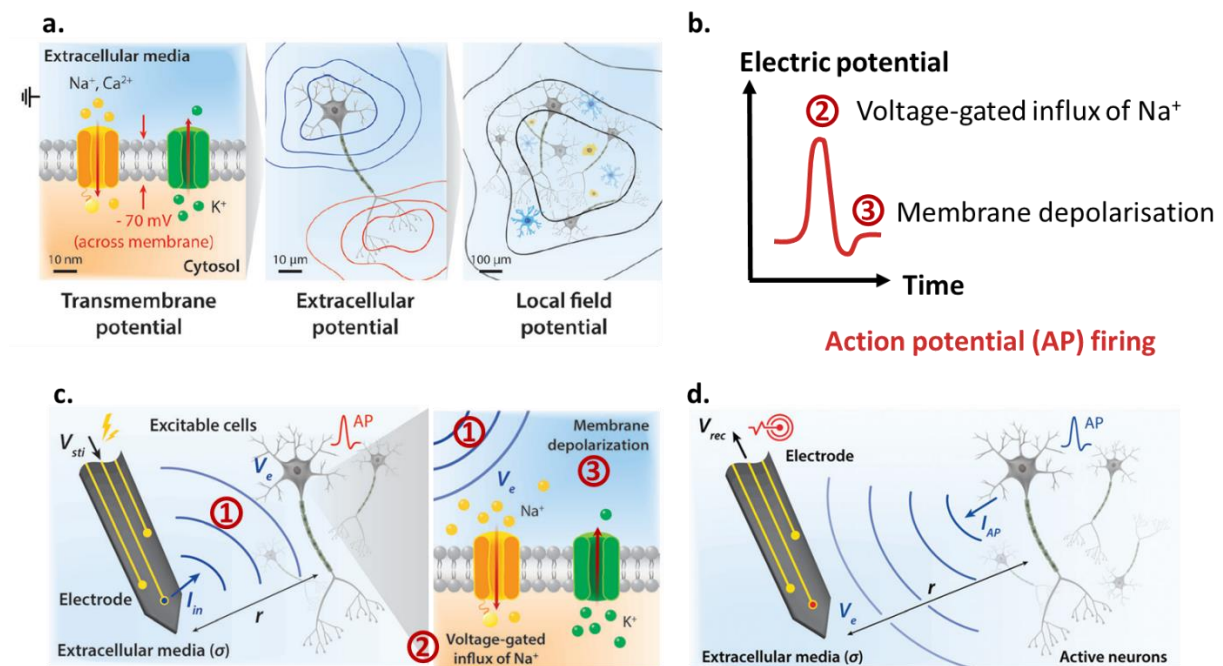


Figure 17. a. Brain electric potential at different scales. b. Action potential firing structure. c. Electrode/neuron interaction in stimulation mode. d. Electrode/neuron interaction in monitoring mode. Adapted from Yuk et al.^[101].

Electrode/tissue interface modelisation

At the electrode/tissue interface, two different charge transport supports are in contact: ions in the extracellular matrix (considered as an electrolyte medium), and electrons in the electrode material (Figure 18a). For electric stimulus to be transmitted from the electrode to the tissues, or reciprocally for action potential to be detected by the electrode, charges need to be injected in both directions at the interface.

This injection of charges may occur via two main mechanisms (Figure 18b): Faradaic charge injection based on surface electro-chemical reactions, or **capacitive charge injection** based on charging/discharging of the electrolyte–electrode interface by accumulation of ions on the electrode without electro-chemical reactions^[116] (Figure 18c). As faradaic mechanism implies redox reactions, it may alter the electrode surface, and generate toxic species, in addition to depleting the electrolyte from important chemicals. Therefore capacitive mechanisms is locally preferred in bioelectronics.

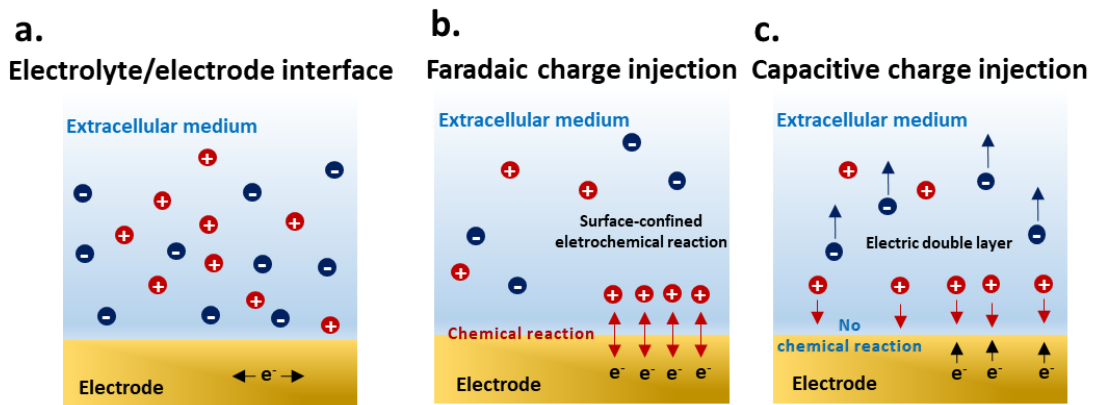


Figure 18. a. Tissue/electrode interface at equilibrium. Faradaic (b) and capacitive (c) charge injection mechanisms at tissue/electrolyte interface.

The simplest way to describe more accurately the interface bioelectronic phenomena is to use the following equivalent circuit^[116] (Figure 19): an electronic device with a resistance R_{ic} applies (or records) a potential V_{sti} (or V_{rec} respectively) on neural tissue. The electrolyte/electrode interface is considered as a leakage resistance R_e in parallel with a capacitance C_e accounting for the electrical double layer (EDL). In stimulation mode, V_{sti} elicits an electric potential V_e on the outer membrane of targeted neurons, triggering action potentials. In recording mode, the electronic activity of neurons generates ionic currents I_{ap} which create an electric potential V_e in the electrolyte, recorded by the electrode.

For more complex interfaces, with porous conductive hydrogels for instance, the capacitance C_e can be coupled with a other equivalent elements, such as Warburg diffusion element to model the diffusion process of electro active species in the hydrogel^[117]. Other equivalent circuits found in literature add ion and electric resistances, plus charge transfer resistance^[118].

a.

Parameter	Definition
V_{sti}	Stimulation electric potential
V_{rec}	Recorded electric potential
V_e	Electrolyte electric potential
I_{ap}	Ionic current injected by action potentials
C_e	Electrode capacitance for capacitive charge injection
R_e	Electrode leakage resistance
R_{ic}	Interconnect resistance for high order circuitry

b.

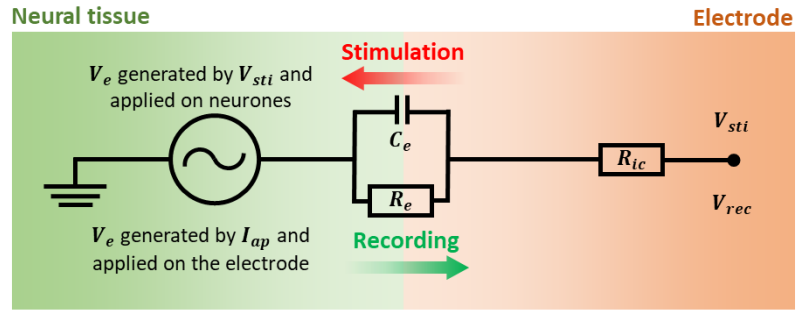


Figure 19. a. Parameters used in the equivalent circuit. b. Equivalent circuit model of tissue–electrode interface for bioelectronic recording.

A detailed analysis of Maxwell’s equations of electromagnetism applied to neural stimulation or recording yields to optimal parameters of the electrode for neural stimulation or recording^[101] (Table 1).

Table 1. Electric requirements for tissue–electrode interfaces and desired electrode features, adapted from Yuk et al.^[101]

Tissue/electrode interaction	Requirements	Desired electrode features
Tissue stimulation	High V_e	Low R_e
		High C_e
		Low R_{ic}
		High V_{sti} ($V_{sti} < V_{reaction}$)
		Close to electrode
Tissue monitoring	High signal/noise ratio	Low R_e
		High C_e
		High R_{ic}
		Close to electrode

Properties of interest

In stimulation mode, the electric potential V_e is proportional to the ionic current I_{in} injected at the electrolyte/electrode interface, preferentially using the capacitive mechanism. To evaluate the prevalence of this mechanism, two values are used in literature: the **charge**

injection capacity (CIC), and the **charge storage capacity of the electrode (CSC)**. The CIC describes the amount of charges that the electrode can inject per unit area without causing irreversible electro-chemical reactions or tissue damage. The CSC corresponds to the amount of charge an electrode can “store”. Both values are in mC/cm². Because it is easier to measure, CSC is a widely spread indicator in literature, to compare the charge transfer capability of electrodes for neural stimulation^[119]. Commercial neural stimulation/recording devices have CSC ranging from 10⁻¹ to 10² mC/cm²: CSC_{sputtered iridium oxide film} = 23 mC/cm² ^[116], CSC_{Platinum} = 0.550 mC/cm² ^[116], CSC_{PEDOT-PSS coatings on ITO} = 3.6 mC/cm² ^[120].

In literature, the tools of predilection to evaluate the electro-chemical properties of an electrolyte, tissue or conductive hydrogel for instance, are cyclovoltametry (CV), pulse experiments, and electrochemical impedance spectroscopy (EIS):

- CV enables to measure the CSC of a tissue or contact hydrogel using the equation $CSC = -\frac{1}{v \cdot S_{electrode}} \int_{i < 0} IdV$ where v is the sweeping rate in V/s, and $S_{electrode}$ the electrode surface contact with the hydrogel or tissue^[121].
- Current pulse experiments enable to assess the capacity of a an electrode material to transmit charges to the surrounding medium when current pulse are applied, without eliciting redox reactions^[122], define as the capacitive charge injection capacity (CIC). The CIC is determined as the maximum injectable charge per surface area^[123], in mC/cm².
- EIS is a powerful investigation tool which can give the impedance Z of the interface according to the frequency (Bode plot), or more quantitative values fitting the Nyquist plot ($-\text{Im}(Z)$ according to $\text{Re}(Z)$) with an equivalent circuit. Such analysis can lead to the conductivity σ of the interfacing hydrogel, its capacitance C_e , leakage and charge transfer resistance R_e and R_{ct} . The measurement is made over a broad frequency range, typically 10 mHz Hz to 10⁵ Hz. The impedance at 1 kHz is mainly used to characterize the recording electrode, ranging in vivo from 50 kΩ to 1 MΩ^[116]. Low impedance is required for recording, but too low impedance may result in a low signal/noise ratio, being detrimental to recording quality.

III.2. Conductive hydrogels

In order to increase the long term biocompatibility of bioelectronic devices, a strategy consists in replacing the traditional hard conductive material electrode by a **conductive hydrogel**. A conductive hydrogel is a hydrogel which displays either a pure ionic conductivity if swollen with an electrolyte, or a mixed ionic/electronic conductivity if combined with a conductive material. It must be understood that conductive hydrogels are not used as electrode coater to enhance biomechanical properties, but as the electrode themselves.

III.2.a. Ionically conductive hydrogels

Pure ionically conductive hydrogels are obtained by dissolving ionic species (NaCl, LiCl) similar to electrolytic tissue media into hydrogels. These hydrogels combine a high ionic conductivity (>10 S/cm) with the soft viscoelastic properties of hydrogel (Young modulus $E < 100$ kPa)^[124]. Due to their high salt concentration (> 1 M), they are suitable skin electrodes for electroencephalography^[124] or electrocardiography recording for instance^[125]. They enable a better signal quality than direct skin electrode contact since they allow impedance adaptation between tissue and electrode. However too high electrolyte concentration may be harmful^[126], and ions can progressively leach out from the hydrogel, making the bioelectronic performances of such gel unstable^[126]. They are not suitable material for long-term implantation.

III.2.b. Composite hydrogels

The drawbacks mentioned above can be overcome by incorporating electronic conductors into the hydrogel, taking advantage of their porous structure: recently, several composite conductive hydrogels have been developed by incorporating metal or carbon nanoparticles, nanowires or nanotubes^[127], or graphene derivatives. The resulting hydrogels display both ionic and electronic conductivity, in addition to the advantageous biomechanical properties of the hydrogel. As metals are susceptible to corrosion in wet environment, noble metals can be used as conductive parts, but in the form of nanoparticles or fibers^[128,129] to avoid major modifications of mechanical properties. The stability of carbon nanomaterials (nanoparticles, carbon nanotubes, graphene) in wet environment is also a great asset for the development of conductive composite hydrogels in alternative to metallic nanoparticles^[130].

For instance, carbon nanotubes were incorporated in gelatin methacrylate networks^[127], and graphene in poly(caprolactone)^[131], both for transient tissue engineering. Reduced graphene oxide has also aroused great interest as it is biocompatible and conductive, and enables “mussel-like chemistry” for adhesive conductive hydrogels^[132–134].

Another possibility lies in the design of purely polymeric composites, combining hydrogels with conductive polymers. The use of conductive polymer is thus of great interest as it enables the design of conductive hydrogels with high electronic and ionic conductivity, and tunable physicochemical properties as described previously. Besides, as hydrogels are highly porous, electrolytes can diffuse inside, resulting in high specific surface conductive biocompatible electrodes. Each conductive polymer chain can be electro-active as it can create a small electronic double layer at its surface, yielding to a high volumetric capacitance.

There is a growing interest in literature concerning PPy, PANI and PEDOT hydrogels. This review will only focus on PEDOT hydrogels as PPy and PANI hydrogels are mainly designed for soft electronic applications, and not necessarily for bioelectronic applications.

III.3. Conductive PEDOT hydrogels

In PEDOT-based conductive hydrogels, the two polymeric networks (the hydrogel matrix and the conductive polymer) can be combined using different strategies.

III.3.a. Interpenetrating networks

The most common conducting polymer hydrogels are based on interpenetrating networks (IPNs) between a conducting polymer (CP = PEDOT and its dopant) and a non-conducting hydrogel template (Table 2). IPN networks are defined as a combination of two or more separately cross-linked networks, composed of two different polymers that do not share covalent bonds. Final hydrogels can either be physically or chemically cross-linked (Figure 20). In PEDOT-based conductive IPN hydrogels, the CP polymer network is physically cross-linked by interaction between EDOT domains. The vast majority of IPN conductive hydrogels use PEDOT:PSS as conductive material. Interestingly, PEDOT:biopolymer hydrogels can also be found (PEDOT:sulfated lignine^[135], PEDOT:chitosan^[136] or PEDOT:starch^[137]). Other anionic

molecule such as benzoic acid^[138], paratoluene sulfonate^[139,140], or orthotoluene sulfonate^[83] have also been used as dopants.

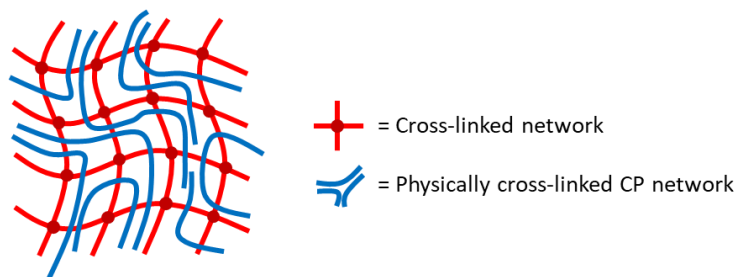


Figure 20. Conductive PEDOT-based IPN structure: two (or more) independent cross-linked networks, one of them being a physically cross-linked CP network.

Conductive PEDOT-based IPN hydrogels are typically prepared through three major approaches, listed in Figure 21:

1. **Filling of a preformed hydrogel with the conductive monomer, then polymerization of the conductive polymer** (via chemical or electrochemical polymerization, Figure 21a). For instance, Wang *et al.*^[136] designed a PEDOT:chitosan hydrogel reaching a conductivity of 0.17 S/cm by chemically polymerizing EDOT into a chitosan/gelatin hydrogel.
2. **Mixing of the conductive polymer and hydrogel precursors followed by the cross-linking of the hydrogel network** (Figure 21b). Using this strategy, Luo *et al.*^[141] and Babeli *et al.*^[142] respectively reported the synthesis of conductive hydrogels, mixing PEDOT:PSS with tannic acid and silk fibroin (or with alginate respectively), before physically cross-linking the hydrogel with calcium chloride. All the gels obtained with this strategy displayed low conductivities below 10^{-3} S/cm.
3. **Mixing of the conductive monomer and hydrogel precursors, followed by the simultaneous polymerization of the conductive polymer and the cross-linking of the hydrogel** (Figure 21c). This approach requires that the conducting monomer and the hydrogel precursors react using either orthogonal chemistry, or the same one. Using orthogonal chemistry, Yang *et al.*^[143] developed a PEDOT:alginate hydrogel polymerizing EDOT with ammonium persulfate, while cross-linking alginate with adipic dihydrazide acid, yielding to a hydrogel with a conductivity up to 0.0607 S/cm.

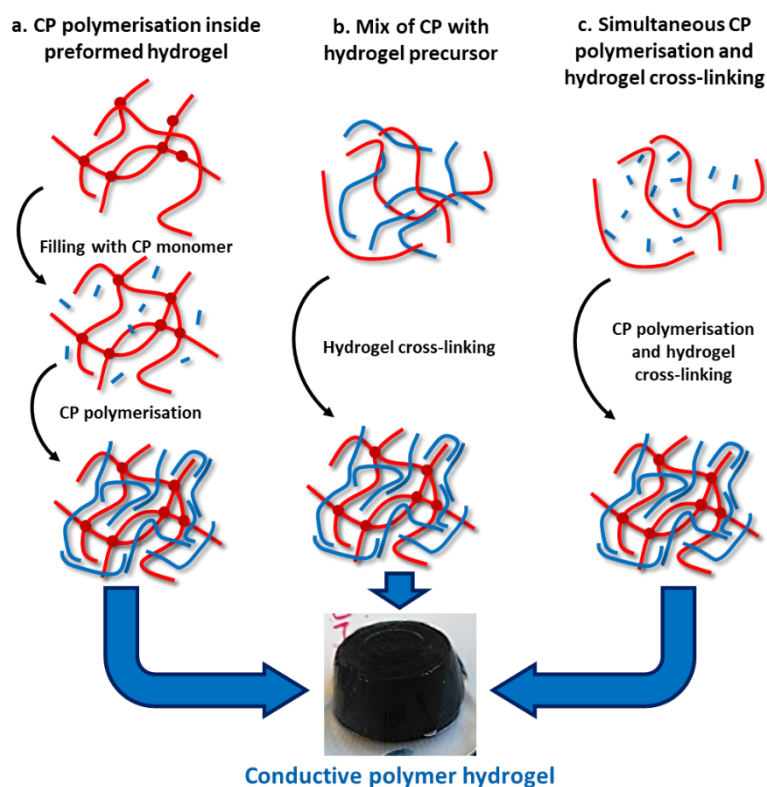


Figure 21. Three synthesis pathways to form interpenetrating conductive hydrogels. Here CP = PEDOT+ dopant.

IPN conductive hydrogels based on PEDOT:PSS without additional conductive material mainly display low conductivity, below 10^{-2} S/cm, with exception of the work of Ding *et al.*^[144]. They developed a PEDOT:PSS hydrogel with a conductivity of 1.2 S/cm, obtained via electro-polymerization of EDOT into a photo-cross-linked poly(2-hydroxyethyl acrylate)/PSS copolymer.

Chapter 1. Towards PEDOT: hyaluronic acid inks for bioelectronics

Table 2. Interpenetrating conductive hydrogels

Hydrogel type		Reference	PEDOT:dopant	Strategy to obtain hydrogel	σ (S/cm)	CSC (mC/cm ²)	Impedance (Ω) at 1 kHz	Biocompatibility	Suggested applications
Physical hydrogel	H-bonds and electrostatic interaction	Luo <i>et al.</i> ^[141]	PEDOT:PSS	PEDOT:PSS in Tannic acid + silk fibroin + CaCl ₂	3.17x10 ⁻⁴	-	-	Cytotoxicity of MC3T3 cells. Antibacterial assays on <i>E. coli</i> and <i>S. aureus</i>	Soft electronics, and human/machine interfaces
		Bhattacharjee <i>et al.</i> ^[145]	PEDOT:PSS	PEDOT:PSS in silk fibroin + PVA, then drying	-	-	~ 10 ³	Human corneal epithelial cell line	Tissue engineering: epithelium regeneration
		Babeli <i>et al.</i> ^[142]	PEDOT:PSS	PEDOT:PSS in alginate/CaCl ₂ hydrogel	7.9x10 ⁻⁵	-	-	-	Pressure sensor/ wearable electronics
		Rastin <i>et al.</i> ^[146]	PEDOT:PSS	PEDOT:PSS mix in Me-cellulose/ κ -carrageenan hydrogel	1.21x10 ⁻³	-	<10 ³	Cytotoxicity and proliferation of HEK-293 (human embryonic kidney cells)	3D bioprinting
		Zhang <i>et al.</i> ^[147]	PEDOT:PSS	PEDOT:PSS in zwitterionic poly(HEAA-co-SBAA) hydrogel	6.25x10 ⁻³	-	~1.5x10 ³	Antifouling + cytotoxicity with bovine aortic endothelial cells (BAECs).	Strain sensor
		Ye <i>et al.</i> ^[148]	PEDOT:PSS	PEDOT:PSS in PVA+PAAM+MWCNTs-COOH cross-linked with borax	-	-	2.00x10 ³	-	Flexible electronics
	π -stacking and electrostatic interaction	Cao <i>et al.</i> ^[149]	PEDOT:PSS	PEDOT:PSS in physical PNIPAM/boron nitride nanosheets NPs hydrogel	-	-	-	-	Skin electronics, photo thermal therapy
Chemical hydrogel	Cross-linking of matrix after CP incorporation	Wang <i>et al.</i> ^[135]	PEDOT:sulfated lignin	PEDOT:SL in cross-linked PAA	-	-	-	Skin healing assay on rat skin. Cytotoxicity on mouse fibroblast cells (NIH/3T3)	Biosensors, strain sensors
		Spencer <i>et al.</i> ^[150]	PEDOT:PSS	PEDOT:PSS in photo cross-linked GelMa	-	-	-	Cytotoxicity and proliferation of C2C12	Recording/stimulating in vivo
		Shih <i>et al.</i> ^[151]	PEDOT:PSS	PEDOT:PSS included in PVA/PMMA hydrogel	3.1	-	500-1000	-	Supercapacitors
		Javadi <i>et al.</i> ^[152]	PEDOT:PSS	Blend PU, PEDOT:PSS and LCGO then polymerization of PU	6-12.5	-	-	Cell Culture and Differentiation of hNCS	Stretchable electronics, biosensors, drug release
		Paradee <i>et al.</i> ^[138]	PEDOT:BA (benzoic acid)	PEDOT:BA particles in alginate hydrogel	3-95	-	-	-	Drug delivery
		Molina <i>et al.</i> ^[153]	PEDOT:ClO ₄	PEDOT:ClO ₄ particles in γ PGA/cystamine hydrogel. Then addition of EDOT-OH	-	-	-	-	Biosensors
		Polat <i>et al.</i> ^[154]	PEDOT:PSS	PEDOT:PSS in GelMa	-	-	~10 ⁴	-	Bioelectronic

Chapter 1. Towards PEDOT: hyaluronic acid inks for bioelectronics

		Aggas <i>et al.</i> ^[3]	PEDOT:PSS	PEDOT:PSS in photo cross-linked poly(HEMA-co-EGMA) hydrogel	-	-	$\sim 10^5$	Attachment and differentiation of PC-12 neural progenitor cells	Tissue engineering
		Lee <i>et al.</i> ^[155]	PEDOT:PSS	PEDOT:PSS in gelatine cross-linked by genepin	$R_{\text{sheet}} = 2500 \Omega/\square$	-	-	-	Biosensors
	Polymerization of EDOT after diffusion in the hydrogel	Zamora-Sequeira <i>et al.</i> ^[137]	PEDOT:starch/k-carrageenan	Diffusion and polymerization of EDOT in starch/k-carrageenan hydrogel	$\sim 3 \times 10^{-7}$	-	$10^6 - 10^7$	Proliferation of SH-SY5Y	Recording/stimulating in vivo
		Sasaki <i>et al.</i> ^[83]	PEDOT:Ots	Polymerization of PEDOT in PU dissolved in THF, with $\text{Fe}(\text{OTs})_3$ as oxidizer.	40-120	-	-	Proliferation of NG108-15 nerve cells or C2C12 muscle cells	Biosensors, strain sensors
		Hassarati <i>et al.</i> ^[139]	PEDOT:PTS (paratoluensulfonate)	Electro-polymerization of EDOT in a PVA/gelMa/heparin matrix		52-72	30-50	Cell adhesion and proliferation of olfactory ensheathing cells (OECs)	Cell culture and differentiation
		Wang <i>et al.</i> ^[136]	PEDOT:Chitosan	Chemical polymerization of EDOT in Chitosan/gelatin gel	$3.4 \times 10^{-2} - 1.7 \times 10^{-1}$	-	-	Adhesion and proliferation of PC12 neural cells	Tissue engineering (neural)
		Xu <i>et al.</i> ^[140]	PEDOT:pTs	Chemical polymerization of EDOT + Na-pTs in CMCs (carboxymethylchitosan) gel	3.47- $5.98 \cdot 10^{-4}$	-	-	Adhesion and proliferation of PC12 neural cells	Tissue engineering (neural)
		Gong <i>et al.</i> ^[156]	PEDOT:PSS	Chemical polymerization of EDOT into a PEG/PSS hydrogel	2.49×10^{-3}	-	-	Cytotoxicity and cell alignment of C2C12 muscle cells	Tissue engineering (muscle)
		Ding <i>et al.</i> ^[144]	PEDOT:PSS	Chemical polymerization of EDOT into a PHEA-PSS hydrogel	1.2	-	-	-	3D printed materials for flexible sensors
	Double inter penetrating network	Spencer <i>et al.</i> ^[157]	PEDOT:PSS	Cross link of PEDOT:PSS with Ca^{2+} , then GelMa with UV	$10^{-3} - 10^{-2}$	-	-	Cytotoxicity and proliferation of C2C12 muscle cells, Subcutaneous implantation of hydrogels in rats	Tissue engineering (muscle)
		Wang <i>et al.</i> ^[158]	PEDOT:PSS	IPN of PEDOT:PSS+MWCNTs in alginate via electrogelation of alginic acid	-	0.5-1.2	$\sim 2.7 \times 10^5$	Proliferation of SH-SY5Y neural cells	Recording/stimulating in vivo (neurons)
		Zhang <i>et al.</i> ^[159]	PEDOT:PSS	IPN of PEDOT:PSS with PNIPAM, physically cross-linked by GO, and chemically by isoacrylamide and PNIPAM	0.08	-	-	-	Flexible electronic devices

III.3.b. Pure conductive hydrogels

To further improve the electrical properties, pure conducting hydrogels have been developed recently. In those hydrogels, PEDOT or its dopant is part of the cross-linking network forming the hydrogel matrix (Table 3). Pure conductive hydrogels are prepared using the same approaches as described above (Figure 21), except that there are no additional materials to form the hydrogel matrix. In this case, the red part in Figure 21 represent PEDOT dopant (Figure 22). Three major cross-linking strategies are implemented:

1. **Physical or chemical cross-linking of PEDOT:dopant from the dopant chains** (Figure 22a). For instance, Del Agua *et al.*^[160] developed PEDOT:PSS free standing films via PSS cross-linking using divinylsulfone as the cross-linker (Figure 23a), with a conductivity reaching 600 S/cm. As another example, Xu *et al.*^[161] synthesized a PEDOT:PSS hydrogel using PEG-peptide as a physical cross-linker for aqueous PEDOT:PSS dispersion (Figure 23b). Finally, Xu *et al.*^[162] designed a self-healing physical hydrogel (Figure 23c), doping PEDOT with sulfated alginate functionalized with adamantanes groups that form host-guest complexes with poly- β -cyclodextrin. This hydrogel exhibited a conductivity up to 0.16 S/cm in a wet state, in addition to high biocompatibility. As the cross-linking was non-covalent, the resulting hydrogel displayed self-healing behaviour and injectability.
2. **Chemical cross-linking of PEDOT:dopant from the PEDOT chains** (Figure 22b), using functionalised EDOT monomers such as carboxyl-EDOT^[80,163] or EDOT-sulfate^[164], that serve as cross-linking points. Mantione *et al.*^[80] reported a conductivity up to 375 S/cm (after a secondary doping with ethylene glycol) using carboxyl-EDOT to cross-link PEDOT:PSS with ethylene glycol (Figure 23d).
3. **Modification of PEDOT:dopant microstructure**, resulting in enhanced inter-PEDOT chain interactions (via π -stacking and hydrophobic interactions), or chains entanglement (Figure 22c). For instance, Yao *et al.*^[165] showed that pure PEDOT/PSS hydrogels can be prepared by adding concentrated sulfuric acid into PEDOT:PSS aqueous solution followed by thermal treatment. This was attributed to the expansion of PEDOT coils, increasing their crystallinity, followed by partial PSS removal. Additionally, using PEDOT:PSS chain entanglements via freeze-drying of commercial PEDOT:PSS and controlled rehydration in various solvent, Yuk *et al.*^[118] and Lu *et al.*^[166] reported pure PEDOT:PSS hydrogels with high conductivity, around 200 S/cm when dry, and around 40 S/cm when hydrated.

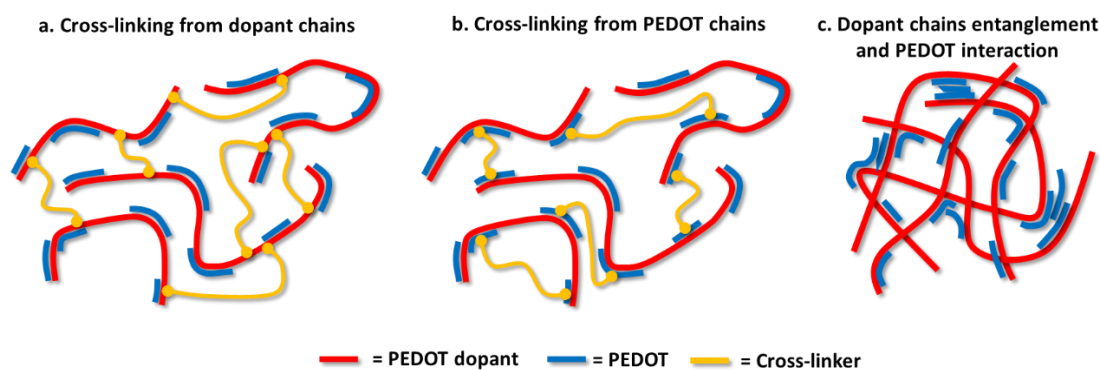


Figure 22. Various cross-linking strategies to form pure conductive hydrogels.

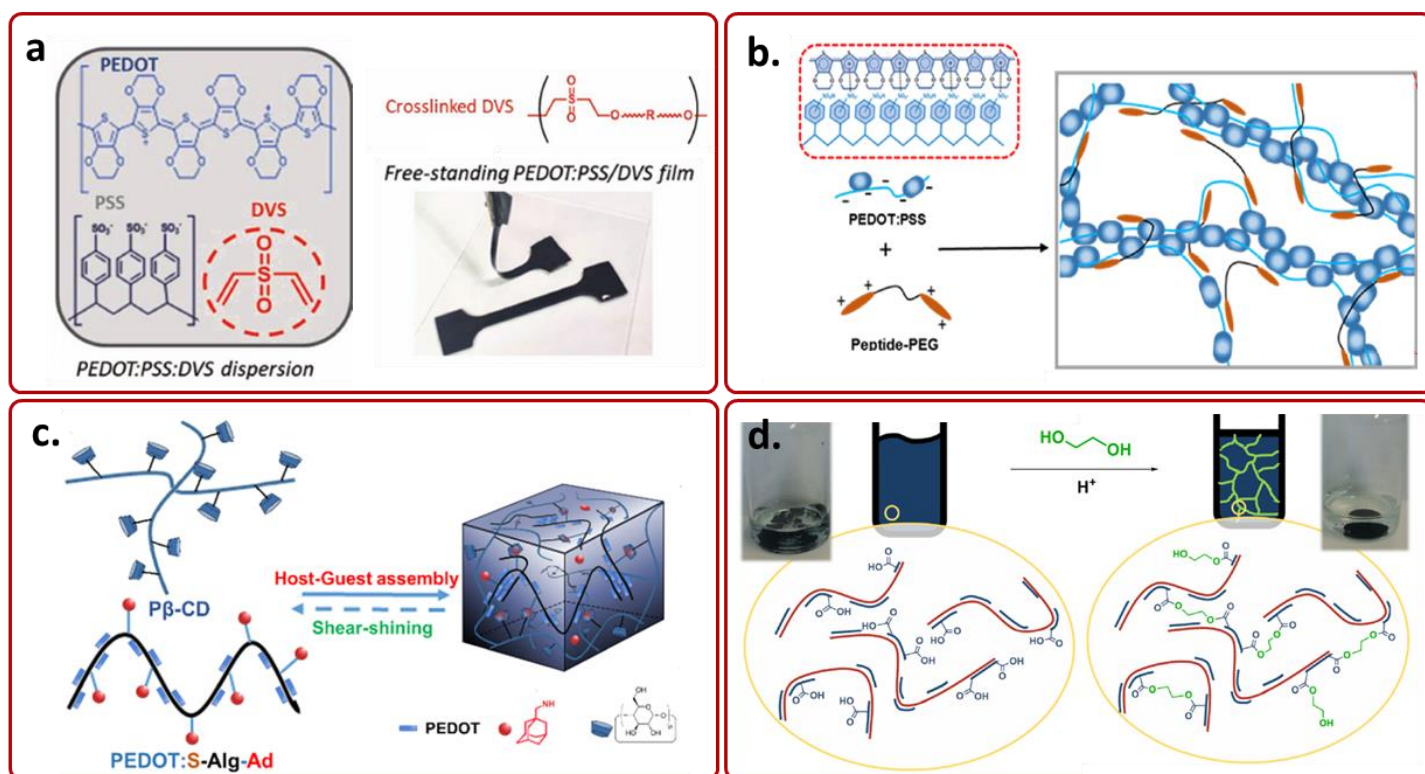


Figure 23. Various PEDOT-based pure conductive hydrogels, relying on different gelation strategies. a) Cross-linking of PSS using divinylsulfone, adapted from del Agua et al.^[160]. b) Electrostatic interaction between peptide-functionalised PEG and PSS, adapted from Xu et al.^[161]. c) Host-guest reversible assembly between poly-β-cyclodextrine and PEDOT:sulfated Alginate-adamantane, adapted from Xu et al.^[162]. d) Cross-linking of carboxyl-PEDOT:PSS with ethylene glycol, adapted from Manton et al.^[80].

Pure conductive hydrogels exhibit the highest conductivities, from 10^1 S/cm to 10^3 S/cm. Among them, the most conductive hydrogels are those relying on chain entanglements of PEDOT:PSS chains, or on covalent cross-linking of PSS chains (Table 3). Pure conductive hydrogels are more conductive than IPN conductive hydrogels (Table 2). This suggests that in the design of a conductive hydrogel, every component that is not conductive may act as an insulator, decreasing the conductivity of the final material.

Chapter 1. Towards PEDOT: hyaluronic acid inks for bioelectronics

Table 3. Pure conductive hydrogels.

Hydrogel type		Reference	PEDOT:dopant	Strategy to obtain hydrogel	σ (S/cm)	CSC (mC/cm ²)	Impedance (Ω) at 1 kHz	Biocompatibility	Suggested applications
Physical hydrogel	Electrostatic interactions	Xu <i>et al.</i> ^[161]	PEDOT:PSS	Physical cross-linking between PEG-peptide and PSS	8.0×10^{-3} – 1.6×10^{-2}	-	$2-9 \times 10^2$	Proliferation of MSCs	Tissue engineering
		Feig <i>et al.</i> ^[167]	PEDOT:PSS	Electrogelation of PEDOT:PSS with high metal dication concentration	-	-	-	-	PEDOT:PSS patterning
		Yang <i>et al.</i> ^[168]	PEDOT:PSS + PANI	Electrostatic gelation of PEDOT:PSS with PANI:phytic acid	12.25 (dry) 6.13×10^{-1} (wet)	-	-	-	Supercapacitors
		Xu <i>et al.</i> ^[169]	PEDOT:PSS or PEDOT:heparin	Reversible covalent bonds HA-aldehyde/glycol-chitosan + electrostatic interaction heparine or PSS / glycol-chitosan	$\sim 3.0 \times 10^{-2}$	-	80-100	Cell proliferation and differentiation of C2C12 +in-vivo implantation and study of degradation and encapsulation	Tissue engineering (muscle)
	π -stacking and hydrophobic interactions	Xu <i>et al.</i> ^[162]	PEDOT:alginate-sulfate-adamantane	Host-guest interaction between PEDOT:Alg-S-Ad and P β -CD	4×10^{-2} – 1.6×10^{-1}	-	100-500	Cell proliferation of C2C12 (muscle cells)	Injectable hydrogels, tissue–electrode interface
		Yao <i>et al.</i> ^[165]	PEDOT:PSS	Clevios PH1000 in 0,1 mol/L H ₂ SO ₄ at 90°C for 3h	0.4-8.8	-	-	-	Supercapacitors
		Novikov <i>et al.</i> ^[170]	PEDOT:PSS	Gelation of PEDOT:PSS with sulfuric acid, then filling with PDMS	6×10^{-3}	20	<100	-	Bioelectronic devices
	π -stacking and electrostatic interactions	Zhang <i>et al.</i> ^[171]	PEDOT:PSS	Gelation when [DBSA] >3 vv%	~ 0.1	-	-	Cytotoxicity and proliferation of C2C12 (muscle cells)	Injectable conductive hydrogel
		Teo <i>et al.</i> ^[84]	PEDOT:PSS/IL	Mix of micro droplets of PEDOT:PSS and ionic liquid	9×10	-	-	-	Advanced bioelectronics process
		Puiggali-Jou <i>et al.</i> ^[172]	PEDOT:alginate	Blend PEDOT:PSS with alginate, then cross-link with CaCl ₂ , elimination of PSS	-	-	-	Cell adhesion and proliferation of Hff and MG-63 fibroblasts	Drug delivery
	Chain entanglements	Lu <i>et al.</i> ^[166]	PEDOT:PSS	Control annealing of PEDOT:PSS +DMSO solution, then rehydration in water	20-40	60	-	-	Bioelectronic devices
		Yuk <i>et al.</i> ^[118]	PEDOT:PSS	Freeze dry of PEDOT:PSS then controlled rehydration in water:DMSO 85:15 v:v	~ 200 (dry) ~ 30 (wet)	-	50-150	In vivo electrophysiology on mice	3D printable flexible electronics
		Maeda <i>et al.</i> ^[173]	PEDOT:PSS	PEDOT:PSS organogel in EtOH, drying, then filling with water	9 (wet) 346 (dry)	-	-	-	Bioelectronic devices
		Peng <i>et al.</i> ^[174]	PEDOT:PVA	Polymerization of EDOT with PVA, then forming PVA hydrogel by successive freeze/thaw cycles. Solidify with PAA/glycerol	9.5×10^{-3}	-	-	-	Bioelectronic devices

Hydrogel type		Reference	PEDOT:dopant	Strategy to obtain hydrogel	σ (S/cm)	CSC (mC/cm ²)	Impedance (Ω) at 1 kHz	Biocompatibility	Suggested applications
Chemical hydrogel	EDOT derivatives, cross-linking from PEDOT	Mantione <i>et al.</i> ^[80]	EDOT-COOH:PSS	Cross-linking between carboxyl-EDOT and EG	375	-		-	Bioelectronics devices
		Xu <i>et al.</i> ^[164]	PEDOT-S/PEDOT	EDOT-sulfate micelles polymerization with EDOT to give PEDOT-S/PEDOT hydrogel	3.8×10^{-2} (wet) 1.2×10^{-1} (wet)	-		-	Dye waste removal, energy storage
		Mawad <i>et al.</i> ^[163]	EDOT-COOH	PEDOT-COOH cross-linked with 1,1'-carbonyldiimidazole	10^{-6} - 10^{-3}	-		Cytotoxicity on L929 fibroblast cells. Cell proliferation of C2C12	Tissue engineering (muscle)
	Cross-linking from PSS or dopant	Heo <i>et al.</i> ^[175]	PEDOT:PSS	Photo polymerization of PEDOT:PSS + EG + PEGDA	$968.0 \pm 245.1 \Omega/\text{sq}$	-		Cytotoxicity on DRG cell	Recording/stimulating in vivo, Tissue engineering (neurons)
		Del Agua <i>et al.</i> ^[160]	PEDOT:PSS	PEDOT:PSS cross-linked by divinylsulfone	400-800	-	~30000	-	Wearable electronic clothing
		Solazzo <i>et al.</i> ^[176]	PEDOT:PSS	PEDOT:PSS cross-linked by PEG-bisepoxy	706 ± 32 (EIS fit) 522 ± 48 (4 probe)	-	100-300	Cytotoxicity and proliferation of C3H10 fibroblasts	Flexible electronic
		Kim <i>et al.</i> ^[177]	PEDOT:PSS	Chemical polymerization of EDOT into a PEG/PSS hydrogel +acidic treatment	$10^{-4} - 10^{-1}$	--		Cytotoxicity and proliferation of H9C2 myocytes	Tissue engineering (muscle)
		Inal <i>et al.</i> ^[66]	PEDOT:PSS	PEDOT:PSS + collagen + DBSA + 3-glycidoxypopyltrimethoxysilane, then freeze drying	-	-	~200-300	Cell adhesion and growth of TIF and MDCK II epithelial cells	3D cell-laden structures
		Yang <i>et al.</i> ^[143]	PEDOT:alginate	Simultaneous polymerization of PEDOT with alginate and alginate cross-linking by dihydrazide adipic acid	$1.4-6.1 \times 10^{-2}$	-	-	Cell adhesion and proliferation of brown adipose-derived stem cells (BADSCs)	Cell culture

To the extent of our knowledge, publications reporting the charge storage capacity of the designed conductive hydrogel are scarce, mostly because it is not a property of interest for the proposed applications. However reported CSC are promising: Yuk *et al.*^[118] reported a CSC of 60 mC/cm² for 3D-printable pure PEDOT: PSS hydrogel. Hassarati *et al.*^[139] electro-polymerized PEDOT in a PVA/GelMa/heparin hydrogel on an ITO electrode leading to a film with a CSC up to 72 mC/cm². Finally, Wang *et al.*^[158] reported the synthesis of an alginate hydrogel including PEDOT:PSS and multi wall carbon nanotubes, with a CSC of 1.2 mC/cm². All those values were at least of the same order of magnitude than simple PEDOT:PSS electro-polymerized on ITO glass (3.6 mC/cm² ^[120]), and were competitive compared to platinum electrodes (0.550 mC/cm² ^[116]).

III.4. Biocompatibility and applications of conductive hydrogels

III.4.a. Biocompatibility

Cytotoxicity assays with conductive hydrogels have been performed on different cell lines depending on the targeted tissues. Conductive hydrogels intended for intracranial stimulation or recording have been tested on NG108-15^[83], SH-SY5Y^[137,158], PC12^[136] or DRG^[175] cell lines, which are all precursors of nervous system cells. L929 Fibroblasts, C2C12 muscle cells and rat H9C2 myocyte precursors^[177] have been also commonly used for cytotoxicity and proliferation assays for devices dedicated to tissue engineering^[162,163,169,171], 3D cell-culture^[156,157] and biosensors^[83]. Pluripotent cells have also been used, such as mesenchymal stromal cells (MSCs)^[161] or C3H10 cells^[176]. All the aforementioned conductive PEDOT hydrogels exhibited good cytocompatibility with the targeted cells, and could promote cell adhesion, differentiation, and directional growth for instance^[161] (Table 2, Table 3).

III.4.b. strain sensors

Conductive hydrogels whose electrical properties depend on applied mechanical constraints can be used as mechanical sensors for electronic-on-skin devices. For instance, Wang *et al.*^[135] designed an IPN conductive hydrogel blending particles of PEDOT doped by sulfated lignin into a polyacrylamide hydrogel. The resulting hydrogel could be stretched up to 1400 % its initial length before breaking, with a linear evolution of resistivity. The authors

designed demonstrators where this hydrogel stuck on the skin could enable to monitor movements, especially of vocal cords (Figure 24).

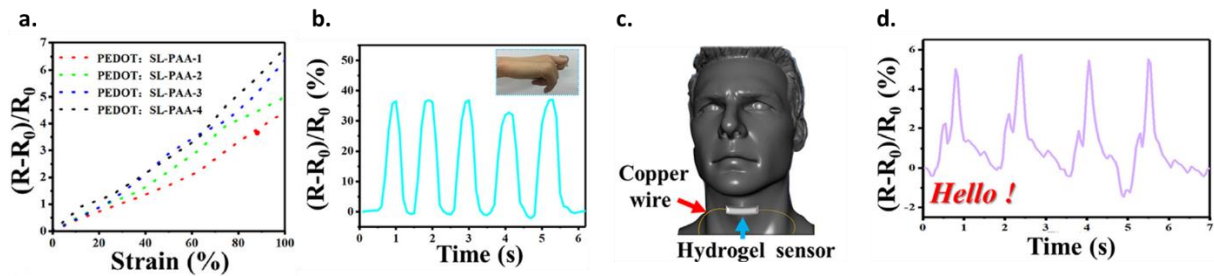


Figure 24. Strain sensors based on PEDOT conductive hydrogels. a. Relative electrical resistance changes of the hydrogel as a function of applied strain. b. Resistance change of the hydrogel sensor in response finger bending. c. Schematic for throat sensing. d. Resistance change in response to sounding of "Hello!" Adapted from Wang et al.^[135].

III.4.c. In-vivo stimulation/recording

The main application for PEDOT-based conductive hydrogels is their use for *in-vivo* stimulation or monitoring of living tissues. Few reported studies have pushed the development of their conductive hydrogels to *in-vivo* testing on animals.

Among others Yuk *et al.*^[118] processed commercial PEDOT:PSS with successive drying/rehydration cycles in water:DMSO mixture to obtain a pure PEDOT:PSS hydrogel resulting from chain entanglement, with high conductivity, up to 30 S/cm when wet. This conductive hydrogel could be 3D-printed on a soft PDMS membrane to form a recording electrode (Figure 25a), then implanted on a mice brain (Figure 25b) to monitor its neuronal action potentials (Figure 25c).

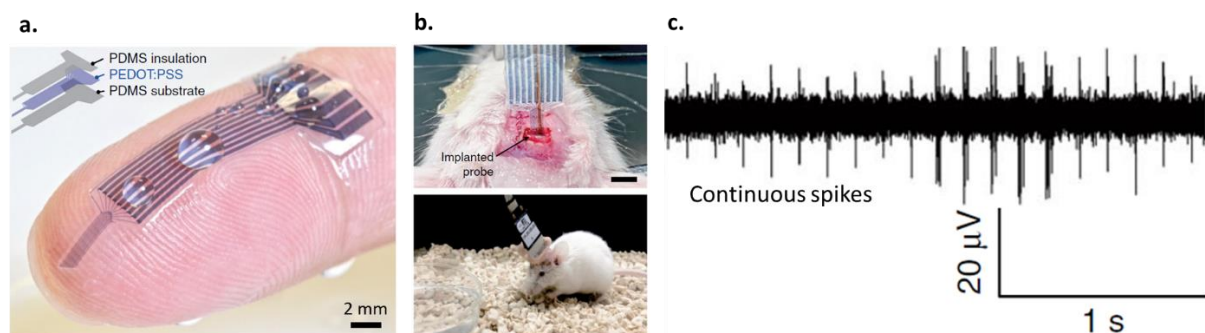


Figure 25. a. Image of the 3D-printed soft neural probe. b. Images of the implanted 3D-printed soft neural probe (top) and a freely moving mouse with the implanted probe (bottom). c. Continuous extracellular action potential traces (300 to 40 kHz) recorded under freely moving conditions Adapted from Yuk et al.^[118].

Even though this reported hydrogel displayed outstanding conductivity, low impedance, great processability, and biocompatibility, no long-term implantation study was performed. Thus, no long-term cytotoxicity data were recorded. Besides, as this hydrogels was made of pure PEDOT:PSS, it was not degradable.

III.5. Degradability

Some of the described conductive hydrogels were degradable, namely they could be decomposed into smaller constituent pieces in physiological or biologically benign conditions, resulting from structural bond cleavage. For clarity, we will use the term **degradation** when structural bond cleavage is done by spontaneous hydrolysis, and **biodegradation** when biological phenomena are involved in the bond cleaving process (enzymatic hydrolysis or oxidation due to reactive oxygen or nitrogen species (ROS and RNS) generated by macrophages^[178,179]).

Designing performing conductive soft materials with degradability of a few months is a key challenge to develop **transient implantable medical devices**. Such devices could open the way to innovative tissue monitoring and could reduce the medical costs and risks of infection as removal surgery would be avoidable. A *sine qua non* condition is the non-cytotoxicity of the (bio)degradation residues, and the possibility for the body to dispose of them through processes like phagocytosis, metabolization, or bioabsorption.

Regarding PEDOT, its degradation entails the breaking of the conjugated backbone. This is hardly achievable in physiological conditions. Therefore, PEDOT is not (bio)degradable in physiological conditions, as most of conductive polymers used in bioelectronics. Numerous studies previously cited in this manuscript have investigated its biocompatibility, but to the best of our knowledge, none of them investigated its long-term cytotoxicity, nor the biological process to assimilate it. Apparently, PEDOT is not degraded or metabolized, but encapsulated by scar tissues, diminishing the quality of the stimulation process^[180].

Therefore, for PEDOT:dopant conductive ink, only the dopant can be potentially degraded. We will speak of **ink disintegration**. Besides, hereafter, the degradation of a

conductive hydrogel refers to the (bio)degradation of the hydrogel matrix and to the disintegration of the PEDOT:dopant conductive part.

To be potentially cleaved into smaller constituents in physiological benign conditions, both PEDOT dopant and the hydrogel matrix should include covalent functions which can be hydrolyzed such as ester, amide, thioester, imine, imide, anhydride, carbonate, urethane and urea functions. Henceforth many conductive PEDOT-based hydrogels matrix intended to be degradable are composed of polymer which backbones include such functions, such as poly(caprolactone)^[131], poly(vinyl alcohol)^[93,181,182], polylactic-co-glycolic acid^[183], poly(methyl methacrylate)^[151], or natural polymers such as cellulose nanofibers^[184] or protein-based materials like gelatin^[136,154], silkworm silk^[139,141,185] or collagen^[66].

Regarding PEDOT dopant, PSS is used in the majority of PEDOT-based conductive hydrogels. But PSS backbone is an aliphatic chain with C-C bonds that are not cleavable in physiological conditions. Like for PEDOT, there are, to the extent of our knowledge, no report investigating long-term PSS toxicity, degradation mechanisms or body clearance mechanisms. Replacing PSS by a potentially (bio)degradable biomolecule is a widely spread strategy described in literature to increase PEDOT:dopant biocompatibility and degradability. Various biomolecules has been used to dope PEDOT in conductive hydrogels, such as alginate^[143,172], starch^[137] and chitosan^[136].

Noticeably, even though those molecules are potentially degradable, no degradation studies have been implemented.

To the best of our knowledge, few degradation studies have been led on chemical PEDOT conductive hydrogels:

- Spencer *et al.*^[157] designed a PEDOT:PSS IPN hydrogel, first cross-linking PEDOT:PSS with Ca²⁺, then penetrating the matrix with GelMa, and finally, photo cross-linking GelMa to obtain the intricate conductive material. They implanted the hydrogel in Wistar rats and measured its mass loss after explanting it from animals after several weeks of treatment: GelMa/PEDOT:PSS hydrogel exhibited a 69.62 ± 11.4% mass loss in 28 days.

- Bhattarcharjee *et al.*^[145] reported the development of an electro-conductive silk fibroin/PEDOT: PSS composite cross-linked by PVA. They investigated its enzymatic biodegradation by proteinase K in PBS at 37°C by measuring the progressive mass loss. They evidenced a biodegradation of 40 to 60 % in 21 days depending on the mass fraction of PEDOT:PSS in the matrix (from 0.1 to 0.3 %).
- Xu *et al.*^[169] reported the degradation study of a conductive hydrogel composed of a hybrid network of reversible covalent bonds between HA-aldehyde and glycol-chitosan, and electrostatic interactions between PSS or heparin and glycol-chitosan. Incubation of the conductive material with lysozymes and hyaluronidase able to degrade chitosan and HA, respectively, resulted in a 20% biodegradation of the hydrogel in 21 days.

Noticeably in all those publications, no cytotoxicity assays were performed on degradation products. No information was brought about the potential cytotoxicity of the degradation products of PEDOT or PSS.

IV. Focus on PEDOT:biomolecules inks

IV.1. PEDOT:biomolecule inks

Even though PSS is acknowledged to be cytocompatible^[186], it still remains an artificial polymer that cannot be (bio)degraded and metabolized by the body. Furthermore, to the extent of our knowledge, there is no report of long time degradation of implanted PSS in the brain, which presents a risk of release of acidic PSS. For mid-term (several months) implantation close to sensitive tissues, alternative conductive materials to PEDOT:PSS with improved clearance rates are required.

To lower the toxicity of PEDOT:dopant material regarding several cell types such as endothelial, epithelial, fibroblasts, macrophages or neural cells, a widely used strategy consists in doping the PEDOT with **biomolecules**. These biomolecules should be negatively charged as they replace PSS. Besides, the use of biomolecules add potential transient properties as they can naturally be degraded.

PEDOT:biomolecules were first synthesized electrochemically, limiting their further processing since they were stuck on the electrode surfaces. Such studies used alginate (Alg)^[187], dextran sulfate (DexS)^[53,187,188], chondroitin sulfate (ChS)^[187], heparin (Hep) and hyaluronic acid (HA)^[139,187,189–191], ulvan^[192], κ -carrageenan^[193,194] or polydopamine^[195]. All those materials displayed low conductivity below 10^{-2} S/cm.

In 2015, Wallace *et al.*^[52] were the first to report the chemical synthesis of a **PEDOT:dextran sulfate ink (PEDOT:DexS)**. PEDOT:DexS displayed a conductivity up to 19 S/cm after secondary treatments with ethylene glycol and annealing (up to 7 S/cm without additional treatments), and promoted cell growth with 25% increase compared to PEDOT:PSS. Additionally, this ink could be inkjet-printed. Over the past six years, PEDOT has been chemically polymerized with several other biomolecules to obtain new bio-inks: pectin^[196], guar^[197], desoxyribo nucleic acid (DNA)^[198,199], sulfated cellulose^[200], Hep, ChS, HA^[201,202].

The PEDOT:biomolecule conductivities have ranged from 10^{-3} to 10^{-1} S/cm (see Table 1 of Chapter 2 of this manuscript). Overall, there are still progress to do to outperform PEDOT:PSS in terms of conductivity in biological conditions. Though, PEDOT:DNA ink

developed by Tekoglu *et al.*^[198], and PEDOT:sulfated cellulose developed by Horikawa *et al.*^[200] displayed promising conductivities close to that of PEDOT:PSS in physiological conditions. But these studies did not investigate their cytotoxicity, and their biological properties still remained unknown.

However, for studies in which biological properties were investigated, all PEDOT:biomolecule inks exhibited equal or better cytocompatibility than PEDOT:PSS. L929 neural cells growth on PEDOT:DexS was slightly improved compared to PEDOT:PSS^[52]. PEDOT: biomolecule synthesized by Mantione *et al.*^[201] (with Hep, ChS and HA) exhibited equal cytocompatibility when incubated with L929 neural cells than PEDOT:PSS.

In addition to biocompatibility, the dopant can be bioactive, enhancing the range of possibilities for the conductive ink. Bioactivity here refers to cell adhesion enhancement, promotion of cell growth, or natural antibacterial properties. Therefore Harman *et al.*^[52] chose DexS as PEDOT dopant since this molecule was acknowledged to display anticoagulant properties, and demonstrated an increased cell growth and adhesion of PC12^[203] and skeletal muscle myoblasts when associated with PPy^[204].

Their acknowledged biocompatibility associated with their bioactive properties led Mantione *et al.*^[201] and others to investigate a precise family of polysaccharides: glycosaminoglycans (GAGs).

IV.2. PEDOT:glycosaminoglycans (GAGs) inks

IV.2.a. Generality on GAGs and PEDOT:GAGs inks

Glycosaminoglycans are natural polysaccharides present in every mammalian tissue, consisting of repeating disaccharide units. They are negatively charged at physiological pH as they possess one carboxylic group on each diade. Chondroitin sulfate, dermatane sulfate, keratin sulfate and heparin are naturally sulfated, hyaluronic acid alone is not sulfated (Figure 26).

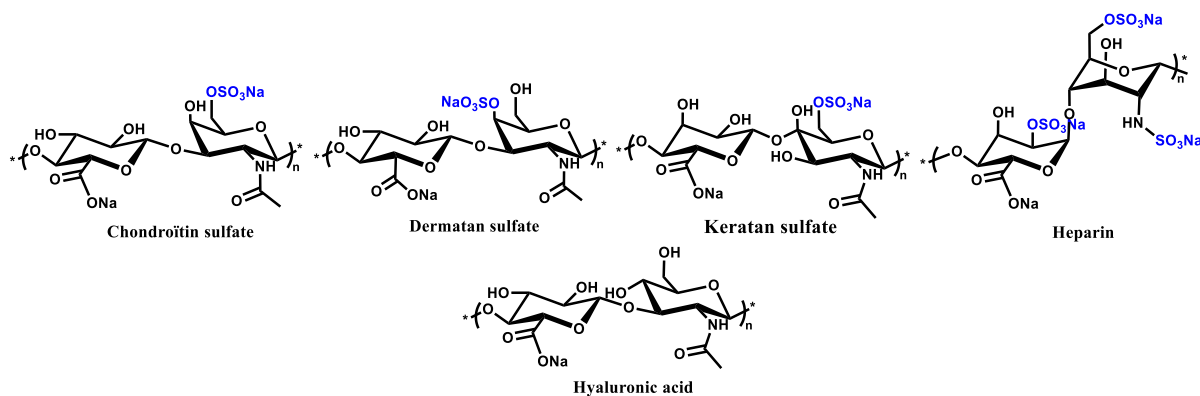


Figure 26. Structure of various glycosaminoglycans, all sulfated except hyaluronic acid.

GAGs are important components of the extracellular matrix (ECM) and play important roles in physiological conditions^[205]. They are considered as key macromolecules that affect cell properties and functions. For instance, they modulate the morphogenesis of tissues and organs^[206,207]. They can support proteins, forming proteoglycans, and regulate molecule movements and signalization in the ECM^[208]. Heparin can bind to several nerve growth factors which stimulate neuron growth and survival^[209,210]. Chondroitin sulfate is involved in neuronal plasticity as it a major component of perineural nets, and seems to protect cells against H₂O₂-induced cell death^[211].

Such physiological properties, added to their structural diversity, wide range of molecular weight and negative charges make them interesting building blocks for the design of biocompatible disintegrable PEDOT inks, with potential bioactive properties. Their utilization as PEDOT dopants could produce bioactive conductive inks with healing properties after device implantation, or could promote interactions with cortical cells.

However PEDOT:GAGs inks display low conductivity^[196,201] ($\sim 10^{-2}$ S/cm), with a poor intrinsic doping of PEDOT chains^[196], which can be a drawback for their wide use in bioelectronics. Nonetheless they proved to be more suitable for SH-SY5Y cell proliferation than PEDOT:PSS, and seemed to protect SH-SY5Y cells from H₂O₂-induced death better than PEDOT:PSS^[201].

IV.2.b. Hyaluronic acid (HA) and PEDOT:HA inks

Among other GAGs, **hyaluronic acid** is of great interest for the design of desintegrable conductive inks at the electronic/tissue interface, especially in neural engineering, as it facilitates nerve regeneration, limits scar formation around implantation sites^[212] and promote neurite outgrowth^[213]. Wang *et al.*^[202] synthesized PEDOT:HA conductive particles included in poly(lactic acid) matrix and the reported material exhibited no significant cytotoxicity, improved cell adhesion compared to pure poly(lactic acid) films, and enhanced neurite outgrowth of PC12 cells under 0.5 mA current stimulation.

HA is a natural ubiquitous polysaccharide, avoiding controversial safety issues^[214,215], and is already widely used in medicine for various applications such as ophthalmic solution^[215], intra-articular injection^[216] or dermal filler^[217]. It used to be extracted and purified from rooster combs^[218] or human umbilical cords^[219], but it is produced nowadays essentially by bacterial fermentation^[220,221], which enables a great control over produced polymer molecular weight and batch-to-batch repeatability. This is a great asset as materials obtained from the biomass often present a wide variability from one batch to another, which prevent semi-industrial production and commercialization. In addition, HA is not sulfated, which makes it a suitable building block to investigate the effect of GAG sulfatation on their capacity to efficiently dope PEDOT.

HA is composed of repeating diades of D-glucuronic acid and N-acetyl-D-glucosamine, linked via alternating β -(1 \rightarrow 4) and β -(1 \rightarrow 3) glycosidic bonds. HA has hydrophilic groups (hydroxyl, carboxyl and acetamido groups) which form intramolecular hydrogen bonds^[222], and interact with water molecules resulting in a high solubility and hydrophilicity^[223]. It also contains axial hydrophobic parts (C-H domains), which form hydrophobic domains, giving HA amphiphilic properties^[222] (Figure 27). Intramolecular interactions added to the amphiphilic character of HA confer to the polymer its rigid structure with a persistence length up to 9.0 nm^[224], and in solution a structure of double strands, or supercoils with helical portions^[225,226]. Contrary to other GAGs whose molecular sizes are mainly below 50 kg/mol, HA can reach very high molecular mass, up to 100.10⁶ g/mol^[227,228].

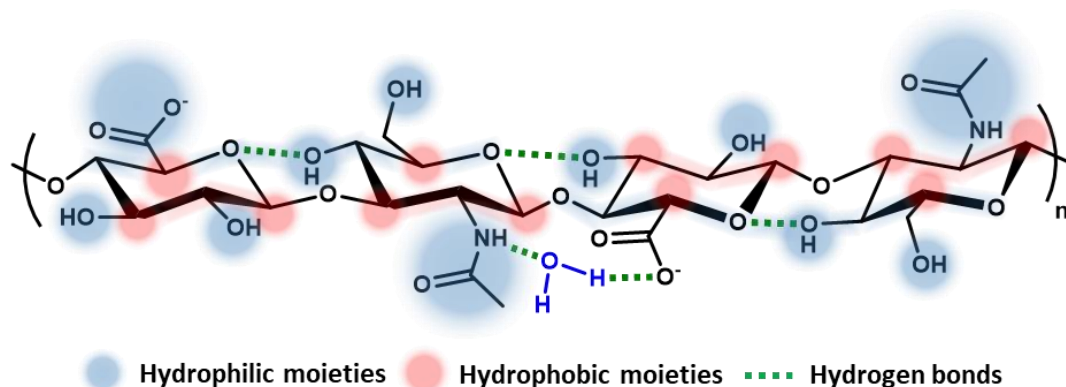


Figure 27 Hyaluronic acid structure and intramolecular interactions.

HA is quickly biodegraded in the human body: its half-life when injected in blood circulation is 20 min, 12 h in knee joints and skin, and 70 days in the vitreous body^[229]. This degradation rate can be tuned by chemical modifications: Feng *et al.*^[230] synthesized sulfated HA (HAS) derivatives with enhanced bioactive properties, with sulfatation degrees of 0.20 and 0.41, which were degraded in 7 and 14 days respectively. Chemical cross-linking is also a strategy to increase degradation time: Patterson *et al.*^[231] grafted glycidyl-methacrylate groups on HA, yielding to cross-linked HA hydrogels with a degradation time over 6-8 weeks.

To the best of our knowledge, only two publications by Mantione *et al.*^[201] and Wang *et al.*^[202] reported the synthesis of PEDOT:HA inks. None of them investigated the degradation of PEDOT:HA inks.

V. Conclusion

The chapter has reviewed the state-of-the-art on conductive polymers dedicated to bioelectronics, with a special focus on PEDOT biomolecules inks.

Numerous conductive soft materials for bioelectronics have been described in the last decade, with the co-development of different conductive polymers, their respective dopants, and the various conditions to post-treat and process them. In particular, PEDOT and the commercial PEDOT:PSS conductive inks have aroused a great interest. Over the past three years, the number of publications on PEDOT-based conductive hydrogels has significantly increased, pointing out the growing need for soft bio-friendly biotic/abiotic contact electrodes. However their lack of biocompatibility and degradability lead to the design of new conductive inks using biopolymers as dopants. Until now, inks using GAGs as PEDOT dopant have displayed low conductivity, in spite of good biocompatibility. Noticeably, to the best of our knowledge, no degradation study on PEDOT:GAG ink or hydrogel has been reported. There is a lack of long-term implantation and degradation studies in the literature.

In this Ph.D. project, the development of highly conductive PEDOT-based printed electronic tracks and contact hydrogels for tissue monitoring and stimulation was targeted. Both tracks and electrode material should be biocompatible, insoluble in water (*i.e.* cross-linked), and biodegradable (Figure 28).

HA was selected as material of choice to dope PEDOT, in order to design conductive materials for electrical contact electrode hydrogel. Its biocompatibility and biodegradability are suitable for intracranial application^[191] and it is adapted to the biotic/abiotic interface^[191,213]. To enhance the conductivity of the resulting material, HA was chemically modified to enhance its properties as a dopant, which has never been done in literature. The resulting PEDOT:HA_{modified} ink served as a building block for both the tracks and the hydrogel (Figure 28).

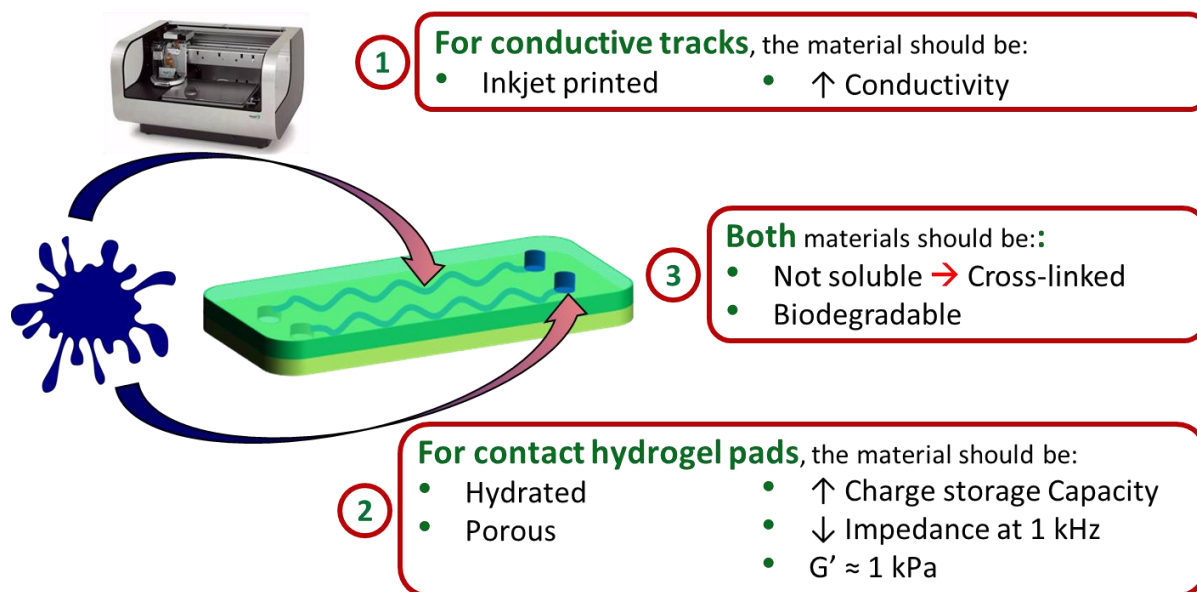


Figure 28. Conductive tracks and hydrogel will be processed from the same PEDOT:HA modified ink, and display precise specifications.

In this work, we have developed PEDOT:HA-based conductive inks and conductive hydrogels, taking benefit from the biocompatibility and biodegradability properties of HA.

The next chapter is dedicated to the chemical modification of HA to enhance its PEDOT doping properties, the study of its biodegradability, and the formulation of a jet-printing PEDOT:HA conductive ink.

VI. Bibliography

- [1] “ANR STRETCH,” can be found under <https://anr.fr/Projet-ANR-18-CE19-0018>, **n.d.**
- [2] K. Bazaka, M. Jacob, *Electronics* **2012**, *2*, 1–34.
- [3] J. R. Aggas, S. Abasi, J. F. Phipps, D. A. Podstawczyk, A. Guiseppi-Elie, *Biosensors and Bioelectronics* **2020**, *168*, 112568.
- [4] Y. Yang, H. Deng, Q. Fu, *Mater. Chem. Front.* **2020**, *4*, 3130–3152.
- [5] J. W. Salatino, K. A. Ludwig, T. D. Y. Kozai, E. K. Purcell, *Nat Biomed Eng* **2017**, *1*, 862–877.
- [6] V. R. Feig, H. Tran, Z. Bao, *ACS central science* **2018**, *4*, 337–348.
- [7] S. Wang, J. Y. Oh, J. Xu, H. Tran, Z. Bao, *Accounts of chemical research* **2018**, *51*, 1033–1045.
- [8] T. Someya, Z. Bao, G. G. Malliaras, *Nature* **2016**, *540*, 379.
- [9] J. Liu, H. Zheng, P. Poh, H.-G. Machens, A. Schilling, *IJMS* **2015**, *16*, 15997–16016.
- [10] S. Sartori, V. Chiono, C. Tonda-Turo, C. Mattu, C. Gianluca, *J. Mater. Chem. B* **2014**, *2*, 5128–5144.
- [11] Y. Liu, M. Pharr, G. A. Salvatore, *ACS nano* **2017**, *11*, 9614–9635.
- [12] N. Matsuhisa, X. Chen, Z. Bao, T. Someya, *Chemical Society Reviews* **2019**, *48*, 2946–2966.
- [13] A. Chortos, J. Liu, Z. Bao, *Nature materials* **2016**, *15*, 937.
- [14] Y. Sun, W. M. Choi, H. Jiang, Y. Y. Huang, J. A. Rogers, *nature nanotechnology* **2006**, *1*, 7.
- [15] T. C. Shyu, P. F. Damasceno, P. M. Dodd, A. Lamoureux, L. Xu, M. Shlian, M. Shtein, S. C. Glotzer, N. A. Kotov, *Nature Mater* **2015**, *14*, 785–789.
- [16] S. Xu, Y. Zhang, J. Cho, J. Lee, X. Huang, L. Jia, J. A. Fan, Y. Su, J. Su, H. Zhang, H. Cheng, B. Lu, C. Yu, C. Chuang, T. Kim, T. Song, K. Shigeta, S. Kang, C. Dagdeviren, I. Petrov, P. V. Braun, Y. Huang, U. Paik, J. A. Rogers, *Nat Commun* **2013**, *4*, 1543.
- [17] M. D. Bartlett, A. Fassler, N. Kazem, E. J. Markvicka, P. Mandal, C. Majidi, *Adv. Mater.* **2016**, *28*, 3726–3731.
- [18] S. Inal, J. Rivnay, A.-O. Suiiu, G. G. Malliaras, I. McCulloch, *Acc. Chem. Res.* **2018**, *51*, 1368–1376.
- [19] J. W. Onorato, C. K. Luscombe, *Mol. Syst. Des. Eng.* **2019**, *4*, 310–324.
- [20] R. Balint, N. J. Cassidy, S. H. Cartmell, *Acta biomaterialia* **2014**, *10*, 2341–2353.
- [21] S. Meng, M. Rouabhia, G. Shi, Z. Zhang, *J. Biomed. Mater. Res.* **2008**, *87A*, 332–344.
- [22] D.-H. Kim, S. M. Richardson-Burns, J. L. Hendricks, C. Sequera, D. C. Martin, *Adv. Funct. Mater.* **2007**, *17*, 79–86.
- [23] S. Cetiner, F. Kalaoglu, H. Karakas, A. S. Sarac, *Textile Research Journal* **2010**, *80*, 1784–1792.
- [24] S. Bousalem, C. Mangeney, M. M. Chehimi, T. Basinska, B. Miksa, S. Slomkowski, *Colloid Polym Sci* **2004**, *282*, 1301–1307.
- [25] A. Akkouch, G. Shi, Z. Zhang, M. Rouabhia, *J. Biomed. Mater. Res.* **2010**, *92A*, 221–231.
- [26] X. Zhang, S. K. Manohar, *J. Am. Chem. Soc.* **2004**, *126*, 12714–12715.
- [27] N. Ferraz, M. Strømme, B. Fellström, S. Pradhan, L. Nyholm, A. Mihranyan, *J. Biomed. Mater. Res.* **2012**, *100A*, 2128–2138.
- [28] I. S. Chronakis, S. Grapenson, A. Jakob, *Polymer* **2006**, *47*, 1597–1603.
- [29] B. Garner, A. J. Hodgson, G. G. Wallace, P. A. Underwood, *J Mater Sci Mater Med* **1999**, *10*, 19–27.
- [30] J.-W. Lee, F. Serna, J. Nickels, C. E. Schmidt, *Biomacromolecules* **2006**, *7*, 1692–1695.
- [31] S. Brahim, A. Guiseppi-Elie, *Electroanalysis* **2005**, *17*, 556–570.
- [32] L. Ghasemi-Mobarakeh, M. P. Prabhakaran, M. Morshed, M. H. Nasr-Esfahani, H. Baharvand, S. Kiani, S. S. Al-Deyab, S. Ramakrishna, *J Tissue Eng Regen Med* **2011**, *5*, e17–e35.
- [33] D. D. Zhou, X. T. Cui, A. Hines, R. J. Greenberg, in *Implantable Neural Prostheses 2* (Eds.: D. Zhou, E. Greenbaum), Springer New York, New York, NY, **2009**, pp. 217–252.
- [34] D. K. Cullen, A. R. Patel, J. F. Doorish, D. H. Smith, B. J. Pfister, *J. Neural Eng.* **2008**, *5*, 374–384.

- [35] Q.-Z. Yu, M.-M. Shi, M. Deng, M. Wang, H.-Z. Chen, *Materials Science and Engineering: B* **2008**, *150*, 70–76.
- [36] M. P. Prabhakaran, L. Ghasemi-Mobarakeh, G. Jin, S. Ramakrishna, *Journal of Bioscience and Bioengineering* **2011**, *112*, 501–507.
- [37] Y. Guo, M. Li, A. Mylonakis, J. Han, A. G. MacDiarmid, X. Chen, P. I. Lekes, Y. Wei, *Biomacromolecules* **2007**, *8*, 3025–3034.
- [38] A. Borriello, V. Guarino, L. Schiavo, M. A. Alvarez-Perez, L. Ambrosio, *J Mater Sci: Mater Med* **2011**, *22*, 1053–1062.
- [39] T. J. Rivers, T. W. Hudson, C. E. Schmidt, *Adv. Funct. Mater.* **2002**, *5*.
- [40] R. Dong, X. Zhao, B. Guo, P. X. Ma, *Biomacromolecules* **2017**, *18*, 2808–2819.
- [41] H. Cui, J. Shao, Y. Wang, P. Zhang, X. Chen, Y. Wei, *Biomacromolecules* **2013**, *14*, 1904–1912.
- [42] B. Guo, A. Finne-Wistrand, A.-C. Albertsson, *Chemistry of Materials* **2011**, *23*, 1254–1262.
- [43] Q. Wang, Q. Wang, W. Teng, *International journal of nanomedicine* **2016**, *11*, 131.
- [44] S. Kirchmeyer, K. Reuter, *Journal of Materials Chemistry* **2005**, *15*, 2077–2088.
- [45] A. Elschner, S. Kirchmeyer, W. Lovenich, U. Merker, K. Reuter, *PEDOT: Principles and Applications of an Intrinsically Conductive Polymer*, CRC Press, **2010**.
- [46] W. Zhao, L. Glavas, K. Odelius, U. Edlund, A.-C. Albertsson, *Chemistry of Materials* **2014**, *26*, 4265–4273.
- [47] A. Kros, N. A. Sommerdijk, R. J. Nolte, *Sensors and Actuators B: Chemical* **2005**, *106*, 289–295.
- [48] R. M. Miriani, M. R. Abidian, D. R. Kipke, in *2008 30th Annual International Conference of the IEEE Engineering in Medicine and Biology Society*, IEEE, Vancouver, BC, **2008**, pp. 1841–1844.
- [49] M. N. Gueye, A. Carella, J. Faure-Vincent, R. Demadrille, J.-P. Simonato, *Progress in Materials Science* **2020**, *108*, 100616.
- [50] C.-F. Chen, C. Dai, W.-Y. Chiu, *e-Polymers* **2008**, *8*, DOI 10.1515/epoly.2008.8.1.955.
- [51] E. Tomšík, I. Ivanko, J. Svoboda, I. Šeděnková, A. Zhigunov, J. Hromádková, J. Pánek, M. Lukešová, N. Velychkivska, L. Janisová, *Macromolecular Chemistry and Physics* **2020**, *221*, 2000219.
- [52] D. G. Harman, R. Gorkin III, L. Stevens, B. Thompson, K. Wagner, B. Weng, J. H. Chung, M. in het Panhuis, G. G. Wallace, *Acta biomaterialia* **2015**, *14*, 33–42.
- [53] A. R. Harris, P. J. Molino, R. M. I. Kapsa, G. M. Clark, A. G. Paolini, G. G. Wallace, *Synthetic Metals* **2016**, *220*, 394–401.
- [54] H. J. Ahonen, J. Lukkari, J. Kankare, *Macromolecules* **2000**, *33*, 6787–6793.
- [55] E. E. Havinga, C. M. J. Mutsaers, L. W. Jenneskens, *Chem. Mater.* **1996**, *8*, 769–776.
- [56] J. L. Bredas, G. B. Street, *Accounts of Chemical Research* **1985**, *18*, 309–315.
- [57] W. A. Muñoz, X. Crispin, M. Fahlman, I. V. Zozoulenko, *Macromolecular Rapid Communications* **2018**, *39*, 1700533.
- [58] I. Zozoulenko, A. Singh, S. K. Singh, V. Gueskine, X. Crispin, M. Berggren, *ACS Applied Polymer Materials* **2019**, *1*, 83–94.
- [59] O. L. Gribkova, O. D. Iakobson, A. A. Nekrasov, V. A. Cabanova, V. A. Tverskoy, A. R. Tameev, A. V. Vannikov, *Electrochimica Acta* **2016**, *222*, 409–420.
- [60] O. L. Gribkova, O. D. Iakobson, A. A. Nekrasov, V. A. Cabanova, V. A. Tverskoy, A. V. Vannikov, *Journal of Solid State Electrochemistry* **2016**, *20*, 2991–3001.
- [61] O. L. Gribkova, N. E. Mitina, A. A. Nekrasov, V. F. Ivanov, V. A. Tverskoi, A. R. Tameev, A. V. Vannikov, *Protection of Metals and Physical Chemistry of Surfaces* **2015**, *51*, 390–395.
- [62] Z. Yi, Y. Zhao, P. Li, K. Ho, N. Blozowski, G. Walker, S. Jaffer, J. Tjong, M. Sain, Z. Lu, *Applied Surface Science* **2018**, *448*, 583–588.
- [63] S. Kim, S. Y. Kim, M. H. Chung, J. Kim, J. H. Kim, *J. Mater. Chem. C* **2015**, *3*, 5859–5868.
- [64] A. Cho, S. Kim, S. Kim, W. Cho, C. Park, F. S. Kim, J. H. Kim, *J. Polym. Sci. Part B: Polym. Phys.* **2016**, *54*, 1530–1536.
- [65] J. Ouyang, Q. Xu, C.-W. Chu, Y. Yang, G. Li, J. Shinar, *Polymer* **2004**, *45*, 8443–8450.
- [66] S. Inal, A. Hama, M. Ferro, C. Pitsalidis, J. Oziat, D. Iandolo, A.-M. Pappa, M. Hadida, M. Huerta, D. Marchat, P. Mailley, R. M. Owens, *Advanced Biosystems* **2017**, *1*, 1700052.

- [67] H. Shi, C. Liu, Q. Jiang, J. Xu, *Advanced Electronic Materials* **2015**, *1*, 1500017.
- [68] W. W. Chiu, J. Travaš-Sejdić, R. P. Cooney, G. A. Bowmaker, *Journal of Raman Spectroscopy* **2006**, *37*, 1354–1361.
- [69] A. M. Nardes, M. Kemerink, R. A. Janssen, J. A. Bastiaansen, N. M. Kiggen, B. M. Langeveld, A. J. Van Breemen, M. M. De Kok, *Advanced Materials* **2007**, *19*, 1196–1200.
- [70] R. Noriega, J. Rivnay, K. Vandewal, F. P. V. Koch, N. Stingelin, P. Smith, M. F. Toney, A. Salleo, *Nature Mater* **2013**, *12*, 1038–1044.
- [71] N. F. Mott, *Philosophical Magazine* **1969**, *19*, 835–852.
- [72] N. Tessler, Y. Preezant, N. Rappaport, Y. Roichman, *Adv. Mater.* **2009**, *21*, 2741–2761.
- [73] P. Sheng, *Phys. Rev. B* **1980**, *21*, 2180–2195.
- [74] L. Zuppiroli, M. N. Bussac, S. Paschen, O. Chauvet, L. Forro, *Phys. Rev. B* **1994**, *50*, 5196–5203.
- [75] W. W. Chiu, J. Travaš-Sejdić, R. P. Cooney, G. A. Bowmaker, *Synthetic Metals* **2005**, *155*, 80–88.
- [76] J. Hao, Z. Piao, J. Yao, Z. Hao, *ChemPlusChem* **2015**, *80*, 1513–1516.
- [77] L. V. Kayser, D. J. Lipomi, *Advanced Materials* **2019**, *31*, 1806133.
- [78] D. Mantione, I. del Agua, A. Sanchez-Sanchez, D. Mecerreyes, *Polymers* **2017**, *9*, 354.
- [79] A. Glasser, É. Cloutet, G. Hadziioannou, H. Kellay, *Chemistry of Materials* **2019**, *31*, 6936–6944.
- [80] D. Mantione, A. V. Marquez, F. Cruciani, C. Brochon, E. Cloutet, G. Hadziioannou, *ACS Macro Lett.* **2019**, *8*, 285–288.
- [81] C. A. Mire, A. Agrawal, G. G. Wallace, P. Calvert, M. in het Panhuis, *Journal of Materials Chemistry* **2011**, *21*, 2671.
- [82] U. Lang, E. Müller, N. Naujoks, J. Dual, *Adv. Funct. Mater.* **2009**, *19*, 1215–1220.
- [83] M. Sasaki, B. C. Karikkineth, K. Nagamine, H. Kaji, K. Torimitsu, M. Nishizawa, *Advanced healthcare materials* **2014**, *3*, 1919–1927.
- [84] M. Y. Teo, N. RaviChandran, N. Kim, S. Kee, L. Stuart, K. C. Aw, J. Stringer, *ACS Applied Materials & Interfaces* **2019**, *11*, 37069–37076.
- [85] M. Kiristi, A. U. Oksuz, L. Oksuz, S. Ulusoy, *Materials Science and Engineering: C* **2013**, *33*, 3845–3850.
- [86] J. Oziat, Electrode 3D de PEDOT: PSS Pour La Détection de Métabolites Électrochimiquement Actifs de Pseudomonas Aeruginosa, PhD Thesis, Lyon, **2016**.
- [87] T. Takano, H. Masunaga, A. Fujiwara, H. Okuzaki, T. Sasaki, *Macromolecules* **2012**, *45*, 3859–3865.
- [88] U. Lang, N. Naujoks, J. Dual, *Synthetic Metals* **2009**, *159*, 473–479.
- [89] T. A. Kung, N. B. Langhals, D. C. Martin, P. J. Johnson, P. S. Cederna, M. G. Urbanchek, *Plastic and Reconstructive Surgery* **2014**, *133*, 1380–1394.
- [90] K. Feron, R. Lim, C. Sherwood, A. Keynes, A. Brichta, P. Dastoor, *IJMS* **2018**, *19*, 2382.
- [91] J.-S. Noh, *Polymers* **2016**, *8*, 123.
- [92] Z. Wang, T. Wang, M. Zhuang, H. Xu, *ACS Appl. Mater. Interfaces* **2019**, *11*, 45301–45309.
- [93] Q. Gao, M. Wang, X. Kang, C. Zhu, M. Ge, *Composites Communications* **2020**, *17*, 134–140.
- [94] C. M. Proctor, I. Uguz, A. Slezia, V. Curto, S. Inal, A. Williamson, G. G. Malliaras, *Advanced Biosystems* **2019**, *3*, 1800270.
- [95] J. E. Collazos-Castro, C. García-Rama, A. Alves-Sampaio, *Acta Biomaterialia* **2016**, *35*, 42–56.
- [96] S. Park, Y. J. Kang, S. Majd, *Advanced Materials* **2015**, *27*, 7583–7619.
- [97] M. Talikowska, X. Fu, G. Lisak, *Biosensors and Bioelectronics* **2019**, *135*, 50–63.
- [98] L. D. Garma, L. M. Ferrari, P. Scognamiglio, F. Greco, F. Santoro, *Lab Chip* **2019**, *19*, 3776–3786.
- [99] G. D. Spyropoulos, J. Savarin, E. F. Gomez, D. T. Simon, M. Berggren, J. N. Gelinas, E. Stavrinidou, D. Khodagholy, *Advanced Materials Technologies* **2019**, 1900652.
- [100] K. A. Ludwig, N. B. Langhals, M. D. Joseph, S. M. Richardson-Burns, J. L. Hendricks, D. R. Kipke, *J. Neural Eng.* **2011**, *8*, 014001.
- [101] H. Yuk, B. Lu, X. Zhao, *Chemical Society Reviews* **2019**, *48*, 1642–1667.
- [102] K. D. Wise, *IEEE Eng. Med. Biol. Mag.* **2005**, *24*, 22–29.

- [103] P. K. Campbell, K. E. Jones, R. J. Huber, K. W. Horch, R. A. Normann, *IEEE Trans. Biomed. Eng.* **1991**, 38, 758–768.
- [104] M. S. Okun, *N Engl J Med* **2012**, 367, 1529–1538.
- [105] J.-W. Jeong, G. Shin, S. I. Park, K. J. Yu, L. Xu, J. A. Rogers, *Neuron* **2015**, 86, 175–186.
- [106] T. D. Y. Kozai, A. S. Jaquins-Gerstl, A. L. Vazquez, A. C. Michael, X. T. Cui, *ACS Chem. Neurosci.* **2015**, 6, 48–67.
- [107] J. Rivnay, H. Wang, L. Fenno, K. Deisseroth, G. G. Malliaras, *Sci. Adv.* **2017**, 3, e1601649.
- [108] S. P. Lacour, G. Courtine, J. Guck, *Nat Rev Mater* **2016**, 1, 16063.
- [109] K. C. Spencer, J. C. Sy, K. B. Ramadi, A. M. Graybiel, R. Langer, M. J. Cima, *Sci Rep* **2017**, 7, 1952.
- [110] Y. Lu, D. Wang, T. Li, X. Zhao, Y. Cao, H. Yang, Y. Y. Duan, *Biomaterials* **2009**, 30, 4143–4151.
- [111] L. Rao, H. Zhou, T. Li, C. Li, Y. Y. Duan, *Acta Biomaterialia* **2012**, 8, 2233–2242.
- [112] E. K. Purcell, J. P. Seymour, S. Yandamuri, D. R. Kipke, *J. Neural Eng.* **2009**, 6, 026005.
- [113] L. M. Y. Yu, N. D. Leipzig, M. S. Shoichet, *Materials Today* **2008**, 11, 36–43.
- [114] N. A. Alba, R. J. Scabassi, M. Sun, X. T. Cui, *IEEE Trans. Neural Syst. Rehabil. Eng.* **2010**, 18, 415–423.
- [115] H. McCann, G. Pisano, L. Beltrachini, *Brain Topography* **2019**, 32, 825–858.
- [116] S. F. Cogan, *Annu. Rev. Biomed. Eng.* **2008**, 10, 275–309.
- [117] L. Masaro, X. X. Zhu, *Progress in Polymer Science* **1999**, 24, 731–775.
- [118] H. Yuk, B. Lu, S. Lin, K. Qu, J. Xu, J. Luo, X. Zhao, *Nat Commun* **2020**, 11, 1604.
- [119] E. M. Hudak, D. W. Kumsa, H. B. Martin, J. T. Mortimer, *J. Neural Eng.* **2017**, 14, 046012.
- [120] T. Nyberg, A. Shimada, K. Torimitsu, *Journal of Neuroscience Methods* **2007**, 160, 16–25.
- [121] N. Torres-Martinez, C. Cretallaz, D. Ratel, P. Mailley, C. Gaude, T. Costecalde, C. Hebert, P. Bergonzo, E. Scorsone, J.-P. Mazellier, J.-L. Divoux, F. Sauter-Starace, *Bioelectrochemistry* **2019**, 129, 79–89.
- [122] C. Boehler, S. Carli, L. Fadiga, T. Stieglitz, M. Asplund, *Nat Protoc* **2020**, 15, 3557–3578.
- [123] N. Torres-Martinez, D. Ratel, C. Crétallaz, C. Gaude, S. Maubert, J.-L. Divoux, C. Henry, D. Guiraud, F. Sauter-Starace, *J. Neural Eng.* **2019**, 16, 066047.
- [124] C. Yang, Z. Suo, *Nat Rev Mater* **2018**, 3, 125–142.
- [125] C. Keplinger, J.-Y. Sun, C. C. Foo, P. Rothmund, G. M. Whitesides, Z. Suo, *Science* **2013**, 341, 984–987.
- [126] S. Zhao, P. Tseng, J. Grasman, Y. Wang, W. Li, B. Napier, B. Yavuz, Y. Chen, L. Howell, J. Rincon, F. G. Omenetto, D. L. Kaplan, *Adv. Mater.* **2018**, 30, 1800598.
- [127] S. R. Shin, S. M. Jung, M. Zalabany, K. Kim, P. Zorlutuna, S. bok Kim, M. Nikkhah, M. Khabiry, M. Azize, J. Kong, K. Wan, T. Palacios, M. R. Dokmeci, H. Bae, X. (Shirley) Tang, A. Khademhosseini, *ACS Nano* **2013**, 7, 2369–2380.
- [128] Y. Ahn, H. Lee, D. Lee, Y. Lee, *ACS Appl. Mater. Interfaces* **2014**, 6, 18401–18407.
- [129] T. Dvir, B. P. Timko, M. D. Brigham, S. R. Naik, S. S. Karajanagi, O. Levy, H. Jin, K. K. Parker, R. Langer, D. S. Kohane, *Nature Nanotech* **2011**, 6, 720–725.
- [130] Y. Shin, S.-J. Song, S. Hong, S. Jeong, W. Chrzanowski, J.-C. Lee, D.-W. Han, *Nanomaterials* **2017**, 7, 369.
- [131] E. Murray, B. C. Thompson, S. Sayyar, G. G. Wallace, *Polymer Degradation and Stability* **2015**, 111, 71–77.
- [132] X. Hu, X.-X. Xia, S.-C. Huang, Z.-G. Qian, *Biomacromolecules* **2019**, 20, 3283–3293.
- [133] X. Jing, H.-Y. Mi, B. N. Napiwocki, X.-F. Peng, L.-S. Turng, *Carbon* **2017**, 125, 557–570.
- [134] X. Jing, H.-Y. Mi, X.-F. Peng, L.-S. Turng, *Carbon* **2018**, 136, 63–72.
- [135] Q. Wang, X. Pan, C. Lin, D. Lin, Y. Ni, L. Chen, L. Huang, S. Cao, X. Ma, *Chemical Engineering Journal* **2019**, 370, 1039–1047.
- [136] S. Wang, C. Sun, S. Guan, W. Li, J. Xu, D. Ge, M. Zhuang, T. Liu, X. Ma, *J. Mater. Chem. B* **2017**, 5, 4774–4788.
- [137] R. Zamora-Sequeira, I. Ardao, R. Starbird, C. A. García-González, *Carbohydrate Polymers* **2018**, 189, 304–312.

- [138] N. Paradee, A. Sirivat, *J. Phys. Chem. B* **2014**, *118*, 9263–9271.
- [139] R. T. Hassarati, H. Marcal, L. John, R. Foster, R. A. Green, *J. Biomed. Mater. Res.* **2016**, *104*, 712–722.
- [140] C. Xu, S. Guan, S. Wang, W. Gong, T. Liu, X. Ma, C. Sun, *Materials Science and Engineering: C* **2018**, *84*, 32–43.
- [141] J. Luo, J. Yang, X. Zheng, X. Ke, Y. Chen, H. Tan, J. Li, *Advanced Healthcare Materials* **2020**, 1901423.
- [142] I. Babeli, G. Ruano, J. Casanovas, M.-P. Ginebra, J. García-Torres, C. Alemán, *Journal of Materials Chemistry C* **2020**, *8*, 8654–8667.
- [143] B. Yang, F. Yao, L. Ye, T. Hao, Y. Zhang, L. Zhang, D. Dong, W. Fang, Y. Wang, X. Zhang, C. Wang, J. Li, *Biomaterials Science* **2020**, *8*, 3173–3185.
- [144] X. Ding, R. Jia, Z. Gan, Y. Du, D. Wang, X. Xu, *Materials Research Express* **2020**, *7*, 055304.
- [145] P. Bhattacharjee, M. Ahearne, *Polymers* **2020**, *12*, 3028.
- [146] H. Rastin, B. Zhang, J. Bi, K. Hassan, T. T. Tung, D. Losic, *Journal of Materials Chemistry B* **2020**, *8*, 5862–5876.
- [147] D. Zhang, Y. Tang, Y. Zhang, F. Yang, Y. Liu, X. Wang, J. Yang, X. Gong, J. Zheng, *J. Mater. Chem. A* **2020**, *8*, 20474–20485.
- [148] F. Ye, M. Li, D. Ke, L. Wang, Y. Lu, *Adv. Mater. Technol.* **2019**, *4*, 1900346.
- [149] S. Cao, X. Tong, K. Dai, Q. Xu, *J. Mater. Chem. A* **2019**, *7*, 8204–8209.
- [150] A. R. Spencer, A. Primbetova, A. N. Koppes, R. A. Koppes, H. Fenniri, N. Annabi, *ACS Biomater. Sci. Eng.* **2018**, *4*, 1558–1567.
- [151] C.-C. Shih, Y.-C. Lin, M. Gao, M. Wu, H.-C. Hsieh, N.-L. Wu, W.-C. Chen, *Journal of Power Sources* **2019**, *426*, 205–215.
- [152] M. Javadi, Q. Gu, S. Naficy, S. Farajikhah, J. M. Crook, G. G. Wallace, S. Beirne, S. E. Moulton, *Macromol. Biosci.* **2018**, *18*, 1700270.
- [153] B. G. Molina, A. Llampayas, G. Fabregat, F. Estrany, C. Alemán, J. Torras, *Journal of Applied Polymer Science* **2020**, 50062.
- [154] T. G. Polat, K. Ateş, S. Bilgin, O. Duman, Ş. Özen, S. Tunç, *Colloids and Surfaces A: Physicochemical and Engineering Aspects* **2019**, *580*, 123751.
- [155] Y. Lee, S.-G. Yim, G. W. Lee, S. Kim, H. S. Kim, D. Y. Hwang, B.-S. An, J. H. Lee, S. Seo, S. Y. Yang, *Sensors* **2020**, *20*, 5737.
- [156] H. Y. Gong, J. Park, W. Kim, J. Kim, J. Y. Lee, W.-G. Koh, *ACS Appl. Mater. Interfaces* **2019**, *11*, 47695–47706.
- [157] A. R. Spencer, E. S. Sani, J. R. Soucy, C. C. Corbet, A. Primbetova, R. A. Koppes, N. Annabi, *ACS Appl. Mater. Interfaces* **2019**, 16.
- [158] K. Wang, L. Tian, T. Wang, Z. Zhang, X. Gao, L. Wu, B. Fu, X. Liu, *Composite Interfaces* **2019**, *26*, 27–40.
- [159] H. Zhang, M. Yue, T. Wang, J. Wang, X. Wu, S. Yang, *New J. Chem.* **2021**, *45*, 4647–4657.
- [160] I. del Agua, D. Mantione, U. Ismailov, A. Sanchez-Sanchez, N. Aramburu, G. G. Malliaras, D. Mecerreyes, E. Ismailova, *Advanced Materials Technologies* **2018**, *3*, 1700322.
- [161] Y. Xu, X. Yang, A. K. Thomas, P. A. Patsis, T. Kurth, M. Kräter, K. Eckert, M. Bornhäuser, Y. Zhang, *ACS Applied Materials & Interfaces* **2018**, *10*, 14418–14425.
- [162] Y. Xu, M. Cui, P. A. Patsis, M. Günther, X. Yang, K. Eckert, Y. Zhang, *ACS Applied Materials & Interfaces* **2019**, *11*, 7715–7724.
- [163] D. Mawad, E. Stewart, D. L. Officer, T. Romeo, P. Wagner, K. Wagner, G. G. Wallace, *Advanced Functional Materials* **2012**, *22*, 2692–2699.
- [164] Y. Xu, Z. Sui, B. Xu, H. Duan, X. Zhang, *Journal of Materials Chemistry* **2012**, *22*, 8579–8584.
- [165] B. Yao, H. Wang, Q. Zhou, M. Wu, M. Zhang, C. Li, G. Shi, *Advanced Materials* **2017**, *29*, 1700974.
- [166] B. Lu, H. Yuk, S. Lin, N. Jian, K. Qu, J. Xu, X. Zhao, *Nat Commun* **2019**, *10*, 1043.
- [167] V. R. Feig, H. Tran, M. Lee, K. Liu, Z. Huang, L. Beker, D. G. Mackanic, Z. Bao, *Adv. Mater.* **2019**, 1902869.

- [168] Z. Yang, D. Shi, W. Dong, M. Chen, *Chem. Eur. J.* **2020**, *26*, 1846–1855.
- [169] Y. Xu, P. A. Patsis, S. Hauser, D. Voigt, R. Rothe, M. Günther, M. Cui, X. Yang, R. Wieduwild, K. Eckert, C. Neinhuis, T. F. Akbar, I. R. Minev, J. Pietzsch, Y. Zhang, *Adv. Sci.* **2019**, 1802077.
- [170] A. Novikov, J. Goding, C. Chapman, E. Cuttaz, R. A. Green, *APL Materials* **2020**, *8*, 101105.
- [171] S. Zhang, Y. Chen, H. Liu, Z. Wang, H. Ling, C. Wang, J. Ni, B. Çelebi-Saltik, X. Wang, X. Meng, H. Kim, A. Baidya, S. Ahadian, N. Ashammakhi, M. R. Dokmeci, J. Travas-Sejdic, A. Khademhosseini, *Advanced Materials* **2020**, *32*, 1904752.
- [172] A. Puiggalí-Jou, E. Cazorla, G. Ruano, I. Babeli, M.-P. Ginebra, J. García-Torres, C. Alemán, *ACS Biomater. Sci. Eng.* **2020**, *6*, 6228–6240.
- [173] R. Maeda, Y. Shinohara, H. Kawakami, Y. Isoda, I. Kanazawa, M. Mitsuishi, *Nanotechnology* **2021**, *32*, 135403.
- [174] Y. Peng, M. Pi, X. Zhang, B. Yan, Y. Li, L. Shi, R. Ran, *Polymer* **2020**, *196*, 122469.
- [175] D. N. Heo, S.-J. Lee, R. Timsina, X. Qiu, N. J. Castro, L. G. Zhang, *Materials Science and Engineering: C* **2019**, *99*, 582–590.
- [176] M. Solazzo, K. Krukiewicz, A. Zhussupbekova, K. Fleischer, M. J. Biggs, M. G. Monaghan, *J. Mater. Chem. B* **2019**, *7*, 4811–4820.
- [177] Y. S. Kim, K. Cho, H. J. Lee, S. Chang, H. Lee, J. H. Kim, W.-G. Koh, *Reactive and Functional Polymers* **2016**, *109*, 15–22.
- [178] F. Buchanan, *Degradation Rate of Bioresorbable Materials: Prediction and Evaluation*, **2008**.
- [179] J. Duan, D. L. Kasper, *Glycobiology* **2011**, *21*, 401–409.
- [180] K. A. Ludwig, J. D. Uram, J. Yang, D. C. Martin, D. R. Kipke, *J. Neural Eng.* **2006**, *3*, 59–70.
- [181] A. Inoue, H. Yuk, B. Lu, X. Zhao, *Sci. Adv.* **2020**, *6*, eaay5394.
- [182] S. Oribe, S. Yoshida, S. Kusama, S. Osawa, A. Nakagawa, M. Iwasaki, T. Tominaga, M. Nishizawa, *Sci Rep* **2019**, *9*, 13379.
- [183] C. J. Bettinger, Z. Bao, *Advanced materials* **2010**, *22*, 651–655.
- [184] Y. H. Jung, T.-H. Chang, H. Zhang, C. Yao, Q. Zheng, V. W. Yang, H. Mi, M. Kim, S. J. Cho, D.-W. Park, H. Jiang, J. Lee, Y. Qiu, W. Zhou, Z. Cai, S. Gong, Z. Ma, *Nat Commun* **2015**, *6*, 7170.
- [185] R. K. Pal, A. A. Farghaly, M. M. Collinson, S. C. Kundu, V. K. Yadavalli, *Advanced Materials* **2016**, *28*, 1406–1412.
- [186] A. Susloparova, S. Halliez, S. Begard, M. Colin, L. Buée, S. Pecqueur, F. Alibert, V. Thomy, S. Arscott, E. Pallecchi, Y. Coffinier, *Sensors and Actuators B: Chemical* **2021**, *327*, 128895.
- [187] P. J. Molino, Z. Yue, B. Zhang, A. Tibbens, X. Liu, Robert. M. I. Kapsa, M. J. Higgins, G. G. Wallace, *Advanced Materials Interfaces* **2014**, *1*, 1300122.
- [188] L. R. Stevens, D. G. Harman, K. J. Gilmore, M. in het Panhuis, G. G. Wallace, *MRS Proc.* **2015**, *1717*, mrsf14-1717-a08-02.
- [189] M. Asplund, E. Thaning, J. Lundberg, A. C. Sandberg-Nordqvist, B. Kostyszyn, O. Inganäs, H. von Holst, *Biomed. Mater.* **2009**, *4*, 045009.
- [190] E. M. Thaning, M. L. M. Asplund, T. A. Nyberg, O. W. Inganäs, H. von Holst, *J. Biomed. Mater. Res.* **2010**, *93B*, 407–415.
- [191] M. Asplund, H. von Holst, O. Inganäs, *Biointerphases* **2008**, *3*, 83–93.
- [192] P. J. Molino, L. Garcia, E. M. Stewart, M. Lamaze, B. Zhang, A. R. Harris, P. Winberg, G. G. Wallace, *Biomaterials Science* **2018**, *6*, 1250–1261.
- [193] P. Hernandez-Suarez, K. Ramirez, F. Alvarado, E. Avendano, R. Starbird, *MRC* **2019**, *9*, 218–223.
- [194] E. Nasybulin, S. Wei, I. Kymissis, K. Levon, *Electrochimica Acta* **2012**, *78*, 638–643.
- [195] R. Kim, Y. Nam, *Journal of Neuroscience Methods* **2019**, *326*, 108369.
- [196] A. I. Hofmann, D. Katsigiannopoulos, M. Mumtaz, I. Petsagkourakis, G. Pecastaings, G. Fleury, C. Schatz, E. Pavlopoulou, C. Brochon, G. Hadziioannou, E. Cloutet, *Macromolecules* **2017**, *50*, 1959–1969.
- [197] I. del Agua, D. Mantione, N. Casado, A. Sanchez-Sanchez, G. G. Malliaras, D. Mecerreyes, *ACS Macro Letters* **2017**, *6*, 473–478.

- [198] S. Tekoglu, D. Wielend, M. C. Scharber, N. S. Sariciftci, C. Yumusak, *Adv. Mater. Technol.* **2020**, 5, 1900699.
- [199] Y. Ner, M. A. Invernale, J. G. Grote, J. A. Stuart, G. A. Sotzing, *Synthetic Metals* **2010**, 160, 351–353.
- [200] M. Horikawa, T. Fujiki, T. Shirosaki, N. Ryu, H. Sakurai, S. Nagaoka, H. Ihara, *J. Mater. Chem. C* **2015**, 3, 8881–8887.
- [201] D. Mantione, I. del Agua, W. Schaafsma, J. Diez-Garcia, B. Castro, H. Sardon, D. Mecerreyes, *Macromol. Biosci.* **2016**, 16, 1227–1238.
- [202] S. Wang, S. Guan, J. Wang, H. Liu, T. Liu, X. Ma, Z. Cui, *Journal of Bioscience and Bioengineering* **2017**, 123, 116–125.
- [203] An. J. Hodgson, M. J. John, A. Georgevich, S. Woodhouse, T. Aoki., N. Ogata, G. G. Wallace, *Smart Structures and Materials* **1996**, 164–76.
- [204] K. J. Gilmore, M. Kita, Y. Han, A. Gelmi, M. J. Higgins, S. E. Moulton, G. M. Clark, R. Kapsa, G. G. Wallace, *Biomaterials* **2009**, 30, 5292–5304.
- [205] U. Freudenberg, Y. Liang, K. L. Kiick, C. Werner, *Advanced Materials* **2016**, 28, 8861–8891.
- [206] S. R. Yu, M. Burkhardt, M. Nowak, J. Ries, Z. Petrášek, S. Scholpp, P. Schwille, M. Brand, *Nature* **2009**, 461, 533–536.
- [207] K. W. Rogers, A. F. Schier, *Annu. Rev. Cell Dev. Biol.* **2011**, 27, 377–407.
- [208] D. Yan, X. Lin, *Cold Spring Harbor Perspectives in Biology* **2009**, 1, a002493–a002493.
- [209] Y. K. Joung, J. W. Bae, K. D. Park, *Expert Opinion on Drug Delivery* **2008**, 5, 1173–1184.
- [210] M. D. Wood, D. Hunter, S. E. Mackinnon, S. E. Sakiyama-Elbert, *Journal of Biomaterials Science, Polymer Edition* **2010**, 21, 771–787.
- [211] N. Cañas, T. Valero, M. Villarroja, E. Montell, J. Vergés, A. G. García, M. G. López, *J Pharmacol Exp Ther* **2007**, 323, 946–953.
- [212] G. Y. Özgenel, *Microsurg.* **2003**, 23, 575–581.
- [213] D. Tarus, L. Hamard, F. Caraguel, D. Wion, A. Szarpak-Jankowska, B. van der Sanden, R. Auzély-Velty, *ACS Appl. Mater. Interfaces* **2016**, 8, 25051–25059.
- [214] V. Voinchet, P. Vasseur, J. Kern, *American Journal of Clinical Dermatology* **2006**, 7, 353–357.
- [215] L. C. Becker, W. F. Bergfeld, D. V. Belsito, C. D. Klaassen, J. G. Marks, R. C. Shank, T. J. Slaga, P. W. Snyder, Cosmetic Ingredient Review Expert P, F. A. Andersen, *Int J Toxicol* **2009**, 28, 5–67.
- [216] M. Pagnano, G. Westrich, *Osteoarthritis and Cartilage* **2005**, 13, 751–761.
- [217] G. D. Monheit, K. M. Coleman, *Dermatol Ther* **2006**, 19, 141–150.
- [218] D. A. Swann, *Biochim. Biophys. Acta* **1968**, 14.
- [219] W. Jeanloz, E. Forchielli, *J. Biol. Chem.* **1950**, 495–511.
- [220] M. R. Johns, L.-T. Goh, A. Oeggerli, *Biotechnol Lett* **1994**, 16, 507–512.
- [221] B. F. Chong, L. M. Blank, R. McLaughlin, L. K. Nielsen, *Appl Microbiol Biotechnol* **2005**, 66, 341–351.
- [222] J. E. Scott, in *Novartis Foundation Symposia* (Eds.: D. Evered, J. Whelan), John Wiley & Sons, Ltd., Chichester, UK, **2007**, pp. 6–20.
- [223] K. Y. Suh, A. Khademhosseini, J. M. Yang, G. Eng, R. Langer, *Adv. Mater.* **2004**, 16, 584–588.
- [224] E. Buhler, F. Boué, *Macromolecules* **2004**, 37, 1600–1610.
- [225] G. Ribitsch, J. Schurz, V. Ribitsch, *Colloid Polymer Sci* **1980**, 258, 1322–1334.
- [226] M. Bathe, G. C. Rutledge, A. J. Grodzinsky, B. Tidor, *Biophysical Journal* **2005**, 88, 3870–3887.
- [227] J. D. de Oliveira, L. S. Carvalho, A. M. V. Gomes, L. R. Queiroz, B. S. Magalhães, N. S. Parachin, *Microb Cell Fact* **2016**, 15, 119.
- [228] H. Knopf-Marques, M. Pravda, L. Wolfova, V. Velebny, P. Schaaf, N. E. Vrana, P. Lavalley, *Adv. Healthcare Mater.* **2016**, 5, 2841–2855.
- [229] T. C. Laurent, J. R. E. Fraser, *FASEB* **1992**, 6, 2397–2404.
- [230] Q. Feng, S. Lin, K. Zhang, C. Dong, T. Wu, H. Huang, X. Yan, L. Zhang, G. Li, L. Bian, *Acta Biomaterialia* **2017**, 53, 329–342.
- [231] J. Patterson, R. Siew, S. W. Herring, A. S. P. Lin, R. Guldberg, P. S. Stayton, *Biomaterials* **2010**, 31, 6772–6781.

Chapter 2.

Development of a new conductive, biocompatible and degradable PEDOT-based ink

I. Introduction.....	64
II. HAS-PBA synthesis	68
II.1. Sulfation of hyaluronic acid	68
II.1.a. Influence of reaction time	71
II.1.b. Influence of reaction temperature	71
II.1.c. Influence of amount and nature of sulfating agent added	72
II.1.d. Influence of HA mean molecular weight Mw	75
II.1.e. Degradability of sulfated HA	76
II.2. Grafting of phenylboronic moieties	77
II.3. Conclusion.....	79
III. Synthesis and characterization of PEDOT:HA _{derivative} inks	80
III.1. Synthesis of PEDOT: HA _{derivative} inks.....	80
III.2. Influence of HA _{derivative} on electric and spectroscopic properties of PEDOT:HA inks.....	81
III.3. Optimization of the synthesis of PEDOT:HAS ₄ -PBA _{0.3} ink	83
III.4. Cytotoxicity using WST-1 assay	88
III.5. Extension of sulfate/PBA synergy to other GAGs	89
III.6. Conclusion.....	90
IV. Ink processing using inkjet printing	92
IV.1. Introduction	92
IV.1.a. Choice of printing process	92
IV.1.b. Inkjet printing with a Dimatix DMP-2800 series inkjet printer	93
IV. 2. Optimization of Ink physico-chemical properties	95
IV.2.a. Pristine ink physico-chemical properties	95
IV.2.b. Experimental design and formulation optimization	97
IV.3. Inkjet printing with Dimatix DMP 2800 inkjet printer	99
IV.4. Characterization of film structure	102
IV.5. Conclusion	103
V. Discussion.....	104
V.1. HA sulfation	104
V.2. Enzymatic biodegradability	106
V.3. Development of highly conductive PEDOT:HAS-PBA ink	108
V.4. Optimization of the polymerization process	109
VI. Conclusion	112
VII. Materials and methods	113
VII.1. Synthesis.....	113

Chapter 2. Development of a new conductive, biocompatible and degradable PEDOT-based ink

VII.1.a. Materials	113
VII.1.b. HA sulfation.....	113
VII.1.c. Synthesis of HAS ₄ -PBA _{0.3}	116
VII.1.d. Synthesis of PEDOT-based inks from HAS _x -PBA _y (Table 5)	117
VII.1.e. Synthesis of PEDOT:HAS ₄ -PBA _{0.3} inks with optimized particle sizes for inkjet printing	117
VII.1.f. Grafting of the phenylboronic acid moiety on ChS	118
VII.2. Characterizations	119
VII.2.a. Sulfation degree	119
VII.2.b. Size exclusion chromatography	120
VII.2.c. Thermogravimetric analysis (TGA)	121
VII.2.d. NMR.....	121
VII.2.e. Ink film deposition on glass slides	122
VII.2.f. Conductivity measurements.....	122
VII.2.g. Absorbance	123
VII.2.h. Dynamic Light Scattering (DLS)	123
VII.2.i. Viscosity measurements for the experimental design	123
VII.2.j. Surface tension.....	123
VII.2.k. Scanning Electron Microscopy	124
VII.2.l. Cytotoxicity experiments	124
VII.3. Experimental design procedure.....	125
VIII. Bibliography.....	129

I. Introduction

The bibliographic review of chapter I has described PEDOT acting as semi-insulator when neutral, and conductive when carrying electronic holes. In the latter case, PEDOT is designated as a p-doped polymer. To counter balance and stabilize those positive charges, dopant counter-anions are needed. They can be small molecules, but also polyanions. Polyanions serve additional roles aside counterbalancing positive charges that propagate into PEDOT conductive domains^[1]. For instance, they can also act as dispersing agents of PEDOT in aqueous solution when 3,4-ethylenedioxythiophene (EDOT) is polymerized through oxidative method in aqueous solution^[2]. This approach results in conductive PEDOT:polyanion dispersions (“inks”) which allow easy processing of the conducting polymer through various printing techniques.

Cloutet *et al.*^[3] reported that to dope PEDOT efficiently, the selected polyanions must have acidic groups in the deprotonated form during the polymerization of EDOT, so as to counter-balance the positive charges of the PEDOT domains. Furthermore, Gribkova *et al.*^[4–6] demonstrated that the rigidity of the backbone of the polyelectrolyte has an influence on the doping degree of PEDOT chains. Rigid polyelectrolytes yield to less doped PEDOT domains, and thus less conductive PEDOT:polyelectrolyte complexes, than more flexible polyelectrolytes. The same team also showed that polyelectrolytes with hydrophobic moieties lead to the formation of more conductive PEDOT-based materials^[5]. This was attributed to the fact that EDOT can interact with hydrophobic parts of the polyelectrolyte chains before polymerization, resulting into more structured PEDOT domains. All those considerations could explain why PEDOT:Poly(styrenesulfonate) (PSS) is such a good conductive material, as PSS meets all those criteria.

To increase the biocompatibility response of PEDOT-based materials and improve their interactions and performance in a biological environment, a widely used strategy consists in doping the PEDOT with biomolecules instead of PSS. Taking into account previous considerations on PEDOT dopants, such biomolecules should be negatively charged. In 2015, Harman *et al.*^[7] reported the chemical synthesis of a PEDOT:dextran sulfate ink (PEDOT:DS) with a conductivity up to 7 S/cm without additional treatments, and better interaction with L-

929 cells than PEDOT:PSS. Besides, the chemical synthesis enabled subsequent processing of the final conductive material.

Over the past six years, several other biomolecules have been investigated to obtain processable PEDOT:biomolecule inks: pectin^[3], guar^[8], deoxyribonucleic acid (DNA)^[9,10], heparin (Hep), chondroitin sulfate (ChS) or hyaluronic acid (HA)^[11,12]. Their properties are summarized in Table 1. In order to increase final PEDOT:biomolecule conductivity and to get closer to extracellular matrix structure, some of these biomolecules (dextran^[7,13], cellulose^[14] or alginate^[15]) were sulfated. As sulfates exhibit a low $pK_a \approx 2$, they are not protonated during PEDOT polymerization, increasing the electrostatic interaction with the conjugated polymer.

Table 1. PEDOT:biomolecule conductive inks reported in literature.

Entry	Reference	PEDOT:biomolecule	Modification of dopant	Conductivity σ (S/cm)	Biocompatibility assay	Biofabrication process
1	Ner <i>et al.</i> ^[10]	PEDOT:DNA	Pristine	1	-	-
2	Tekogluet <i>al.</i> ^[9]	PEDOT:DNA		550 Ω/\square	-	-
3	Mantione <i>et al.</i> ^[11]	PEDOT:heparin		0.05–0.001	Cytotoxicity, L-929 cells cellular attachment, CCF-STTG1 cells, proliferation of SH-SY5Y (neurons)	-
		PEDOT: chondroitin sulfate		0.075–0.002		
		PEDOT: HA		0.071–0.003		
4	Wang <i>et al.</i> ^[12]	PEDOT:HA		0.069	Differentiation of neuronal PC-12 (neurons)	-
5	Del Agua <i>et al.</i> ^[16]	PEDOT:xanthan		0.01	Cell proliferation of MDCK II eGFP (epithelial cells)	Aerogel formation
6	Hofmann <i>et al.</i> ^[3]	PEDOT:pectin		<0.01	-	-
7	Del Agua <i>et al.</i> ^[8]	PEDOT:guar	Sulfation	0.028–0.129	-	Conductive ionic gel
8	Zamora-Sequeira <i>et al.</i> ^[17]	PEDOT:starch/k-carrageenan		0.00029–0.00035	Proliferation of SH-SY5Y (neurons)	-
9	Horikawa <i>et al.</i> ^[14]	PEDOT:sulfated cellulose ($DS_S=1.03$) ^a		0.576	-	-
		PEDOT:sulfated cellulose ($DS_S=1.53$) ^a		0.014		
10	Harman <i>et al.</i> ^[7]	PEDOT:dextran sulfate ($DS_S=1.84$)		7	Cytotoxicity, L-929 cells	Inkjet printing
11	Xu <i>et al.</i> ^[15]	PEDOT:sulfated alginate		0.16	Cell proliferation of C212 (muscle)	Hydrogel formation

a: DS_S is the sulfation degree of the biomolecule, namely the average number of sulfate function per repeating unit.

Interestingly, glycosaminoglycans (GAGs), namely hyaluronic acid, chondroitin sulfate and heparin (Table 1, entry **3** and **4**, Figure 1), led to highly biocompatible PEDOT:GAGs conductive material, suitable for *in-vivo* recording and stimulation. But they all displayed low conductivity^[11,12] ($\sigma < 10^{-1}$ S/cm, see Table 1, entry **3** and **4**). Moreover, no correlation between the sulfation degree (DS_s) of these three GAGs and the conductivity of the resulting PEDOT:GAG films could be made..

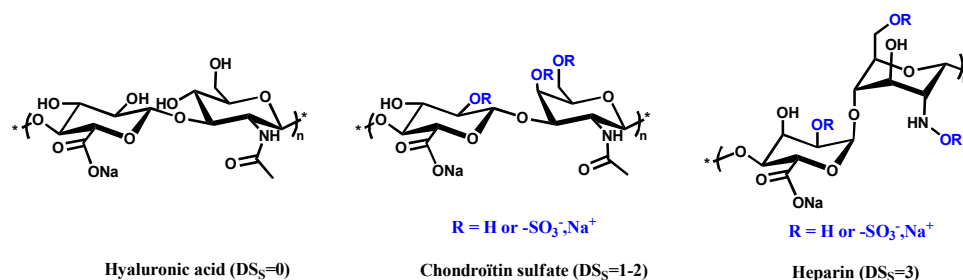


Figure 1. Various glycosaminoglycans used in PEDOT:GAGs inks.

The work of Horikawa *et al.*^[14] (Table 1, entry **9**) exhibited the complex effect of biomolecule sulfation degree on PEDOT:biomolecule conductivity: DS_s impacted sulfated biomolecule ability to crystallize, and therefore the ability of PEDOT domains to organize themselves. But both Horikawa *et al.*^[14] and Hofmann *et al.*^[3] demonstrated that sulfated polyelectrolytes are better PEDOT dopant than pristine ones (Table 1, entries **6** and **9**).

In this work, in order to assess thoroughly the influence of chemical modification on the final ink properties for the rational design of conductive HA-based biomaterials, HA was chosen as a building block as it is not sulfated in its pristine state, enabling a fine control of its chemical modification (Figure 1). Besides, it is a natural polysaccharide ubiquitous in the body, avoiding controversial safety issues^[18,19], and is already widely used in medicine for various applications such as ophthalmic formulations^[19], intra-articular injections^[20] or dermal fillers^[21]. Finally, it is produced nowadays essentially by bacterial fermentation^[22,23], which enables a great control over its molar mass, and batch-to-batch reproducibility.

Chemical moieties, sulfates and aromatic groups, that “mimic” the chemical functions of PSS were introduced on HA backbone and the dopant properties of these HA derivatives were studied. First, the effect of sulfation was investigated. In addition, aromatic groups were introduced in order to increase hydrophobic interactions and potential π -stacking between

PEDOT and HA chains. To the extent of our knowledge, the systematic study of GAG sulfation and introduction of an aromatic group has never been investigated before.

Then EDOT was polymerized with the modified hyaluronic acid, resulting in a new PEDOT:HA_{derivative} material. While a lot of attention has been given to the understanding and to the optimization of EDOT polymerization with small molecules or PSS, only few studies tackle those issues for PEDOT:biomolecule. Wallace *et al.*^[7,13] investigated many parameters for the polymerization protocol of PEDOT:dextran sulfate ink such as temperature, EDOT/DexS ratio. Mantione *et al.*^[11] studied the influence of the biomolecule on the final conductivity and absorbance. In this work, we investigated the electrical, spectroscopic and biological properties of different PEDOT:HA_{derivative} inks, in order to understand the influence of the chemical modification of HA on final properties.

II. HAS-PBA synthesis

In order to mimic the structure of PSS, chemical functions of interest were grafted on HA. HA hydroxyl functions were sulfated, and aromatic groups were introduced via the grafting of aminophenyl boronic acid (PBA) groups on its carboxylate functions. The resulting HA derivative is abridged HAS-PBA (Figure 2). PBA was chosen to introduce an aromatic group as previous work at CERMAV evidenced its biocompatibility^[24].

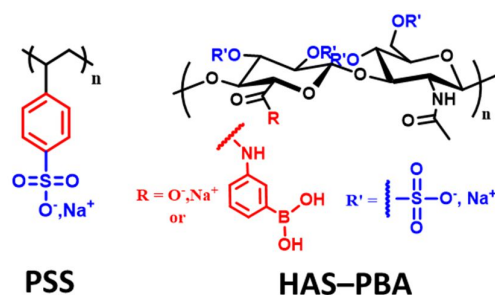


Figure 2. Structure of HAS-PBA compared to PSS.

II.1. Sulfation of hyaluronic acid

The first step of HA modification consists in its sulfation. HA was sulfated using two commonly used sulfating reagents: pyridine complex, $\text{SO}_3\text{-Py}$, and *N,N*-dimethylformamide complex $\text{SO}_3\text{-DMF}$.

In the literature, HA sulfation procedures are composed of two main steps^[25–30] (Figure 3). The first step consists in converting the HA sodium salt to the tetrabutylammonium salt (HA-TBA) by an ion exchange process in order to enhance its solubility in DMF. In the second step, HA-TBA is reacted with $\text{SO}_3\text{-Py}$ or $\text{SO}_3\text{-DMF}$ using DMF as a solvent. In these conditions, sulfated HA derivatives (HAS) were obtained with sulfation degrees (DS_s , defined as the mean number of sulfate groups per HA disaccharide repeating unit) in the range of 0.2–3.2^[25–30].

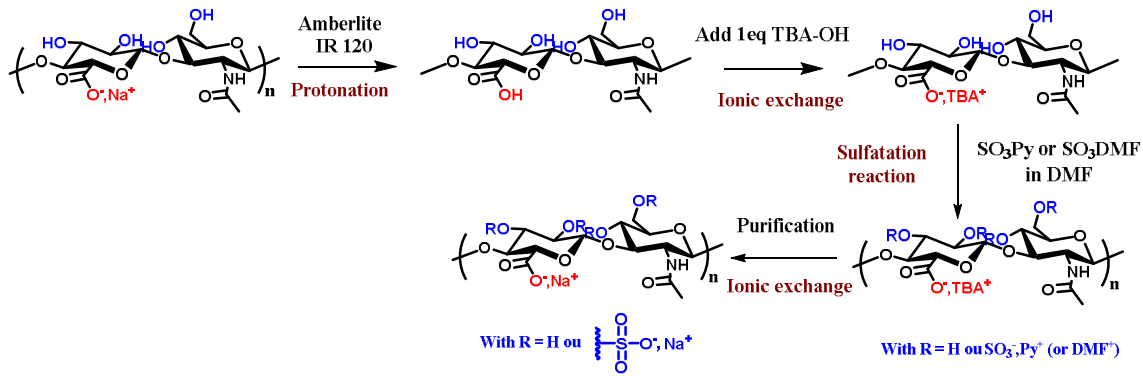


Figure 3. Sulfation reaction.

To quantify the degradation of HA chains during the sulfation reaction, the decrease of the polymerization degree DP_w was chosen as a characteristic value since new chemical groups were introduced on HA chains during sulfation. HA chain degradation during the reaction can be evidenced by the decrease of the ratio

$$DPw_{final}/DPw_{initial} = \frac{M_w \text{ final} / M_{\text{sulfated HA repeating unit}}}{M_w \text{ initial} / M_{\text{HA repeating unit}}} = \frac{M_w \text{ final} / (M_{\text{HA repeating unit}} + DS_S \cdot M_{\text{sulfate}})}{M_w \text{ initial} / M_{\text{HA repeating unit}}}$$

Where DPw_{final} and $DPw_{initial}$ are the final and initial degrees of polymerization after and before the sulfation reaction, M_w the weight average molar masses of polymer x , and M_x is the molar mass of x . The evolution of the polydispersity \mathcal{D} was also monitored.

In the literature, it was reported that important degradation of HA chains occurs during the sulfation reaction ($DPw_{final}/DPw_{initial} \leq 0.11$ for HA samples with average molar masses M_w in the range 380-440 kg/mol^[25,26], and $DPw_{final}/DPw_{initial} \leq 0.07$ for HA samples with M_w around 1 million g/mol^[27-30]).

Herein, several reaction parameters, including the reaction time, reaction temperature, amount and nature of sulfating agent, as well as the quenching method, were investigated in order to optimize the sulfation of HA without degradation. Studies were carried starting from HA samples with different average molar weights M_w of 113, 219, 478, and 1070 kg/mol (referred to as **HA113**, **HA219**, **HA478** and **HA1070**, respectively).

The sulfation degree, DS_s , was quantified using either C, H, N, S elemental analysis, or a combination of turbidimetric and colorimetric absorption measurements to estimate the sulfate and sugar mass fraction. The average molar masses were measured at 30 °C using size exclusion chromatography coupled to multi-angle light scattering (SEC-MALS), using 0.1 M $NaNO_3$ containing 5 mM NaN_3 as eluent. The dn/dc values used in SEC-MALS analysis were determined for each sulfated HA in order to obtain more accurate measurements (Figure 4).

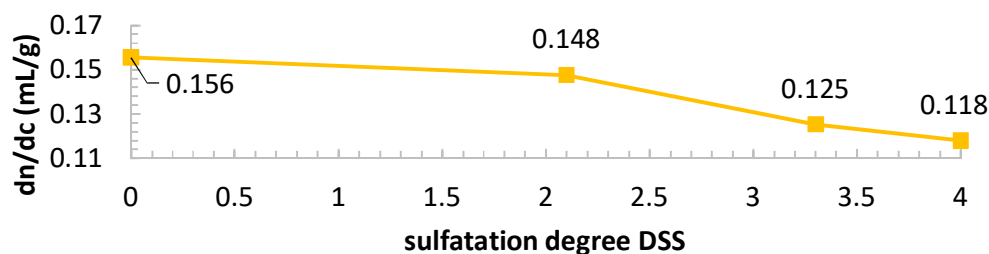


Figure 4. Values of dn/dc of HA **113** with different sulfation degrees, (0.1 M $NaNO_3$ /0.005 M NaN_3 , at 30 °C).

For all the syntheses, for n equivalents of sulfating reagent with respect to HA repeating unit, $n+1$ equivalents of NaOH were added to the reaction medium at the end of the sulfation reaction in order to directly neutralize the formed sulfuric acid. The pH of the reaction medium was then adjusted to neutral pH, and HAS was precipitated with ethanol instead of acetone, differently from literature^[27–30]. Finally, HAS was solubilized in water and the solution was dialyzed against water and freeze-dried.

The quenching of the reaction by the addition of aqueous NaOH was chosen as we suspected that the high degradation of the polysaccharide chains reported in the literature was due to the formation of sulfuric acid upon addition of water^[31], according to the following reaction: $SO_3 + H_2O \rightarrow H_2SO_4$. Moreover, as concentrated sulfuric acid can also be used as a de-sulfating agent for polysaccharides^[31,32], this may provide explanation for the non-reproducibility and the relatively low sulfation degrees (DS_s in the range 0.4–3.2) reported in the literature^[26,27,29,30]. In the present work, high sulfation degrees ranging from 1.2 to 4 were achieved with this new quenching and purification procedure.

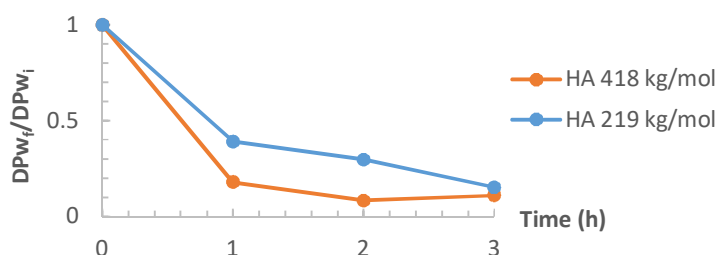
II.1.a. Influence of reaction time

HAS **1** and HAS **2** were sulfated for 1, 2 or 3 hours (Table 2), resulting in more important chain degradation as reaction time increased (Figure 5), without linear augmentation of sulfation degree. Therefore, the reaction time was set to 1 hour.

Table 2. Influence of reaction time on HA sulfation.

Entry	Mw _i (kg/mol)	Sulfating agent	Equivalent of sulfating agent /HA (n)	Reaction time (h)	Reaction temperature	DS _s ^a	DPw _f /DPw _i	Đ _f /Đ _i
1	478	SO ₃ -DMF	20	1 to 3	r.T.	1.5 < DS _s < 4	0.17 to 0.08	1.06 to 1.12
2	219	SO ₃ -DMF	20	1 to 3	r.T.	1.7 < DS _s < 2.9	0.39 to 0.15	1.09 to 1.18

^a determined by a combination of turbidimetric and colorimetric absorption measurements

Figure 5. Chain degradation according to sulfating time, for HA **1** (478 kg/mol) and HA **2** (219 kg/mol).

II.1.b. Influence of reaction temperature

It was observed that reaction at room temperature resulted in non-reproducible sulfation degree. To overcome this problem, the reaction temperature, which influences the reaction kinetics, was controlled. As can be seen from entry **3** to **8** in Table 3, reactions performed in these conditions resulted in reproducible sulfation degrees. Besides, HA sulfated at 30 °C was much more degraded than when the reaction was performed at 4 °C ($DPw_{final}/DPw_{initial} \leq 0.23$ and ≥ 0.38 respectively, Table 3 and Figure 6). In order to minimize polymer backbone degradation, the reaction temperature was set at 4 °C.

In these conditions, HAS **8** using HA with initial Mw of 113 kg/mol was synthesized, with almost no chain degradation ($DPw_{final}/DPw_{initial} = 0.77$), high sulfation degree ($DS_s = 4$), and a yield higher than 95%.

Table 3. Influence of reaction temperature on HA sulfation.

Entry	Mw _i (kg/mol)	Sulfating agent	Equivalent of sulfating agent / HA (n)	Reaction time (h)	Reaction temperature	DS _s ^a	DPw _f /DPw _i	D _f /D _i
3	478	SO ₃ -DMF	20	1	30°C	4	0.06	1.04
4	478	SO ₃ -DMF	20	1	4°C	4	0.38	1.04
5	219	SO ₃ -DMF	20	1	30°C	4	0.11	1.08
6	219	SO ₃ -DMF	20	1	4°C	4	0.51	1.17
7	113	SO ₃ -DMF	20	1	30°C	4	0.23	1.01
8	113	SO ₃ -DMF	20	1	4°C	4	0.77	1.01

^a determined by a combination of turbidimetric and colorimetric absorption measurements

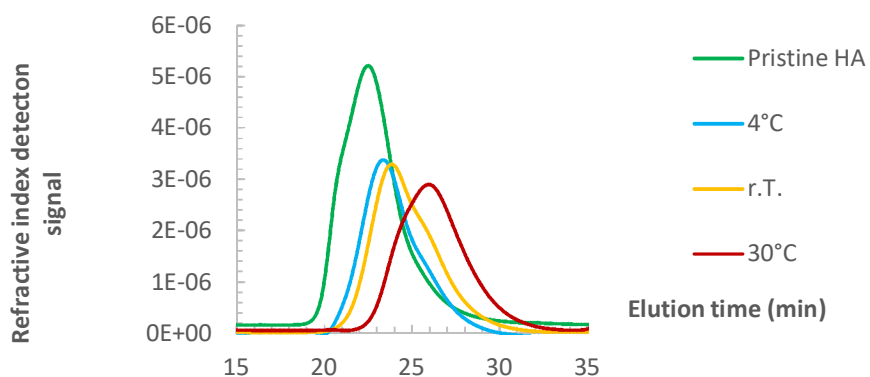


Figure 6. Size exclusion chromatograms of HA113, sulfated at 4°C, room temperature and 30°C.

II.1.c. Influence of amount and nature of sulfating agent added

Another set of experiments (HAS in entry **9-21** in Table 4) were performed with **HA113**, **HA219**, **HA478** and **HA1070**, by varying the nature of the sulfating agent (SO₃-Py or SO₃-DMF), and its amount, in order to investigate the influence of these parameters on the sulfation degree. A sulfation range from 1.8 to 4 was obtained (Figure 7), with low chain degradation.

Table 4. Influence of amount and nature of sulfating agent on HA sulfation.

Entry	Mw _i (kg/mol)	Sulfating agent	Equivalent of sulfating agent /HA (n)	Reaction time (h)	Reaction temperature	DS _s ^a	DPw _f /DPw _i	D _f /D _i
9	1070	SO ₃ -Py	10	1	4°C	1.5	0.56	1.01
10	1070	SO ₃ -Py	15	1	4°C	1.8	0.33	0.98
11	478	SO ₃ -Py	10	1	4°C	1.2	0.64	1.13
14	478	SO ₃ -Py	15	1	4°C	1.4	0.71	1.16
15	1070	SO ₃ -DMF	8	1	4°C	2.2	0.11	0.92
16	1070	SO ₃ -DMF	13	1	4°C	3	0.13	0.9
17	478	SO ₃ -DMF	10	1	4°C	1.6	0.48	1.15
18	478	SO ₃ -DMF	15	1	4°C	3.3	0.25	1.15
19	219	SO ₃ -DMF	10	1	4°C	1.6	0.64	1.08
20	219	SO ₃ -DMF	15	1	4°C	3.3	0.41	1.08
21	113	SO ₃ -DMF	10	1	4°C	2.2	0.68	1.01

^a determined by a combination of turbidimetric and colorimetric absorption measurements

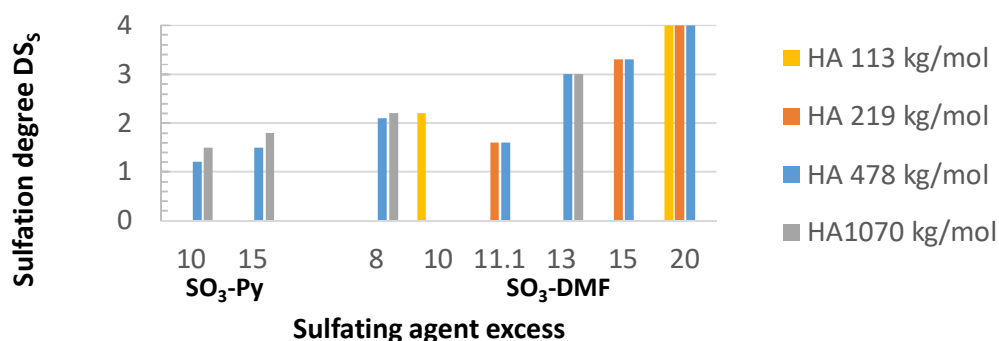


Figure 7. Sulfation degrees obtained according to the type and excess of sulfating agent for HAS **3** to **19**. The DSs values were determined by a combination of turbidimetric and colorimetric absorption measurements.

The ¹H and ¹³C NMR spectra of HAS₄ were assigned using 2D homonuclear ¹H–¹H COSY (Figure 33), as well as heteronuclear ¹H–¹³C HSQC-DEPT (Figure 8) and heteronuclear long distance ¹H–¹³C HMBC experiments (Figure 35). From the 2D ¹H–¹³C HSQC-DEPT spectrum of this derivative shown in Figure 8, it can be seen that the ¹H and ¹³C signals can be clearly identified, which is due to the full substitution of the OH groups.

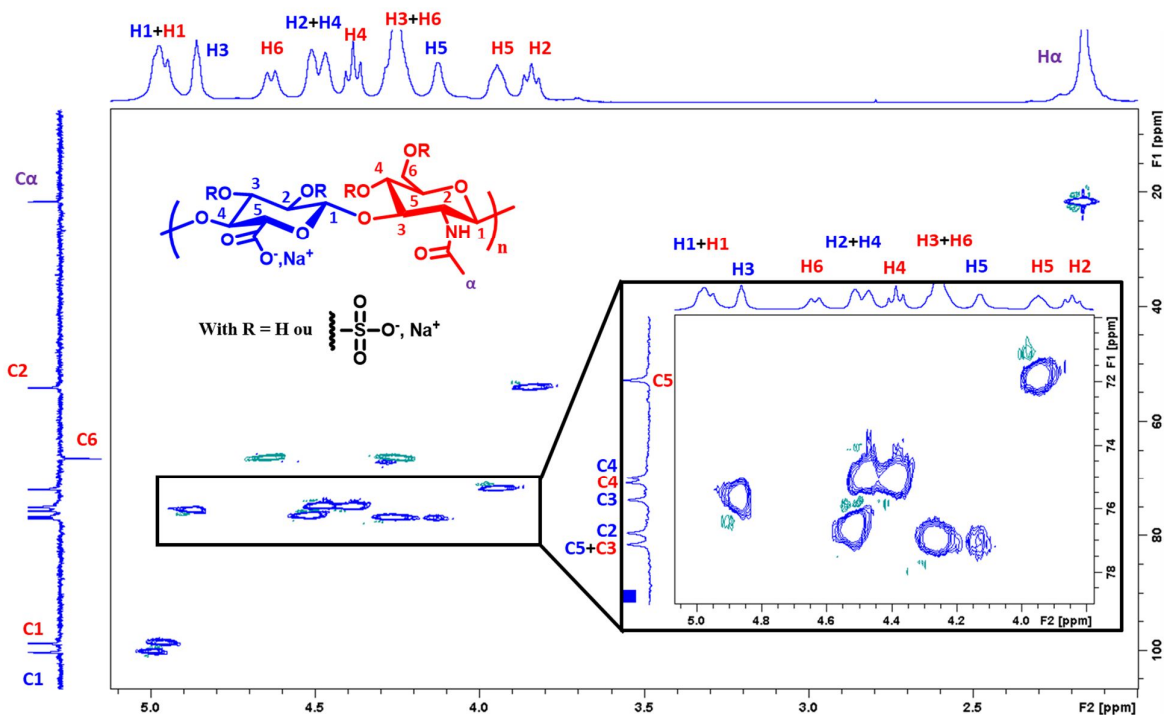


Figure 8. HSQC-DEPT NMR spectrum of HAS₄ at 17 mg/mL at 80°C in D₂O.

Interestingly, as the DS_S increased, the δ values of the proton signals of the HA sugars were shifted to lower magnetic fields owing to the lower field (4.74 and 4.63 ppm) due to the presence of the sulfate groups (Figure 9).

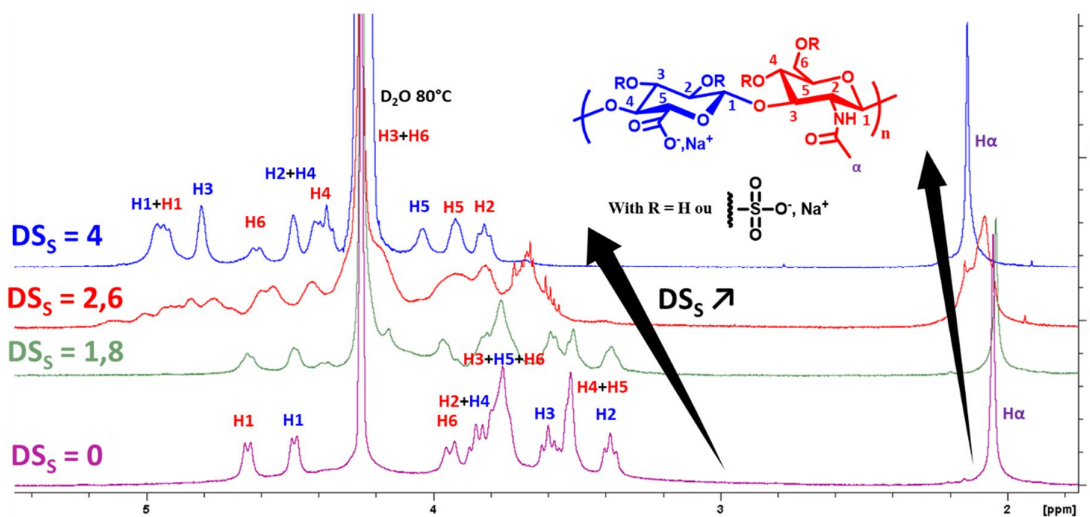


Figure 9. ¹H NMR spectrum of sulfated HA **113** with various sulfation degree, in D₂O, 353K.

Similarly, the δ values of the sulfate bearing carbon signals of the HA sugars were shifted to lower magnetic fields (**C6**, **C4**, **C3** and **C2** on Figure 10).

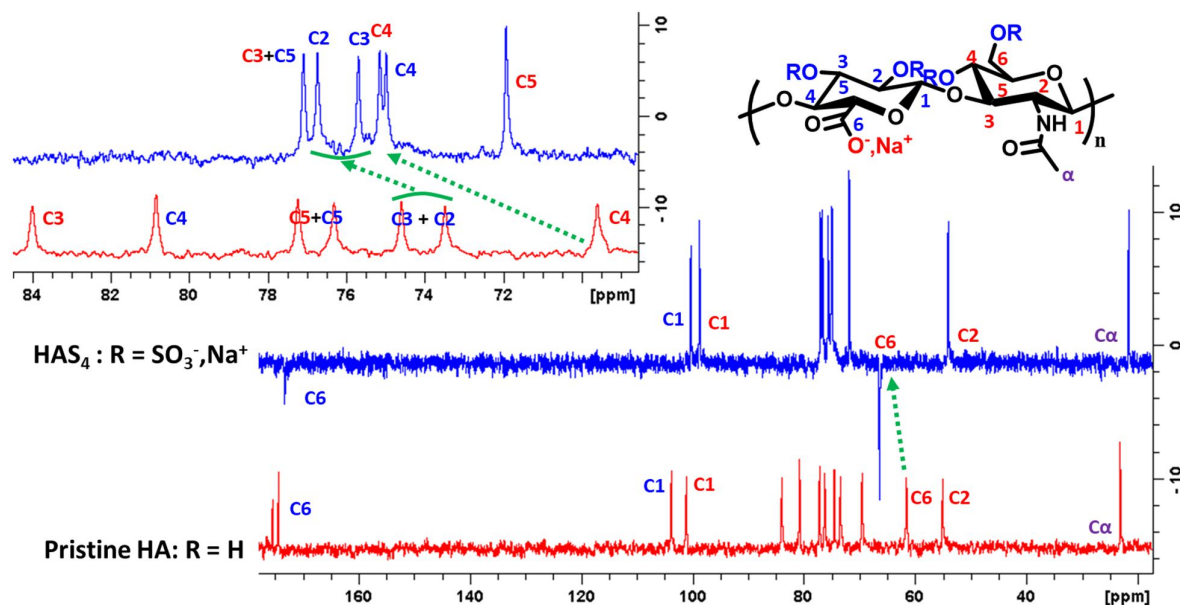


Figure 10. ^{13}C DEPT NMR spectrum of HAS₄ **8** and ^{13}C ZG NMR spectrum of HA113, in D₂O at 17 g/L at 80°C.

II.1.d. Influence of HA mean molecular weight Mw

Size exclusion chromatography (SEC-MALLS) showed that HAS prepared from HA samples with different molar masses (**HA113**, **HA219**, **HA478** and **HA1070**, Table 4) exhibited a slight increase of polydispersity \mathcal{D} ($\sim 10\%$) in comparison to initial HA. No major degradation was observed for the derivatives prepared from **HA113**, **HA219**, **HA478** ($\text{DP}_{\text{wf}}/\text{DP}_{\text{wi}} > 0.40$ in most cases). On the other hand, the decrease of DP_{w} was much more significant for the HAS derivatives prepared from **HA1070** using $\text{SO}_3\text{-DMF}$ (entry **15** and **16** in Table 4), in agreement with the literature^[25].

Conclusion

After thorough study of the sulfation reaction, we selected sulfated HA with an initial M_{w} of 113 kg/mol, prepared in conditions of entries **21** and **8** for the rest of this work. Both possess a sulfation degree of 2.2 and 4, respectively. They were selected as they displayed the minimum chain degradation during sulfation reaction ($\text{DP}_{\text{wf}}/\text{DP}_{\text{wi}} \sim 0.7$).

II.1.e. Degradability of sulfated HA

The biodegradation of HAS **8** and **21** (Table 4 and Table 5) as well as native HA with $M_w = 113$ kg/mol by hyaluronidase (HAase) using an enzyme concentration of 1000 U/mL was then investigated. HAase cleaves the β 1,4-glucosaminidic bond between glucosamine and glucuronic acid moieties^[33], leading to the formation of a *N*-Acetyl-glucosamine reducing end (Figure 11).

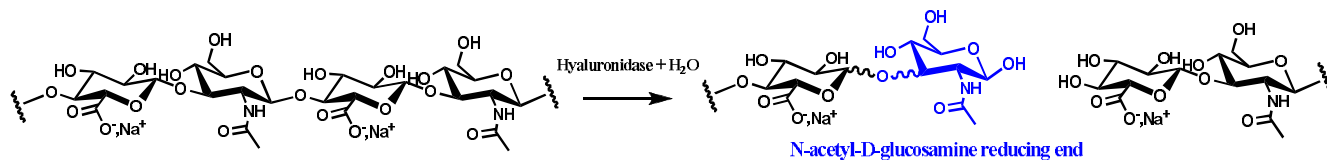


Figure 11. Cleavage reaction of HA by HAase.

Incubation conditions were adapted from Asteriou *et al.*^[33]. Samples were incubated at 37°C for several weeks, in ammonium acetate buffer at pH 5, in the presence of 1000 U/mL of hyaluronidase from bovine testes. Then sample fractions were aliquoted at different times and analyzed by SEC-MALS to determine their average molar mass. Noticeably Asteriou *et al.*^[33] reported that in these incubation conditions, the activity of HAase is optimal. Furthermore, the concentration of HAase is by far superior to physiological concentrations. Therefore, the degradation rate obtained in this study were expected to be higher than those of the final sulfated HA in physiological conditions. The results are summarized in Figure 12.

To quantify the degradation of HAS chains during the incubation, the decrease of the average molar mass M_w was chosen as a characteristic value since no chemical groups were introduced on HAS chains hydrolysis. Noticeably, here, $\frac{DPw_{final}}{DPw_{initial}} = \frac{Mw_{final}}{Mw_{initial}}$.

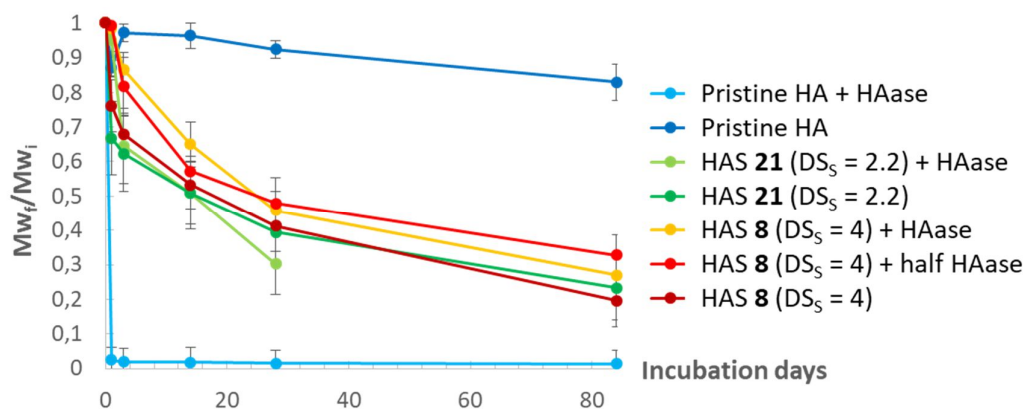


Figure 12. Degradation of various sulfated HA in ammonium acetate 5 mM pH 5 with or without 1000 U/mL of hyaluronidase (except HAS **8** + half HAase which was incubated with 500 U/mL of HAase).

While native HA degraded rapidly in the presence of HAase at a concentration of 1000 U/mL ($Mw_{final}/Mw_{initial} < 0.02$ in 24 hours), HA without HAase was stable, with a degradation of 18% in 3 months ($Mw_{final}/Mw_{initial} < 0.82$). Interestingly, HAS **8** and **21** displayed the same degradation behavior, regardless of the concentration of HAase. All demonstrated a degradation of roughly $40 \pm 10\%$ in two weeks ($Mw_{final}/Mw_{initial} \sim 0.6$), and roughly $70 \pm 10\%$ in three months ($Mw_{final}/Mw_{initial} \sim 0.3$).

Comparing the degradation curves of sulfated HA without HAase, it appeared that sulfated HA are less stable than pristine HA. Regarding the degradation rate of HAS **8** and **21** in the presence of HAase, no difference was observed by varying the sulfation degree or the HAase concentration, indicating that sulfated HA were not affected by the presence of the enzyme.

Sulfated HAS are therefore degradable, but not biodegradable as their degradation seemed to be not linked to enzymatic activity. Having the sulfated HA in hand, we further introduced the aromatic PBA moiety.

II.2. Grafting of phenylboronic moieties

HAS was then further modified by a phenylboronic acid (PBA) group. PBA was grafted on HAS **8** (Table 4, $DS_s = 4$, prepared from HA113) via an amide coupling reaction between the carboxylic acid function of HAS and the amine function of 3-APBA using 4-(4,6-dimethoxy-

1,3,5-triazin-2-yl)-4-methylmorpholinium chloride (DMTMM) as a coupling agent, at pH 6.5, according to the conditions of Figueirido *et al.*^[24] (Figure 13).

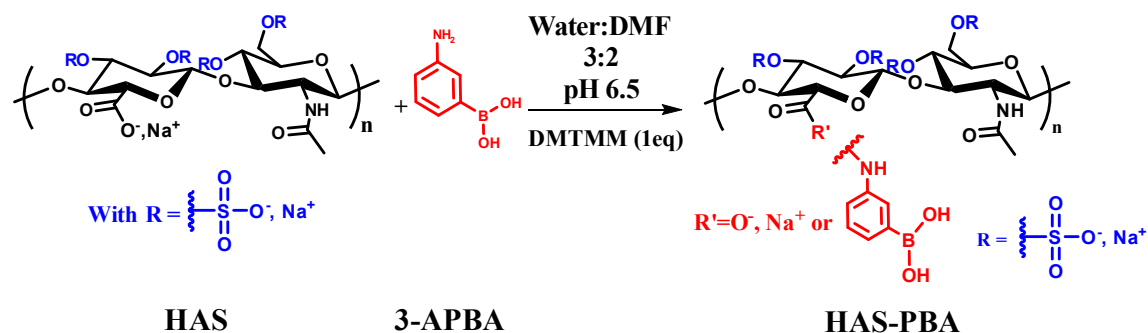


Figure 13. Amide coupling reaction of sulfated HA with 3-APBA.

The substitution degree in PBA (DS_{PBA}) was determined by ^1H NMR spectroscopy, from the integration of the proton signals of PBA and of the acetyl proton H_α of HA (Figure 14).

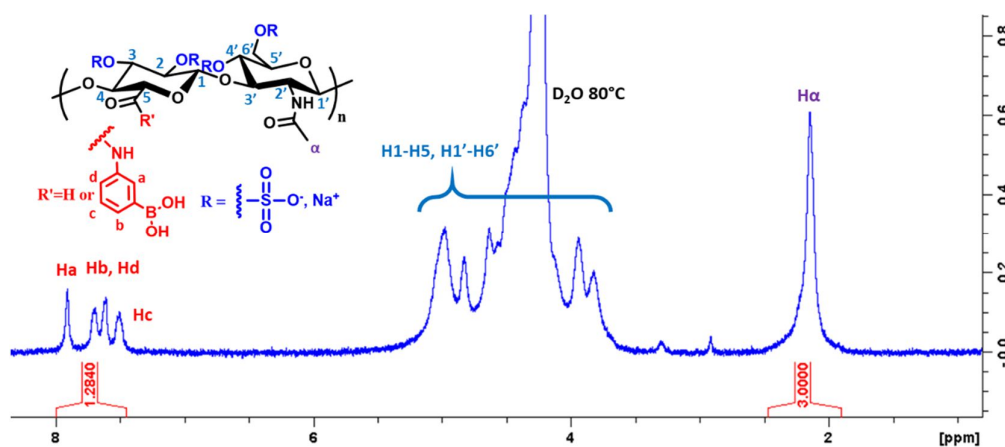


Figure 14. ^1H NMR spectrum of $\text{HAS}_4\text{-PBA}_{0.32}$ (5 mg/mL), at 80 °C in D_2O .

Two different HAS-PBA derivatives, referred to as $\text{HAS}_x\text{-PBA}_y$ (x and y being the DSs and DS_{PBA} values, respectively) were synthesized from HAS **8** (of from pristine HA) with a mass yield higher than 95% (Table 5).

II.3. Conclusion

We synthesized 5 different modified HA derivatives with various substitution degrees in sulfate and PBA (Table 5). Their synthesis required a total time of 2 weeks including purification and freeze drying times, with a sulfation yield higher than 85%, and a grafting of PBA yield higher than 95%. Using these different derivatives, various PEDOT:HA_{derivative} inks were synthesized, and their properties investigated.

Table 5. Various HAS_x-PBA_y synthesized.

HA derivative	Sulfation degree (x)	DS in PBA (y)	Total mass yield from HA (%)
HAS _{1.6}	1.6	0	84
HAS ₃	3	0	82
HAS ₄	4	0	85
HA-PBA _{0.3}	0	0.30	96
HAS ₄ -PBA _{0.3}	4	0.30	81

III. Synthesis and characterization of PEDOT:HA_{derivative} inks

III.1. Synthesis of PEDOT: HA_{derivative} inks

In this work, the five HAS_x-PBA_y derivatives as well as initial HA were used as dopants to prepare PEDOT dispersions by oxidative chemical polymerization (Figure 15 and Table 6). The polymerization procedure was adapted from Harman *et al.*^[7], with minor modifications. Briefly, the HA derivatives and EDOT were first dissolved in a mixture of water:MeCN (9:1, v:v) and stirred for 18 h at 25 °C. Herein, MeCN was added to improve EDOT solubility. In all reactions, the molar ratio EDOT/ HAS_x-PBA_y was set to 2, which corresponds to one EDOT per saccharide unit. Ammonium persulfate (NH₄)₂S₂O₈ (APS), as oxidant, and iron II sulfate Fe(SO₄), as catalyst, were then added. Although 1 molar equivalent of APS with respect to EDOT should be enough to achieve polymerization, 1.33 molar equivalent of APS were used to also oxidize the PEDOT backbone, forming charge-propagating carriers. 0.05 equivalent of Fe(SO₄) was added.

During polymerization, the reaction medium became deep blue as a result of PEDOT formation (Figure 16). The polymerization was considered as finished when the pH became constant, usually between 1.1 and 1.5, within 18 to 48 hours. The PEDOT dispersions were finally homogenized by mixing for 10 minutes at 25000 rpm, dialyzed against deionized water, and then freeze-dried to recover inks as solid deep blue powders.

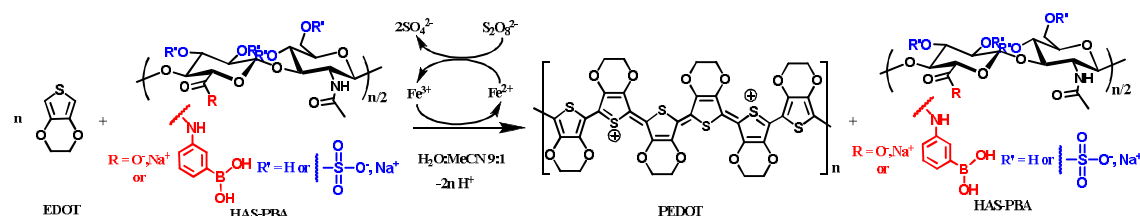


Figure 15. EDOT polymerization in the presence of HAS_x-PBA_y.

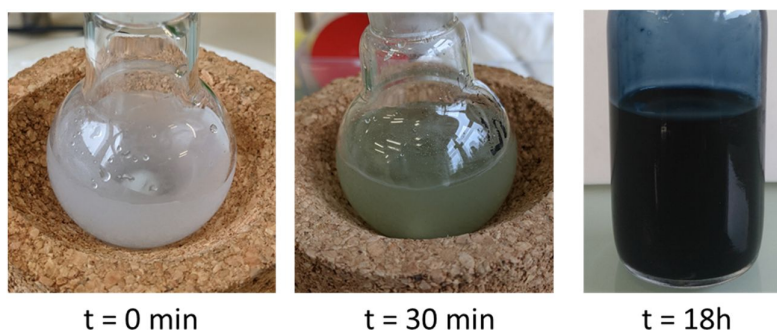


Figure 16. Change of color during EDOT polymerization.

Next, ultraviolet–near infrared spectroscopy, conductivity measurements and cytotoxicity tests were carried out to characterize the different PEDOT:HAS_x-PBA_y inks (see Table 6) and to gain a better understanding of the influence of the chemical modifications of HA on the material properties.

Table 6. Synthesized PEDOT:HA_{derivative} inks.

Ink	Sample name	Sulfation degree (x)	DS in PBA (y)	σ (S/cm) ^a
1	Clevios PH1000 PEDOT:PSS	NA	NA	$7.2 \times 10^{-2} \pm 1.3 \times 10^{-2}$
2	PEDOT:HA	0	0	
3	PEDOT:HAS _{1.6}	1.6	0	$3.2 \times 10^{-2} \pm 0.7 \times 10^{-2}$
4	PEDOT:HAS ₃	3	0	$1.4 \times 10^{-1} \pm 0.5 \times 10^{-2}$
5	PEDOT:HAS ₄	4	0	$1.6 \times 10^{-1} \pm 0.4 \times 10^{-2}$
6	PEDOT:HA-PBA _{0.3}	0	0.30	$3.5 \times 10^{-3} \pm 0.9 \times 10^{-3}$
7	PEDOT:HAS ₄ -PBA _{0.3}	4	0.30	1.57 ± 0.2

^aThe conductivity was obtained using a 4-point probe according to the protocol described in section VII.2.f.

III.2. Influence of HA_{derivative} on electric and spectroscopic properties of PEDOT:HA inks

Visible-NIR absorbance spectroscopy measurements were carried out on drop-casted films on a glass slide, and allowed us to quantify the ink intrinsic doping state, as PEDOT neutral chain, radical cation and dications (the charge carriers) display specific absorbance bands^[4,34–37] (Figure 17). These are between 350 and 550 nm for neutral PEDOT, around 800 nm for radical cations, and superior to 1100 nm for dications (Sample preparation is detailed in section VII.2.g). All spectra were normalized to the film thickness to compare respective

absorbance from one sample to another. The various inks displayed absorption bands of different intensities (Figure 17). The more the absorption bands of radical cations and dications were intense, the more intrinsically doped the PEDOT domains were^[34].

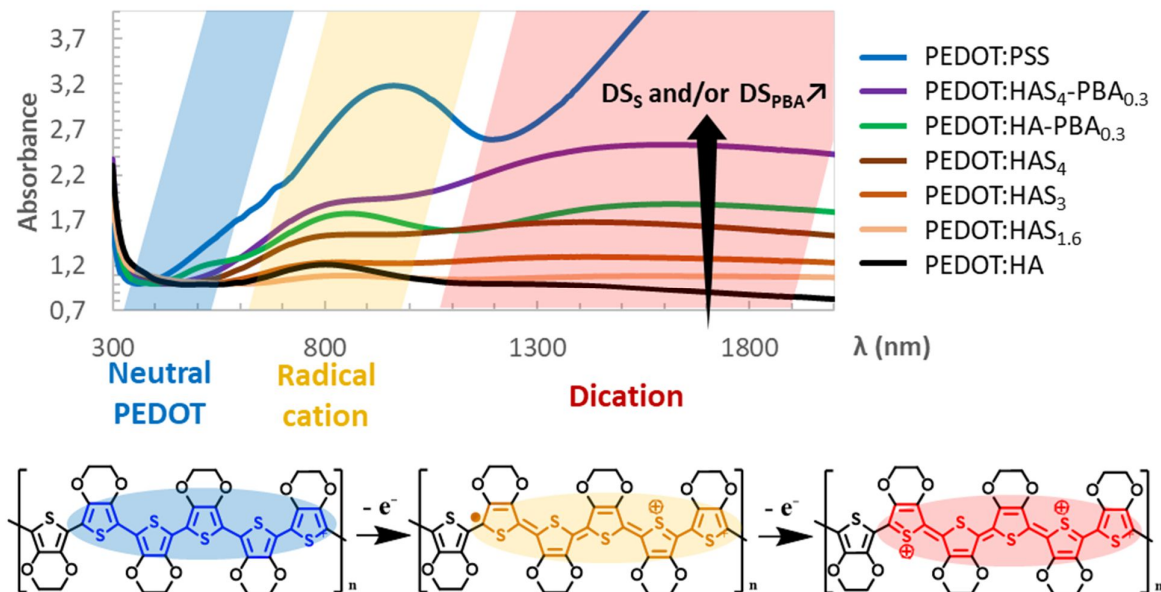


Figure 17. UV-visible-NIR absorption spectra of PEDOT:HA_{derivative} inks and PEDOT:PSS.

We observed that for all samples, the absorption band of neutral PEDOT was almost not present, as expected since 1.33 equivalent of APS with respect to EDOT were added during polymerization. Comparing PEDOT:HA, PEDOT:HAS_{1.6}, PEDOT:HAS₃ and PEDOT:HAS₄ (inks **2** to **5**), we observed that the absorption band intensity of charge carriers increased as the DS_s increased. However PEDOT:HA-PBA_{0.3} (ink **6**) exhibited higher absorption in the charge carrier bands. When both sulfate and PBA were present (PEDOT:HAS₄-PBA_{0.3}, ink **7**), charge carriers absorption bands were even more intense. Those results demonstrated the importance of negatively charged sulfate and hydrophobic groups on the polyelectrolyte to dope efficiently the PEDOT chains, and the synergy between them.

The obtained inks were compared to a commercial formulation of PEDOT:PSS (Clevios PH1000) which pH was adjusted to 7.4. Commercial PEDOT:PSS displayed more intense charge carriers absorption bands, especially for the dication.

For conductivity measurements, inks were dropped on glass slides, dried, and film thickness h were measured with a mechanical profilometer. Then their sheet resistivity R_{sheet}

were measured using a 4-points probe device. Their conductivity was calculated using the following equation:

$$\sigma = 1/R_{sheet} \cdot h \cdot c$$

where c was a geometric corrector coefficient determined by the software. Conductivity are reported in Table 6.

PEDOT:HA displayed no conductive behavior (Table 6). Comparing **PEDOT:HAS_{1.6}**, **PEDOT:HAS₃** and **PEDOT:HAS₄**, we observed that the conductivity increased as the sulfation degree, DS_s, increased (Table 6). Interestingly **PEDOT:HA-PBA_{0.3}** displayed lower conductivity than all **PEDOT:HAS_x** inks, whereas it is more intrinsically doped according to absorbance measurements (Figure 17). **PEDOT:HAS₄-PBA_{0.3}** presented an unprecedented conductivity for a PEDOT:GAG ink ($\sigma = 1.6$ S/cm), demonstrating the synergy between the sulfate and aromatic groups.

This synergistic effect could be interpreted in terms of PEDOT/polyelectrolyte interactions: hydrophobic moieties in **PEDOT:HA-PBA_{0.3}** enabled close association of PEDOT domains along HA-PBA_{0.3}, resulting in stable radical cations and dications. However, because of the absence of sulfate groups along the polyelectrolyte, they cannot efficiently propagate, resulting in a low conductivity. By contrast, the numerous sulfate groups in the **PEDOT:HAS_x** samples enabled charge propagation all along the chains, but did not increase charge carrier concentration in PEDOT domains. HAS₄-PBA_{0.3} hydrophobic moieties enhanced charge carrier concentrations, and its negative sulfated charges enabled their propagation.

Interestingly, **PEDOT:HAS₄-PBA_{0.3}** ink displayed better conductive properties than **PEDOT:PSS** in physiological conditions (pH \approx 7.4 in PBS, Table 6), without secondary doping. HAS₄-PBA_{0.3} was selected for the rest of this Ph.D. project in order to develop processable conductive inks.

III.3. Optimization of the synthesis of PEDOT:HAS₄-PBA_{0.3} ink

An experimental design was implemented in order to optimize the physico-chemical properties of the ink for processing it using ink-jet printing (section IV.2.). Prediction models

were obtained to adjust viscosity, surface tension and particle size measured by dynamic light scattering, but we were unable to validate them since at this stage of the work, ink particle sizes were not reproducible. Therefore, the polymerization of EDOT in the presence of HAS₄-PBA_{0.3} had to be further optimized in order to get reproducible ink particle size, with a diameter range between 200 and 1000 nm.

At the beginning of EDOT polymerization in the presence of HAS₄-PBA_{0.3}, the medium was an emulsion of EDOT organic domains in water. Indeed EDOT solubility in water is very low (2.1 mg/mL at 20 °C)^[2], though enhanced by the addition of polyelectrolyte containing aromatic groups or a solvent such as acetonitrile. As polymerization progressed, EDOT organic droplets polymerize to yield PEDOT clusters stabilized and entangled with HAS₄-PBA_{0.3}, resulting in a final ink suspension of particles (Figure 18). The quality and stability of the initial PEDOT emulsion was identified as a key parameter to obtain a final ink with monodisperse and reproducible particle size.

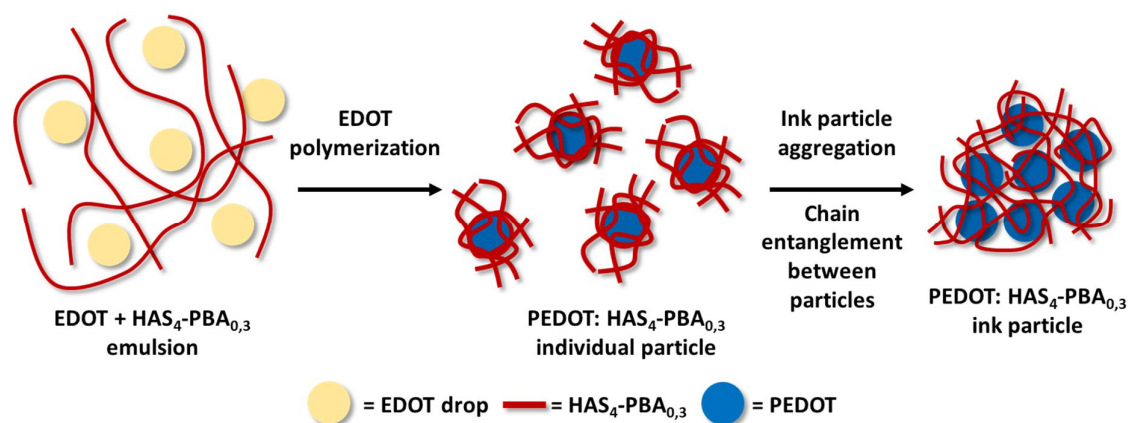


Figure 18. PEDOT:HAS-PBA ink particle formation.

In order to optimize the synthesis of PEDOT: HAS₄-PBA_{0.3}, Harman *et al.* procedure^[7] was modified. Different parameters were investigated.

First, as the initial EDOT droplet size seemed crucial, a homogenization step was performed at the very beginning of the polymerization to obtain, as far as possible, an EDOT emulsion composed of small and monodisperse EDOT droplets.

Second, in order to stabilize the initial EDOT emulsion, the addition of a surfactant (dodecylbenzene sulfonic acid, DBSA) was investigated to stabilize the EDOT / water interface,

and to prevent EDOT droplet coalescence^[38]. Besides, the addition of acetonitrile to the aqueous solvent was also investigated to lower the medium surface tension, as acetonitrile surface tension ($\gamma_{\text{acetonitrile}} = 29.29 \text{ mN/m}$) is much lower than water surface tension ($\gamma_{\text{water}} = 71.97 \text{ mN/m}$ at 25°C).

Then, to minimize aggregation of PEDOT: HAS₄-PBA_{0.3} particles, our strategy was to decrease the concentration of HAS-PBA and EDOT during polymerization. Therefore, the concentration of HAS-PBA and EDOT were varied during polymerization to investigate the effect of these parameters on the size of PEDOT: HAS₄-PBA_{0.3} particles.

At the end, an optimized polymerization protocol was defined with the following steps: HAS₄-PBA_{0.3} was first dissolved in water, then EDOT was added, and then, DBSA and/or acetonitrile depending on the reaction conditions. Finally, the oxidant and catalyst (APS + FeSO₄) were added. After adding all reagents in this order, the medium was mixed for 10 minutes at 25000 rpm to create the EDOT emulsion. At the end of the polymerization step (18 – 24 hours), the medium was dialyzed against water to remove by-products, adjusted to pH 7.4 and filtered successively through 3 μm , 1.2 μm , 0.8 μm and finally 0.45 μm filters whenever it was possible (see detailed protocol in experimental part VII.1.e).

Several inks were synthesized to gain a better understanding of the influence of each EDOT polymerization parameter on the size of the final particles, their polydispersity as well as the resistivity of drop-casted films of PEDOT: HAS₄-PBA_{0.3} (Table 7).

For this study, film sheet resistivity was used as validation technique. For a uniform sheet thickness, sheet resistivity is a special case of resistivity. Its unity is $\Omega/\square = \Omega/(\text{m/m})$. The “ \square ” is adimensionnal, but kept to not confuse the sheet resistance from the bulk resistance.

Previously synthesized PEDOT: HAS₄-PBA_{0.3} films displayed a conductivity between 1 and 2 S/cm, with films thickness between 5 and 15 μm . Thus, in this study, the PEDOT-based films were expected to display a sheet resistivity below 5-10 k Ω/\square . Entries **1** to **5** in Table 7 indicate that the addition of DBSA at 1.5 g/L, without acetonitrile resulted in the formation of ink particles between 240 and 400 nm. Besides, a EDOT + HAS₄-PBA_{0.3} concentration above 10 g/L tended to lead to larger particles than at 10 g/L, confirming that high concentrations lead to ink particle aggregation.

Table 7. Ink synthesis with [DBSA] = 1.5 g/L, varying [HAS-PBA + EDOT] concentration.

Entry	Synthesis parameters					Characterization			
	Ratio EDOT / HAS-PBA	[HAS ₄ -PBA _{0.3} + EDOT] (g/L)	Vol% MeCN	[DBSA] (g/L)	Equivalent FeSO ₄	Smaller filtration size	Z _{Average} (nm)	PDI	Resistivity (Ω/\square)
1	2	10	0	1.5	0.015	0.45 μm	241 \pm 4	0.20 \pm 0.04	
2	2	18.5	0	1.5	0.015	0.8 μm	331 \pm 6	0.3 \pm 0.05	
3	2	25	0	1.5	0.015	0.8 μm	361 \pm 5	0.27 \pm 0.05	
4	2	37.5	0	1.5	0.015	0.8 μm	401 \pm 5	0.23 \pm 0.03	2.8x10 ⁴ \pm 0.3x10 ⁴
5	2	40	0	1.5	0.015	0.8 μm	331 \pm 5	0.26 \pm 0.02	

However, when those inks were dropped on glass slides to form ink films to measure conductivity with a 4-points probe, a new behavior occurred: during the drying process, ink particles migrated to the border of the film, making a final halo (Figure 19), displaying no conductivity behavior, or at least very high resistivity. The same effect was observed for ink dropped on soft polyurethane substrate, or silicon substrate. This phenomenon prevented the measurements of inks conductivity.

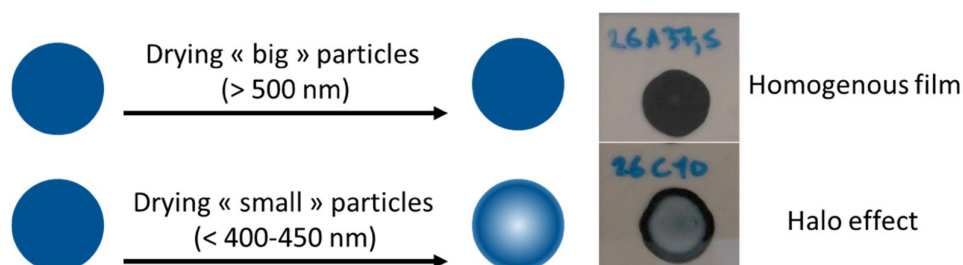


Figure 19. Halo effect during the drying of ink films.

Additional experiments with initial mixing, but without DBSA surfactant, were performed, varying [HAS-PBA + EDOT], volume fraction of acetonitrile and amount of catalyst (entries **6** to **10** in Table 8). Once again, it was observed that decreasing concentration resulted in smaller ink particles, from 800-1000 nm at 37.5 g/L to 300-400 nm at 10 g/L. Smaller ink particles were obtained when adding 10 vol% of acetonitrile, even at high concentration (entry 10). The presence of acetonitrile, like DBSA, seemed to decrease solvent surface tension, enabling lower particle size. Interestingly, the same halo effect on ink films was observed, even without DBSA, but only for ink with small particles below 450-500 nm. Inks with larger particles around 800-1000 nm displayed a resistivity around 1-10 k Ω/\square , consistent with the previously measured conductivity (Table 6, Ink **7**, $\sigma \approx 1.5$ S/cm for 2-10 μm thick films).

Table 8. Ink synthesis varying amount of catalyzer and acetonitrile concentration.

Entry	Synthesis parameters					Characterization			
	Ratio EDOT / HAS-PBA	[HAS ₄ -PBA _{0.3} + EDOT] (g/L)	Vol% MeCN	[DBSA] (g/L)	Equivalent FeSO ₄	Smaller filtration size	Z _{Average} (nm)	PDI	Resistivity (Ω/\square)
6	2	10	0	0	0.015	0.8 μm	411 \pm 14	0.36 \pm 0.04	2.4x10 ⁶ \pm 0.4x10 ⁶
7	2	10	0	0	0.005	0.45 μm	443 \pm 7	0.26 \pm 0.04	
8	2	37.5	0	0	0.015	0.8 μm	1004 \pm 22	0.42 \pm 0.06	1.5x10 ³ \pm 0.2x10 ³
9	2	37.5	0	0	0.005	0.8 μm	892 \pm 54	0.31 \pm 0.03	1.0x10 ⁴ \pm 1.2x10 ³
10	2	37.5	10	0	0.015	0.45 μm	385 \pm 2	0.17 \pm 0.02	7.6x10 ⁵ \pm 0.8x10 ⁵

Furthermore, this set of experiments showed that the halo effect was more likely due to ink particle size, rather than the presence of a surfactant.

Keeping in mind that ink conductivity should be as high as possible, additional inks with an EDOT/HAS₄-PBA_{0.3} ratio of 4 were synthesized (entries **11** to **17** in Table 9). Like for a molar ratio of 2, smaller ink particles were obtained when adding acetonitrile and/or DBSA, but the “halo effect” prevented the measurement of effective conductivity. Finally, ink synthesis at low concentration without DBSA or acetonitrile (entries **14** to **16**) yielded ink with particles with sizes around 650-800 nm, with coherent resistivity (1443-6469 k Ω/\square) compared to previous conductivity measurements (Table 6, Ink 7, $\sigma \approx 1.5$ S/cm for 2-10 μm thick films, corresponding to resistivity between 0.7 and 3.3 k Ω/\square). Interestingly, decreasing the amount of catalyst did not affect the particle size, but appeared to decrease their polydispersity index.

Table 9. Ink synthesis with a molar ratio EDOT/HAS-PBA of 4.

Entry	Synthesis parameters					Characterization			
	Ratio EDOT / HAS-PBA	[HAS ₄ -PBA _{0.3} + EDOT] (g/L)	Vol% MeCN	[DBSA] (g/L)	Equivalent FeSO ₄	Smaller filtration size	Z _{Average} (nm)	PDI	Resistivity (Ω/\square)
11	4	10	0	1,5	0,005	0,45 μm	306 \pm 6	0.25 \pm 0.01	
12	4	10	10	0	0,005	0,45 μm	251 \pm 6	0.29 \pm 0.02	
13	4	10	10	1,5	0,005	0,8 μm	490 \pm 5	0.26 \pm 0.00	
14	4	10	0	0	0,015	0,8 μm	763 \pm 15	0.33 \pm 0.04	1.4x10 ³ \pm 0.2x10 ³
15	4	10	0	0	0,005	1,2 μm	767 \pm 29	0.27 \pm 0.01	4.4x10 ³ \pm 0.3x10 ³
16	4	10	0	0	0,005	1,2 μm	680 \pm 19	0.25 \pm 0.04	6.5x10 ³ \pm 0.7x10 ³
17	4	10	0	0	0	Visible particle in suspension			

Conclusion

In summary to obtain monodisperse and reproducible PEDOT:HAS₄-PBA_{0.3} inks, with large enough particles to avoid the “halo effect” during film drying, no DBSA or acetonitrile should be added to the medium, the amount of FeSO₄ catalyst should be kept to the minimum (0.005 eq) to lower particle size polydispersity, and [EDOT + HAS₄-PBA_{0.3}] during polymerization should be around 10 g/L. Concerning the molar ratio EDOT/ HAS₄-PBA_{0.3}, increasing it from 2 to 4 resulted in a slight decrease of resistivity at equal particle size (entries **8** and **14**). Interestingly, it was observed that bigger ink particles resulted in lower resistivity: for example ink in entry **8** with a ratio EDOT/ HAS₄-PBA_{0.3} of 2 and 1004 nm wide particles displayed a lower resistivity of 1500 Ω/□ than ink in entry **16** with a ratio EDOT/HAS₄-PBA_{0.3} but 680 nm wide ink particle.

It is important to note that this new polymerization procedure with initial mixing was reproducible, as same particle size and polydispersity index were obtained on batches synthesized at different scales (from 50 mg to 650 mg, ink **16** and **17** in Table 9), contrary to first experiments without mixing.

III.4. Cytotoxicity using WST-1 assay

The cytotoxicity of PEDOT:HAS₄-PBA_{0.3} (ink **7**, Table 6) and its precursors (HAS₄-PBA_{0.3} in Table 5, HAS **8** in Table 4, and initial HA**113**) was assessed using a cell proliferation and viability WST-1 assay. Briefly, murine NIH3T3 fibroblast cells were cultured in a 96-well plate and adhered to the surface of the wells. Then, growth medium was removed and replaced by PEDOT:HAS₄-PBA_{0.3} ink **7**, HAS₄-PBA_{0.3}, HAS₄ **8** or initial HA**113** solubilized in PBS, at different concentrations (50 to 750 µg/L). After 24h of exposure, cell viability was measured using WST-1 assay, and compared to a negative control (cells alone), and a positive control (cells incubated 24h with H₂O₂).

A high fibroblast cells viability of incubated with PEDOT:HAS₄-PBA_{0.3} ink was observed at all concentrations, similarly to initial HA (Figure 20). Values above 100% indicate that pristine HA or the ink even slightly promoted cell proliferation in comparison to cells cultivated alone. This means that PEDOT:HAS₄-PBA_{0.3} ink appeared to be cytocompatible (IC₅₀ > 750 µg/mL,

where IC_{50} is the dose of cytotoxic compound at which 50% mortality is achieved) and even, enabled cell growth. Such results are in line with those reported by Mantione *et al.*^[11] for which L929 fibroblasts were incubated with PEDOT:GAGs inks, showing a 100% cell viability after 24h. Regarding both intermediates HAS_4 and $HAS_4-PBA_{0.3}$, cell viability was still above 80 % at the concentration of 750 $\mu g/mL$, demonstrating their very low cytotoxicity towards fibroblast cells.

On an indicative basis, the IC_{50} value of PEDOT:PSS was reported to be below 1000 $\mu g/mL$ ^[39].

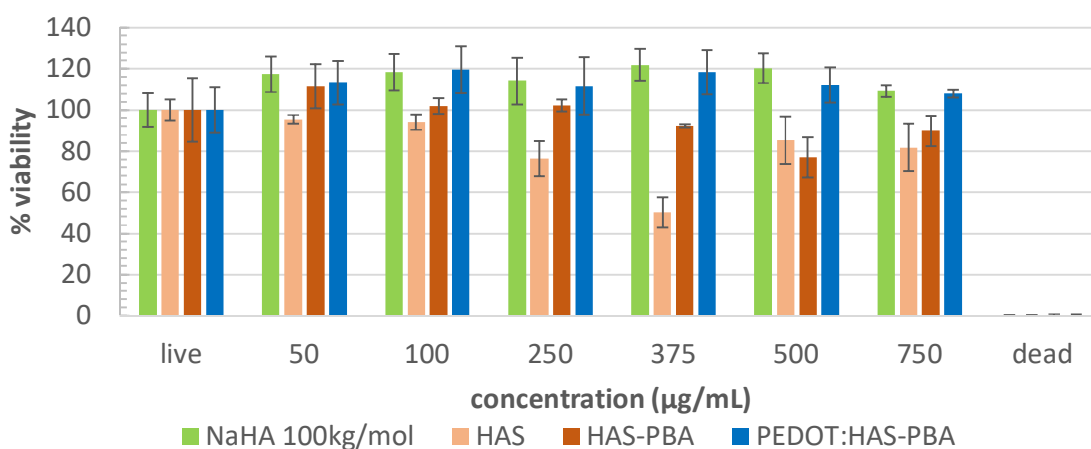


Figure 20. Cytotoxicity at 24h on NIH3T3 cells (WST-1) (n=3).

III.5. Extension of sulfate/PBA synergy to other GAGs

Previously, it was described how the simultaneous presence of both sulfates and PBA moieties resulted in a high intrinsic doping of PEDOT chains and a high conductivity. To confirm this synergy, additional inks were synthesized using another GAG: chondroitin sulfate.

ChS is a GAG with a structure close to HA, possessing one to two sulfates per repeating unit^[40] (Figure 1). Somehow, it can be considered as a sulfated HA with a controlled DS_s between 1 and 2. Specifications from the supplier indicated a DS_s of 1.5 for the ChS that was used. Using the same protocol than for HA, PBA moieties were grafted on ChS, resulting in $ChS-PBA_{0.3}$. To assess the influence of both sulfate and PBA, three new inks were synthesized

using the optimized ink polymerization protocol: PEDOT:HA, PEDOT:ChS_{1.5} and PEDOT: ChS_{1.5}-PBA. Particle size and conductivity were measured using the same methodology as described above (Table 10).

Table 10. Properties of additional inks based on ChS_{1.5}.

Ink	Sample name	Sulfation degree	DS in PBA	Z _{average} (nm)	PDI	σ (S/cm)
8	PEDOT:HA	0	0	541 ± 27	0.29 ± 0.01	
9	PEDOT:ChS	1	0	351 ± 16	0.30 ± 0.04	8.2x10 ⁻² ± 0.5x10 ⁻²
10	PEDOT:ChS-PBA _{0.3}	1	0.30	734 ± 76	0.62 ± 0.16	1.1 ± 0.2

As previously observed, **PEDOT:HA** ink **8** displayed no conductivity, as for PEDOT:HA ink **2**, confirming that the optimized polymerization protocol did not change the ink conductive properties. However **PEDOT:ChS_{1.5}** displayed a conductivity slightly above those of **PEDOT:HAS_{1.6}** (0.032 S/cm, ink 3 in Table 6), which is consistent as the sulfation degrees are similar. Interestingly, **PEDOT:ChS_{1.5}-PBA_{0.3}** ink displayed a conductivity of 1.078 S/cm, ~ 3 times higher than **PEDOT:ChS_{1.5}**. This sample demonstrates that the synergy between sulfate and PBA moieties to boost PEDOT:biomolecule conductivity is not restricted to HA but could also be observed for other glycosaminoglycans.

III.6. Conclusion

In this part, it was demonstrated that the presence of both sulfate functions and aromatic groups on a PEDOT dopant resulted in a synergistic effect, greatly improving the conductivity of the final PEDOT:dopant material. Thus, a new biocompatible PEDOT:HAS₄-PBA_{0.3} ink was synthesized, displaying a conductivity up to 1.5 S/cm. This ink was selected for the rest of this Ph.D. project.

The ink synthesis protocol adapted from literature^[7] was improved by adding an initial mixing step. This enabled to get a reproducible batch-to-batch ink particle size, regardless of the batch size. Besides, the ink particle size could be tuned by varying [dopant + EDOT] during polymerization.

The next step of this study consisted in adjusting the physico-chemical properties of the PEDOT:HAS₄-PBA_{0.3} ink in order to process it to create conductive tracks. Inkjet printing process of the material was investigated as described in the next section.

IV. Ink processing using inkjet printing

IV.1. Introduction

The next step was to process the PEDOT:HAS₄-PBA_{0.3} ink in order to fabricate conductive tracks on flexible substrates using inkjet printing.

IV.1.a. Choice of printing process

There is an abundant literature about the processing of PEDOT:PSS ink, as its physicochemical properties can be finely tuned to be adapted to several processes: ink surface tension, viscosity and wettability can be modified by adjusting PEDOT:PSS concentration, the pH, the ionic force of the solution, or by adding surfactants, cross-linkers or co-solvent^[41–43]. PEDOT:PSS is currently the most widely used conductive ink for the design of soft electronic devices. PEDOT:PSS films and patterns can be obtained by several methods: spin coating^[44], doctor blading^[41], spray coating, inkjet printing^[43,45], flexography, roll-to-roll printing^[46], lithography or electro-spinning^[47] (Figure 21).

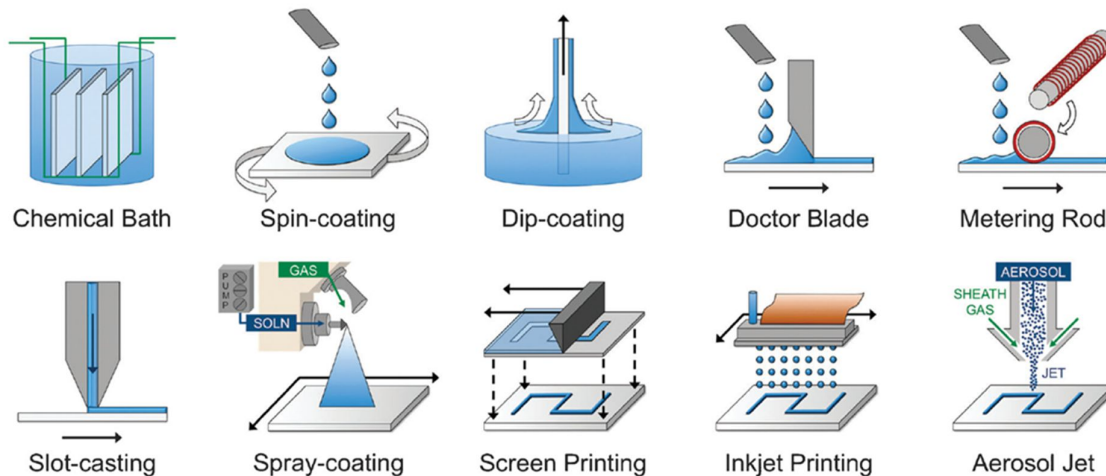


Figure 21. Scheme of various solution deposition methods, adapted from Pasquarelli et al.^[48].

However in this Ph.D. project, several physico-chemical parameters were constrained as the final designed material was intended for implantation in the brain. Therefore, physiological pH (pH \approx 7.4) and ionic strength should be matched with those of tissues (\approx 150 mM). Besides, additional restrictions were imposed by the small mass and volume of ink

available in this project. Printing techniques such as roll-to-roll printing, lithography, doctor blading, spray coating or spin coating require a large amount of printing material^[48,49], and a lot can be wasted during the process.

Those considerations led us to consider inkjet printing or extrusion printing as processing solutions. However, as PEDOT:HAS₄-PBA_{0.3} ink was fluid at working concentration (viscosity < 50 mPa.s at a shear rate of 10 s⁻¹ for concentration below 40 g/L), extrusion printing was dismissed as this technique requires high viscosity, around or above 1 Pa.s. Finally, inkjet printing was selected as a processing method.

IV.1.b. Inkjet printing with a Dimatix DMP-2800 series inkjet printer

Inkjet printing is the most widely used printing technology for domestic application worldwide. This printing technology relies on the propulsion of ink droplets from a reservoir to a substrate. Ink is pumped into a printing chamber, and is expelled through a nozzle, a few micrometer wide. This flow of droplets can be continuous (continuous inkjet (CIJ) technology), or droplets can be ejected one by one (drop on demand (DoD) inkjet technology). DoD printing enables to work on smaller ink volume, and avoid wastes as each ejected drop ends on the printing substrate.

As inkjet printing relies on the formation and expulsion of small droplets of ink through a nozzle a few micrometers wide, the ink must satisfy three key parameters to be printable:

- Ink pigment particles in suspension should be small enough to avoid clogging the nozzle;
- The ink must be fluid enough to be propelled through the nozzle at high speed and frequency without excess pressure, which could damage the printer or propelling system. However, it must not be too fluid as it may otherwise flow through the nozzle without control;
- Finally, ink surface tension must be adapted to the nozzle geometry in order to form round droplets without satellites behind, in order to have a good printing quality.

The inkjet printer available for this project was a Dimatix DMP-2800 series inkjet printer, from Fujifilm (Düsseldorf, Germany, Figure 22). This fully configurable printer is widely used in ink development projects^[41,41,42,50,51] as it enables to work with small volumes (0.5 – 2 mL) and a wide variety of solvents and pigments. It is a drop on demand (DoD) printer, using a piezoelectric transducer in the print-head which allows the user, depending on the cartridge, to create and eject 10 pL or 1 pL nominal drops by applying a time-varying voltage signal. This signal is converted into translational motion by the receiving piezo transducer (Figure 23), enabling a fine tuning of the ejection speed, volume, and amount of ejected ink.

The print-head offers 16 nozzles of 21 μm width. The number of firing nozzles, the firing frequency, the ejection speed and the print-head temperature can be controlled independently via the software. The time varying-voltage used to control the piezo material can also be adjusted. The printing substrate can be as large as A4 dimension, and control cameras enable to determine finely the printing origin.



Figure 22. Dimatix DMP-2800 inkjet printer.

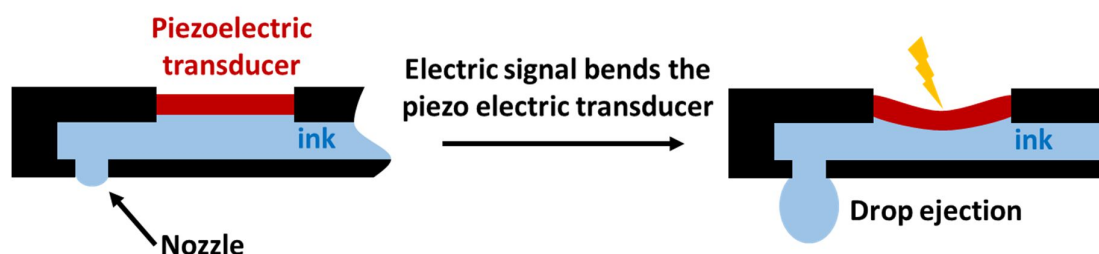


Figure 23. Drop on demand inkjet print-head.

Ink optimal physicochemical specifications for this printer are indicated by the manual:

- A surface tension between 28 and 33 mN/m;
- A viscosity between 10 and 12 mPa.s. Noticeably, no further specifications are given concerning the mode of viscosity measurement (such as the shear rate or the kind of geometry used in case of Brookfield viscometer);
- Particle size below 200 nm;
- pH between 4 and 9.

Thus, the previously designed PEDOT:HAS₄-PBA_{0.3} ink **4** (Table 7) was formulated to match these specifications.

IV. 2. Optimization of Ink physico-chemical properties

The physico-chemical properties (viscosity and surface tension) of pristine PEDOT:HAS₄-PBA_{0.3} ink **4** (Table 7) were first investigated to assess which physico-chemical parameters needed to be adjusted. The parameters to adjust those properties could be modified independently, but their effects on ink physico-chemical, structural and conductive properties were interconnected. Therefore, an experimental design was implemented.

IV.2.a. Pristine ink physico-chemical properties

PEDOT:HAS₄-PBA_{0.3} **4** (Table 7) was dissolved at 20 g/L in water and pH adjusted to 7.4 with 0.1 M NaOH.

Viscosity

Viscosity measurements were performed on a cone-plate AR2000 rheometer (section VII.2.i.). At this concentration and at room temperature, ink **4** exhibited a shear thinning behavior with a minimum viscosity of 1.8 mPa.s at 10 s⁻¹ (Figure 24a). To meet Dimatix printer specifications, dynamic viscosity should be increased to 10-12 mPa.s. Increasing ink concentration above 20 g/L or addition of glycerol could be a solution to increase viscosity. Moreover, glycerol may also increase ink boiling point to prevent nozzle clogging as glycerol boiling temperature is very high (T_{eb} = 290°C).

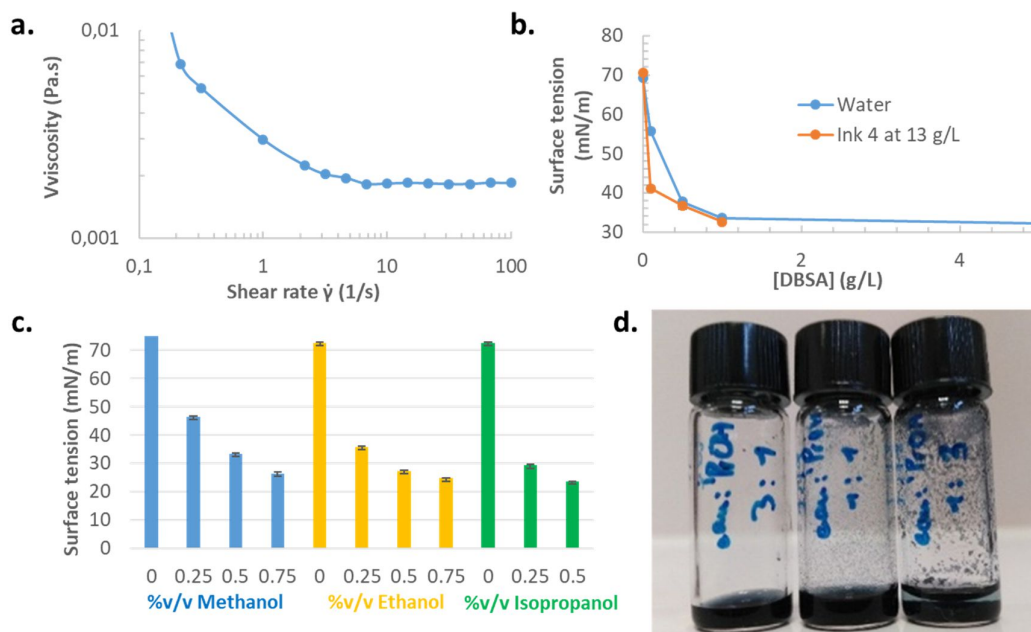


Figure 24. Physico-chemical properties of ink 4. a. Viscosity versus shear rate of PEDOT:HAS-PBA ink 4 at 20 g/L at 25°C. b. Surface tension of water or PEDOT:HAS-PBA ink 4 containing DBSA. c. Surface tension of PEDOT:HAS-PBA ink 4 at 20 g/L with various alcohols as co-solvents. d. Formation of large ink particles as isopropanol volume fraction in water increases (from left to right: 25, 50 and 75 vol% of isopropanol).

Surface tension

Surface tension measurements of ink 4 at 20 g/L in water performed with the pending drop technique indicated a surface tension of 70.4 ± 0.8 mN/m (Figure 24b), namely almost the surface tension of water at room temperature (72.0 mN/m at 25°C). The presence of PEDOT:HAS₄-PBA_{0.3} in water did not seem to affect too much the surface tension of the solvent.

A first attempt to lower the surface tension to targeted values around 30 mN/m was to use an alcohol as a co-solvent of the aqueous dispersion of PEDOT:HAS₄-PBA_{0.3} (Figure 24c), as low molar mass alcohols display low surface tensions ($\gamma_{\text{methanol}} = 22.6$ mN/m, $\gamma_{\text{ethanol}} = 22.27$ mN/m, $\gamma_{\text{isopropanol}} = 21.7$ g/L). Those three alcohols are used in some laser printed inks, as there are volatile and lower surface tension. PEDOT:HAS₄-PBA_{0.3} was dissolved in water:alcohol 75:25, 50:50 and 25:75 v:v, and an effective decrease of surface tension was observed (Figure 24c).

However, the presence of alcohol with low electric permittivity ($\epsilon_{\text{water}} = 80.1$, $\epsilon_{\text{methanol}} = 32.7$, $\epsilon_{\text{ethanol}} = 24.5$ and $\epsilon_{\text{isopropanol}} = 17.9$) was detrimental to the PEDOT:HAS-PBA ink which

formed large aggregates, visible with naked eye, that sedimented in a few hours (Figure 24d). This was incompatible with inkjet printing as too large particles would have clogged the print-head nozzles.

Finally, the use of surfactant was tested to decrease the surface tension of the ink. Dodecylbenzene sulfonic acid (DBSA) was selected since it is already widely used in the field of printable electronic, especially with PEDOT:PSS^[41,42,52,53]. Although pure DBSA appears to be toxic and corrosive, previous studies performed at L2CB have demonstrated that the addition of DBSA in conducting materials did not induce cytotoxicity if washed thoroughly^[16]. Indeed we observed that adding DBSA enabled to lower water surface tension, even at low concentrations (Figure 24b, critical micellar concentration (CMC) = 0.819 g/L at 25 °C and γ_{water} with [DBSA] at CMC = 36.09 mN/m^[54]).

In summary, these physico-chemical characterizations led us to conclude that the viscosity of PEDOT:HAS₄-PBA_{0.3} solution should be increased, by increasing PEDOT:HAS-PBA concentration or adding glycerol. Besides, the surface tension of PEDOT:HAS₄-PBA_{0.3} solution should be decreased, using DBSA as a surfactant. Moreover, during ink formulation, focus should be kept on particle size to keep the ink printable, as the impact of additives incorporation on particle aggregation was unknown. Finally, the ink conductivity should be maximized. A possibility to achieve this goal could be to increase the EDOT/HAS₄-PBA_{0.3} ratio.

IV.2.b. Experimental design and formulation optimization

To optimize PEDOT:HAS₄-PBA_{0.3} ink physicochemical properties (surface tension, viscosity, particle size), while maximizing final printed tracks conductivity, an experimental design was implemented. This work has been done in collaboration with Luc Choisnard from the Molecular Pharmaco-Chemistry department of University Grenoble Alpes. The aim of this experimental design was to establish mathematical prediction models which enabled to predict the outcome values of surface tension, viscosity, ink particle size and ink conductivity as a function of independent input variables. The input variables were ink concentration (A), DBSA surfactant concentration (B), EDOT/HAS₄-PBA_{0.3} molar ratio during ink polymerization (C) and addition of glycerol (D).

These input parameters could be controlled independently from one another, but their respective effects were interdependent. Indeed, while glycerol mainly has an effect on ink volatility and viscosity, and DBSA mainly has an effect on surface tension, both may affect the micro structuration of the printed conductive tracks once dried. Indeed, in the literature, glycerol can be used as a secondary dopant to increase PEDOT:PSS conductivity^[44,55–58], and DBSA can be used as a dopant of PEDOT^[59], or as secondary dopant as its presence affects the microstructure of the dried film^[53]. Besides, changing the EDOT/HAS₄-PBA_{0.3} ratio has an effect on both particle size and conductivity.

Briefly, an experimental design in 21 experiments was implemented as described in the experimental section, and enabled to obtain prediction models for all physicochemical parameters (surface tension (R1), viscosity (R2), ink particle size (R3) and resistivity (R4)), where each of the response could be defined as a function of the reduced entry factors (Table 11).

Table 11. Prediction models obtained from the analysis of experimental data. *a*, *b*, *c* and *d* are reduced entry factor obtained from entry factor *A*, *B*, *C* and *D* with a mathematical transformation which eased data treatment (see experimental section for details).

Response	Name	Units	Target	modelled response	R ²	Predicted R ²
R1	Surface tension	mN/m	[27-32] mN/m	$R1 = 39,419 + 2,61649a - 1,21673b + 1,63065c + 1,20239ac + 0,95691b^2 - 2,14922c^2$	0.9373	0.8705
R2	Viscosity	mPa.s	≈ 10 mPa.s	$1/\text{Sqrt}(R2) = 0,368901 - 0,186116a - 0,00108652b - 0,03594c - 0,0179638d - 0,0338625ac - 0,00490352bc - 0,0208548bd + 0,0162035a^2 + 0,0638737c^2 + 0,0132498d^2$	0.9991	0.9963
R3	Z _{average}	nm	< 500 μm	$\text{Ln}(R3) = 7,57144 - 0,0136538a + 0,838918c + 0,268876a^2 - 0,77394c^2$	0.919	0.8745
R4	Resistivity	Ω/□	As low as possible	$R4^{0.34204} = 859.4 - 3.918A + 81.4B - 945.8C + 0.0181A^2 + 274C^2 + 1.385AB + 0.790AC - 61BC$	0.9910	0.9027

For all responses, signal/noise ratio was superior to 4, and R² correlation coefficient was close to 1, with a difference with predicted R² below 0.2. Therefore, the calculated prediction models relevantly fitted the measured data. Prediction models for viscosity, conductivity and surface tension were statistically validated with complementary experiments.

However, the prediction model calculated for particle size could not be validated. This was attributed to the poor quality data sets used to establish it, with high ink particle size and

high polydispersity index, due to lack of batch-to-batch reproducibility. Indeed, this experimental design was implemented before the optimization of the PEDOT:HAS₄-PBA_{0.3} synthesis protocol described beforehand in section III.3. of this chapter, and was the reason for us to conduct this optimization.

The experimental design however allowed us to conclude that:

- Optimal ink concentration was calculated to be [PEDOT:HAS₄-PBA_{0.3}] = 31.2 g/L.
- The surface tension corresponding to the maximum DBSA concentration explored in the experimental design (1 g/L) resulted in surface tension around 39 mN/m, still too high in regards of Dimatix specifications. Complementary measurements were made: DBSA concentration of 1.5 g/L yielded to surface tension around 34 mN/m, and of 2 g/L to surface tension around 33 mN/m.

Besides, all prediction models exhibited that the initial volume fraction of glycerol only had a minor impact on viscosity. Optimal ink glycerol volume fraction were calculated at 2.3 vol% as too little glycerol resulted in crackled dried ink films, while too much glycerol resulted in films that did not dry well, preventing the measurement of conductivity.

Concerning the EDOT/HAS₄-PBA_{0.3} molar ratio during ink polymerization, the experimental design exhibited that ratio below 2 resulted in too low conductive inks. It was set at 2 or more for ulterior experiments.

Based on these results, PEDOT:HAS₄-PBA_{0.3} inks were formulated in water at 31.2 g/L, with 2.3 vol% of glycerol and 2 g/L of DBSA, for further inkjet-printed experiments with using the Dimatix DMP-2800 inkjet printer previously described.

IV.3. Inkjet printing with Dimatix DMP 2800 inkjet printer

PEDOT:HAS₄-PBA_{0.3} inks were formulated with different additives (DBSA, glycerol), and sonicated 30 seconds in an ultrasound bath, then vortexed right before printing. 500 µL to 1 mL of ink was charged in the cartridge using a syringe, the print-head was clipped on the cartridge, and the whole system plugged in the printer. Different PEDOT:HAS₄-PBA_{0.3} inks with different particle sizes and EDOT/HAS₄-PBA_{0.3} ratio were investigated (Table 12).

In first experiments, it was just assessed whether the ink could be printed or not, without consideration of printing quality, printing resolution, or wettability of the surface. Inks were printed on soft polyurethane films.

Formulation **1** (Table 12) with a surface tension of 33.3 mN/m was printable, but nozzles clogged quickly, as particle were very large (1704 nm). Inks with various particle size ranging from 334 nm to 1095 nm, and polydispersity index below 0.27 (Formulations **2** to **5**), could be printed. However, formulation **6** with a high polydispersity (0.89) could not be printed.

Table 12. Various formulation of PEDOT:HAS₄-PBA_{0.3} ink for inkjet printing. Glycerol was added in all formulations at a concentration of 2.3 vol%.

Formulation	ratio EDOT/HAS ₄ -PBA _{0.3}	[DBSA] (g/L)	Surface tension (mN/m)	Z _{average} (nm)	PDI	Printable?
1	2	2	33.3 ± 0.3	1704 ± 135	0.38 ± 0.03	V for few minutes
2	2	1.5	28.8 ± 0.4	334 ± 3	0.2 ± 0.03	V
3	4	2	31.8	680 ± 14	0.25 ± 0.03	V
4	2	2	32.1 ± 0.5	767 ± 27	0.27 ± 0.01	V
5	4	2	32.0	1095 ± 69	0.26 ± 0.04	V
6	4	2	34.6	1155 ± 188	1.00 ± 0.0	X

Various patterns were then printed to measure the conductivity of printed tracks. The 4-points probe was used to measure track sheet resistivity (as the substrate was soft, the thickness of the track was not measured, and thus tracks conductivities could not be obtained). In the 4-points probe software, sample geometric parameters are required to take border effect into account, as sheet resistivity would vary depending on surface dimension. However the software could not consider the dimension of straight thin tracks (5 to 6 mm long, and 0.2 mm large), and crashed systematically: these parameters were set by default to a rectangular sample of 15 by 20 mm. As a result, tracks sheet resistivity reported below do not take into account the small width of the tracks. Real effective resistivity might be much lower.

To start, the pattern “Dimatix Antenna” was printed using formulation **5** (1095 nm particles, to investigate high particle size printability) on a soft polyurethane film using 14 out of 16 nozzles, superimposing 5 successive layers. Vertical printed tracks displayed irregularities, with visible separated dots (Figure 25a). As Dimatix printer prints patterns line by line, horizontally, this was attributed to a clogged nozzle. On the other hand, horizontal

lines were continuous. Resistivity of zones 1 and 2 (Figure 25a) were much higher ($\sim 10^5 \Omega/\square$) than values obtained for non-formulated PEDOT:HAS₄-PBA_{0.3} on a glass slide ($\sim 0,5-1 \text{ k}\Omega/\square$). Probing the central zone 3 yielded resistivity just slightly higher than values obtained for PEDOT:HAS₄-PBA_{0.3} (Figure 25c). In addition to the absence of geometric correction due to software limitations, the high resistivities were attributed to the low thickness of printed tracks.

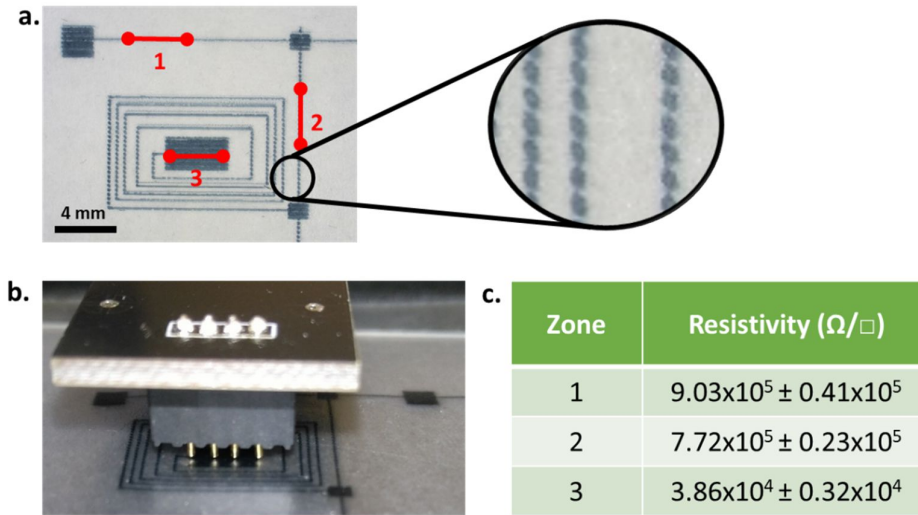


Figure 25. Measurement of track resistivity using 4-point probe. a. Pattern "Dimatix Antenna". b. 4-points probes on printed tracks. c. Track resistivity for the different track sections.

In order to decrease track resistivity, additional tracks were printed with formulation **4** to evaluate the influence on conductivity of EDOT/HAS₄-PBA_{0.3} ratio (EDOT/HAS₄-PBA_{0.3} ratio = 2 for formulation **4** and 4 for formulation **5**), and particle size (767 nm for formulation **4** and 1095 nm for formulation **5**, Figure 26). Several tracks with 160 μm width set value were printed, increasing progressively the number of layers. As the number of printed layers increased, the printing resolution decreased, resulting into wider tracks (Figure 26a).

However, even with a high number of ink layers, resulting in a low printing resolution incompatible with the printing of 100 μm wide tracks for a medical device, the resistivities remained very high in comparison to values obtained for non-formulated PEDOT:HAS₄-PBA_{0.3} dried ink films on glass slide ($\sim 0,5-1 \text{ k}\Omega/\square$).

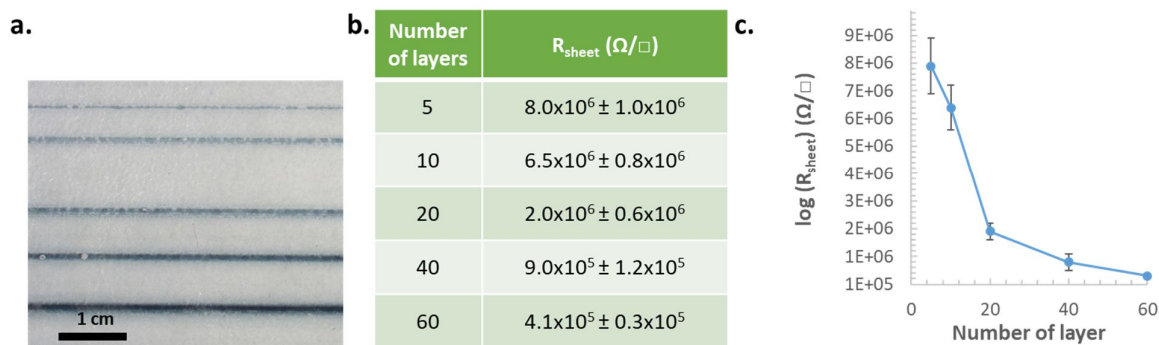


Figure 26. a. Printed lines with increasing number of layers. b. Number of ink layers and corresponding sheet resistivity. c. Sheet resistivity according to number of ink layers.

To understand this observed high film resistivity, structural analysis of PEDOT:HAS₄-PBA_{0.3} printed tracks were performed.

IV.4. Characterization of film structure

Printed tracks were analyzed by scanning electron microscopy (SEM) to observe their structure (Figure 27). Ink **4** (764 nm particle diameter) was printed on a silicon substrate (to get maximum planarity). 50 layers were printed at once and dried overnight in a clodes petri dish at room temperature. The track width set value was 160 μm , but the effective width of the tracks were around 500 μm , exhibiting that successive ink layers flowed on each other, widening the tracks. Plus zoomed picture displayed some granularity, in accordance with DLS measurements that reported ink particles around 767 nm diameter (Table 12).

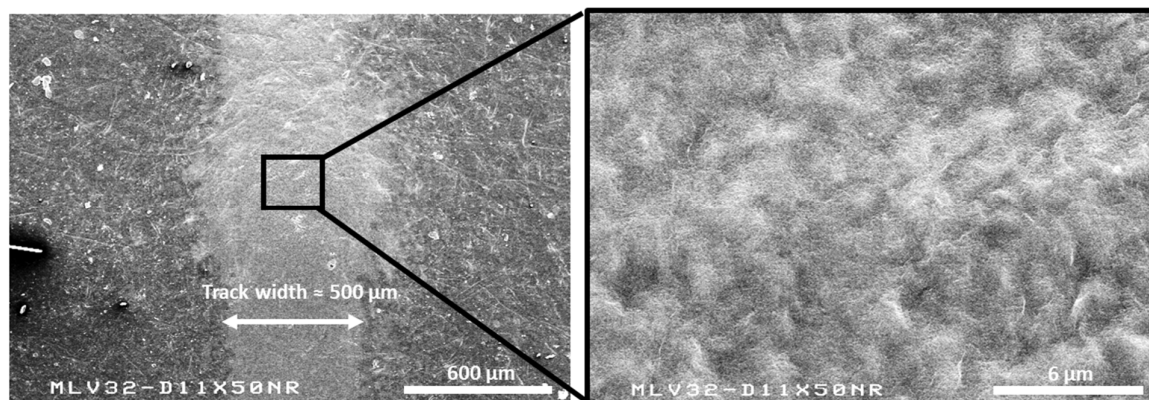


Figure 27. SEM picture of printed inks **4**, 50 successive layers. Left: zoom X50 right: zoom X5000.

IV.5. Conclusion

The developed PEDOT :HAS₄-PBA_{0.3} ink was formulated with a surfactant and glycerol in water to tune its surface tension and viscosity to process it using inkjet-printing. The formulation was established with the help of an experimental design. Yet, the latter could not be exploited to the fullest due to a lack of batch-to-batch reproducibility concerning the ink particle size, and wide particle size polydispersity.

This issue led us to optimize the ink synthesis protocol previously described in section III.3. of this chapter, implementing a mixing step at the beginning of the polymerization reaction. Unfortunately, due to lack of time, this experimental design was not implemented again once this issue solved, but could have led to a deeper understanding of ink physico-chemical properties.

The ink was printed with a Dimatix inkjet printer, and led to tracks with high resistivity. This issue could be solved optimizing the printing protocol and drying of the printed pattern.

V. Discussion

In this chapter, the chemical modification of hyaluronic acid was reported (sulfation and grafting of an aromatic group), leading to different HA derivatives with controlled degradation properties. The ability of these derivatives to efficiently dope PEDOT was investigated, and the resulting inks were formulated in order to be processed using inkjet printing.

V.1. HA sulfation

In the literature, HA has been sulfated to increase its interaction with growth factors (human bone morphogenetic protein-4^[27] or TGF- β 1^[30]) or with rSDF-1 α protein^[25], to develop antiherpetic activity as sulfation degree increases antiviral properties of HA^[28], or to slow down its biodegradation as sulfates may hinder enzymatic activity^[26]. In all these studies, HA was sulfated using two main sulfur trioxide complexes as sulfating reagents: SO₃-Py complex, and SO₃-DMF complex. As pyridine is a stronger Lewis base than DMF, SO₃-Py is less reactive than SO₃-DMF. Therefore, SO₃-Py was used to achieve low sulfation degree ($0.2 < DS_s < 1.9$), and SO₃-DMF was used to achieve higher sulfation degree ($0.4 < DS_s < 3.5$) (Table 13).

Although sulfation conditions and purification procedures varied from one publication to another, all of them pointed out important chain degradation after sulfation. Therefore, high molar mass HA ($M_w \sim 1 \times 10^6$ g/mol) had been used in many studies to obtain sulfated HA derivatives with $M_w \sim 30$ -70 kg/mol (Table 13).

Table 13. Sulfation reaction in literature.

Reference	Aim of sulfation	Mw _i (kg/mol)	Sulfating agent	Excess	Time and T	Purification	DS _s	DPw _f /DPw _i
Feng <i>et al.</i> ^[26]	Slow down enzymatic degradation	380	SO ₃ -DMF	20	24 h at r.T.	Dialysis vs water	0.4	NP
			SO ₃ -Py	7	20 min at r.T.		0.2	
Purcell <i>et al.</i> ^[25]	Increase protein binding affinity	440	SO ₃ -DMF	20	1 h at r.T.	Precipitation in acetone, neutralization with NaOH in EtOH, washing with acetone, and dialysis vs water	2.8	0.11
Hintze <i>et al.</i> ^[27]		1100	SO ₃ -DMF	20	1 h at r.T.		2.8	0.04
			SO ₃ -Py	7	20 min at r.T.		1	0.02
Kunze <i>et al.</i> ^[30]		1150	SO ₃ -DMF	20	time not precised. at r.T.		2.8	0.04
		1150	SO ₃ -Py	7			1	0.02
Möller <i>et al.</i> ^[28]	Increase antiviral activity	1000	SO ₃ -DMF	20	1 h at r.T.		3	0.03
			SO ₃ -Py	7	20 min at r.T.		1.5	0.01
		130	SO ₃ -DMF	20	1 h at r.T.		3.2	0.16
			SO ₃ -Py	7	20 min at r.T.		1.9	0.07

In this work, we developed new sulfation conditions and a purification procedure which resulted in much lower chain degradation ($DPw_f/DPw_i \sim 0.67$) in addition to higher sulfation degree ($DS_s = 4$) for the same amount of sulfating agent (20 eq of SO₃-DMF) compared to HA. To the extent of our knowledge, this is unprecedented.

The increase of sulfation degree was attributed to the basic quenching of sulfation reaction, neutralizing the formed sulfuric acid when water was added^[31], according to the following reaction: $SO_3 + H_2O \rightarrow H_2SO_4$. As concentrated sulfuric acid can also be used as a de-sulfating agent for polysaccharides^[31,32], this could explain why literature protocols based on pure water quenching and hence on the production of sulfuric acid result in lower DS_s . HA **478** sulfated at room temperature for 1h with 20 equivalents of SO₃-DMF (Table 2, HA **1**) displayed a chain degradation DPw_f/DPw_i of 0.17, relevant with the chain degradation of same molar weight HA in the publication of Purcell *et al.*^[25] ($DPw_f/DPw_i = 0.16$), but with a much higher sulfation degree (4 in our case, versus 2.8 in Purcell work).

The decrease of chain degradation we observed may be due to the cold reaction temperature we used (4°C), slowing down the kinetics of HA hydrolysis (Table 3).

Our optimized protocol could enable to design highly sulfated HA with low chain degradation to promote even more protein binding affinity, or antiviral activities. Furthermore, the better control on both chain length and sulfation degree is promising as it could allow the development of HA derivatives with controlled enzymatic degradability.

V.2. Enzymatic biodegradability

In physiological conditions, hyaluronic acid is depolymerized by hyaluronidase (HAase), which can be found in different species. These enzymes cleave the β 1,4-glucosaminidic bond between glucosamine and glucuronic acid^[60], leading to the formation of a N-Acetyl-glucosamine reducing end (Figure 11). Tam and Chan^[61] reported in 1985 that testes HAase degrades HA, producing multiple intermediates like tetra or hexasaccharides.

Hyaluronidases can degrade HA quickly, but are also able to degrade chondroitin sulfate (ChS), albeit at slower rate^[62]. This decrease of degradation rate can be attributed to the presence of bulky sulfate groups on the polysaccharide backbone^[26,63]. They limit enzyme access to the polysaccharide chain, since HAase needs a pristine HA octasaccharide to bind to HA^[26,64].

In this work, sulfates were expected to increase HA backbone acidity to dope efficiently the PEDOT chains, but also to slow down the biodegradation. Feng *et al.*^[26] showed that the more sulfated HA is, the slower it will be degraded by HAase; in their study, HA sulfation degrees of 0.21 and 0.40 resulted in a total degradation in 7 and 14 days respectively^[26] versus a few hours for pristine HA. In our case, we targeted a lifespan of 2 to 3 months for the resorbable medical device ; so we aimed for high HA sulfation degree.

Sulfated HAS **8** and **21** with sulfation degree of 4 and 2.2 respectively (Table 3 and Table 4), were incubated at 37°C in ammonium acetate buffer at 5 mM pH 5, to maximize the activity of HAase, according to the work of Asteriou *et al.*^[33]. The degradation of sulfated HA were monitored over time measuring the chains average molar weight using SEC-MALS (Figure 12). It was observed that the degradation rate of sulfated HA, with or without HAase, were more important than the degradation of pristine HA without HAase, but less important than the degradation of pristine HA with HAase. Besides, the degradation rate of sulfated HA were independent of HAase presence and concentration.

These observations indicated that the sulfated HA was not degraded by enzymatic reactions, but by auto-hydrolysis. This could be attributed to the sulfates, which could contribute to hydrolytic auto-cleavage of the β 1,4-glucosaminidic bond between glucosamine and glucuronic acid, as it has been observed in other sulfated polysaccharides such as carrageenan^[32].

Regarding the lack of HAase activity on sulfated HA, it was first assumed that the sulfate groups on HAS backbone prevented the HAase/HAS complex to form as HAase needs an available unmodified HAS octasaccharide substrate to bind to HA^[64]. However, the SEC-MALS chromatograms for all samples incubated with enzymes displayed an important signal in light scattering before the signal of the differential refractometer, suggesting the formation of large aggregates during the incubation (Figure 28). This fact suggested complexation of HAase and sulfated HAS during incubation, inhibiting all activity of HAase as it was bound to sulfated HAS likely due to electrostatic interactions. Indeed, sulfated glycosaminoglycans are known to bind proteins^[40].

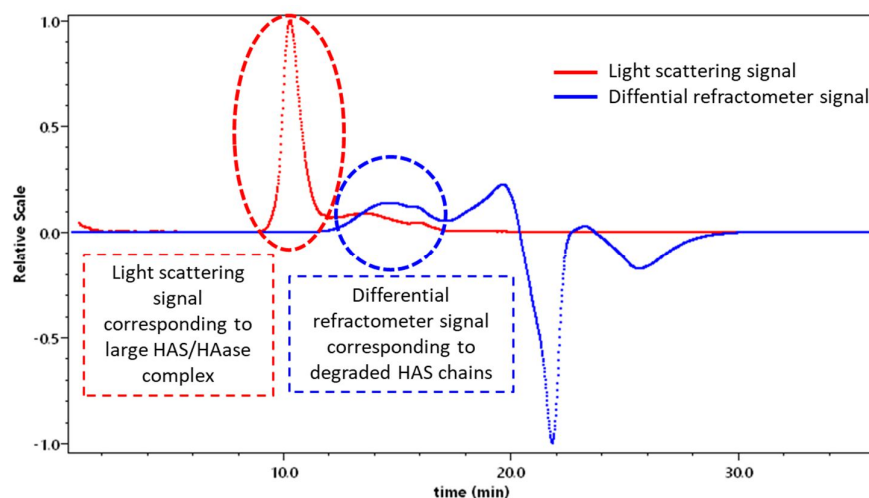


Figure 28. SEC-MALS chromatogram of HAS 21 incubated with HAase 4 weeks in ammonium acetate 5 mM pH 5 at 37°C.

In conclusion we developed a protocol with low HA degradation during HA sulfation, and a HAS degradation of $65 \pm 10\%$ in three months. Noticeably, we demonstrated that sulfated HA is degradable, but not biodegradable as its degradation results from auto-hydrolysis and not enzymatic hydrolysis. HAS₄ was adapted to the design of a conductive PEDOT-based ink with controllable degradation time.

V.3. Development of highly conductive PEDOT:HAS-PBA ink

The use of biomolecules to dope PEDOT enables to design more biocompatible and bioactive PEDOT:biomolecule conductive inks than PEDOT:PSS, but to the detriment of conductivity. To the best of our knowledge, only DNA^[9,10] and DexS^[7] based PEDOT inks have displayed conductivity > 1 S/cm (Table 1). This can be attributed to the acidity of their negative groups (phosphate groups ($pK_a \approx 2.15$) on DNA, and sulfate groups ($pK_a \approx 2$) on DexS), which make them negatively charged even at low pH, increasing electrostatic interactions with positively charged doped PEDOT domains.

However, additional work highlighted that simply increasing the amount of negative charges by adding chemical groups like sulfates on a biomolecule was not enough to increase the PEDOT:biomolecule final conductivity. Horikawa *et al.*^[14] sulfated cellulose to make it more GAG-like in order to design more biocompatible PEDOT:sulfated cellulose ink. Though they observed that sulfated cellulose yielded more conductive ink than pristine cellulose, an optimal degree of sulfation was to be found. They concluded that the electrical conductivity of PEDOT/sulfated cellulose tended to increase with the crystallinity of the cellulose as PEDOT chains could line up around the rigid cellulose chains and crystallize easily. Too much sulfate groups on cellulose chain could hinder the crystallization process. Their conclusions were consistent with the work of Takano *et al.*^[65] in which the authors demonstrated using X-ray scattering that more crystallized PEDOT domain yielded more conductive PEDOT-based material.

Increasing PEDOT degree of organization while maintaining its close contact with its dopant to counter balance its positive charges results in an increase of conductivity. This close PEDOT/dopant contact could be achieved via π -stacking with aromatic groups on dopant chains, as it is the case for PEDOT:PSS.

In this work, we introduced both sulfate groups and aminophenylboronic acid moieties on HA, to increase its acidity and global negative charge, as well as its hydrophobic and π -stacking interactions with PEDOT. We demonstrated that the introduction of sulfate or PBA moieties alone on a HA chain resulted in almost no conductivity enhancement of

PEDOT:HA_{derivative} ink (σ (**PEDOT:HAS_x**) = 0.032-0.016 S/cm for $x = 1.6-4$, and σ (**PEDOT:HA-PBA_{0.3}**) = 0.0035 S/cm, Table 6). In contrast, the simultaneous introduction of both sulfate and PBA resulted in a high increase of conductivity, up to 2 S/cm. This synergy was observed on another GAG, natural ChS ($DS_S = 1.5$). The **PEDOT:ChS_{1.5}** ink displayed a conductivity of 0.082 S/cm, whereas the **PEDOT:ChS_{1.5}-PBA_{0.3}** ink displayed a conductivity of 1.078 S/cm, showing a synergetic effect of sulfate and PBA to enhance PEDOT:biomolecule conductivity.

To the best of our knowledge, the introduction of aromatic moieties on biomolecules to design new PEDOT bio-dopants has never been described in the literature. This work highlights the potential of this strategy, and could enable to develop even more conductive PEDOT:biomolecule inks, that could compete with PEDOT:PSS inks.

V.4. Optimization of the polymerization process

The procedures reported for synthesis of the PEDOT:biomolecule inks are all derived from the same procedure described by Harman *et al.*^[7]. Briefly, the bio-dopant is dissolved in water, then EDOT is added, the medium is stirred vigorously, and finally the oxidant is added. When polymerization is completed, the medium is either purified by dialysis against water, or by centrifugation^[16]. These works characterize the final inks as particle suspensions, without further investigation of their structure, except the measurement of particle size.

It is generally accepted that during polymerization of EDOT with PSS, a PEDOT-rich core composed of 6 to 18 repeating units long PEDOT chains, surrounded by a PSS-rich outer shell is formed.^[66] Water removal results in a solid-state nanostructure that resembles this core-shell structure. For instance, Lang *et al.*^[67] studied PEDOT:PSS films by bright field transmission electron microscopy (TEM) and high angle annular dark field scanning TEM. They showed that PEDOT:PSS suspension after polymerization was constituted of particles from 30 to 50 nm, resulting from the aggregation of several tangles, where each tangle was composed of a single PSS chain with several PEDOT domains attached to it (Figure 29). Particles of PEDOT are thus stabilized in aqueous solution by PSS (Figure 29). The size of the final ink particles thus partly depended only on the used polyelectrolyte and its physico-chemical properties.

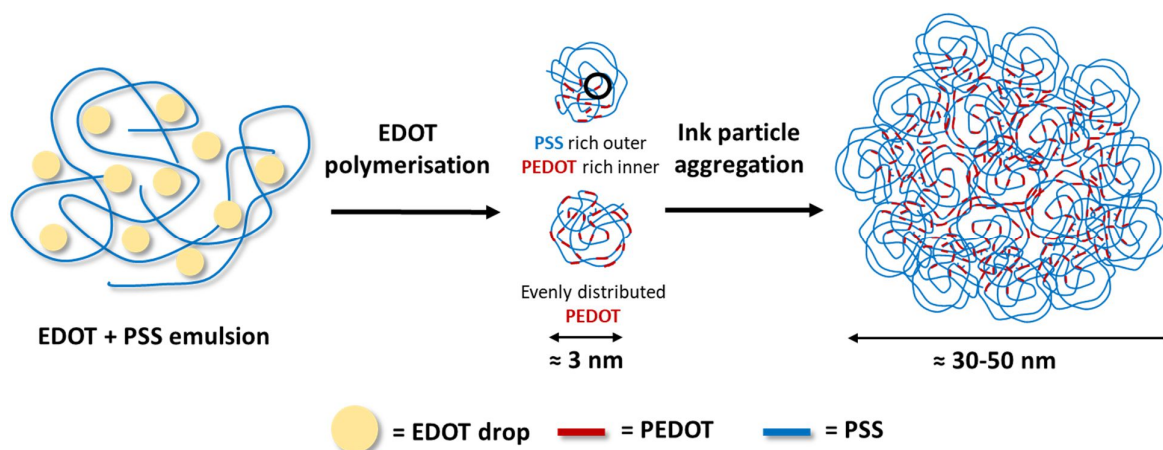


Figure 29. Molecular scheme of PEDOT:PSS ink particle formation according to work from Lang et al.^[67].

In this PhD thesis, the oxidative polymerization of EDOT in the presence of HAS₄-PBA_{0.3} had to be optimized to obtain aqueous dispersions of PEDOT:HAS₄-PBA_{0.3} particles with controlled sizes and high reproducibility. In this regard, we showed that the final ink suspension parameters (particle size and polydispersity) were highly dependent on reaction medium surface tension, concentration and homogenization. Initial mixing of the EDOT + dopant dispersion enabled batch-to-batch reproducibility, regardless of reaction scale-up, in addition to a strong decrease of polydispersity. Moreover, decreasing medium surface tension using either a surfactant or a polar co-solvent with low surface tension, and medium reagents concentration, enabled to reduce particle size.

Based on these observations, we assumed that final PEDOT:HAS₄-PBA_{0.3} ink particles consist of PEDOT clusters entangled and stabilized by HAS₄-PBA_{0.3} chains (Figure 30).

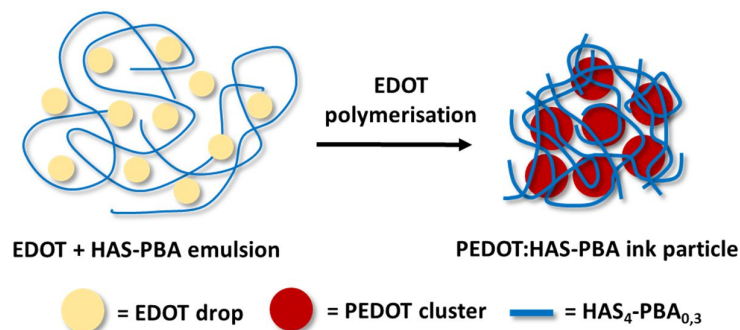


Figure 30. Assumed molecular scheme of PEDOT:HAS₄-PBA_{0.3} ink particle formation.

The identification of the parameters impacting PEDOT:HAS₄-PBA_{0.3} particle size enabled us to finely tune the PEDOT:HAS₄-PBA_{0.3} particle size, making this PEDOT:HAS₄-PBA_{0.3} ink suitable for various processing, such as inkjet printing. Usually, PEDOT:biomolecules inks are processed by electrospinning^[47], drop casting^[10–12], spin coating^[7] or extrusion printing^[7]. To the best of our knowledge, this work reports the first printing of a conductive biocompatible PEDOT-based ink using a GAG as a dopant of PEDOT. Beforehand, only Harman *and al.*^[7] have reported inkjet printing of a PEDOT:DexS ink. Noticeably, they did not reported the conductivity of the printed tracks.

To the best of our knowledge, the only work reporting the conductivity of printed PEDOT:PSS tracks without secondary doping or other treatments is the publication of Mire *et al.*^[43] in which they printed commercial PEDOT:PSS on different substrates. When printed on glass, the 80 μm wide and 0.7 μm thick tracks displayed a conductivity of 2.8 S/cm. When printed on a soft chitosan-HA free standing film, the tracks were 40 μm wide and 1.2 μm thick with a conductivity of 0.7 S/cm, corresponding to a 2 cm long track resistance of ≈ 400 k Ω . This value is comparable with what was obtained for 60 layers of printed PEDOT:HAS₄-PBA_{0.3} ink ($R_{\text{sheet}} \approx 410$ k Ω/\square). Our ink is competitive. Noticeably, those conductivities are far below those reported for PEDOT:PSS when secondary doping process are implemented.

VI. Conclusion

In order to develop a new PEDOT-based conductive and resorbable ink, hyaluronic acid was modified to design an efficient PEDOT dopant displaying biocompatibility and degradability.

In this project, we developed a new sulfation protocol of HA with enhanced sulfation yield combined with lower HA chain degradation than reported in the literature. Several sulfated HA derivatives were synthesized, including or not an additional aminophenylboronic acid group on HA. We demonstrated that the simultaneous presence of both sulfates and PBA groups on HA greatly enhanced its ability to dope PEDOT efficiently, leading to the design of a new conductive ink PEDOT:HAS₄-PBA_{0.3} exhibiting a conductivity up to 1.5 S/cm. This ink is biocompatible, and HAS₄ displayed resistance to enzymatic degradation ($M_w_i/M_w_f \approx 0.4 \pm 0.1$ in 1 month in extreme degradation conditions (pH 5 which is known to be the optimal HAase degradation pH^[33], and high HAase concentration of 1000 U/mL). Therefore, the developed PEDOT:HAS₄-PBA_{0.3} ink was expected to degrade in physiological conditions in several month, as expected in this Ph.D. project.

This synthesis of this PEDOT-based ink was optimized. The polymerization protocol was improved compared to the literature, with a deeper understanding of the role of the various reaction parameters. This new protocol was reproducible, batch-size independent, and enabled to finely tune the size of final ink particles. It enabled to formulate this ink to adjust its physico-chemical properties to process it using inkjet printing. The resulting printing tracks displayed resistivity slightly above those of printed PEDOT:PSS tracks and soft polymer substrate, without additional treatment^[43].

In bioelectronics, conductive materials are exposed to wet mediums. For PEDOT:HAS₄-PBA_{0.3} ink to be suitable for bioelectronics, it should be stable in such conditions, and keep its conductive properties unchanged when wet. However as described in this chapter, PEDOT:HAS₄-PBA_{0.3} ink was readily soluble in water. The next chapter of this manuscript will be dedicated to the cross-linking of PEDOT:HAS₄-PBA_{0.3} ink, in order to obtain insoluble conductive PEDOT:biomolecule tracks.

VII. Materials and methods

VII.1. Synthesis

VII.1.a. Materials

Hyaluronic acid sodium salts were obtained from different suppliers (Table 14).

Table 14. Suppliers of hyaluronic acid sodium salts.

Mw (kg/mol)	PDI	Supplier
113	1.56	Lifecore Biomedical (Chaska, Minesotta, USA)
219	1.44	
478	1.43	
1070	1.62	Kikkoman biochemifa company (Tokyo, Japan)

Chondroitin sulfate sodium salt from shark cartilage (product number C3484, batch # BCBW8637), tetrabutylammonium hydroxide 30-hydrate (TBA-OH,(H₂O)₃₀), sulfur trioxide N,N-dimethylformamide (SO₃-DMF), ammonium persulfate (APS), 4-(4,6-dimethoxy-1,3,5-triazin-2-yl)-4-methylmorpholinium chloride (DMTMM), 3-aminophenylboronic acid hemisulfate salt (3APBA), dodecylbenzene sulfonic acid (DBSA), carbazole, sodium tetraborate and sodium hydroxide pellets were obtained from Sigma-Aldrich (Saint-Quentin Fallavier, France). Barium chloride (BaCl) was from Touzart et Matignon (Evry, France). 3,4-ethylenedioxythiophene (EDOT) and iron^{II} sulfate heptahydrate were from Alfa Aesar. Hydrochloric acid and glycerol were from Fischer Scientific. N,N-dimethylformamide (DMF), ethanol 96% (EtOH) and acetonitrile (MeCN) were from VWR International (Fontenay-sous-Bois, France). All reagents were used as received without further purification.

VII.1.b. HA sulfation

The sulfation protocol was adapted from the literature^[25–30]. 1 g of HA was converted to tetrabutylammonium hyaluronate (HA-TBA) through elution on a H⁺-form ion exchange resin (Amberlite IR-130 from Sigma Aldrich), then basification to pH 4.25 with a 0.4 M TBA-OH solution and freeze-drying. (Figure 31, NMR ¹H (D₂O, 80°C) : 4.68-4.36 (2H, dd), 4.25 (HOD

signal), 3.95-3.25 (10H, m), 3.18-3.10 (8Ha, t), 2.10-1.84 (3H, s), 1.70-1.56 (8Hb, quint), 1.42-1.28 (8Hc, hex), 1.00-0.86 (12Hd, t)).

1 g of HA-TBA was suspended in DMF at 4.7 g/L, then degassed and cooled down to 4 °C. *n* equivalents of SO₃-DMF dissolved in DMF at 123 g/L were added at once. The reaction medium was degassed and stirred 1 h à 4 °C under nitrogen. The reaction was quenched by the addition of 667 mL of a NaOH solution containing (*n*+1) equivalent of OH⁻ ions. The medium was neutralized, and NaCl was added to obtain a final NaCl concentration of 0.5 M. HAS was precipitated with 1.7 L of EtOH. HAS was dissolved in 0.3 M NaCl and dialyzed against water with a 6-8 kg/mol dialysis membrane (Spectrum Laboratories, CA, USA) until bath conductivity was below 8 µS/cm, then recovered by freeze-drying with a yield of around 95%. The degree of sulfation, DS_S, was analyzed by elementary analysis or chemical quantification, as described in below. (¹H NMR (D₂O, 80°C, Figure 32): 5.04-4.9 (2H,m), 4.9-4.8 (1H, s), 4.68-4.58 (1H, d), 4.54-4.45 (2H, d), 4.42-3.4.33 (1H, t), 4.31-4.19 (HOD signal + 2H), 4.18-4.10 (1H, s), 3.99-3.91 (1H, m), 3.89-3.80 (1H, t), 2.27-2.06 (3H, s); ¹³C NMR (D₂O, 80°C, Figure 33), 173.2, 103, 98.8, 77.2, 76.8, 75.7, 75.2, 75.0, 72.0, 66.5, 54.2, 21.7).

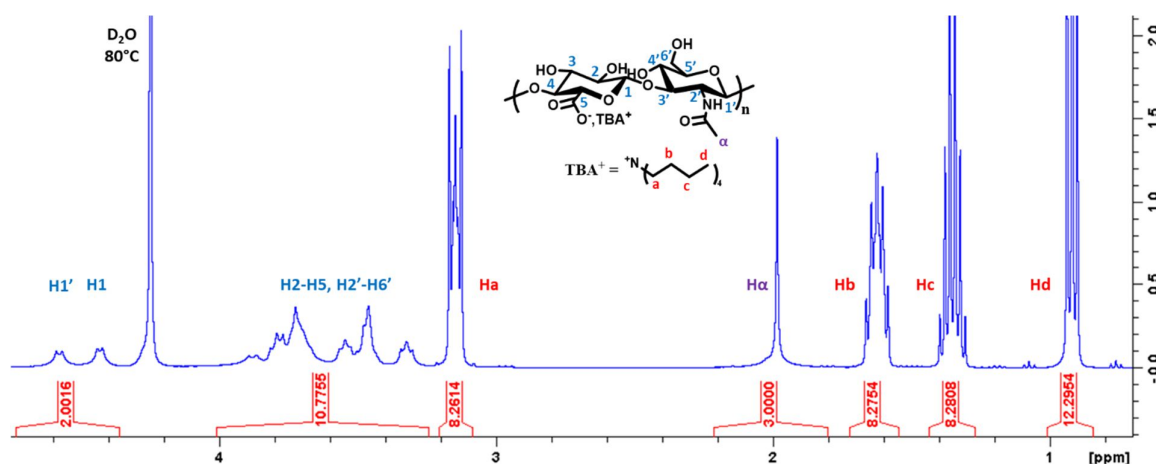


Figure 31. ¹H NMR spectrum of HA-TBA, 5 mg/mL at 80°C in D₂O.

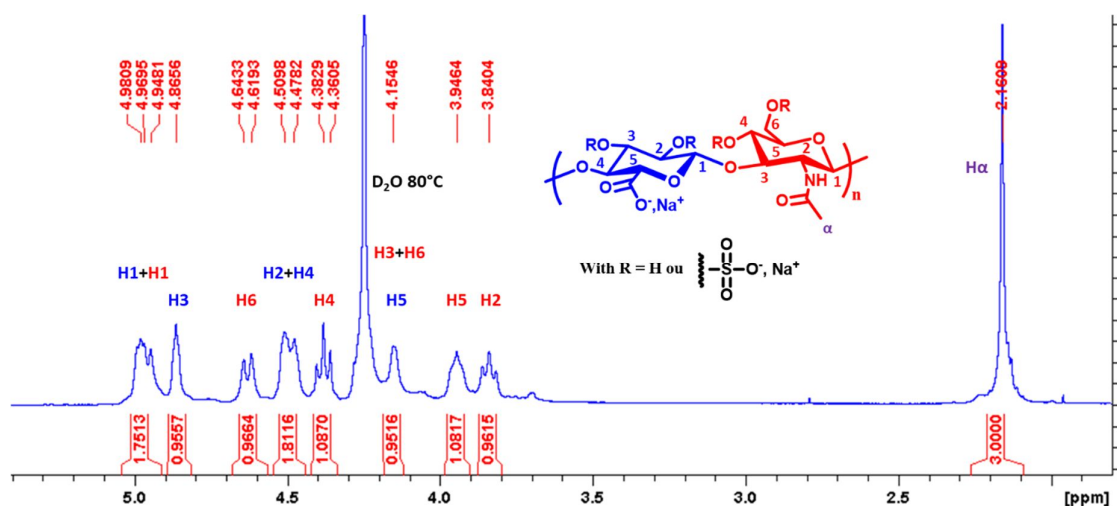


Figure 32. ^1H NMR spectrum of HAS_4 at 80°C (17 mg/mL) in D_2O .

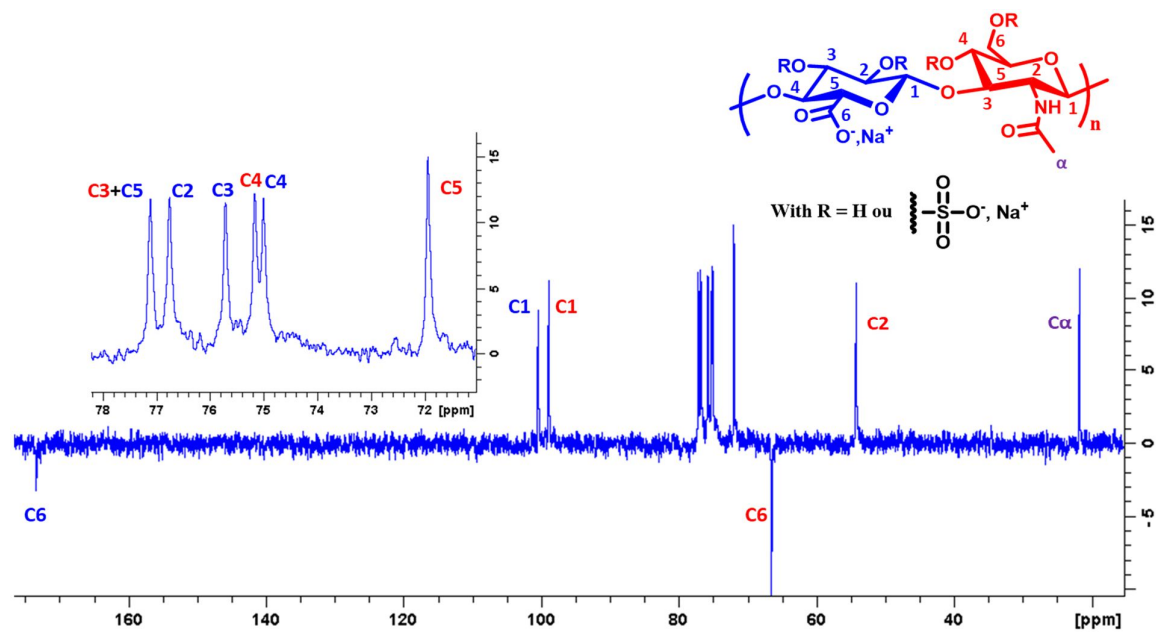


Figure 33. NMR ^{13}C DEPT of HAS_4 at 17 mg/mL at 80°C in D_2O .

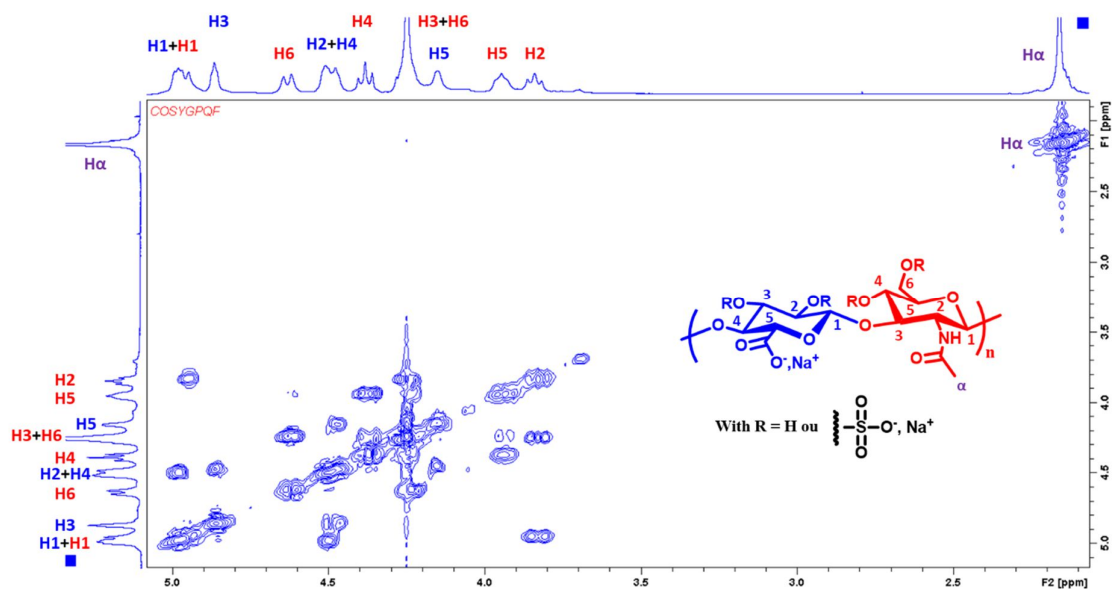


Figure 34. ^1H NMR COSY of HAS_4 at 17 mg/mL at 80°C in D_2O .

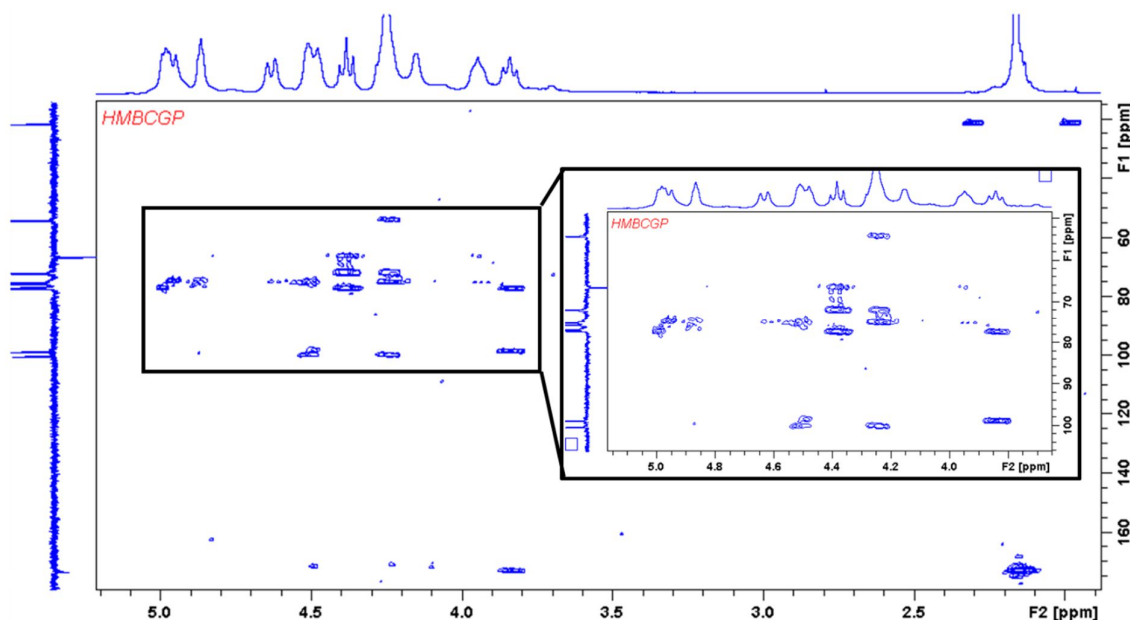


Figure 35. ^{13}C HMBC NMR of HAS_4 at 17 mg/mL at 80°C in D_2O .

VII.1.c. Synthesis of $\text{HAS}_4\text{-PBA}_{0.3}$

The protocol was adapted from Auzély *et al.*^{43, 44}. 1 g of HAS_4 was dissolved in 492 mL of water:DMF 3:2 v:v. 1 equivalent of DMTMM dissolved in 4 mL of water was added then 0.3 equivalent of 3APBA dissolved in 4 mL of water. The pH was adjusted to 6.5 and the medium stirred overnight at room temperature. NaCl was added to obtain a final NaCl concentration

of 0.3 M, then the medium was purified by ultrafiltration on a 10 kDa ultra-filtration membrane (Amicon Bioseparations, Millipore, NH, USA), and freeze-dried. HAS-PBA was recovered with a yield superior to 90%. The degree of PBA substitution on the HA backbone, DS_{PBA} , was analyzed by 1H NMR using the integration of HA methyl protons as a reference, and the sum of integration of aromatic protons of PBA divided by 4. DS_{PBA} was found to be equal to 0.3. (Figure 14 1H NMR (D_2O , 80°C): 7.92-7.81 (0.3Ha, s), 7.70-7.53 (0.6Hb+c, dd), 7.50-7.40 (0.3H,d t), 5.08-3.56 (10H + HOD signal at 4.25, m), 2.32-1.94 (3H, s)).

VII.1.d. Synthesis of PEDOT-based inks from HASx-PBAy (Table 5)

The protocol was adapted from Harman *et al.*^[7] with minor modifications. 1 g of HAS₄-PBA_{0.30} (1 equivalent) was dissolved into 16 mL of degassed water:MeCN 9:1 v:v. 251 μ L (334 mg, 2 equivalent) of EDOT were added (so as [HAS-PBA + EDOT] = 37.5 g/L). The medium was stirred overnight at 4 °C under nitrogen. 9.81 mg of FeSO₄ were added (0.015 eq compared to EDOT). 714 mg of APS (1.33 equivalent compared to EDOT) were dissolved in 16 mL of degassed and cold water:MeCN 9:1 v:v, then added dropwise in 1h to the medium using a syringe pump. The medium was stirred 4 h at 4 °C under nitrogen, then at room temperature until pH was stable below 1.1-1.2. The reaction was quenched adding 32 mL of water, then homogenized at 10,000 rpm for 10 minutes using an IKA Ultra Turrax T-10 basic disperser with a S 10 N-8G dispersing tool (Roth, Karlsruhe, Germany). The medium was dialyzed against osmosed water with dialysis membrane MWCO 6-8 kDa (Spectrum Laboratories, California, USA), changing the bath until water conductivity was below 8 μ S/cm. Then pH was adjusted to 7.4 and PEDOT:HAS₄-PBA_{0.3} was recovered by freeze-drying as a deep blue powder, with a yield superior to 85%.

VII.1.e. Synthesis of PEDOT:HAS₄-PBA_{0.3} inks with optimized particle sizes for inkjet printing

1 g of HAS₄-PBA_{0.30} (1 equivalent) was dissolved into 111 mL of degassed water. 255 μ L (339 mg, 2 equivalent) of EDOT were added (so as [HAS₄-PBA_{0.3} + EDOT] = 10 g/L). 3.32 mg of FeSO₄ was added (0.005 equivalent compared to EDOT) and 724 mg of APS (1.33 equivalent compared to EDOT) were dissolved in 10 mL of degassed water and added at once to the HAS₄-PBA_{0.30} solution. Quickly after, the solution was mixed 10 minutes at 25,000 rpm using an Ultra

Turrax T-10 basic disperser with a S 10 N-8G dispersing tool (Roth, Karlsruhe, Germany). After mixing, the solution was stirred at room temperature under nitrogen until pH was stable below 1.4-1.5. The medium was dialyzed against deionized water with a 6-8 kg/mol dialysis membrane (Spectrum Laboratories, California, USA), changing the bath until water conductivity was below 8 $\mu\text{S}/\text{cm}$. Then pH was adjusted to 7.4. The medium was then filtered successively through 3 μm and 1.2 μm cellulose acetate filters to remove large aggregates. PEDOT:HAS₄-PBA_{0.3} was recovered by freeze-drying as a deep blue powder, with a yield superior to 80%.

VII.1.f. Grafting of the phenylboronic acid moiety on ChS

The protocol was adapted from Auzély *et al.*^{43, 44}. 1 g of ChS was dissolved in 492 mL of water:DMF 3:2 v:v. 1 equivalent of DMTMM dissolved in 4 mL of water was added, then 0.3 equivalent of 3APBA dissolved in 4 mL of water. The pH was adjusted to 6.5 and the medium stirred overnight at room temperature. NaCl was added to obtain a final NaCl concentration of 0.3 M, then the medium was purified by ultrafiltration on a 10 kg/mol ultra-filtration membrane (Amicon Bioseparation, Millipore, New Hampshire, USA), and freeze-dried. ChS-PBA was recovered with a yield superior to 87%. The PBA degree of substitution on the ChS backbone, DS_{PBA} , was analyzed by ^1H NMR using the integration of ChS acetyl protons as a reference, and the sum of the integration of aromatic protons of PBA divided by 4. Noticeably, the acetyl protons of ChS repeating units grafted with a PBA groups gave another signal than acetyl protons of pristine ChS repeating unit. DS_{PBA} was found to be equal to 0.3. (Figure 36, ^1H NMR (D_2O , 80°C): 7.96-7.86 (0.29H, d), 7.73-7.58 (0.68H, m), 7.55-7.45 (0.37H, t), 4.86-3.63 (m), 2.14-1.94 (2H, m), 1.79-1.49 (1H, dxd)).

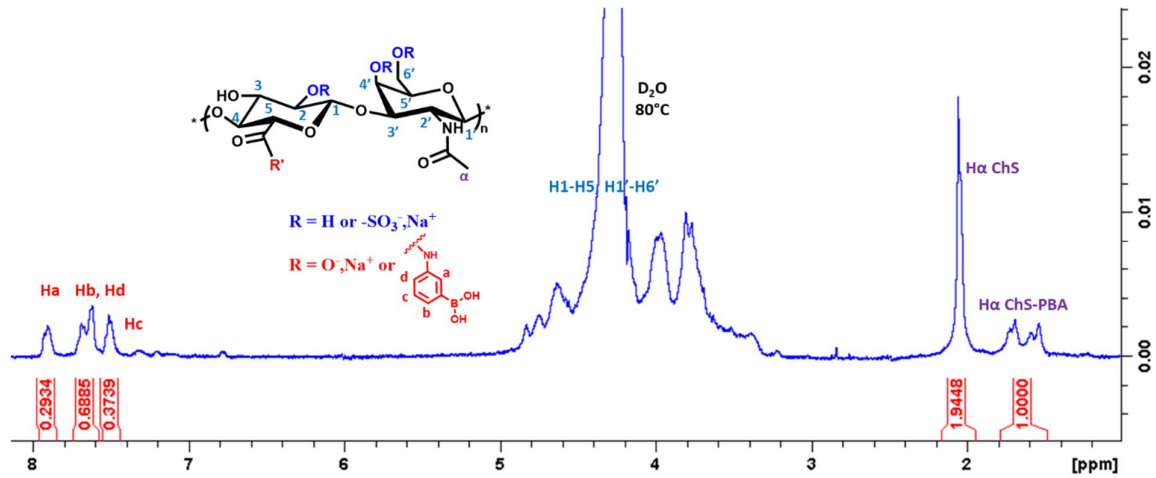


Figure 36. ^1H NMR spectrum of ChS-PBA_{0.3} at 80°C (4 mg/mL) in D_2O .

VII.2. Characterizations

VII.2.a. Sulfation degree

The sulfation degree DS_S defined as the mean amount of sulfate groups by HA repeating unit was determined using the following equation:

$$\text{DS}_\text{S} = \frac{w_{\text{SO}_3\text{Na}} / M_{\text{SO}_3\text{Na}}}{w_{\text{HA repeating unit}} / M_{\text{HA repeating unit}}}$$

Where w_x is x mass fraction in the sample, $M_{\text{SO}_3\text{Na}} = 102.05 \text{ g/mol}$ and $M_{\text{HA repeating unit}} = 401.30 \text{ g/mol}$. For hyaluronic acid, DS_S can range from 0 to 4.

The sulfate mass fraction of the sample was analyzed using a turbidimetric method adapted from the literature^[69]. Briefly, HAS was hydrolyzed releasing SO_4^{2-} anions, forming a precipitate with Ba^{2+} that remained in suspension due to gelatin as a viscosity enhancer. Practically, 1.5-2 mg of sulfated hyaluronic acid were dissolved in HCl 1M to obtain $[\text{HAS}] = 1.5 \text{ g/L}$, then hydrolyzed for 3 h at 107 °C. 20 to 55 μL of sample were aliquoted, completed to 100 μL with HCl 1M. For the calibration curve, HAS was replaced by 40, 60, 80 and 100 μL of 0.59 g/L Na_2SO_4 . The blank control contained only 100 μL of HCl 1M. To all solutions, 700 μL of 30 g/L trichloroacetic acid solution was added, then 200 μL of a solution containing 5 g/L of gelatin and 5 g/L of BaCl_2 . Solutions were vortexed each 5 minutes for 25 minutes, before

measuring the absorbance at 360 nm. The sulfate mass fraction was averaged from three measurements performed at different sample concentrations.

The HA repeating unit mass fraction of the sample was analyzed using a colorimetric method adapted from the literature^[70–72]. First, HAS was hydrolyzed in concentrated sulfuric acid mixed with sodium tetraborate, releasing one uronic acid by HA repeating unit. In concentrated sulfuric acid, uronic acid mixed with sodium tetraborate yielded 5-formyl-2-furancarboxylic acid, reacting with carbazole to produce a chromophore that could be quantitated by absorbance measurements^[72]. Sodium tetraborate and carbazole solutions were prepared the day before analysis without introducing any magnetic bar to avoid contamination. 0.7-1 mg of sample were dissolved in 1.5 mL of water. A volume containing 40 µg was aliquoted and completed to 200 µL with water. For establishing the calibration curve, HAS was replaced by 7.27, 21.8, 36.34 and 58.14 µL of 688 µg/mL original sodium hyaluronate. The blank control contained only 200 µL of water. To all solutions, 800 µL of 25 mM Na₂B₄O₇ in concentrated sulfuric acid were added. The vials were vortexed, hydrolyzed 10 min at 100 °C and cooled down in water for 15 minutes. 200 µL of 7.48 mM carbazole in anhydrous ethanol were added. The vials were vortexed, hydrolyzed 10 min at 100 °C and cooled down in water for 15 minutes. The absorbance was measured at 530 nm.

Additionally, DS_S was determined for a few samples by elemental analysis (C, H, N, S) . Analysis were performed on a CHNS Flash EA1112Series analyzer (ThermoFinnigan Inc.), heated at 950 °C in a quartz tube filled with copper and zinc oxide, and quartz wool for separation. Gases were carried by helium, separated at 54 °C in the chromatography column, and detected with a thermal conductivity detector.

VII.2.b. Size exclusion chromatography

The molar mass distribution and the weight-average molar mass of sulfated hyaluronic acids were determined by size exclusion chromatography (SEC) using a Waters GPC Alliance chromatograph (Waters, Saint-Quentin-en-Yvelines, France) equipped with a differential refractometer and a light scattering detector (MALS) from Wyatt (Santa Barbara, USA). The solutions was injected at a concentration of 0.7 mg/mL in 0.1 M NaNO₃/0.005 M NaN₃, at a flow rate of 0.5 mL/min and at a column temperature of 30 °C. Samples and mobile phases were filtered under 0.1 µm before injection in the column.

The variation of refractive index according to concentration (dn/dc) values of sulfated and pristine hyaluronic acid (sulfation degree of 2.1, 3.3 and 4) were determined with the same refractometer, using five concentrations between 0.05 and 0.40 g/mol (Figure 4). Stock solution at 0.5. g/L were prepared for each sample in 0.1 M NaNO_3 /0.005 M NaN_3 . Diluted solution at 80, 60, 40 20 and 10% were prepared. To be as precise as possible on concentrations, the hydration degree of the freeze-dried sulfated HA samples was measured by thermogravimetry analysis as detailed below, and the diluted solutions were prepared by weighting the aliquoted volumes.

VII.2.c. Thermogravimetric analysis (TGA)

The water mass fraction of freeze-dried samples was assessed using a TG-92-12 from Setaram (Caluire et Cuire, France) using the following temperature sequence: threshold at 20°C for 300 s, the temperature ramps at 5°C / min until 120°C, threshold at 120°C for 60 s, then temperature decrease at 10°C/min until 20°C, using N_2 as carrying gas. Water mass fractions of HAS samples are listed in Table 15.

Table 15. Water mass fraction of various sulfated HA determined by TGA.

Sample	Water mass fraction determined by TGA
Pristine HA 113	12.0 %
HAS _{2.}	15.9 %
HAS _{3.3}	16.1 %
HAS ₄	11.7 %

VII.2.d. NMR

NMR spectra of the polysaccharide derivatives dissolved in deuterium oxide were recorded at 25 °C or 80 °C (depending on the viscosity of the solution) using a Bruker AVANCE III HD spectrometer operating at 400.13 MHz (^1H) and 100.61 MHz (^{13}C). Deuterium oxide was obtained from SDS (Vitry, France). All NMR spectra were analyzed with Topspin 3.1 software from Bruker AXS. The ^1H and ^{13}C -NMR assignments were based on ^1H - ^1H homonuclear and ^1H -

^{13}C heteronuclear correlation experiments (correlation spectroscopy, COSY and heteronuclear single quantum correlation, HSQC).

All ^1H NMR spectra were recorded using a 4000 Hz spectral width, 65,536 data points, 8.192 s acquisition times applying at 90° tip angle, 10 s relaxation delays for accurate integration of the proton signals, and 16 to 64 scans. The ^{13}C NMR DEPTQSP spectra were recorded using a 20,161 Hz spectral width, 65,536 data points, 1.638 s acquisition time at 90° tip angle, 2 s recycle delay and 8,192 scans. Chemical shifts were given relative to external tetramethylsilane (TMS = 0 ppm) and calibration was performed using the signal of the residual protons of the solvent as a secondary reference.

VII.2.e. Ink film deposition on glass slides

Glass slides were washed with acetone and ethanol. Freeze-dried PEDOT-based ink was dissolved in water at 13 g/L and the suspension was strongly stirred for 10 minutes and sonicated in an ultrasound bath for 30 seconds. 60 μL of suspension were deposited on a glass slide inside a silicon ring of 1 cm inner diameter. The ink was dried at room temperature. Ink film thickness h was measured with a Dektak DXT profilometer (Brüker, Palaiseau, France).

VII.2.f. Conductivity measurements

Film sheet resistivity R_{sheet} was determined using a 4-point probe from Ossila (Power Cord Type, Sheffield, England), over a wide range of tension and current to certify the ohmic behaviour. Conductivity σ was calculated as $\sigma = 1/R_{\text{sheet}} \cdot h \cdot c$ where c was a geometric corrector coefficient determined by the software and h the film thickness measured with a Dektak DXT profilometer (Brüker, Palaiseau, France). Conductivity was measured in several locations of the film, then averaged.

For a uniform sheet thickness, sheet resistivity is a special case of resistivity. Its unity is $\Omega/\square = \Omega/(\text{m}/\text{m})$. The “ \square ” is adimensionnal, but kept to not confuse the sheet resistance from the bulk resistance.

VII.2.g. Absorbance

Absorbance was measured from 300 to 2000 nm using a Cary 7000 Universal Measurement Spectrophotometer (Agilent, Santa Clara, USA), on ink films on glass slides prepared according to protocol described in section VII.2.e. All spectra were normalized by film thickness h , which was measured using a Dektak DXT profilometer (Brüker, Palaiseau, France).

VII.2.h. Dynamic Light Scattering (DLS)

DLS measurements were recorded on a Zeta sizer NanoZS from Malvern Instruments Ltd. (Worcestershire, England). For DLS measurements, samples were diluted at 0.05 g/L in water and equilibrated at 25°C. Measurements were made 3 times in a row. The “Zaverage” value was reported. The Zaverage is the intensity weighted mean hydrodynamic size of the ensemble collection of particles measured by DLS.

VII.2.i. Viscosity measurements for the experimental design

Viscosity experiments were performed with an AR 2000 EX cone-plate rheometer (TA Instruments, Eschborn, Germany). The cone had a diameter of 4 cm and an angle of 4°. 1150 μ L were deposited on the plate, and the cone set 75 μ m above. In a steady-state flow, three shear rate ramps from 0.1 Hz to 700 Hz at 25°C, with 6 points per decade were performed. The average viscosity at 10 Hz was reported for the experimental design. To prevent water evaporation, the measuring system was surrounded with a low-viscosity silicon oil (50 mPa.s) carefully added to the edges of the cone.

VII.2.j. Surface tension

Surface tensions were measured using a DSA100 drop shape analyzer from Krüss (Hamburg, Germany) using DSA4 software from Krüss. The pending drop technique was used, with a Laplace-Young drop fitting algorithm. The needle used was a NE45 KRÜSS needle with an inner diameter of 1.8 mm (Hamburg, Germany). The density of the gas surrounding phase was set at 0.0012 g/L and the density of the ink was considered as the same of water at 25°C: 0.997 g/L.

VII.2.k. Scanning Electron Microscopy

Scanning electron microscopy pictures were made using an ULTRA+ microscope from Zeiss (Fougères, France) equipped with a Gemini electron gun from Zeiss (Fougères, France) and a high efficiency In-Lens SE2 detector from Zeiss (Fougères, France). The electron gun firing voltage was set at 5 kV.

VII.2.l. Cytotoxicity experiments

These experiments were performed by Mathilde Menneteau from the LSMB laboratory at CEA Grenoble/LETI/DTBS.

To assess the cytocompatibility of the materials, fibroblasts cells were selected as they play an important role in wound repair. NIH3T3 murine fibroblasts were seeded in 96-well plates at a density of 4.000 cells per well and incubated during 24 h at 37°C with growth medium. After 24 hours of culture, the growth medium was removed and replaced with 200 µL of growth medium added with PEDOT:HAS₄-PBA_{0.3} ink, or one of its precursors at increasing concentrations (50, 100, 250, 375, 500 and 750 µg/mL). A positive control (live) and a negative control with 10 mM of H₂O₂ (dead) were performed. After 24 h, the growth medium was removed and replaced with 100 µL of growth medium and 10 µL of WST-1 reagent (4-[3-(4-Iodophenyl)-2-(4-nitro-phenyl)-2H-5-tetrazolio]-1,3-benzene sulfonate). In the presence of mitochondrial succinate dehydrogenase, the reagent was reduced and formed a yellow formazan compound whose quantity was proportional to the number of living cells. After 2 h of incubation at 37°C, the viability was deduced by reading the absorbance at 450 nm with an Infinite-M1000 TECAN microplate reader as

$$Viability\% = \frac{Absorbance\ (sample) - Absorbance\ (positive\ control)}{Absorbance\ (negative\ control) - Absorbance\ (positive\ control)}.$$

Experiments were conducted three times, in sextuplicate.

VII.3. Experimental design procedure

To optimize PEDOT:HAS-PBA ink physicochemical properties, a set of independently controlled factors were determined: ink concentration (A), DBSA surfactant concentration (B), addition of glycerol (C) and EDOT/HAS-PBA (D) molar ratio during ink polymerization. The domain of variations of those entry factors A-D within which the prediction model was relevant is defined as the experimental domain (Table 16).

Table 16. Design experimental domain.

Factor	Name	Units	Minimum	Maximum	Coded Low	Coded High	Reduced factor
A	[ink]	g/L	10.00	45.00	-1 ↔ 10.00	+1 ↔ 45.00	a
B	[DBSA]	g/L	0.5000	1.0000	-1 ↔ 0.50	+1 ↔ 1.00	b
C	EDOT / HAS ₄ -PBA _{0,3}	ratio	1.0000	2.00	-1 ↔ 1.00	+1 ↔ 2.00	c
D	Glycerol vol%	%	0.0000	4.00	-1 ↔ 0.00	+1 ↔ 20.00	d

To facilitate data treatment data, and obtain a mathematical prediction model without unities, each entry factor A-D was mathematically transformed into a reduced factor a-d, using transformation as follows: $a = \frac{A - A_{mean}}{A_{max} - A_{mean}} = \frac{A - A_{mean}}{A_{mean} - A_{min}}$. This transformation enables to change the experimental domain into an adimensional interval [-1;1] (Figure 37).

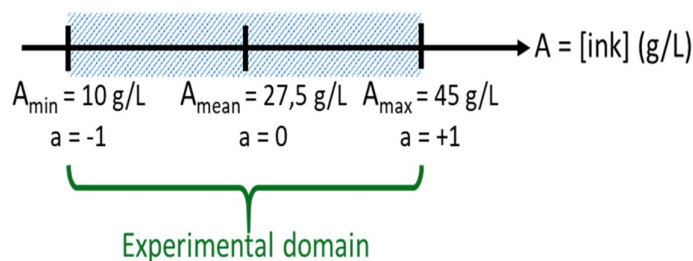


Figure 37. Illustration of transforming factor into reduced factor: example of entry A.

The physicochemical properties to optimize were the surface tension (R1), the viscosity (R2), the particle size (R3) and the conductivity of the ink (R4). These parameters will be referred to as response factors R1-R4 (Table 17).

Table 17. Design outcome responses.

Response	Name	Units	Target
R1	Surface tension	mN/m	$\approx 27 - 32$ mN/m
R2	Viscosity	mPa.s	$\approx 10 - 12$ mPa.s
R3	Particle size	μm	$< 500\text{nm}$ ideally
R4	Resistivity	Ω/\square	As low as possible

Several set of experiments were suggested by the software to optimize the ink formulation, ranging from 13 to 35 experiments. The greater the number of experiments, the more robust and reliable the statistical model is, as abnormal results are more compensated, and as experimental fluctuations can be rigorously taken into account. As the amount of required PEDOT:HAS₄-PBA_{0.3} was quickly increasing with the number of experiments, a compromise was set using a design matrix of 21 experiments, corresponding to a face-centered composite design to study the four input variables A-D. In order to take into account experimental fluctuations and systematic operator biases, the order to carry out the experiments was then randomized. Concerning the experimental methodology, several measures were taken to reduce as much as possible the experimental fluctuations:

- The whole experimental design was performed in the shortest amount of time to avoid potential external fluctuations (sample degradation, important variation of air humidity, etc...);
- Each set of manipulation (sample preparation, characterization) was done the same day, in the same room, using the same glassware, micropipettes, machine, or any other laboratory apparatus;
- Each deviation from this guideline was recorded to track back any potential abnormal result.

This experimental design required inks with 3 different EDOT/HAS-PBA ratio of 1, 2 and 3. Those three batches were synthesized the same day, purified simultaneously and freeze-dried. These inks were formulated at different concentrations with DBSA and glycerol. In addition, PEG ($M_n = 3.35$ kg/mol) was added to all formulations so as $[\text{PEG } 3.35 \text{ kg/mol}] = 6.5$

g/L, in order to take into account the potential viscosity of an ulterior 3.5 kg/mol PEG dithiol cross-linker.

Surface tension, viscosity, ink particle size and resistivity was measured according to protocol described previously in experimental section. The full design matrix and the corresponding resulting data are shown below (Table 18).

Table 18. Design of experiment experimental matrix and measured answers.

Std	Run	Factor 1	Factor 2	Factor 3	Factor 4	Response 1	Response 2	Response 3	Response 4
		A: ink concentration	B : DBSA concentration	C : EDOT/HAS ₄ -PBA _{0.3}	D:Glycerol vol%	Surface tension	Viscosity	Particle size	Resistivity
		g/L	g/L	ratio	%	mN/m	mPa.s	nm	Ω/□
3	1	44.86	0.50	2	4	45.3	20.9	2229	1331
5	2	44.86	0.50	1	4	39.1	8.4	525	214400
11	3	27.41	0.50	1.5	2	42.1	7.2	1902	5215
9	4	9.95	0.75	1.5	2	36.0	3.1	2380	16680
14	5	27.37	0.75	2	2	39.0	6.2	1977	2631
8	6	9.99	0.50	1	0	35.7	2.4	552	18500000
21	7	27.37	0.75	1.5	2	39.4	7.3	2579	5086
10	8	44.79	0.75	1.5	2	42.0	25.0	2350	3405
13	9	27.37	0.75	1	2	36.3	4.6	352	1102000
4	10	9.939	0.99	1	4	34.5	2.6	594	1895330
19	11	27.37	0.75	1.5	2	39.2	7.2	1636	28047
1	12	44.72	0.99	2	0	41.7	17.5	3801	4222
18	13	27.37	0.75	1.5	2	41.5	7.2	2158	8582
7	14	9.939	0.99	2	4	35.1	2.7	2873	11630
12	15	27.33	0.99	1.5	2	39.3	7.0	1283	5439
20	16	27.37	0.75	1.5	2	39.5	7.2	1641	5960
15	17	27.37	0.75	1.5	0	39.1	6.3	2655	6061
6	18	9.969	50	2	0	37.1	2.4	2305	11593
2	19	44.72	0.99	1	0	36.4	6.5	415	6042000
17	20	27.37	0.75	1.5	2	38.8	7.9	2686	6032
16	21	27.37	0.75	1.5	4	38.5	7.5	1737	20673

Data were analyzed using a multilinear regression^[73] using a Cox-Box analysis^[74]. When needed, responses were transformed in order to normalize the distribution of values^[75]. Regression models were refined selecting the most relevant coefficients using a step by step forward march algorithm, using the AICc quality criteria^[76].

Optimal formulation for inkjet printing was nevertheless calculated using the following priority order between different responses: surface tension < resistivity < viscosity. Taking into

account those constraints, an optimal formulation to inkjet-print PEDOT:HAS₄-PBA_{0.3} ink with the highest conductivity was determined, with corresponding predicted values (Table 19). To confirm this prediction model, the corresponding formulation was prepared 3 times and analyzed.

Table 19. Optimal factor values and expected values of responses.

Factors and answers	Solution	Expected values	Obtained values (n=3)	Relative difference (%)
A: [ink] (g/L)	31.238			
B: [DBSA] (g/L)	0.903			
C: EDOT/ HAS ₄ -PBA _{0.3}	2			
D: Glycerol vol%	2.264			
R1: Surface tension (mN/m)		39.330	39.66 ± 0.22	6.79
R2: Viscosity (mPa.s)		8.494	9.99 ± 0.68	17.61
R3: Z _{average} (nm)		2091	1359 ± 272	35.01
R4: Resistivity (Ω/□)		1052	1500 ± 45	42.58

The experimental difference between the predicted surface tension and viscosity was acceptable (Table 19). However, the relative difference between the predicted particle size and resistivity was not acceptable, highlighting that there was a problem in the whole process inducing reproducibility issues, and statistical mistakes.

This variability was attributed to the high particle size and polydispersity index of all samples. Thus, DLS data that were used to establish the regression model were unreliable and meaningless, as the three inks used for this experimental design all displayed a high polydispersity. This resulted in an inaccurate prediction model. This problem was solved afterwards by adding a mixing step at the beginning of the polymerization reaction.

VIII. Bibliography

- [1] J. Hao, Z. Piao, J. Yao, Z. Hao, *ChemPlusChem* **2015**, *80*, 1513–1516.
- [2] A. Elschner, S. Kirchmeyer, W. Lovenich, U. Merker, K. Reuter, *PEDOT: Principles and Applications of an Intrinsically Conductive Polymer*, CRC Press, **2010**.
- [3] A. I. Hofmann, D. Katsigiannopoulos, M. Mumtaz, I. Petsagkourakis, G. Pecastaings, G. Fleury, C. Schatz, E. Pavlopoulou, C. Brochon, G. Hadziioannou, E. Cloutet, *Macromolecules* **2017**, *50*, 1959–1969.
- [4] O. L. Gribkova, O. D. Iakobson, A. A. Nekrasov, V. A. Cabanova, V. A. Tverskoy, A. R. Tameev, A. V. Vannikov, *Electrochimica Acta* **2016**, *222*, 409–420.
- [5] O. L. Gribkova, O. D. Iakobson, A. A. Nekrasov, V. A. Cabanova, V. A. Tverskoy, A. V. Vannikov, *Journal of Solid State Electrochemistry* **2016**, *20*, 2991–3001.
- [6] O. L. Gribkova, N. E. Mitina, A. A. Nekrasov, V. F. Ivanov, V. A. Tverskoi, A. R. Tameev, A. V. Vannikov, *Protection of Metals and Physical Chemistry of Surfaces* **2015**, *51*, 390–395.
- [7] D. G. Harman, R. Gorkin III, L. Stevens, B. Thompson, K. Wagner, B. Weng, J. H. Chung, M. in het Panhuis, G. G. Wallace, *Acta biomaterialia* **2015**, *14*, 33–42.
- [8] I. del Agua, D. Mantione, N. Casado, A. Sanchez-Sanchez, G. G. Malliaras, D. Mecerreyes, *ACS Macro Letters* **2017**, *6*, 473–478.
- [9] S. Tekoglu, D. Wielend, M. C. Scharber, N. S. Sariciftci, C. Yumusak, *Adv. Mater. Technol.* **2020**, *5*, 1900699.
- [10] Y. Ner, M. A. Invernale, J. G. Grote, J. A. Stuart, G. A. Sotzing, *Synthetic Metals* **2010**, *160*, 351–353.
- [11] D. Mantione, I. del Agua, W. Schaafsma, J. Diez-Garcia, B. Castro, H. Sardon, D. Mecerreyes, *Macromol. Biosci.* **2016**, *16*, 1227–1238.
- [12] S. Wang, S. Guan, J. Wang, H. Liu, T. Liu, X. Ma, Z. Cui, *Journal of Bioscience and Bioengineering* **2017**, *123*, 116–125.
- [13] A. R. Harris, P. J. Molino, R. M. I. Kapsa, G. M. Clark, A. G. Paolini, G. G. Wallace, *Synthetic Metals* **2016**, *220*, 394–401.
- [14] M. Horikawa, T. Fujiki, T. Shirosaki, N. Ryu, H. Sakurai, S. Nagaoka, H. Ihara, *J. Mater. Chem. C* **2015**, *3*, 8881–8887.
- [15] Y. Xu, M. Cui, P. A. Patsis, M. Günther, X. Yang, K. Eckert, Y. Zhang, *ACS Applied Materials & Interfaces* **2019**, *11*, 7715–7724.
- [16] I. del Agua, S. Marina, C. Pitsalidis, D. Mantione, M. Ferro, D. Iandolo, A. Sanchez-Sanchez, G. G. Malliaras, R. M. Owens, D. Mecerreyes, *ACS Omega* **2018**, *3*, 7424–7431.
- [17] R. Zamora-Sequeira, I. Ardao, R. Starbird, C. A. García-González, *Carbohydrate Polymers* **2018**, *189*, 304–312.
- [18] V. Voinchet, P. Vasseur, J. Kern, *American Journal of Clinical Dermatology* **2006**, *7*, 353–357.
- [19] L. C. Becker, W. F. Bergfeld, D. V. Belsito, C. D. Klaassen, J. G. Marks, R. C. Shank, T. J. Slaga, P. W. Snyder, Cosmetic Ingredient Review Expert P, F. A. Andersen, *Int J Toxicol* **2009**, *28*, 5–67.
- [20] M. Pagnano, G. Westrich, *Osteoarthritis and Cartilage* **2005**, *13*, 751–761.
- [21] G. D. Monheit, K. M. Coleman, *Dermatol Ther* **2006**, *19*, 141–150.
- [22] M. R. Johns, L.-T. Goh, A. Oeggerli, *Biotechnol Lett* **1994**, *16*, 507–512.
- [23] B. F. Chong, L. M. Blank, R. McLaughlin, L. K. Nielsen, *Appl Microbiol Biotechnol* **2005**, *66*, 341–351.
- [24] T. Figueiredo, J. Jing, I. Jeacomine, J. Olsson, T. Gerfaud, J.-G. Boiteau, C. Rome, C. Harris, R. Auzély-Velty, *Biomacromolecules* **2020**, *21*, 230–239.
- [25] B. P. Purcell, I. L. Kim, V. Chuo, T. Guenin, S. M. Dorsey, J. A. Burdick, *Biomater. Sci.* **2014**, *2*, 693–702.
- [26] Q. Feng, S. Lin, K. Zhang, C. Dong, T. Wu, H. Huang, X. Yan, L. Zhang, G. Li, L. Bian, *Acta Biomaterialia* **2017**, *53*, 329–342.

- [27] V. Hintze, S. Moeller, M. Schnabelrauch, S. Bierbaum, M. Viola, H. Worch, D. Scharnweber, *Biomacromolecules* **2009**, *10*, 3290–3297.
- [28] S. Möller, M. Schmidtke, D. Weiss, J. Schiller, K. Pawlik, P. Wutzler, M. Schnabelrauch, *Carbohydrate Polymers* **2012**, *90*, 608–615.
- [29] R. Barbucci, A. Magnani, S. Lamponi, M. Casolaro, *Macromolecular Symposia* **1996**, *105*, 1–8.
- [30] R. Kunze, M. Rösler, S. Möller, M. Schnabelrauch, T. Riemer, U. Hempel, P. Dieter, *Glycoconjugate Journal* **2010**, *27*, 151–158.
- [31] E. E. Gilbert, *Chemical Reviews* **1962**, *62*, 549–589.
- [32] V. A. Cosenza, D. A. Navarro, C. A. Stortz, **n.d.**, 40.
- [33] T. Asteriou, B. Deschrevel, B. Delpech, P. Bertrand, F. Bultelle, C. Merai, J.-C. Vincent, *Analytical Biochemistry* **2001**, *293*, 53–59.
- [34] N. Massonnet, A. Carella, O. Jaudouin, P. Rannou, G. Laval, C. Celle, J.-P. Simonato, *J. Mater. Chem. C* **2014**, *2*, 1278–1283.
- [35] J. Hwang, D. B. Tanner, I. Schwendeman, J. R. Reynolds, *Physical Review B* **2003**, *67*, DOI 10.1103/PhysRevB.67.115205.
- [36] W. A. Muñoz, X. Crispin, M. Fahlman, I. V. Zozoulenko, *Macromolecular Rapid Communications* **2018**, *39*, 1700533.
- [37] I. Zozoulenko, A. Singh, S. K. Singh, V. Gueskine, X. Crispin, M. Berggren, *ACS Applied Polymer Materials* **2019**, *1*, 83–94.
- [38] S. Arditty, F. L.-C. et V. Schmitt, Fabrication, stability and rheological properties of solid-stabilized emulsions, Fabrication, stabilité et propriétés rhéologiques des émulsions stabilisées par des particules colloïdales, Université Sciences et Technologies - Bordeaux I, **2004**.
- [39] S. Baek, R. A. Green, L. A. Poole-Warren, *J. Biomed. Mater. Res.* **2014**, *102*, 2743–2754.
- [40] L. Djerbal, H. Lortat-Jacob, J. Kwok, *Glycoconj J* **2017**, *34*, 363–376.
- [41] A. Glasser, É. Cloutet, G. Hadziioannou, H. Kellay, *Chemistry of Materials* **2019**, *31*, 6936–6944.
- [42] D. Mantione, A. V. Marquez, F. Cruciani, C. Brochon, E. Cloutet, G. Hadziioannou, *ACS Macro Lett.* **2019**, *8*, 285–288.
- [43] C. A. Mire, A. Agrawal, G. G. Wallace, P. Calvert, M. in het Panhuis, *Journal of Materials Chemistry* **2011**, *21*, 2671.
- [44] M. Sasaki, B. C. Karikkineth, K. Nagamine, H. Kaji, K. Torimitsu, M. Nishizawa, *Advanced healthcare materials* **2014**, *3*, 1919–1927.
- [45] M. Y. Teo, N. RaviChandran, N. Kim, S. Kee, L. Stuart, K. C. Aw, J. Stringer, *ACS Applied Materials & Interfaces* **2019**, *11*, 37069–37076.
- [46] S. Kim, S. Y. Kim, M. H. Chung, J. Kim, J. H. Kim, *J. Mater. Chem. C* **2015**, *3*, 5859–5868.
- [47] M. Kiristi, A. U. Oksuz, L. Oksuz, S. Ulusoy, *Materials Science and Engineering: C* **2013**, *33*, 3845–3850.
- [48] R. M. Pasquarelli, D. S. Ginley, R. O’Hayre, *Chem. Soc. Rev.* **2011**, *40*, 5406.
- [49] A. BLAYO, *Formulation Des Encres Pour l’impression*, Ed. Techniques Ingénieur, **2007**.
- [50] K. Dimic-Misic, A. Karakoc, M. Ozkan, H. Ghufuran, T. Maloney, J. Paltakari, *Journal of Applied Engineering Science* **2015**, *13*, 207–212.
- [51] X. Cao, Y. Ye, Q. Tang, E. Chen, Z. Jiang, J. Pan, T. Guo, *The Journal of Physical Chemistry Letters* **2020**, *11*, 8442–8450.
- [52] J. Oziat, Electrode 3D de PEDOT: PSS Pour La Détection de Métabolites Electrochimiquement Actifs de Pseudomonas Aeruginosa, PhD Thesis, Lyon, **2016**.
- [53] A. Lima, P. Schottland, S. Sadki, C. Chevrot, *Synthetic Metals* **1998**, *93*, 33–41.
- [54] M. Yang, Z. Wei, H. Duan, Y. Lin, *Chem. Res. Chin. Univ.* **2018**, *34*, 440–443.
- [55] M. N. Gueye, A. Carella, J. Faure-Vincent, R. Demadrille, J.-P. Simonato, *Progress in Materials Science* **2020**, *108*, 100616.
- [56] H. Yamaguchi, K. Aizawa, Y. Chonan, T. Komiyama, T. Aoyama, E. Sakai, J. Qiu, N. Sato, *Journal of Electronic Materials* **2018**, *47*, 3370–3375.
- [57] H. Shi, C. Liu, Q. Jiang, J. Xu, *Advanced Electronic Materials* **2015**, *1*, 1500017.
- [58] J. Ouyang, Q. Xu, C.-W. Chu, Y. Yang, G. Li, J. Shinar, *Polymer* **2004**, *45*, 8443–8450.

- [59] C.-F. Chen, C. Dai, W.-Y. Chiu, *e-Polymers* **2008**, *8*, DOI 10.1515/epoly.2008.8.1.955.
- [60] S. Ernst, R. Langer, C. L. Cooney, R. Sasisekharan, *Critical Reviews in Biochemistry and Molecular Biology* **1995**, *30*, 387–444.
- [61] Y. C. Tam, E. C. Chan, *Infect. Immun.* **1985**, *47*, 508.
- [62] R. Stern, M. J. Jedrzejewski, *Chem. Rev.* **2006**, *106*, 818–839.
- [63] R. Moseley, R. J. Waddington, G. Embery, *Biochimica et Biophysica Acta (BBA) - Molecular Basis of Disease* **1997**, *1362*, 221–231.
- [64] B. Deschrevel, F. Tranchepain, J.-C. Vincent, *Matrix Biology* **2008**, *27*, 475–486.
- [65] T. Takano, H. Masunaga, A. Fujiwara, H. Okuzaki, T. Sasaki, *Macromolecules* **2012**, *45*, 3859–3865.
- [66] R. Kroon, D. A. Mengistie, D. Kiefer, J. Hynynen, J. D. Ryan, L. Yu, C. Müller, *Chemical Society Reviews* **2016**, *45*, 6147–6164.
- [67] U. Lang, E. Müller, N. Naujoks, J. Dual, *Adv. Funct. Mater.* **2009**, *19*, 1215–1220.
- [68] D. Tarus, E. Hachet, L. Messenger, B. Catargi, V. Ravaine, R. Auzély-Velty, *Macromolecular Rapid Communications* **2014**, *35*, 2089–2095.
- [69] K. Dodgson, R. Price, *Biochemical Journal* **1962**, *84*, 106–110.
- [70] S. B. Frazier, K. A. Roodhouse, D. E. Hourcade, L. Zhang, *Open Glycoscience* **2008**, *1*, 31–39.
- [71] M. Plätzer, J. H. Ozegowski, R. H. H. Neubert, *Journal of Pharmaceutical and Biomedical Analysis* **1999**, *21*, 491–496.
- [72] J. Li, K. Kisara, S. Danielsson, M. E. Lindström, G. Gellerstedt, *Carbohydrate Research* **2007**, *342*, 1442–1449.
- [73] G. E. P. Box, W. G. Hunter, J. S. Hunter, *Statistics for Experimenters: Design, Innovation, and Discovery, 2nd Edition*, **n.d.**
- [74] G. E. P. Box, D. R. Cox, *Journal of the Royal Statistical Society: Series B (Methodological)* **1964**, *26*, 211–243.
- [75] D. M. Miller, *The American Statistician* **1984**, *38*, 124–126.
- [76] Y. Yin, C. W. Carter, *Nucleic Acids Research* **1996**, *24*, 1279–1286.

Chapter 3.

Ink cross-linking

I. Introduction.....	136
II. First cross-linking assays.....	139
II.1. Dynamic cross-linking of PEDOT: HAS ₄ -PBA _{0.3}	139
II.2. First assays for cross-linking the ink via thiol-ene chemistry	140
II.2.a. Choice of thiol-ene chemistry and photoinitiator	141
II.2.b. Incorporation of PEDOT:HAS ₄ -PBA _{0.3} ink into a hydrogel	143
II.2.c. Cross-linking from functionalized EDOT	148
III. Development of alkene-functionalized HAS-PBA.....	152
III.1. Synthesis of HAS ₄ -PBA _{0.3} -PEGene _{0.22}	152
III.1.a. Grafting of pentenoate moiety in place of a sulfate	152
III.1.b. Introduction of a PEG spacer arm	154
III. 2. Polymerization of EDOT in the presence of HAS ₄ -PBA _{0.3} -PEGene _{0.22} and cross-linking	157
III.2.a. HAS ₄ -PBA _{0.3} -PEGene _{0.22} particle size	157
III.2.b. PEDOT: HAS ₄ -PBA _{0.3} -PEGene _{0.22} based ink conductivity.....	157
III.3. Stability of PEDOT:HAS ₄ -PBA _{0.3} -PEGene _{0.22} cross-linked films.....	159
III.3.a. Evolution of conductivity.....	159
III.3.b. Evolution of film microstructure when immersed in water.....	160
IV. Inkjet printing of PEDOT: HAS ₄ -PBA _{0.3} -PEGene _{0.22}	162
IV.1. Ink formulation.....	162
IV.2. Inkjet printing with Dimatix DMP-2800 printer	163
IV.2.a. Printing optimization.....	164
IV.2.b. Stability of conductive properties in humid medium	166
IV.2.c. Conclusion	167
V. Discussion.....	168
V.I. Inclusion of a conductive ink inside a cross-linked matrix.....	168
VI.2. Cross-linking PEDOT:HAS ₄ -PBA _{0.3} from PEDOT chains.....	169
VI.3. Cross-linking PEDOT:HAS ₄ -PBA _{0.3} from HAS ₄ -PBA _{0.3} chains	171
VI.4. Inkjet printing of cross-linkable PEDOT:HAS ₄ -PBA _{0.3} -PEGene _{0.22} ink.....	173
VI. Conclusion	175
VII. Materials and methods	176
VII.1. Synthesis	176
VII.1.a. Materials	176
VIII.1.b. Synthesis and characterization of HA-Fru	176
VII.1.c. Determination of the degree of substitution (DS) of HA-fructose by the follow of the amide coupling reaction.....	177

VII.1.d. Synthesis of HA-pentenoate	178
VII.1.e. Synthesis of N-(2,3-dihydroxypropan)-penten-5-amide	179
VII.1.f. Synthesis of methyl-EDOT-pentenoate	180
VIII.1.g. Synthesis of pent-5-enoxymethyl-EDOT	181
VII.1.h. Synthesis of PEDOTene _x :HAS ₄ -PBA _{0.3} ink	182
VII.1.i. Synthesis of PEGene	183
VII.1.k. Grafting of PBA and PEGene on HAS.....	184
VII.1.l. PEDOT:HAS ₄ -PBA _{0.3} -PEGene _{0.22} ink polymerization protocol	185
VII.2. Characterizations	185
VII.2.a. Rheology.....	185
VII.2.b. Photorheometry.....	186
VII.2.c. Ink film deposition on glass slides	187
VII.2.d. Conductivity measurements	187
VII.2.e. Functionalization of glass-slides with thiol moieties	187
VII.2.f. Dynamic Light Scattering (DLS)	188
VII.2.g. Viscosity measurements.....	188
VII.2.h. Surface tension	188
VII.2.i. Atomic force microscopy (AFM) analysis	189
VIII. Bibliography	190

I. Introduction

In the previous chapter, the development of a new conductive, biocompatible and degradable material was described. The PEDOT:HAS₄-PBA_{0.3} ink displayed unprecedented conductive properties for an ink based on a modified glycosaminoglycan, and was furthermore processable as it could be formulated to be inkjet-printed. However, dried films based on PEDOT: HAS₄-PBA_{0.3} dissolved in water, which prevented their use in wet medium. Thus, this low stability in the presence of water affected their suitability for biomedical applications.

A first solution to prevent material dissolution could be to include it in a waterproof sheath. This strategy has been implemented in many publications.

In the domain of neural recording/stimulation, Proctor *et al.*^[1] developed an electrocorticography device with an integrated microfluidic ion pump for simultaneous neural recording and electrophoretic drug delivery in vivo, embedding PEDOT:PSS conductive tracks into parylene C membrane. Leleux *et al.* also described the design of an electroencephalography device, including PEDOT:PSS tracks into a polyimide sheath^[2], as well as the development of an electrode for long-term cutaneous electrophysiological recordings, by embedding PEDOT:PSS between kapton membranes^[3]. Chiu *et al.*^[4] developed a glucose biosensor able to detect glucose concentration in blood from 100 μ M to 1 M. The conductive PEDOT:PSS tracks of this device were sandwiched between PET films.

But those different works still present a limitation: in case of damage of the protective sheath, the conductive tracks might be exposed to humidity and dissolve, resulting in an ineffective device. A way to overcome this is to cross-link the conductive material in order to make it insoluble in water and suitable for biomedical applications.

In soft electronics, cross-linkers can be added to the conductive ink formulation, to increase film stability or to anchor it to on a surface. Various cross-linkers have been used for PEDOT:PSS: 3-glycidoxypropyltrimethoxysilane (GOPS)^[5–7] (Figure 1), and more recently divinylsulfone (DVS)^[8] and poly(ethylene glycol)diglycidyl ether (PEGDE)^[9]. GOPS and PEGDE rely on the formation of a covalent bond with the sulfate moieties of PSS, while DVS reacts with free alcohol or amine groups present in commercial PEDOT:PSS formulation (addition of

ethylene glycol). The increase of GOPS concentration increases the film mechanical strength to the detriment of conductivity^[6], while DVS seems to have a small effect on conductivity while increasing film stability^[8].

Concerning their biocompatibility, GOPS and DVS have been used to stabilize PEDOT:PSS films on electrodes^[10], or PEDOT:PSS deposits on wearable monitoring devices^[8]. None of these studies have investigated the degradability of the cross-linked materials, nor their long term biocompatibility. However GOPS has been used to develop conductive biocompatible PEDOT:PSS scaffolds for 3D cell culture^[11]. Solazzo *et al.*^[9] have selected PEGDE, as PEG is widely used for biomedical applications. PEGDE seemed to enhance cytocompatibility, conductivity and hydrophilicity of PEDOT : PSS films. PEGylated cross-linkers therefore appeared as promising candidates for the development of water-stable PEDOT-based conductive materials for bioelectronics.

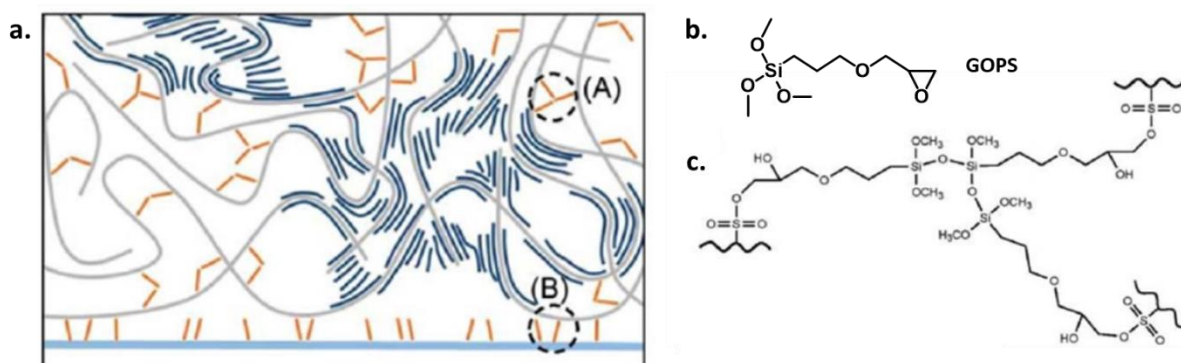


Figure 1. a. Structure of a PEDOT : PSS film cross-linked with GOPS. b. GOPS structure. c. GOPS cross-linking network.
adapted from Hånkansson *et al.*^[6].

However, all those studies have described the cross-linking of synthetic PEDOT:PSS with non-hydrolysable covalent bonds. The resulting insoluble material was not disintegrable in physiological conditions whereas the aim of this Ph.D. project was to design a transient conductive and biocompatible material. Therefore, hereafter, the cross-linking of biocompatible PEDOT:HAS₄-PBA_{0.3} conductive ink by biocompatible cross-linker via hydrolysable bonds was investigated.

The cross-linking of PEDOT:HAS₄-PBA_{0.3} was first investigated using PBA moieties that can form reversible boronate ester bonds with diol-containing molecules, such as

carbohydrates. Then, functional EDOT units were copolymerized with EDOT in order to cross-link the ink from the functional PEDOT chains. Finally, a new cross-linkable HAS₄-PBA_{0.3} derivative was synthesized for cross-linking the ink from the HAS₄-PBA_{0.3} chains.

II. First cross-linking assays

In the previous chapter, the best conductive ink was PEDOT: HAS₄-PBA_{0.3} ink **7** (chapter 2, Table 6). In this part, various strategies for cross-linking the ink were implemented in order to obtain water-stable ink films and tracks.

II.1. Dynamic cross-linking of PEDOT: HAS₄-PBA_{0.3}

The first strategy implemented to cross-link the PEDOT: HAS₄-PBA_{0.3} ink was to use the chemistry of boronic acid functions of HAS₄-PBA_{0.3}. Previous work at CERMAV showed the ability to prepare dynamic covalent hydrogels at physiological pH via the formation of reversible boronate ester bonds between two hyaluronic acid partners modified, respectively, by PBA and fructose moieties^[12]. Hydrogel networks were formed at a total polymer concentration of 15 g/L, higher than the overlap concentration of initial HA (initial HA M_w = 100 kg/mol, C^* \approx 3 g/L), with a molar ratio of PBA-to-grafted fructose of 1.

Herein, this strategy was exploited to cross-link the PEDOT: HAS₄-PBA_{0.3} ink **7** (chapter 2, Table 6) in PBS at pH = 7.4 by mixing it with HA (M_w = 100 kg/mol) modified with fructose (HA-Fru, DS_{Fru} = 0.15, Figure 2a). Based on the fact that the desired final concentration of HA-Fru in the mixture was 20 g/L, the PEDOT: HAS₄-PBA_{0.3} ink **7** was added at a concentration of 26 g/L corresponding to a molar ratio of PBA-to-grafted fructose of \sim 1. Indeed, assuming that 100 % of HAS₄-PBA_{0.3} had reacted with EDOT during ink **7** polymerization, HAS₄-PBA_{0.3} mass fraction in ink **7** can be calculated. Therefore the corresponding ink **7** concentration to have the desired amount of PBA moieties in the medium was 26 g/L.

However, no gelation was observed. Based on this result, PEDOT:HA-PBA_{0.3} ink **6** (chapter, Table 6), without sulfates, was mixed in the same conditions as described above with HA-Fru. A gel immediately formed in this case (Figure 2b), displaying an elastic modulus (G') around 1 kPa at 1 Hz (Figure 2c, detailed protocol). Furthermore, when the hydrogel was exposed to a series of several cycles of breaking and reforming, which consisted in applying high oscillation stresses (950 Pa) for 2 minutes, intercalated with low stresses (48 Pa) for 3 minutes, it was able to recover its initial rheological moduli, demonstrating its self-healing property (Figure 2d).

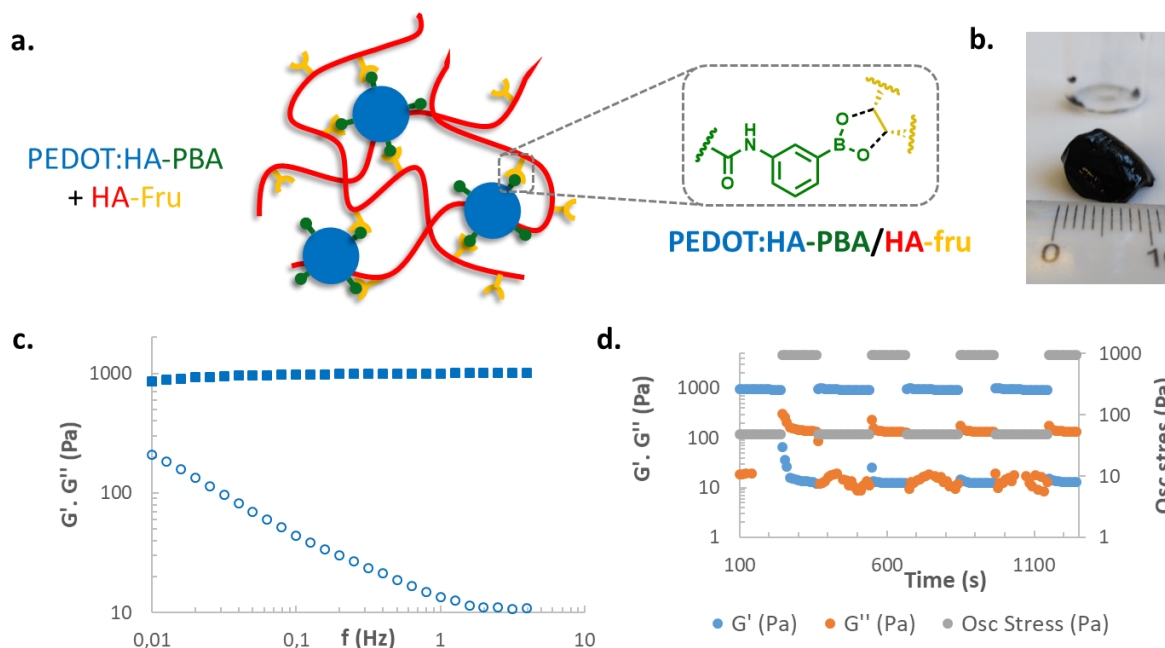


Figure 2. Structure and properties of PEDOT:HA-PBA_{0.3} / HA-Fru hydrogel. a. Scheme of cross-linking network of PEDOT:HA-PBA_{0.3} ink with HA-Fru. b. Resulting hydrogel. c. Frequency sweep of PEDOT:HA-PBA_{0.3} + HA-Fru hydrogel at 5% strain. d. Auto healing behavior of PEDOT:HA-PBA_{0.3} + HA-Fru hydrogel.

This experiment thus demonstrated the ability to obtain a hydrogel by crosslinking HA-Fru with PEDOT:HA-PBA_{0.3} particles (diameter of 300-700 nm), in contrast to PEDOT: HAS₄-PBA_{0.3} particles. This result may be attributed to a reactivity problem of PBA groups due to steric hindrance between adjacent sulfate groups.

However, the PEDOT:HA-PBA_{0.3} /HA-Fru hydrogel was not stable in diluted aqueous medium and dissolved in a few minutes, due the dynamic nature of the boronate ester cross-linkages. Based on these results, we investigated other crosslinking strategies based on the formation of covalent bonds between HA chains.

II.2. First assays for cross-linking the ink via thiol-ene chemistry

We proposed to use thiol-ene chemistry for crosslinking PEDOT: HAS₄-PBA_{0.3} films, as it benefits from mild reaction conditions, and allows for spatial and temporal tuning of material properties. Besides, it demonstrated several times its compatibility with sensitive biomolecules^[12,13]. Three crosslinking strategies were considered (Figure 3):

- Incorporation of the conductive ink into a polymer network cross-linked via thiol-ene chemistry.
- Cross-linking of PEDOT: HAS₄-PBA_{0.3} from the PEDOT domains.
- Cross-linking of PEDOT: HAS₄-PBA_{0.3} from the HAS₄-PBA_{0.3} chains.

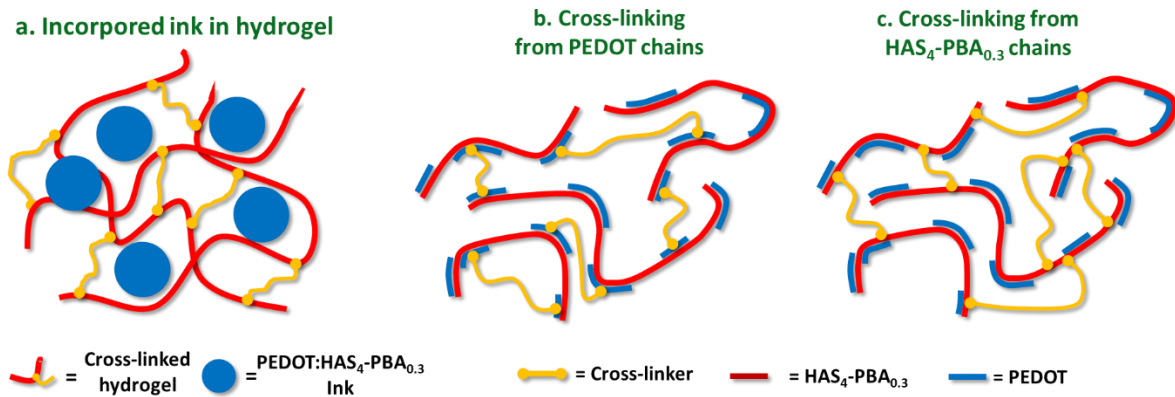


Figure 3. Three strategies to cross-link PEDOT:HAS₄-PBA_{0.3} material.

These will be successfully presented, after a short presentation of thiol-ene chemistry.

II.2.a. Choice of thiol-ene chemistry and photoinitiator

The chemical reaction used to cross-link the ink should create covalent irreversible though (bio)degradable bonds, without affecting the conductive properties of the ink, namely without modifying its chemistry, or the microstructure of the film. This excluded some usual cross-linking chemistry such as ring-opening, esterification, reductive amination or reaction with epoxides, as they require complex chemical environment, harsh conditions leading to polymer chain degradation, and lack of orthogonality in their selection of a chemical substrate.

Click chemistry reactions appeared promising as they are fast, effective, reliable, and selective. The radical addition of thiols on alkene double bonds can be considered as click chemistry because of its high reactivity and yield, simplicity, orthogonality with other reactions and broad variety of available reagents^[14,15]. It was known for a long time, but reintroduced in 2001 by Sharpless *et al.*^[16]. The admitted chemical mechanism starts with the formation of a thiyl radical resulting from the cleavage of the sulfur-hydrogen bond, which can react with almost all unhindered alkene bond. The thiyl radical propagates via the alkene,

forming a thioether bond with anti-markovnikov region-selectivity (Figure 4). Ideally, the same amount of thiol and alkene are consumed, without ene-to-ene coupling.

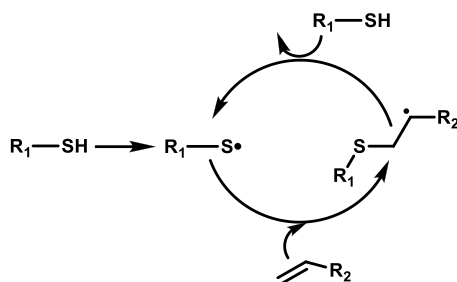


Figure 4. Thiol-ene reaction mechanism.

Contrary to methacrylate systems, thiol-ene reactions are not inhibited by oxygen species dissolved in the medium, which enables to work under atmospheric conditions. The initial thiyl radical can be formed by direct irradiation under UV light, but the use of photo-initiator is preferred. The concentration of photo-initiator should be optimized as too little photo initiator will result in slow cross-linking kinetics and incomplete cross-linking, but too much photo-initiator may result into competitive reactions between the thiyl and initiator radicals.

UV or visible light is required to activate the photo-initiator and form radical. Since PEDOT highly absorbs light, with a minimum of absorption around 400-450 nm, depending on the dopant, it is important to select a photo initiator with high reactivity and high molar extinction coefficient in this wavelength range. In addition, the photo initiator should be biocompatible, and soluble in water.

Three different photo-initiators were considered: hydroxy-1-[4-(2-hydroxyethoxy)phenyl]-2-methyl-1-propanon (Irgacure 2959), lithium phenyl-2,4,6-trimethylbenzoylphosphinate (LAP) and phenylbis(2,4,6-trimethylbenzoyl)phosphine oxide (Irgacure 819) (Figure 5a). All of them appeared to be biocompatible^[17,17-19]. However, Irgacure 819 was hardly soluble in water, and reported protocols to solubilize it in water were not adapted to our system^[20]. This photo-initiator was discarded in spite of its high absorbance at high wavelength, which would have been very convenient (Figure 5c). As Irgacure 2959 is very soluble in water, it is one of the most used photo-initiator in thiol-ene chemistry. However

LAP displays a higher molar extinction coefficient for wavelengths higher than 350 nm (Figure 5c), has been reported more biocompatible and reactive than Irgacure 2959^[19]. Therefore, this photo-initiator was selected for this Ph.D. project.

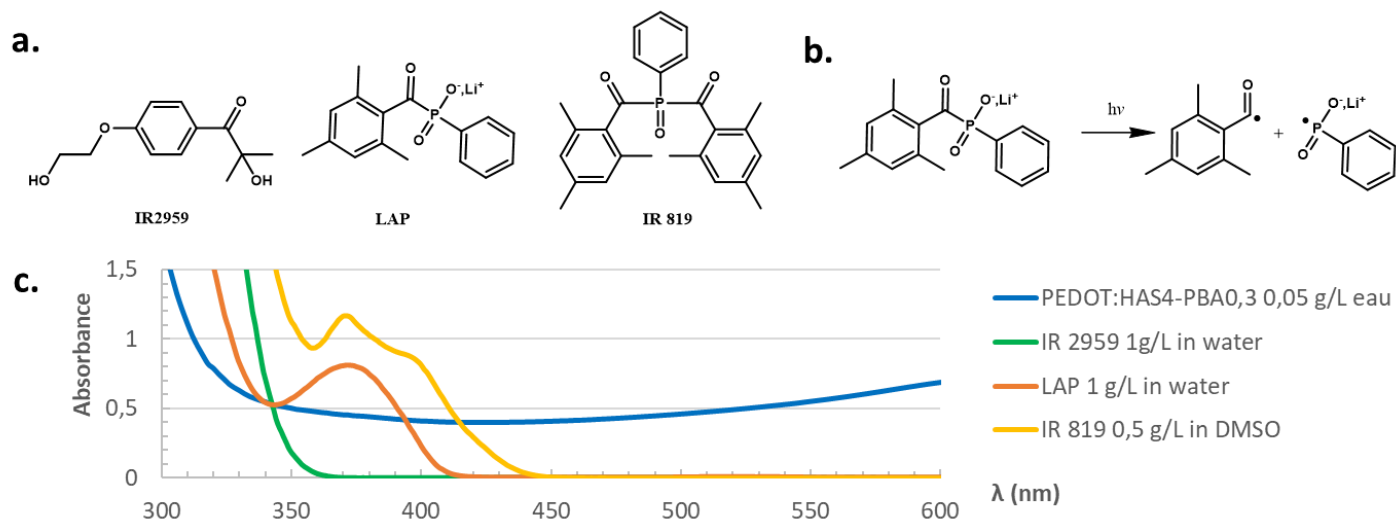


Figure 5. Structure and absorbance properties of various photoinitiators. a. Three assessed photoinitiators. b. UV-induced cleavage of LAP yielding to radical formation. c. Absorbance of photoinitiators and PEDOT:HAS4-PBA ink.

II.2.b. Incorporation of PEDOT:HAS₄-PBA_{0.3} ink into a hydrogel

As the polymer network should display the same properties of biocompatibility and degradability as PEDOT: HAS₄-PBA_{0.3} ink, hyaluronic acid appeared as the best candidate as matrix component. HA ($M_w = 113$ kg/mol) was thus functionalized by alkene groups by reaction with pentenoic anhydride according to a procedure reported by Mergy *et al.*^[13], and the resulting HA-pentenoate derivative ($DS_{\text{pentenoate}} = 0.2$) was cross-linked with different bis-thiol derivatives (Figure 6). 1,4-Dithiothreitol (DTT) was used as a short cross-linker, and a PEG bis-thiol (PEG-(SH)₂), with $M_n = 750$ g/mol, was used as a long cross-linker.

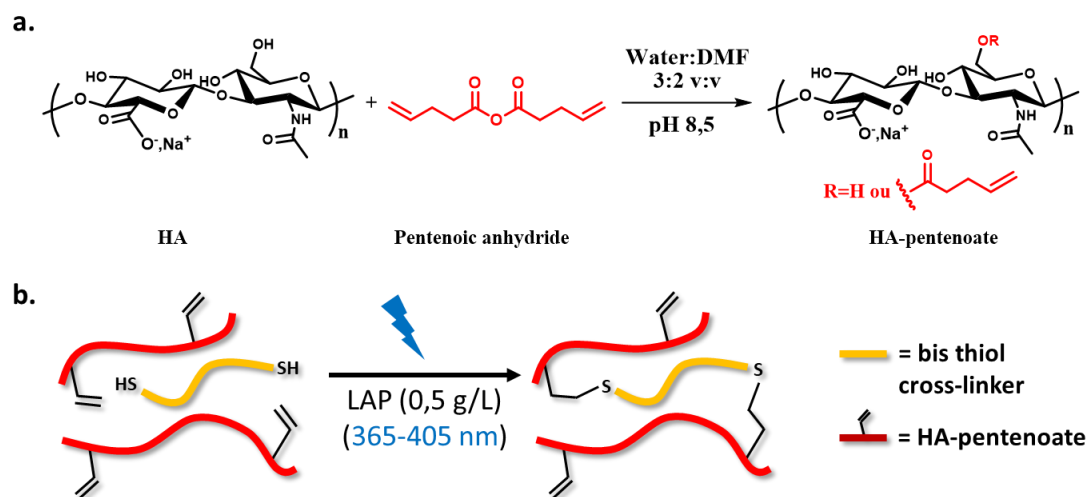


Figure 6. a. Synthesis of HA-pentenoate. b. Cross-linking by thiol-ene chemistry.

Cross-linking kinetics

The kinetics of the cross-linking reaction photoinitiated by LAP was first investigated using a rheometer equipped with a UV curing cell (detailed protocol in section VII.2.b.). Various hydrogel precursor mixtures (HA-pentenoate + cross-linker + photoinitiator in PBS), were added to PEDOT: HAS₄-PBA_{0.3} ink, and photocross-linked (Table 1). The elastic (storage) and loss moduli, G' and G'' , were monitored over time (Figure 7).

The samples were equilibrated for 2 min before being exposed to UV light for a time of 35 to 100 min. Initially, G'' was larger than G' , which reflected the viscous behavior of the sample. After an induction period, the storage and loss moduli increased due to the formation of intermolecular cross-links. The gelation time was recorded at the crossover of G' and G'' ^[21]. Formulations **1** and **2** (Table 1), prepared without PEDOT: HAS₄-PBA_{0.3} ink, formed quickly a gel, as seen from the variation of the elastic and loss moduli upon UV exposure (Figure 7). This G' modulus increased quickly before reaching progressively a plateau. On the other hand, the gelation time was dramatically increased for formulation **3**, prepared with PEDOT: HAS₄-PBA_{0.3} ink at a concentration of 6.5 g/L, while no crossover point of G' and G'' could be observed for formulation **4**, containing PEDOT: HAS₄-PBA_{0.3} ink at a concentration of 13 g/L, within the time of experiment (Figure 7). This indicated that the gelation time was not yet reached for the latter formulation.

Chapter 3. Ink cross-linking

Table 1. Photo-cross-linking of various formulations under irradiation at 365 nm at 20 mW/cm². All reactions were performed using LAP at a concentration of 1 g/L.

Hydrogel #	DS _{pentenoate}	[HA-pentenoate] (g/L)	Cross-linker	n _{SH} /n ₌	[PEDOT:HAS ₄ -PBA _{0.3}] (g/L)	Gelation time (min)	G' / G'' at the end of the experiment (Pa)	
							G'	G''
1	0.25	14	PEG-(SH) ₂ 750 g/mol	0.5	0	3.3	827	2.2
2	0.25	27	DTT	1	0	7.4	5678	78
3	0.25	27	PEG-(SH) ₂ 750 g/mol	1	6.5	28	2600	183
4	0.25	27	PEG-(SH) ₂ 750 g/mol	1	13	>100	NA	NA

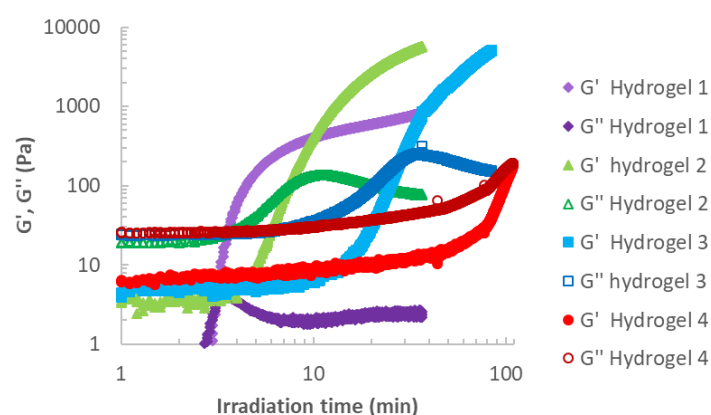


Figure 7. Variation of the G' and G'' moduli for various HA-pentenoate/bis-thiol cross-linker formulations.

These results revealed a significant slowing down of the gelation process of HA-pentenoate/bis-thiol mixtures upon addition of PEDOT: HAS₄-PBA_{0.3} ink. This was likely due to UV light absorption of the ink, which reduced radical formation. It should be noted that these experiments were carried out from 400 μ L of formulations deposited on the rheometer plate with a diameter of 2 cm, resulting in a gel thickness of \sim 320 μ m. Increasing the UV light power and decreasing the thickness of the gelling solution could have decreased the gelation time.

Ink film deposition on thiol-functionalized glass slides

To assess the influence of ink incorporation in a cross-linked matrix on conductivity, various hydrogel precursor mixtures were deposited on glass-slides, irradiated and dried. In order to evaluate the variation of the conductivity of the cross-linked film after immersion in water, the glass slides were functionalized by thiols in order to covalently link the hydrogel matrix to the surface (Figure 8). Glass slides were functionalized using a protocol developed previously at CEA.

Chapter 3. Ink cross-linking

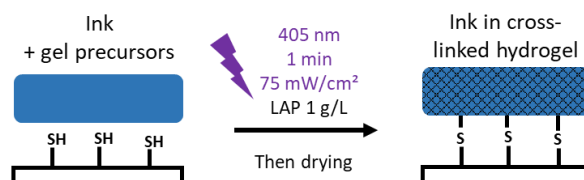


Figure 8. Cross-linking of HA-pentenoate + PEG-(SH)₂ including dissolved PEDOT: HAS₄-PBA_{0.3} ink **4** on a thiol functionalized glass slide.

PEDOT: HAS₄-PBA_{0.3} ink **4** was dissolved at 13 g/L, in a mixture of HA-pentenoate solubilized in water (15 g/L) in the presence of LAP (1 g/L) and PEG-(SH)₂ (M_n = 750 g/mol, 4.7 g/L to have [SH] = [alkene]). 60 μ L were deposited on a glass slide inside a silicon ring of 1 cm inner diameter (which serves as a removable well). Then, the mixture was either dried overnight, then photocross-linked, or immediately cross-linked under UV light and then, dried overnight. All films were irradiated 1 minute at 405 nm at a light power of 75 mW/cm² to deliver a high amount of energy to the photoinitiator, in the minimum absorption band of PEDOT: HAS₄-PBA_{0.3}.

Conductivity and appearance

Film thickness and resistivity were measured to deduce their conductivity as described in chapter 2. Depending on whether they were irradiated then dried, or dried then irradiated, films displayed different characteristics and behavior (Table 2).

Table 2. Characteristics of ink films grafted to a thiol functionalized glass slide.

Process sequence	Irradiated then dried	Dried then irradiated
Film Aspect	Homogenous, visually smooth	Heterogeneous, visually rough
Electric behavior	Linear U/I electrical characteristic	Irregular U/I electrical characteristic. but increasing I as U increased.
Conductivity σ (S/cm)	$\approx 10^{-4} - 10^{-3}$ S/cm	$\approx 10^{-2} - 10^{-1}$ S/cm

It was observed that the presence of the PEDOT: HAS₄-PBA_{0.3} ink into a cross-linked HA-pentenoate/PEG-(SH)₂ network resulted in important conductivity decrease, dropping from 1.5–2 S/cm for pure PEDOT: HAS₄-PBA_{0.3} ink based films to 10⁻¹ to 10⁻⁴ S/cm. It is interesting to note that films that were cross-linked and then dried displayed a better aspect than films that were dried and then cross-linked, but a conductivity one to two orders of magnitude lower than the latter ones.

Stability in water

To investigate the stability of those films in aqueous medium, glass slides were immersed in water or in PBS. In a few minutes, all films detached from the glass slides, and rolled on themselves to form tubes. After 10 to 20 additional minutes, all films unrolled, yielding to floating discs, whose diameters were two to three times larger than initial ink films. Films immersed in PBS swelled less than films immersed in water due to screening of electrostatic repulsion in PBS (Figure 9).

This behavior may be attributed to a differential cross-linking in the thickness of the film during irradiation: upper layers of ink were more cross-linked than bottom layers, as UV photons were absorbed by PEDOT. Therefore, less cross-linked layers swelled more when immersed in water. This differential swelling throughout the film thickness resulted in the self-rolling. Films finally unrolled as the swelling equilibrium was reached in all the thickness of the cross-linked ink film.

The important swelling of the films was too high to keep them attached to the surface.

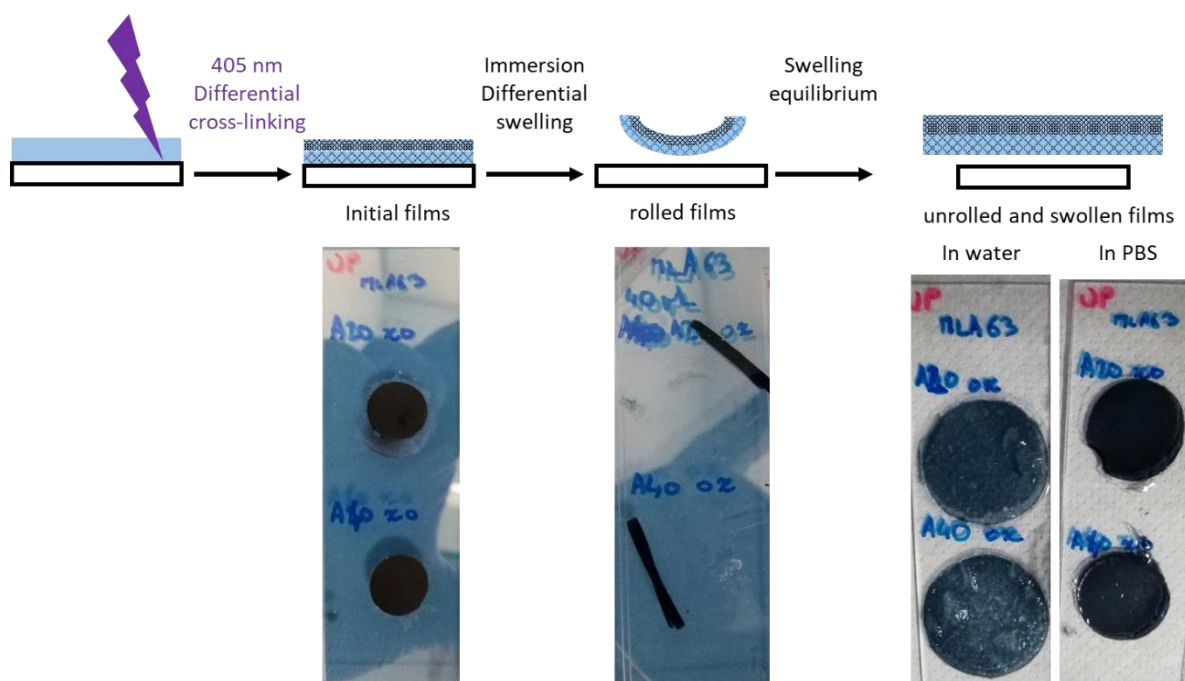


Figure 9. Cross-linked ink film behavior and interpretation when immersed.

Conclusion

Films that were cross-linked before drying had the most important drop of conductivity of 3 to 4 orders of magnitude. It is probable that the cross-linking of HA-ene with PEG-(SH)₂ prevented the structuration of ink particles as conductive domains could not adjust one to

another via hydrophobic interactions or π -stacking. Besides, films that were cross-linked after drying suffered a conductivity drop of 1 or 2 orders of magnitude, which was less important than in the former case. This suggested that in this case, the film could reorganize itself during the drying process, but that the hydrogel matrix acted as an insulator.

Those results evidenced that the strategy consisting in incorporating the conductive ink into a non-conductive cross-linked network was not relevant. Indeed, the non-conductive hydrogel matrix may act as an insulator, decreasing conductivity. As a consequence, the ink must be part of the cross-linking network itself, in order to minimize the addition of insulating components, and to constraint the swelling of the final material. Finally, the ink should be cross-linked after drying in order to enable the re-organization of conductive domains during drying.

II.2.c. Cross-linking from functionalized EDOT

Based on the previous results, we investigated the possibility to crosslink the PEDOT: HAS₄-PBA_{0.3} films from the PEDOT domains. This required the functionalization of EDOT with suitable groups.

To the best of our knowledge, there are only few publications reporting the cross-linking of PEDOT:dopant conductive material from the PEDOT domains. Mantione *et al.*^[22] cross-linked PEDOT:PSS introducing EDOT functionalized with carboxyl groups, using an esterification reaction with ethylene glycol to cross-link PEDOT domains. Inspired by this work, we aimed to design an EDOT monomer, functionalized with an alkene function to cross-link PEDOT: HAS₄-PBA_{0.3} by a thiol-ene coupling reaction. This targeted molecule was referred to as EDOT-ene in the following sections (Figure 10).

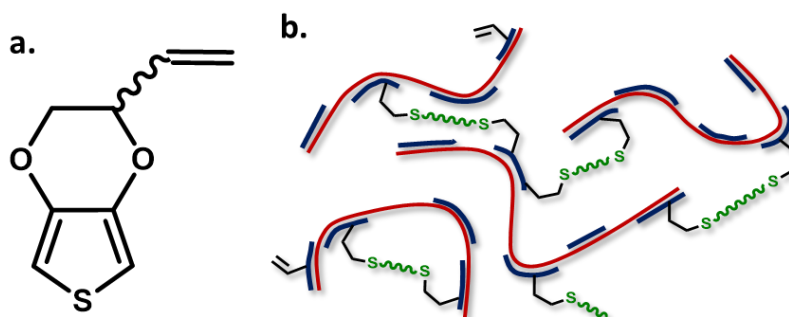


Figure 10. a. Structure of targeted EDOT-ene. b. Hypothetic structure of PEDOT:HAS-PBA cross-linked by dithiols using alkene moieties of EDOT-ene.

Three synthesis were attempted to obtain EDOT-ene derivatives, starting from two different molecules: 3,4-dimethoxythiophene (Entry 1, Table 3), or hydroxymethyl-EDOT (Entry 2 and 3, Table 3).

Table 3. Synthesized EDOT-ene molecules.

Entry	EDOT-ene	Synthetic pathway	Synthesis completed?
1		<p>I. $r = 75 \%$</p> <p>II. $r = 51 \%$</p>	X
2		$r = 51 \%$	V
3		$r = 35 \%$	V

Synthesis from 3,4-dimethoxythiophene

We first aimed to synthesize EDOT-ene in entry 1 (referred to as EDOT-ene 1) in two steps from 3,4-dimethoxythiophene^[13]. The first step relied on an amidation reaction between 2,3-dihydroxypropylamine and pentanoic anhydride carried out in DMF in the presence of *N,N*-diisopropylamine to neutralize the formed pentanoic acid (Table 3). The resulting

pentenamide derivative was then reacted with 3,4-dimethoxythiophene in toluene according to a previously reported procedure^[22,23]. However, no transesterification reaction occurred, which was attributed to the poor low solubility of the pentamide derivative in the reaction medium.

Synthesis from hydroxymethyl EDOT

Hydroxymethyl-EDOT, a commercial EDOT derivative, was then used to synthesize the EDOT-ene derivatives shown in entry **2** and **3** of Table 3, and referred to as EDOT-ene **2** and **3**. Hydroxymethyl-EDOT has been widely used as a precursor for functionalizing EDOT, especially to increase the EDOT solubility in polar protic solvent^[7].

Hydroxymethyl-EDOT was successfully esterified with pentenoic anhydride using conditions similar to the first step of EDOT **1** synthesis, yielding EDOT-ene **2** with a 51 % yield (Table 3). EDOT-ene **3** was synthesized with a 35 % yield by reaction between bromopent-5-ene and hydroxymethyl-EDOT according to literature methods^[24,25]. The reactivity of both EDOT-ene **2** and **3** with thiols in photo-activated chemistry could not be assessed directly as none of them were soluble in water.

Each EDOT-ene derivative was then co-polymerized with EDOT in the presence of HAS₄-PBA_{0.3} as described previously, yielding PEDOT-ene_x: HAS₄-PBA_{0.3} inks, where x was the fraction of EDOT-ene (**2** or **3**) on total EDOT. Inks with x = 0.25 and 0.5 were thus synthesized. Different sets of cross-linking parameters were tested (PEG-(SH)₂ with M_n = 750 or 3500 kg/mol, [LAP] = 0.5 or 1 g/L, [PEDOT-ene_x: HAS₄-PBA_{0.3}] = 13, 20 or 40 g/L, water or PBS, and pH = 5.6 or 7.4). Yet, none of them enabled to cross-link those inks under UV light exposure at 365 nm in the presence of PEG-(SH)₂ and LAP.

¹H NMR spectra of those inks displayed no signal in the alkene region (between 4.7 and 6.2 ppm), but interestingly, also not signal corresponding to EDOT or EDOT-ene **2** or **3** (Figure 11). Only proton signals of HAS₄-PBA_{0.3} could be observed, despite PEDOT domains were present, as evidenced by the deep blue color of the inks.

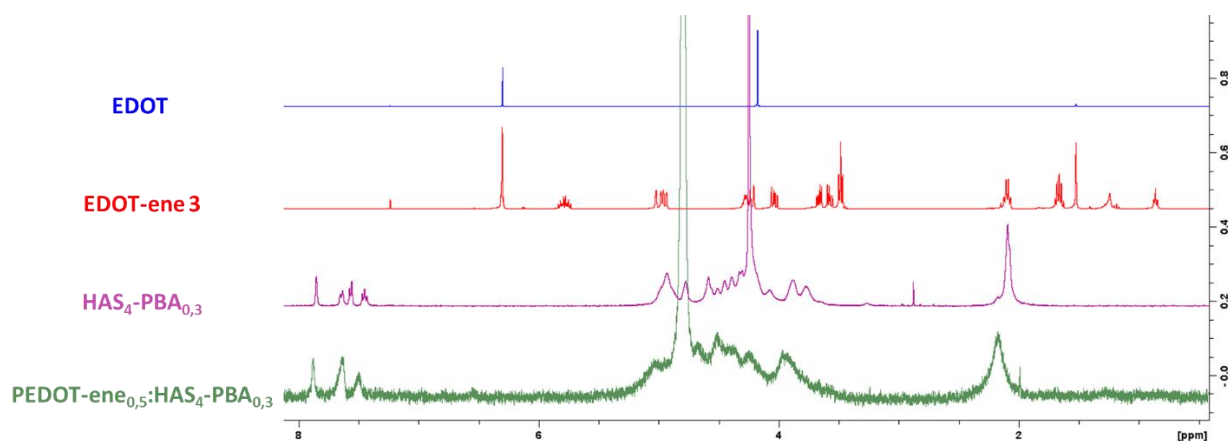


Figure 11. ^1H NMR spectra of PEDOT-ene_{0.5}:HAS₄-PBA_{0.3} ink in D_2O at 25 °C, HAS-PBA in D_2O at 80 °C, EDOT and EDOT-ene 3 in CDCl_3 at 25 °C.

The absence of proton signals from PEDOT suggested that the PEDOT domains were “buried” deep inside the PEDOT-ene_x: HAS₄-PBA_{0.3} particles. This assumption was supported by the fact that like EDOT, EDOT-ene monomers were hydrophobic, since the aliphatic chain added to EDOT did not increase its affinity with water. The structure of PEDOT-ene_x: HAS₄-PBA_{0.3} particles was likely similar to the one of PEDOT: HAS₄-PBA_{0.3} particles, with a core rich in EDOT, stabilized by and entangled in HAS₄-PBA_{0.3} chains, which are hydrophilic. Therefore, the alkene anchors introduced to cross-link the ink were probably sterically not available, preventing the thiol-ene reaction and hydrogel formation.

III. Development of alkene-functionalized HAS-PBA

Based on the previous results, we finally focused on crosslinking PEDOT-HAS-PBA films via thiol-ene chemistry after introducing alkene groups on HAS-PBA.

III.1. Synthesis of HAS₄-PBA_{0.3}-PEGene_{0.22}

Two strategies were explored to introduce an alkene group on HAS₄-PBA_{0.3}. They are described in the following section.

III.1.a. Grafting of pentenoate moiety in place of a sulfate

As HAS₄-PBA_{0.3} was already heavily substituted by sulfates ($DS_S = 4$) and PBA moieties ($DS_{PBA} = 0.3$), the first attempt consisted in introducing pentenoate groups in place of some sulfate functions. HA-pentenoate was synthesized as described before ($DS_{\text{pentenoate}} = 0.2$), then sulfated in order to replace all remaining hydroxyl groups by sulfates functions (using the sulfatation protocol detailed in chapter 2). The resulting sulfated HA with pentenoate moieties (abridged HAS-ene) was then further modified by introducing PBA moieties (according to PBA grafting protocol detailed in chapter 2) (Figure 12). ¹H NMR analysis of the final product HAS-ene-PBA gave $DS_{\text{pentenoate}} = 0.12$ and $DS_{PBA} = 0.35$ as expected (Figure 13).

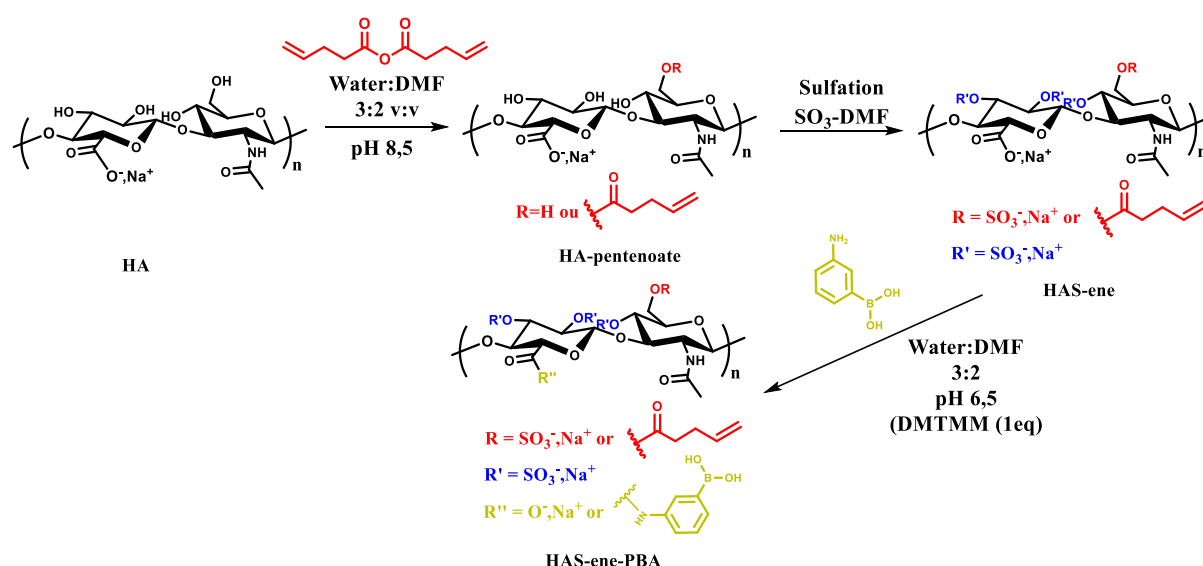


Figure 12. 3 steps synthesis of HAS₄-ene-PBA_{0.3}. To simplify this scheme, it is assumed that the primary OH group of the N-acetylglucosamine unit of HA has been converted into pentenoate and that the other remaining OH groups have been sulfated. However, the esterification reaction with pentenoic anhydride can occur at other positions.

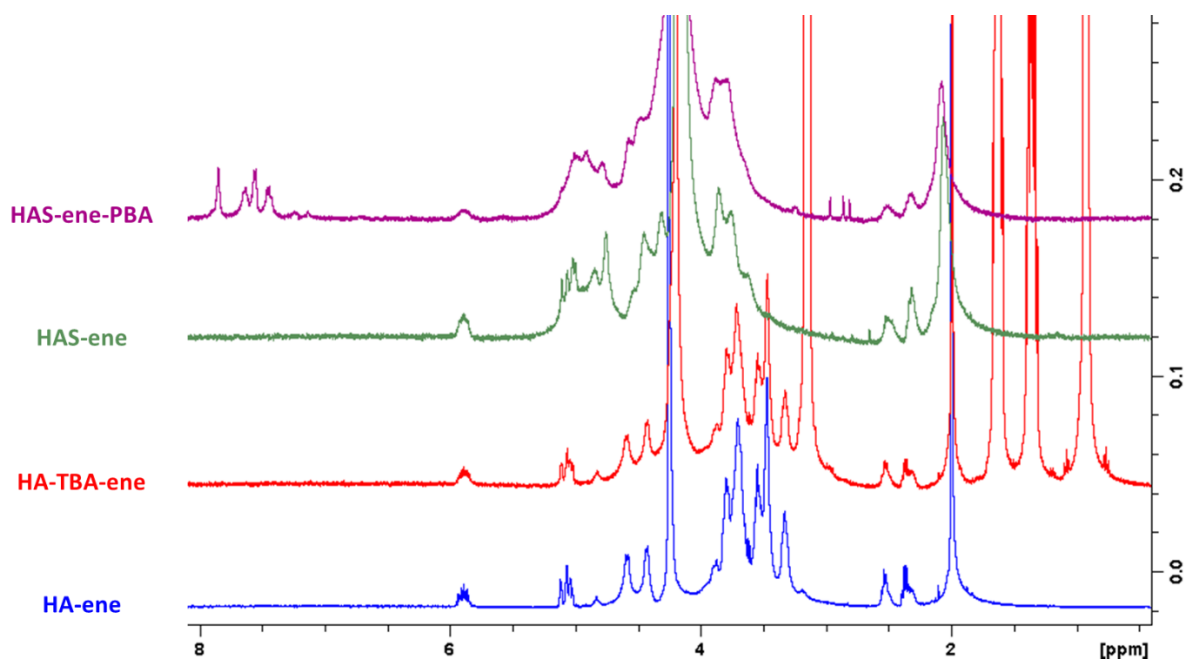


Figure 13. ^1H NMR spectrum of various intermediates from HA-pentenoate (abridged HA-ene) to HAS-ene-PBA.

Based on previous observations indicating reactivity problems of PBA moieties due to steric hindrance caused by adjacent sulfate groups (Chapter 3, section II.1.), we verified by ^1H NMR the reactivity of the alkene groups of HAS-ene-PBA using a highly reactive thiol, 3-mercaptopropionic acid (3MPA), after UV exposure in the presence of 1g/L of LAP (Figure 14a). To this end, HAS-ene-PBA was dissolved in D_2O in the presence of LAP (1 g/L), and 3MPA (1 molar equivalent with respect to alkene functions). The mixture was analyzed by ^1H NMR before and after irradiation at 365 nm for 10 minutes at 65 mW/cm^2 (Figure 14b). The integration of the signal corresponding to the alkene proton of HAS-ene-PBA at 5.9 ppm did not change before and after irradiation, indicating that no thiol-ene coupling occurred between 3MPA and HAS-ene-PBA.

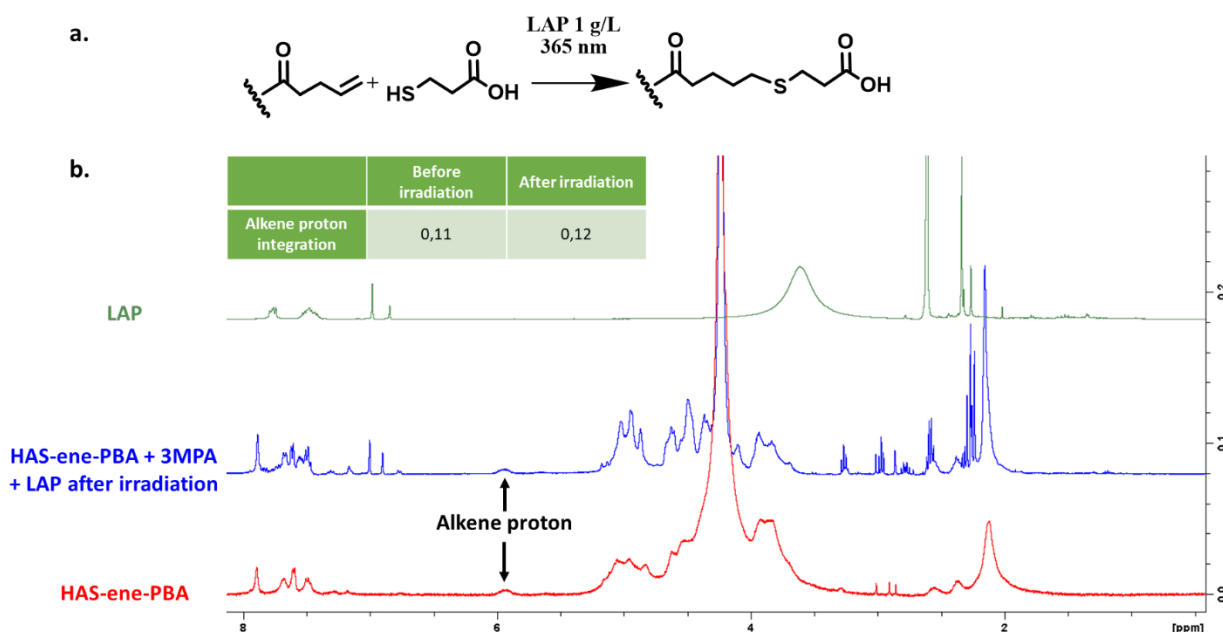


Figure 14. a. Expected reaction of HAS-ene-PBA with 3MPA, under irradiation, in the presence of LAP. b. ^1H NMR spectrum of HAS-ene-PBA and (HAS-ene-PBA + 3MPA + LAP) after UV irradiation, in D_2O at 80 °C, and LAP in CDCl_3 at 25 °C.

This absence of reactivity supported our assumption that the sulfate groups induced steric hindrance and thereby prevented chemical reactions with the HA backbone. This suggested that a spacer between the sulfated HA backbone and the alkene moiety should be introduced to cross-link HAS-PBA by a thiol-ene coupling reaction.

III.1.b. Introduction of a PEG spacer arm

In order to overcome the absence of reactivity of the pentenoate groups directly linked to HA, we used an heterobifunctional oligo(ethylene glycol) (oligoPEG) spacer arm with a pentenoate group at one end, and an amine group at the other end. This PEG oligomer will be referred to as “PEGene” in the following. The use of a hydrophilic PEG oligomer ensured the solvation of the spacer and thus its distancing from the $\text{HAS}_4\text{-PBA}_{0.3}$ backbone.

PEGene was synthesized in two steps from commercial O-(2-aminoethyl)-O'-[2-(Boc-amino)ethyl]deca(ethylene glycol) ($\text{H}_2\text{N}-(\text{PEG})_{11}\text{-NH-Boc}$, Figure 15). Briefly, pentenoic anhydride was first reacted with $\text{H}_2\text{N}-(\text{PEG})_{11}\text{-NH-Boc}$ to yield the pentenamide derivative $\text{CH}_2=\text{CH}-(\text{CH}_2)_2\text{-CO-HN}-(\text{PEG})_{11}\text{-NH-Boc}$. After purification, the protective Boc group was

removed by treatment with trifluoroacetic acid. After purification, PEGene was recovered with a total yield higher than 80%.

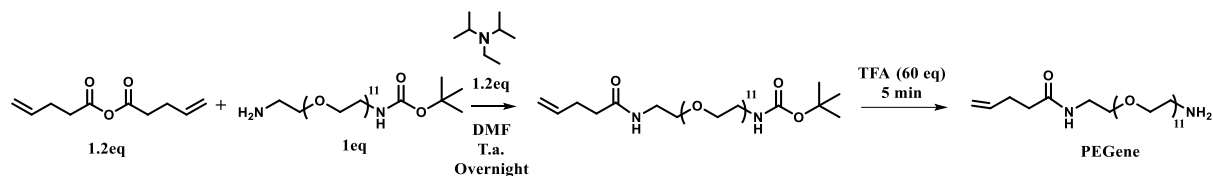


Figure 15. Synthesis of PEGene in two steps from *O*-(2-aminoethyl)-*O'*-[2-(Boc-amino)ethyl]deca(ethylene glycol).

PEGene was then reacted with the remaining carboxylates on HAS-PBA using DMTMM as a coupling agent, at pH 6.5. Reactions with various equivalents of PEGene compared to HAS-PBA were implemented (Table 4a), resulting in different substitution degrees in PEGene (DS_{PEGene}). The DS_{PEGene} value was determined by ^1H NMR, from the integration of the alkene proton signal at 5.9 ppm, using the integration of HAS acetyl protons signal at 2.15 ppm as a reference (Table 4a). The grafting ratio was constant around 0.4.

Table 4. Grafting of PEGene on $\text{HAS}_4\text{-PBA}_{0.3}$ (a) or simultaneous grafting of PEGene and 3-APBA on HAS_4 (b).

a.

Grafting of PEGene on HAS-PBA		
Equivalent of PEGene	DS_{PEGene}	Grafting yield (%)
0.3	0.11	37
0.4	0.15	38

b.

Simultaneous grafting of PEGene and 3APBA on HAS					
Equivalent of PEGene	DS_{PEGene}	Grafting yield (%)	Equivalent of 3APBA	DS_{PBA}	Grafting yield (%)
0.3	0.12	40	0.3	0.3	100
0.4	0.16	40	0.3	0.3	100
0.6	0.22	37	0.3	0.3	100

Interestingly, PEGene could be grafted on HAS_4 simultaneously with 3APBA in the same conditions (Table 4b, Figure 16). PEGene and 3APBA grafting ratio were the same as when they were grafted separately: those two reagents did not interfere. Noticeably, the grafting yield of PEGene (≈ 0.4) was much lower than the grafting yield of 3-APBA on HAS, close to 100 % in less than 24h. This could be explained by the highest nucleophilicity of the amine of 3-APBA, as it is in ortho position of an electro-attractor boron atom, whereas the amine of PEGene is connected to an aliphatic chain, with almost no inductive donor effect.

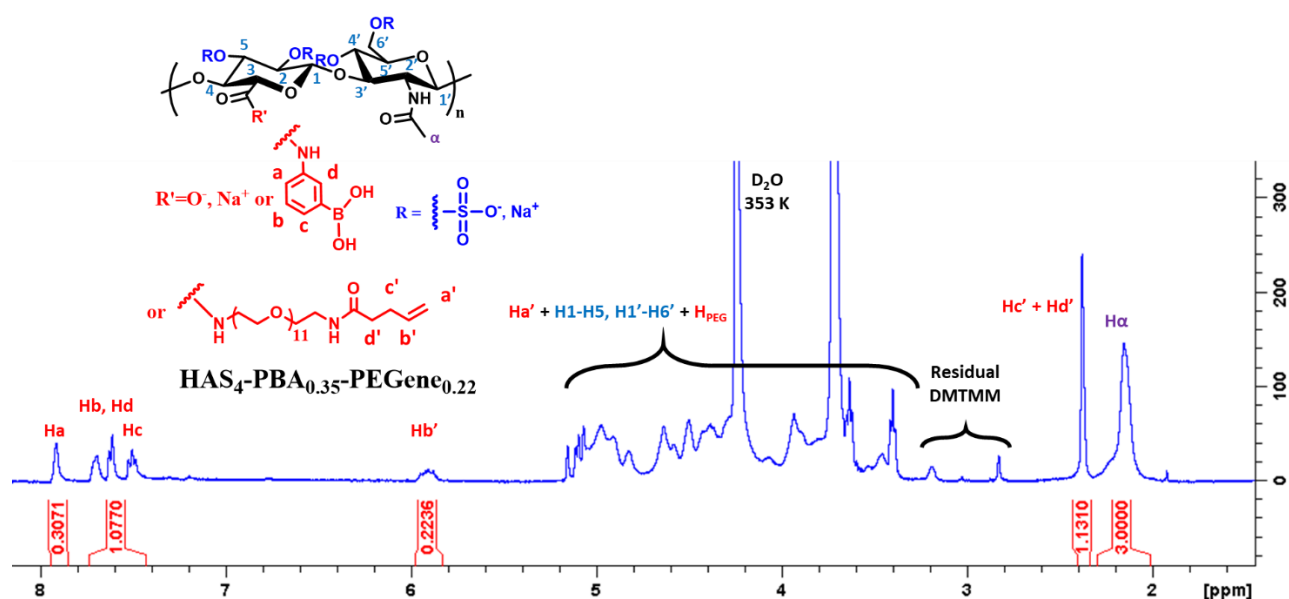


Figure 16. ^1H NMR spectrum of $\text{HAS}_4\text{PBA}_{0.35}\text{-PEGene}_{0.22}$, in D_2O (4mg/mL) at 80°C .

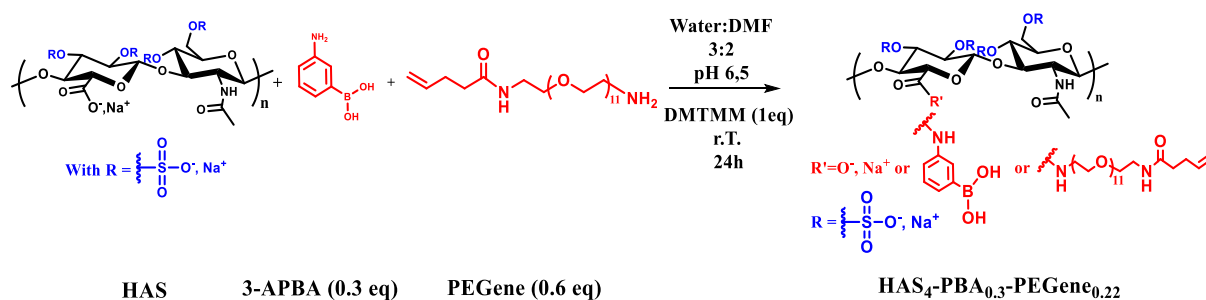


Figure 17. Coupling of PEGene and 3-APBA with HAS.

The reactivity of $\text{HAS}_4\text{-PBA}_{0.3}\text{-PEGene}_{0.22}$ towards thiols was also investigated. To this end, $\text{HAS}_4\text{-PBA}_{0.3}\text{-PEGene}_{0.22}$ was solubilized in water at a concentration of 25 g/L in the presence of LAP (1g/L) and PEG-(SH)₂ ($M_n = 3.5$ kg/mol, 7.6 g/L to have $[\text{SH}] = [=]$). After exposure to UV light at 365 nm at 20 mW/cm² for 10 min, a gel was observed. This confirmed successful thiol-ene coupling reaction between $\text{HAS}_4\text{-PBA}_{0.3}\text{-PEGene}_{0.22}$ and PEG-(SH)₂. Thus, this result demonstrated that the presence of a long PEG spacer arm between $\text{HAS}_4\text{-PBA}_{0.3}$ backbone and the alkene function is key for cross-linking the ink.

$\text{HAS}_4\text{-PBA}_{0.3}\text{-PEGene}_{0.22}$, possessing the highest $\text{DS}_{\text{PEGene}}$ value, was then used for the ink cross-linking experiments.

III. 2. Polymerization of EDOT in the presence of HAS₄-PBA_{0.3}-PEGene_{0.22} and cross-linking

EDOT was polymerized in the presence of HAS₄-PBA_{0.3}-PEGene_{0.22}, following the optimized protocol previously established in chapter 2 (section III.3.). All PEDOT: HAS₄-PBA_{0.3}-PEGene_{0.22} inks (referred to as **inkXL** for cross-linkable ink) were polymerized without acetonitrile, nor surfactant, with 0.005 eq of FeSO₄ as catalyst, and a molar ratio EDOT / HAS₄-PBA_{0.3}-PEGene_{0.22} of 4.

III.2.a. HAS₄-PBA_{0.3}-PEGene_{0.22} particle size

The effect of the concentration of (HAS₄-PBA_{0.3}-PEGene_{0.22} + EDOT) on the final particle size was investigated (Table 5). Similar to the PEDOT:HAS₄-PBA_{0.3} ink, the PEDOT: HAS₄-PBA_{0.3}-PEGene_{0.22} ink particle size increased when the concentration during polymerization increased (Chapter 2, Table 8), enabling a fine tuning of particle size for subsequent processing.

Table 5. Effect on ink particle size of HAS₄-PBA_{0.3}-PEGene_{0.22} + EDOT concentration during EDOT polymerization.

InkXL #	[HAS-PBA-PEGene + EDOT] (g/L)	Characterization		
		Filter	Z _{Average} (nm)	PDI
1	10	0.8 µm	320 ± 12	0.22 ± 0.03
2	17	1.2 µm	370 ± 18	0.28 ± 0.03
3	20	1.2 µm	370 ± 13	0.23 ± 0.03
4	25	1.2 µm	656 ± 53	0.32 ± 0.04
5	40	Not filterable		

III.2.b. PEDOT: HAS₄-PBA_{0.3}-PEGene_{0.22} based ink conductivity

The conductivity of films based on inkXL **1** (Table 5) alone or cross-linked with PEG-(SH)₂ was measured using a 4 point probe to determine their resistivity, and a profilometer to determine film thickness. InkXL **1** was suspended in water at 13 g/L. If cross-linked, PEG-(SH)₂ 3.5 kg/mol and LAP were added to obtain a molar ratio $n_{\text{thiol}}/n_{\text{alkene}} = 1$, and so as to have [LAP] = 1 g/L. To calculate the cross-linker concentration, it was assumed that during PEDOT: HAS₄-PBA_{0.3}-PEGene_{0.22} polymerization, 100 % of HAS₄-PBA_{0.3}-PEGene_{0.22} reacted with EDOT. The mass fraction of HAS₄-PBA_{0.3}-PEGene_{0.22} in final inkXL, and the corresponding quantity of alkene function can thus be calculated. 60 µL of inks were spread on a glass slide without surface modification and immediately irradiated for 5 minutes at 405 nm at 75 mW/cm², then

dried overnight (Table 6). It was chosen to cross-link inkXL **1** before drying to get the most visually homogenous films, without cracks.

Table 6. Conductivity of PEDOT:HAS-PBA-PEGene ink films, cross-linked or not

InkXL	[inkXL] (g/L)	Ratio $n_{SH}/n_{=}$	[LAP] (g/L)	Irradiation	Film aspect	σ (S/cm)	Stability in water
1	13	0	0	X	Homogenous No halo effect	3.8 ± 0.2	X
		1	1	5 min 405 nm 75 mW/cm ²		0.6 ± 0.08	V

The film based on inkXL **1** alone displayed a conductivity of 3.8 S/cm, better than that of PEDOT:HAS₄-PBA_{0.3} ($\sigma = 1.5$ S/cm). The cross-linked inkXL **1** film displayed a conductivity of 0.6 S/cm, almost one order of magnitude smaller than the non-cross-linked film. Like for PEDOT:HAS₄-PBA_{0.3} ink included in a cross-linked matrix, the addition of non-conductive material (the cross-linker) and the introduction of crosslinkages which hinder film structuration, lowered conductivity. Nevertheless, the conductivity drop was much lower in this case, yielding values close to the conductivity of PEDOT:HAS₄-PBA_{0.3}. Interestingly, even though ink particles were small, below 350 nm, no halo effect was observed after drying, contrary to uncross-linked films of PEDOT:HAS₄-PBA_{0.3} inks with similar particle size (Chapter 2, section III.3.). When immersed in water, the pure inkXL **1** film dissolved in a few minutes, while the cross-linked one detached from the glass slide and floated in water, swelling a bit (Figure 18).



Figure 18. Cross-linked PEDOT:HAS₄-PBA_{0.3}-PEGene_{0.22} ink film, swollen in water.

III.3. Stability of PEDOT:HAS₄-PBA_{0.3}-PEGene_{0.22} cross-linked films

III.3.a. Evolution of conductivity

PEDOT: HAS₄-PBA_{0.3}-PEGene_{0.22} inks appeared to be cross-linkable and stable in water, with conductivities above 0.5 S/cm (Figure 6). The influence of hydration/dehydration cycles on film conductivity was investigated. InkXL **1** was suspended in water at 50 g/L with PEG-(SH)₂ (M_n = 3.5 kg/mol) at 13 g/L to obtain a molar ratio $n_{\text{thiol}}/n_{\text{alkene}} = 1$, and LAP at 1 g/L. 60 μL of the mixture were spread on a glass slide functionalized with thiol functions, and immediately irradiated for 7 minutes at 405 nm at 75 mW/cm², then dried overnight. The grafted film was immersed in water 1 h, then dried, several times. At each cycle, film thickness and conductivity were measured (Figure 19).

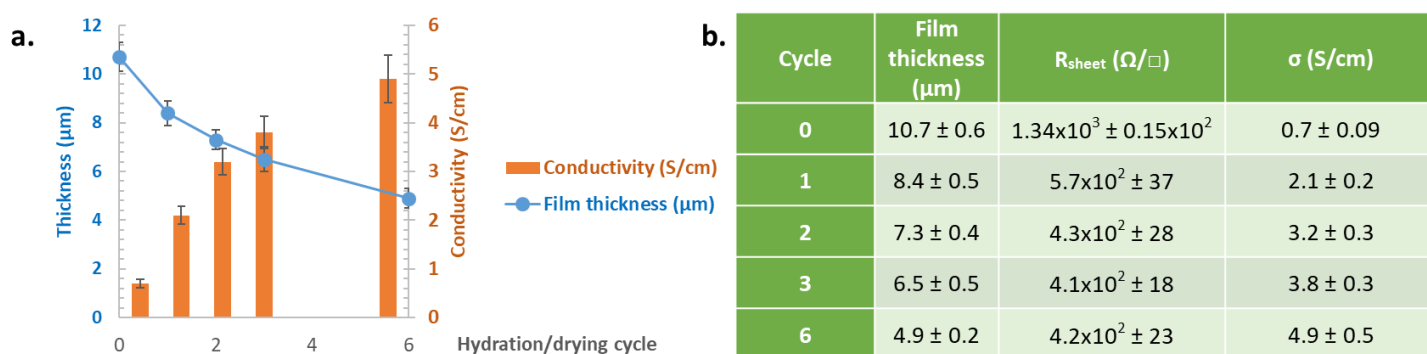


Figure 19. *a.* Conductivity and thickness of a cross-linked film of inkXL **1** after several hydration/drying cycles. *b.* Corresponding thickness, conductivity and sheet resistance.

As the number of hydration/drying cycles increased, the film thickness decreased, dropping from 10.7 μm to 4.9 μm , causing the film conductivity to rise from 0.7 S/cm to 4.9 S/cm, coherently with conductivity equation: $\sigma = 1/(R_{\text{sheet}} \cdot h)$. However, the increase of film conductivity was not only due to a diminution of its thickness, but also to the rapid diminution then stabilization of film sheet resistance (Figure 19b). This could be due to a progressive modification of film microstructure.

III.3.b. Evolution of film microstructure when immersed in water

To investigate modifications of the film microstructure, atomic force microscopy analysis were carried out. The AFM observations were performed at the Platform for Nano Characterization (PFNC) of CEA LETI by Denis Mariolle.

InkXL **1** was suspended in water at 25 g/L with PEG-(SH)₂ ($M_n = 3.5$ kg/mol) at 13 g/L (molar ratio $n_{\text{thiol}}/n_{\text{alkene}} = 0.9$), and LAP at 1 g/L. Two identical cross-linked thin films were realized: 150 μL of the mixture were spin coated at 1000 rpm on a thiol-functionalized glass-slide, and immediately irradiated for 2 minutes at 405 nm at 75 mW/cm², then dried overnight. One of the two films was immersed for 2 hours in water, then dried in a close petri dish at room temperature. Both films were analyzed by atomic force microscopy and compared to investigate the effect of the 2 hours washing on the film structure (Table 7 and Figure 20).

Table 7. Influence of 2 hours immersion in water on the conductivity of spin-coated inkXL **1** cross-linked films.

Film	Film thickness (nm)	R_{sheet} (Ω/\square)	σ (S/cm)
Pristine	930 \pm 56	$1.26 \times 10^5 \pm 1.2 \times 10^4$	0.085 \pm 0.009
After 2 h immersion in water	620 \pm 38	$1.11 \times 10^5 \pm 2.3 \times 10^4$	0.145 \pm 0.031

As observed in section III.3.a., film thickness and sheet resistivity decreased after immersion in water, while conductivity increased. AFM topology pictures (Figure 20) showed that the pristine film was relatively flat, with some impurities on the surface. After immersion in water, the surface impurities disappeared, and the surface appeared much more “wavy”. Adhesion pictures, indicating the variation of adhesion of the AFM tip depending on its position on the surface, were much more homogenous for immersed films.

This suggested that the immersion of the film for two hours resulted in the removal of a part of the film (potentially the uncross-linked chains), while simultaneously homogenizing the rest of the film, since adhesion map was less contrasted.

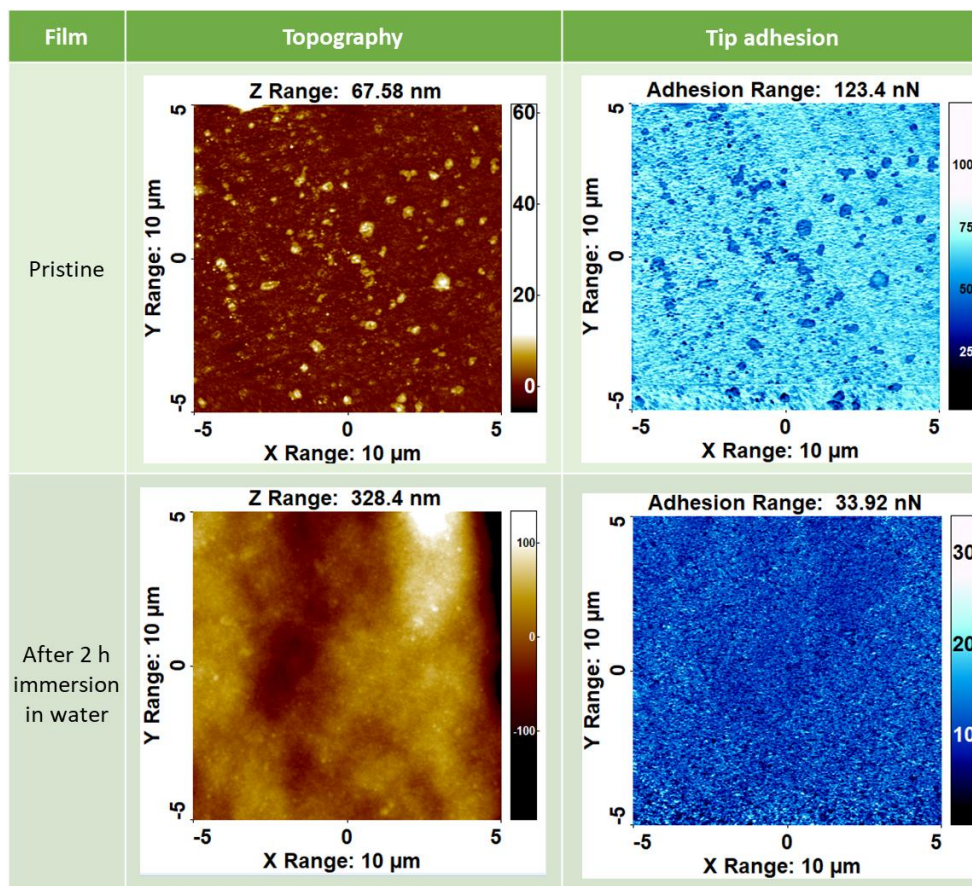


Figure 20. AFM picture of pristine and washed cross-linked films based on inkXL 1 Tip AD-2.8-AS, $F = 20$ nN, DC sample bias = 0.5 V.

IV. Inkjet printing of PEDOT: HAS₄-PBA_{0.3}-PEGene_{0.22}

IV.1. Ink formulation

The developed PEDOT:HAS₄-PBA_{0.3}-PEGene_{0.22} ink appeared to meet all the expected requirements: it was conductive, cross-linkable with thiol-ene chemistry, and its particle size appeared to be compatible with inkjet printing. Taking into account the formulation of PEDOT:HAS₄-PBA_{0.3} ink for inkjet printing described in chapter 2, inkXL were formulated with:

- 2 g/L of DBSA to lower formulation surface tension to around 32-33 mN/m;
- 2.3 vol% of glycerol to avoid ink evaporation in print head nozzles;
- 1 g/L of LAP to cross-link it after printing;
- PEG-(SH)₂ (M_n = 3.5 kg/mol) to obtain a molar ratio $n_{\text{thiol}}/n_{\text{alkene}} = 1$.

To calculate [PEG-(SH)₂], it was assumed that during PEDOT: HAS₄-PBA_{0.3}-PEGene_{0.22} polymerization, 100 % of HAS₄-PBA_{0.3}-PEGene_{0.22} reacted with EDOT, enabling to calculate the mass fraction of HAS₄-PBA_{0.3}-PEGene_{0.22} in final inkXL $w_{\text{HAS-PBA-PEGene}}$.

Thus:

$$[\text{PEG} - (\text{SH})_2] = \frac{[\text{HAS-PBA-PEGene}] \cdot w_{\text{HAS-PBA-PEGene}}}{M_{\text{HAS-PBA-PEGene}}} \cdot DS_{\text{PEGene}} \cdot \frac{\text{cross-linking degree}}{2} \cdot M_n(\text{PEG} - (\text{SH})_2)$$

$$\text{Where } \text{cross-linking degree} = n_{\text{thiol}}/n_{\text{alkene}}.$$

Regarding the viscosity of PEDOT: HAS₄-PBA_{0.3}-PEGene_{0.22}, it was much higher than that of PEDOT:HAS₄-PBA_{0.3} ink at equal concentration (Figure 21a), and seemed to depend on ink particle size: inkXL with larger particles were more viscous (Figure 21b). Therefore, the optimal inkXL concentration for inkjet printing had to be determined for each PEDOT: HAS₄-PBA_{0.3}-PEGene_{0.22} ink. InkXL **1** to **3** with a Z_{average} of 320-370 nm were printed at 9.5 g/L, and inkXL **4** with a Z_{average} of 656 nm was printed at 12 g/L. It is important to note that printing concentrations of PEDOT: HAS₄-PBA_{0.3}-PEGene_{0.22} ink were much lower than PEDOT:HAS₄-PBA_{0.3} one (31.2 g/L).

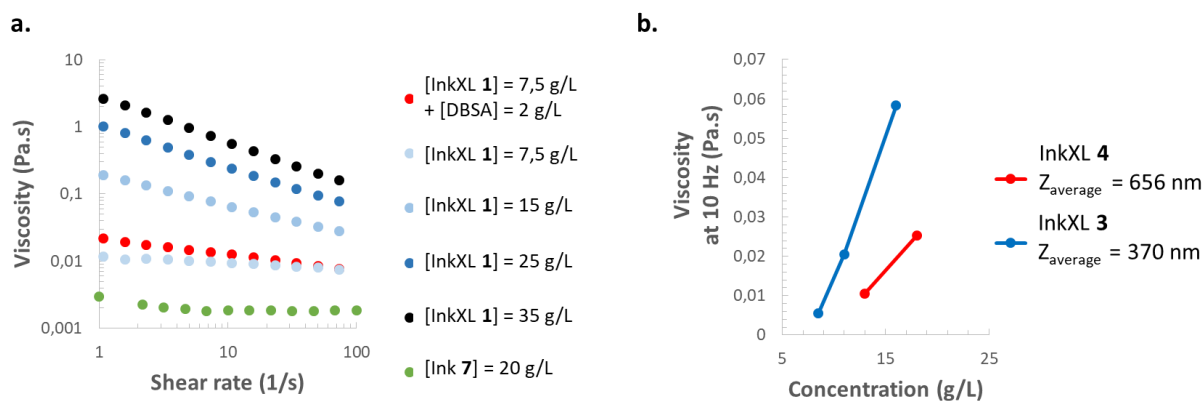


Figure 21. a. Viscosity of PEDOT:HAS₄-PBA_{0.3}-PEGene_{0.22} inkXL 1 ($Z_{\text{average}} = 320$ nm, Table 5) in water at different concentration, compared to viscosity of PEDOT:HAS₄-PBA_{0.3} ink 7 at 20 g/L. b. Viscosity at 10 Hz of PEDOT:HAS₄-PBA_{0.3}-PEGene_{0.22} inkXL 4 and 3 of different particle size.

IV.2. Inkjet printing with Dimatix DMP-2800 printer

A Dimatix DMP-2800 printer was used to create with PEDOT: HAS₄-PBA_{0.3}-PEGene_{0.22} inks a pattern comprising a series of parallel lines with expected line width of ~ 200 μm . This line width was selected to reproduce the conditions of other printed intracranial electrode reported in the literature^[26–28]. For this purpose, PEDOT: HAS₄-PBA_{0.3}-PEGene_{0.22} inks were formulated at different concentrations according to their particle size as described above (Table 8), and sonicated 30 seconds in an ultrasound bath, then vortexed right before printing. 500 μL to 1 mL of ink was charged in the cartridge using a syringe, the print head was clipped on the cartridge, and the whole system plugged in the printer. All inks were printed successfully on soft polyurethane films. After printing the desired number of layers, tracks were irradiated 5 minutes at 405 nm at 75 mW/cm² and dried overnight in a closed petri dish at room temperature.

Table 8. InkXL formulation used for inkjet printing

FormulationXL	InkXL #	Z_{average} (nm)	InkXL] (g/L)	[PEG-(SH) ₂] (g/L) so as $n_{\text{alkene}} = n_{\text{thiol}}$	[DBSA] (g/L)	Glycerol vol%	[LAP] (g/L)
1	4	656 \pm 53	9.5	2.34	2	2.64	1
2	3	370 \pm 13	12	2.95			

First, tracks were printed and cross-linked at once using formulationXL **1** (Table 8). Small squares were added to the line to align more precisely the 4-points probe (Figure 22a). Tracks sheet resistivity were measured as described in chapter 2. Then, the PU film was immersed 1 h in water and dried overnight in a closed petri dish at room temperature. Tracks did not dissolve or detach from the substrate. As previously observed for inkXL **1** films (Figure 19), the conductivity of tracks after immersion in water and drying was higher than before immersion (Figure 22b). Like tracks printed with PEDOT:HAS₄-PBA_{0.3} ink, those cross-linked tracks displayed resistivity much higher than films, but still smaller than PEDOT:HAS₄-PBA_{0.3} at equal number of ink layers (Figure 22c). Those resistivity were still very high, and required printing optimization, which will be described further.

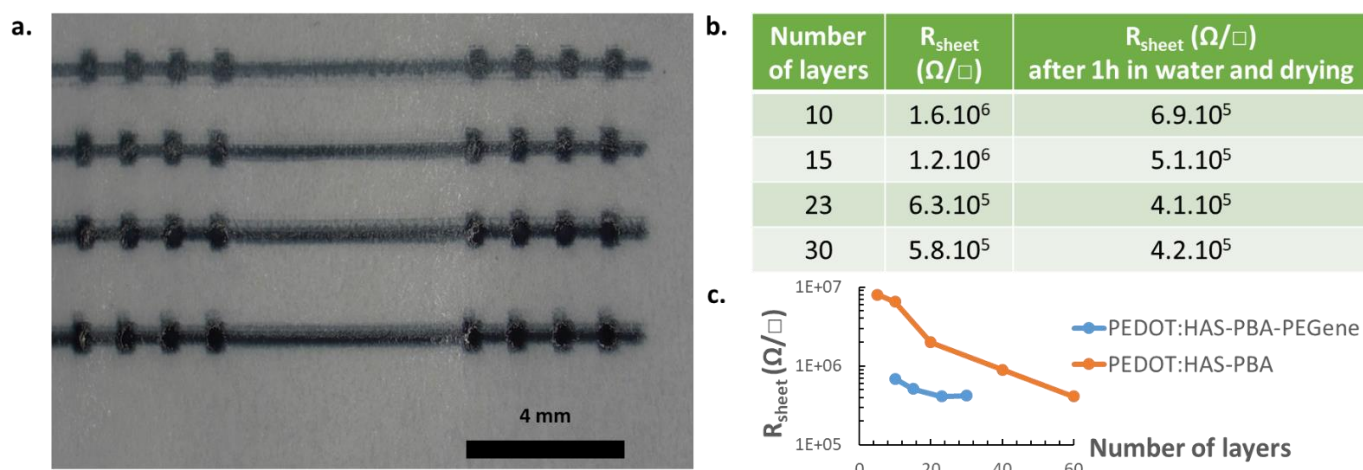


Figure 22. a. Cross-linked PEDOT:HAS-PBA-PEGene tracks, with various number of printed layers. b. Tracks resistivity before and after immersion in water. c. Track resistivity according to the number of layers for PEDOT:HAS₄-PBA_{0.3}-PEGene_{0.22} and PEDOT:HAS₄-PBA_{0.3} inks.

IV.2.a. Printing optimization

For a large homogenous film, sheet resistance only depends on film thickness. A correction factor can be applied to take into account the real film geometry. But for thin tracks, the conductivity depends on the track cross-section. Thus, the thickness of printed tracks should be increased to increase conductivity, while its width should be kept as thin as possible.

It was observed that the tracks width increased with the number of ink layers. This revealed that upper ink layers did not stack on lower ink layers, but progressively flowed on

them or merged with them as they were not dried enough or correctly cross-linked. To address this issue, it was suggested to progressively cross-link ink tracks to enable a better stacking of upper ink layers on lower ones, as they would be partially dried and cross-linked by the irradiation process.

Formulations XL **1** and **2** (Table 8) were printed on PU films. For each ink, 50 layers were printed in total, using three different cross-linking protocols. The total irradiation time was the same for all three protocols that are described below:

- 50 layers were printed and cross-linked at once with 5 minutes of irradiation at 405 nm at 75 mW/cm² (protocol 1).
- 5 series of 10 layers were printed, with 1 minute of irradiation at 405 nm at 75 mW/cm² between each series (protocol 2).
- 10 series of 5 layers were printed, with 30 seconds of irradiation at 405 nm at 75 mW/cm² between each series (protocol 3).

The track resistivity measured for each protocol is reported in Table 9. Visually, the tracks printed with protocol 2 and 3 were thinner than tracks printed with protocol 1, though no precise measurements were performed.

Table 9. Conductivities of printed tracks using various cross-link protocols.

FormulationXL #	InkXL #	Z _{average} (nm)	PDI	Printing and cross-linking protocol	R _{sheet} (Ω/□)
1	4	656 ± 53	0.3	1	4.90x10 ⁴
				2	7.72x10 ⁴
				3	8.28x10 ⁴
2	3	370 ± 13	0.28	1	3.90x10 ⁵
				2	4.29x10 ⁵
				3	4.97x10 ⁵

This set of experiments exhibited that it was better to print all tracks at once to obtain the lowest track resistivity. Taking into account that tracks printed with protocol 1 were larger, it appeared that increasing track width was more important to increase its conductivity, than trying to increase its thickness. In addition, as inkXL **4** particles were almost twice as large as inkXL **3** particles, it appeared that films composed of larger particles were more conductive.

This experimental fact was consistent with what was observed with PEDOT:HAS₄-PBA_{0.3} inks (Chapter 2, Table 8).

IV.2.b. Stability of conductive properties in humid medium

In section IV.2., it was observed that the printed tracks displayed an increase of conductivity after being immersed in water for 1 hour and then dried. Here, the stability of tracks conduction properties when immersed in water were investigated, to assess their capacity to conduct electricity, even when wet.

FormulationXL 1 (Table 9) was used to print several parallel straight lines of 3 cm long and 200 μm width, on a soft 50 μm thick PU film (following protocol 1, section IV.2.a.). 40 layers were printed on top of each other and then irradiated for 5 minutes at 405 nm at 75 mW/cm^2 and dried overnight in a closed petri dish at room temperature. The extremities of the lines were sandwiched between metallic plates (Figure 23a), and the total resistance measured using an Ohm-meter (Figure 23b). Noticeably, with this set up, the conductivity of several printed tracks was taken into account to get a smaller total resistance. PBS drops were deposited on the middle of the printed tracks, and the total resistance was monitored over time.

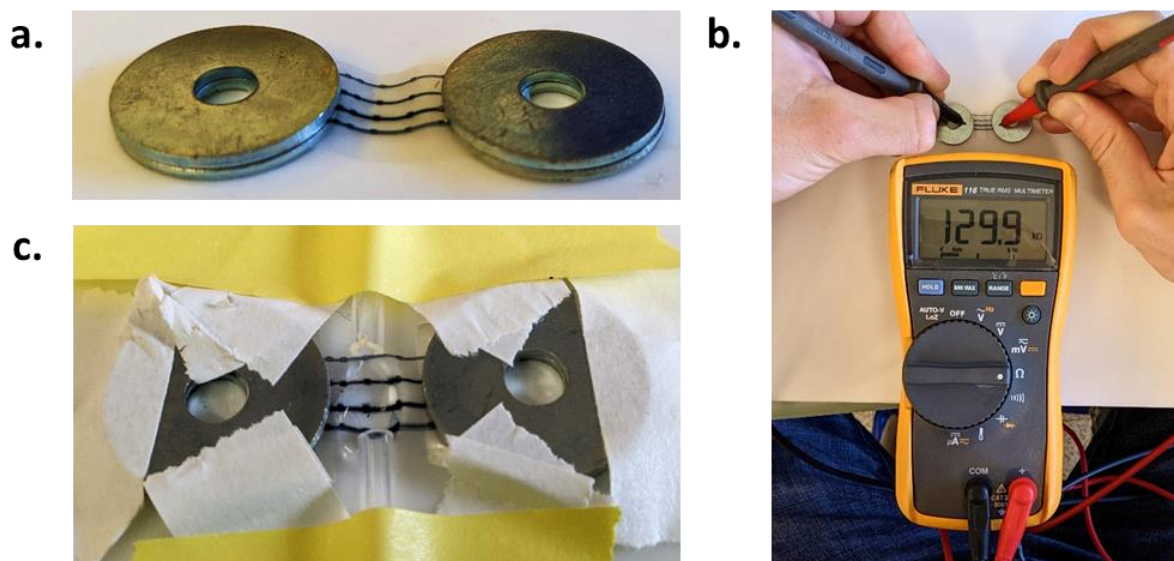


Figure 23. Experimental set up to evaluate the conductivity of wet cross-linked PEDOT:HAS₄-PBA_{0.3}-PEGene_{0.22} tracks.

The initial total resistance of the system was $130 \pm 20 \text{ k}\Omega$. After pouring PBS on the tracks (Figure 23c), it increased to $600 \pm 50 \text{ k}\Omega$ in a few minutes, and stabilised to this value. The resistance was monitored over the next 4 hours, adding water if necessary (to compensate PBS evaporation), and remained between 600 and 700 k Ω . After drying, the total resistance decreased to $100 \pm 20 \text{ k}\Omega$, which was a little lower than initially, similar to the observation made in section IV.2.

IV.2.c. Conclusion

In conclusion, the developed PEDOT: HAS₄-PBA_{0.3}-PEGene_{0.22} ink could be inkjet-printed and cross-linked, yielding conductive tracks, even when immersed in water, though displaying an important increase of resistance. However, the initial resistance seemed to be recovered when dried, and even slightly decreased.

V. Discussion

In this chapter, different strategies to stabilize the developed PEDOT:HAS₄-PBA_{0.3} ink and prevent its dissolution in water or biological fluids during use were investigated. The bulky sulfates along the HAS₄-PBA_{0.3} backbone prevented the use of the boronic acid functions to form reversible ester boronate with planar vicinal diol. Therefore, three other strategies of ink-cross-linking based on thiol-ene photochemistry were investigated.

V.1. Inclusion of a conductive ink inside a cross-linked matrix.

PEDOT:HAS₄-PBA_{0.3} was first included in a matrix of alkene-functionalized hyaluronic acid (HA-pentenoate) cross-linked by PEG-bis-thiols using a photo-activated thiol-ene chemistry. The incorporation of PEDOT-based conductive materials in a cross-linked matrix has been already widely reported in the literature to obtain water-stable conductive PEDOT:PSS-based materials, mainly interpenetrating hydrogel networks (Chapter 1, tables 2 and 3). In this work, only thin films could be cross-linked using thiol-ene chemistry due to the high absorbance at UV wavelengths of PEDOT. Thus the obtained materials could not be properly referred to as hydrogels.

The resulting composite material displayed conductivity two to three orders of magnitude lower than PEDOT:HAS₄-PBA_{0.3} ink alone (10^{-4} to 10^{-1} S/cm versus 1.5 S/cm). This drop of conductivity was also observed in the literature. While pristine PEDOT:PSS conductivity was reported to be between 0.1 to 10 S/cm^[29], materials relying on this strategy displayed conductivity between 10^{-3} and 8.10^{-2} S/cm^[30,31]. The decrease of conductivity was attributed to: 1) the presence of the HA-pentenoate/bis-thiol matrix acting as an insulator, and 2) the fact that the cross-linking hindered the conductive ink to structure itself, contrary to films based on PEDOT:HAS₄-PBA_{0.3} inks. Indeed, ink microstructuration during film drying has been demonstrated to be crucial to increase its final conductivity, as evidenced by the large literature data about PEDOT:PSS film annealing and secondary doping process which modify film microstructure (chapter 1 section II.2.c.).

To circumvent this insulation problem, an alternative strategy could consist in using the cross-linking matrix as a secondary dopant of PEDOT:PSS, drastically increasing its final conductivity. Mantione *et al.*^[32] and then Del Agua *et al.*^[8] added divinylsulfone (DVS) to a commercial solution of PEDOT:PSS containing conductivity-boosting additives such as ethylene glycol. DVS reacted with ethylene glycol, cross-linking the formulation, yielding PEDOT:PSS free-standing-films with conductivity up to 700 S/cm. Although this strategy relied on the use of toxic ethylene glycol, the reported materials exhibited satisfactory biocompatibility with L929 fibroblast cells and SH-SY5Y neural cells. However, those formulations processing required an annealing at high temperature ($> 130^{\circ}\text{C}$) to remove excess ethylene glycol (otherwise the material might be cytotoxic), which prevented its adaptation to our system, as HA derivatives would be degraded at such temperature.

Therefore, another solution was explored to introduce as less non-conductive material as possible: it consisted in cross-linking the conductive ink itself.

VI.2. Cross-linking PEDOT:HAS₄-PBA_{0.3} from PEDOT chains

To cross-link PEDOT-based materials in order to make them more stable in aqueous medium, some authors designed functional EDOT monomers whose functionality was used as an anchor point to implement a cross-linking reaction.

This strategy has been used to cross-link PEDOT alone. Xu *et al.*^[33] designed a chemical hydrogel composed of a mixture of EDOT and sulfated EDOT, which formed EDOT micelles in suspension. When the oxidizing agent was added, the EDOT micelles polymerized internally and between themselves, leading to a hydrogel with enhanced electrochemical capacitance and high absorption ability to various guest substances, such as dye stuffs and heavy metal ions. Mawad *et al.*^[34] synthesized a single component hydrogel composed of poly(3-thiopheneacetic acid) with a final conductivity around 10^{-6} S/cm, which could be enhanced to 10^{-3} S/cm when doped with perchlorate anions. Noticeably, when no dopant PEDOT was used, the final conductivity was very low. Besides, the degradability of these materials was not investigated. However, considering the cross-linking points of those materials were composed of hydrolysable esters, they should be degradable.

To design more conductive water-stable PEDOT-based materials, the cross-linking of functional EDOT with a dopant has also been described. Mantione *et al.*^[22] cross-linked a PEDOT_x:PSS ink (where x was the fraction of carboxyl-EDOT introduced in the polymer chain) by an esterification reaction with ethylene glycol. They obtained water-stable films with conductivity between 140 and 375 S/cm, compared to pristine soluble PEDOT:PSS film which displayed a conductivity of 171 S/cm using their film preparation protocol. No biocompatibility, nor degradability studies were conducted.

With our cross-linking strategy based on thiol-ene photochemistry, the ink made of alkene-functional PEDOT had to react with a bis-thiol. A closely related molecule found in literature, “emEDOT” (Figure 24a), has been described and synthesized to obtain, after electropolymerization, P(emEDOT) films that could be post-functionalized using thiol-ene chemistry^[35,36]. Yet, emEDOT was not reactive enough and required 1 h under 356 nm UV light at 100 mW/cm² to react quantitatively (probably due to high UV-photon absorption of EDOT, as it was observed during this project). Such conditions were not compatible with the use of polysaccharides that would be highly degraded in such reaction conditions. Similarly, ProDOT-diene (Figure 24b) has been synthesized and electro-polymerized by Wei *et al.*^[37] to obtain Poly(ProDOT-diene) films that could be post-functionalized using thiol-ene click chemistry. As for emEDOT, this molecule was not reactive enough as it required 3 hours under UV light exposure at 365 nm (power density was not specified) to react quantitatively.

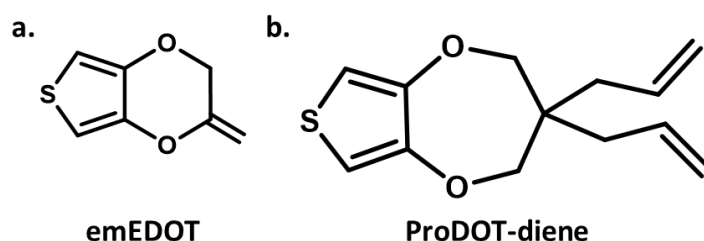


Figure 24. Example of alkene-functionalized EDOT or ProDOT derivatives from the literature. a. emEDOT, adapted from Wu *et al.*^[35]. b. ProDOT-diene, adapted from Wei *et al.*^[37].

EDOT-ene **2** and **3** developed in this project (Table 3) were not soluble in water. Though they could have been synthesized and polymerized with EDOT in the presence of HAS₄-PBA_{0.3} to obtain PEDOT_x:HAS₄-PBA_{0.3} inks (where x was the molar fraction of EDOT-ene over total EDOT), those inks were not cross-linkable by thiol-ene chemistry. The ¹H NMR spectra of those

inks displayed no signals corresponding to EDOT or EDOT-ene (Figure 11), indicating that the EDOT and alkene moieties were deeply buried inside HAS₄-PBA_{0.3} tangles due to their hydrophobicity. By contrast, Mantione *et al.*^[22] designed a hydrophilic carboxyl-EDOT, resulting in an ink of which the cross-linking points were accessible to the cross-linkers.

This fact demonstrated the importance of hydrophilic/hydrophobic considerations in the design of a cross-linkable PEDOT-based ink. A first solution to increase PEDOT-ene/PEDOT hydrophilicity could be to replace EDOT by hydroxymethyl-EDOT in the polymer. A second solution could consist in introducing the alkene functions at the end of a hydrophilic spacer that would ensure its solvation in water and accessibility to bis-thiols cross-linkers.

We selected this last strategy in this work, and designed a new molecule with a thiol-ene reactive pentenoate group grafted to an oligo-PEG chain.

VI.3. Cross-linking PEDOT:HAS₄-PBA_{0.3} from HAS₄-PBA_{0.3} chains

The cross-linking of PEDOT: HAS₄-PBA_{0.3} ink was performed using thiol-ene photochemistry after introducing alkene groups on HAS₄-PBA_{0.3} through an poly(ethylene glycol) spacer arm. The resulting HAS₄-PBA_{0.3}-PEGene_{0.22} derivative was then used to polymerize EDOT, leading to the formation of a new PEDOT: HAS₄-PBA_{0.3}-PEGene_{0.22} conductive and cross-linkable ink. The latter afforded films with a pristine conductivity of 3.8 S/cm, higher than PEDOT: HAS₄-PBA_{0.4} (conductivity of 1.5 S/cm). When this new PEDOT: HAS₄-PBA_{0.3}-PEGene_{0.22} ink was cross-linked with a bis-thiol under irradiation, the final dried ink films displayed a conductivity around 0.6 S/cm.

This decrease of conductivity after cross-linking was consistent with the literature. Indeed, PEDOT:PSS films cross-linked by 3-glycidoxypropyltrimethoxysilane (GOPS) have been shown to display enhanced water-stability, but decreased conductivity. In the work from Mantione *et al.*^[32], PEDOT:PSS conductivity dropped from ≈ 600 S/cm to ≈ 300 S/cm when cross-linked with 3 % v/v of GOPS, which was corroborated by Solazzo *et al.*^[9] Both studies used commercial PEDOT:PSS formulations containing secondary dopants, hence the high reported conductivity compared to pristine PEDOT:PSS ($\sigma \approx 10^{-1}$ - 10^1 S/cm). Håkansson *et al.*^[6] observed the same behavior with pristine PEDOT:PSS without any secondary doping

treatment, with a conductivity drop from 1 S/cm for PEDOT:PSS alone to 0.002 S/cm for PEDOT:PSS cross-linked with 1% v/v of GOPS.

This drop of conductivity between cross-linked and non-cross-linked ink films could be interpreted in terms of film micro-structuration. Indeed, pristine PEDOT: HAS₄-PBA_{0.3}-PEGene_{0.22} exhibited a higher conductivity than PEDOT: HAS₄-PBA_{0.3} ink (3.8 S/cm vs 1.5 S/cm): the additional PEGene side groups may enhance film crystallization during its formation, as PEGene side groups are composed of long linear hydrophilic chains that could well organize themselves. But when PEDOT: HAS₄-PBA_{0.3}-PEGene_{0.22} films were cross-linked, the conductivity dropped to 0.6 S/cm. The cross-linking could prevent the micro-organization and crystallization of the film during its drying.

Interestingly, Solazzo *et al.*^[9] observed an increase of conductivity when they cross-linked PEDOT:PSS with poly(ethylene glycol)diglycidyl ether. They attributed this increase to a secondary doping process due to the PEGylated nature of the cross-linker, as EG are well-known PEDOT:PSS secondary dopants. The difference of behavior between their study and ours, where a PEGylated side chain was grafted to HAS₄-PBA_{0.3} backbone in addition to the utilization a PEG-bis thiol cross-linker (Mn = 3.5 kg/mol), could not be interpreted.

Noticeably, cross-linked films based on PEDOT: HAS₄-PBA_{0.3}-PEGene_{0.22} became more conductive when immersed in water and then dried. Successive hydration/drying cycles enabled to increase the conductivity from 0.6 S/cm to 4.9 S/cm after 6 cycles. The simultaneous decrease of film thickness and film sheet resistivity (Figure 19) enabled us to attribute this increase to both a washing of the film, removing excess HAS₄-PBA_{0.3}-PEGene_{0.22} chains, yielding more concentrated PEDOT domains, and to a modification of the film micro structuration. To investigate the modification of micro-structuration, AFM analysis was performed. The AFM pictures showed a decrease of film flatness, in addition to an increase of film homogeneity after immersion 2 hours in water. Thus, the increase of conductivity could be attributed to both the removal of non-cross-linked chains and to a restructuration of the conductive and nonconductive domains of the film, leading to a more homogenous surface.

A similar film structure reorganization was evidenced by Alemu *et al.*^[38] in the study of the mechanism of conductivity enhancement of PEDOT:PSS films by film treatment with methanol. They attributed the conductivity enhancement of PEDOT:PSS films immersed in

methanol to the removal of PSS which led to thicker films, yielding bigger and better connected PEDOT chains, in addition to a modification of structure of PEDOT:PSS core-shell structure. In our case, the immersion in water may have removed the uncross-linked HAS₄-PBA_{0.3}-PEGene_{0.22} chains, leading to a concentration of PEDOT domains, in addition to a swelling and reorganization of PEDOT:HAS₄-PBA_{0.3}-PEGene_{0.22} particles.

VI.4. Inkjet printing of cross-linkable PEDOT:HAS₄-PBA_{0.3}-PEGene_{0.22} ink

The newly developed PEDOT: HAS₄-PBA_{0.3}-PEGene_{0.22} ink could be processed via inkjet printing after formulation to tune its physico-chemical properties. Based on the conditions previously studied for PEDOT-HAS₄-PBA_{0.3} in chapter 2, we formulated the ink to obtain such as the final ink viscosity was around 10 mPa.s, the surface tension was between 30 and 33 mN/m, and the material was prepared at concentrations between 9.5 and 12 g/L depending on its particle size. The conductivities of the various films and tracks are summarized in (Table 10).

Table 10. Conduction properties of PEDOT:HAS₄-PBA_{0.3} and PEDOT:HAS₄-PBA_{0.3}-PEGene_{0.22} inks with various process and treatments.

Ink	PEDOT:HAS ₄ -PBA _{0.3}	PEDOT:HAS ₄ -PBA _{0.3} -PEGene _{0.22}
σ (Drop-cast film) (S/cm)	1.57 ± 0.2	3.8 ± 0.2
σ (Cross-linked drop-cast film) (S/cm)	NA	0.6 ± 0.08
σ (Washed cross-linked drop-cast film) (S/cm)	NA	4.9 ± 0.5 (6 hydration/drying cycles)
R_{sheet} (Printed track) (Ω/\square)	$4.1 \times 10^5 - 2 \times 10^6$	NA
R_{sheet} (Printed then cross-linked track) (Ω/\square)	NA	$4.9 \times 10^4 - 5.0 \times 10^5$

Interestingly, the cross-linked printed tracks exhibited lower resistivity than the previously printed PEDOT:HAS₄-PBA_{0.3} tracks (Chapter 2, section IV.3.), whereas the cross-linked drop-cast PEDOT: HAS₄-PBA_{0.3}-PEGene_{0.22} ink films displayed lower conductivity than non-cross-linked drop cast PEDOT: HAS₄-PBA_{0.3} ink film. Moreover, the cross-linked printed tracks were insoluble in water after cross-linking, and still conductive when totally immersed in PBS (though displaying an increase of resistivity). Notably, a decrease of resistivity in the dry state was observed after one hydration/drying cycle. Interestingly, the cross-linked tracks

did not delaminated from the soft PU film when immersed in water, whereas the PU film was not functionalized by thiols functions. This could be attributed to the partial penetration of the ink in the PU film surface, resulting in track adhesion after cross-linking. This fact is supported by the work of Mire *et al.*^[29] where they observed a partial interpenetration of inkjet-printed PEDOT:PSS and a soft polymeric substrate.

To the best of our knowledge, only one paper has reported the printing of a solvent resistant PEDOT-based ink: Tang *et al.*^[39] processed commercial PEDOT:PSS with ([3-(methacryloyloxy)propyl]-trimethoxysilane hardener, which is structurally close to GOPS, and printed it using electro-hydrodynamic jet printing, yielding to PEDOT:PSS tracks with improved solvent resistance and electrical conductivity. However, the biocompatibility of this cross-linked material was not investigated, and as it displayed no hydrolysable bonds, the resulting material might be not desintegrable.

VI. Conclusion

In conclusion, after exploring different strategies to cross-link the PEDOT:HAS₄-PBA_{0.3} ink developed in chapter 2, we designed and characterized a PEDOT:HAS₄-PBA_{0.3}-PEG_{0.22} ink, which can be photocross-linked in the presence of bis-thiols via thiol-ene chemistry. This afforded water-stable ink-based films with an initial conductivity of 0.6 S/cm, which could be enhanced up to 4.6 S/cm after successive hydration/drying cycles.

Furthermore, this ink could be formulated to be inkjet-printed. Once cross-linked after printing, the PEDOT:HAS₄-PBA_{0.3}-PEG_{0.22} tracks were not soluble in water, still conductive when immersed in PBS, and even displayed an increase of conductivity when dried again (R_{Sheet} dropped from $5.8 \cdot 10^5$ to $4.2 \cdot 10^5 \Omega/\square$).

These conductive cross-linkable inks could be used for the design of conductive tracks for medical bioelectronic devices, without the risk of failure in case of contact of the circuitry with biological fluids. Though the biodegradability of this material could not be investigated, it is expected to be disintegrable as it is composed of degradable HAS₄-PBA_{0.3} cross-linked via amide functions, which are hydrolysable.

In this section, only thin films or tracks could be photocross-linked. But provided that thicker material could be cross-linked, bulky conductive hydrogels could be synthesized. This would enable to design soft electrodes at the electronic/tissue interface, or conductive 3D culture platforms for electroactive cells. The design of such conductive hydrogels is described in the 4th chapter of this manuscript.

VII. Materials and methods

VII.1. Synthesis

VII.1.a. Materials

Sodium Hyaluronate ($M_w = 219$ kg/mol, PDI = 1.44) was obtained from Lifecore Biomedical (Chaska, Minnesota, USA). Fructosamine hydrochloride, 4-(4,6-Dimethoxy-1,3,5-triazin-2-yl)-4-methylmorpholinium chloride (DMTMM), 3-aminophenylboronic acid hemisulfate salt (3APBA), 2,4,6-Trinitrobenzene Sulfonic Acid (TNBS), pentenoic anhydride, 2,3-dihydroxypropylamine, N,N-diisopropylamine, hydroxymethyl-EDOT, 3,4-Ethylenedioxythiophene (EDOT), sodium hydride in mineral oil at 60 %, 5-bromopentene, dodecylbenzene sulfonic acid (DBSA), sodium hydroxide pellets and O-(2-aminoethyl)-O'-[2-(Boc-amino)ethyl]deca(ethylene glycol) were obtained from Sigma-Aldrich (Saint-Quentin Fallavier, France). Trifluoroacetic acid was obtained from Merck (Lyon, France). Hydrochloric acid and glycerol were from Fischer Scientific. N,N-dimethylformamide (DMF), Ethanol 96% (EtOH), dichloromethane, methanol and acetonitrile (MeCN) were from VWR International (Fontenay-sous-Bois, France). All reagents were used as received without further purification.

VII.1.b. Synthesis and characterization of HA-Fru

HA-fructose was synthesized by an amide coupling reaction with fructosamine (containing free primary amine groups, Figure 25). To this end, fructosamine (0.024 g, 0.112 mmol) was added to a water/DMF (3/2, v/v) mixture containing DMTMM (0.207 g, 0.75 mmol) and HA (0.3 g, 0.75 mmol, $M_w = 400$ kg/mol) and the pH was adjusted to 6.5 using 0.5 M aqueous NaOH. After stirring for 24 h at room temperature, the HA derivative was purified by ultrafiltration using deionized water and the products were recovered by freeze-drying. The fructose substitution degree DS_{Fru} was found to be 0.15 as detailed below.

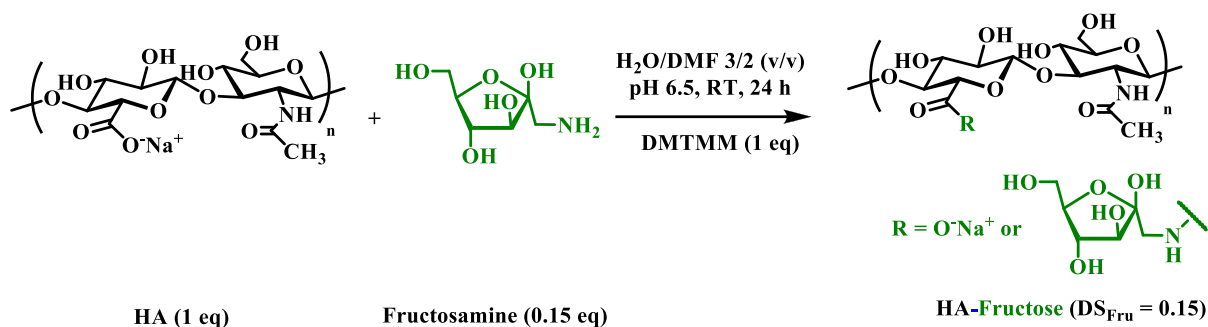


Figure 25. Amide coupling of HA with fructosamine.

VII.1.c. Determination of the degree of substitution (DS) of HA-fructose by the follow of the amide coupling reaction

As the superposition of ¹H signals of HA and grafted fructose moieties precluded the determination of the DS of HA-fructose by ¹H NMR, it was estimated by the following up of the reaction, by quantifying the free primary amine groups in the reaction medium as a function of time. This was based on the reaction of fructosamine with 2,4,6-trinitrobenzene sulfonic acid (TNBS), which gave an orange-colored final product (trinitrophenylamine) that absorbed in the UV region, around 340 nm (Figure 26). The protocol was adapted from Figueiredo *et al.*^[12].

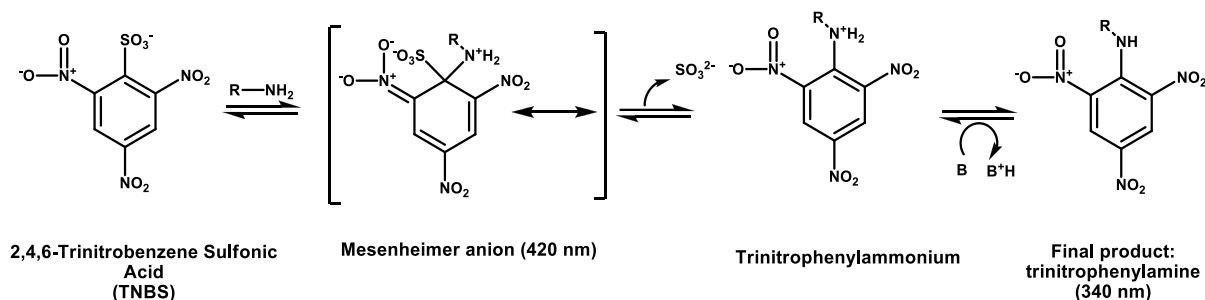


Figure 26. Mechanism of trinitrophenylation of primary amines with TNBS.

Standard curve was prepared by diluting 1 mg/mL fructosamine stock solutions in 0.1 M sodium bicarbonate buffer pH 9.17 at known concentrations of amine (10 to 25 µg/mL). Various volumes of a fresh solution of 0.01 % TNBS (w/v) in the same buffer were added in each solution, in order to get a molar ratio of TNBS/amine of 1, and samples were incubated at 37 °C for 2 h. Then, 150 µL of HCl 1 M were added to the samples, and the product of reaction between the amine and TNBS was analyzed by UV spectroscopy (from 280 to 580

nm). A standard curve was plotted with the maximal absorbance values (Figure 27b). It is important to note that the wavelength of the maximal absorbance depends on the primary amines (355 nm for fructosamine).

The same procedure was used to quantify amines during the amide coupling reactions with HA, by taking small aliquots of the reaction medium as a function of time (Figure 27a). We estimated approximately 100 % of conversion for HA-fructose within 20 h, which gave values of DS of 0.15

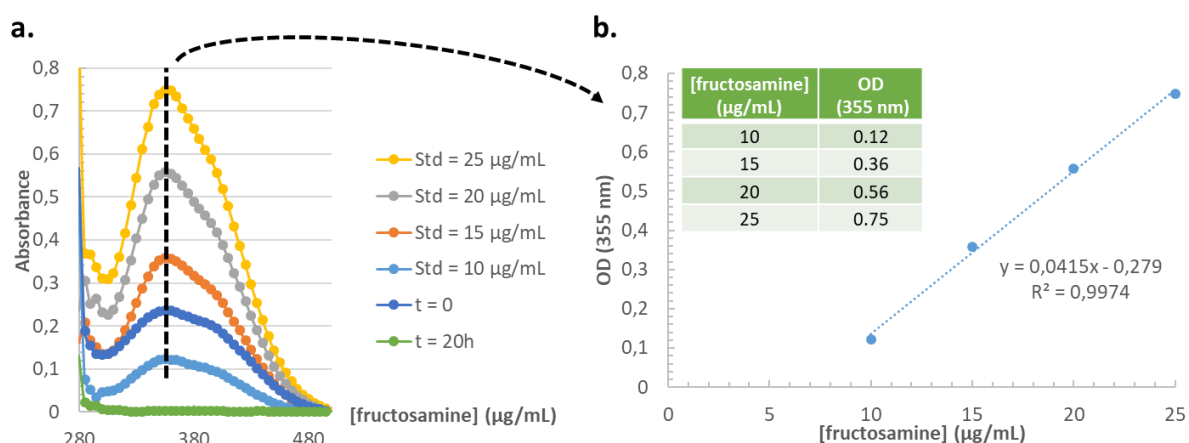


Figure 27. a. Absorbance spectrum of standard fructosamine reacted with TNBS, and aliquots of reactional medium at $t=0$ and $t=20$ min after reaction with TNBS. b. Calibration curve for fructosamine at 355 nm.

VII.1.d. Synthesis of HA-pentenoate

Sodium hyaluronate (0.30 g, 0.75 mmol, $M_w = 200$ kg/mol) was dissolved in ultrapure water (15 mL) at 4°C, and the resulting mixture was kept at 4°C under continuous stirring overnight for complete dissolution. DMF (10 mL) was then added dropwise in order to have a water/DMF ratio of 3/2, v/v. Pentenoic anhydride (0.137g, 0.75 mmol, 1 molar equivalent with respect to the repeating unit of HA,) was added while maintaining the pH between 8 and 9 (by adding 0.5 M NaOH) for 4 h. The reaction was kept at 4°C under continuous stirring for one night. After this time, NaCl was added to the reaction mixture to have a NaCl concentration of 0.5 M. Then the reaction mixture was dialyzed against water with a 6-8 kg/mol dialysis membrane (Spectrum Laboratories, CA, USA) until bath conductivity was below 8 μS/cm with ultrapure water. The purified product was recovered by freeze-drying ($\eta = 97\%$) and characterized by ^1H NMR spectroscopy (Figure 28). The degree of substitution $\text{DS}_{\text{pentenoate}}$ was

determined to be 0.2 (Figure 29, ^1H NMR (HOD): 5.95-5.92 (0.2H, m, Hc), 5.13-5.00 (0.4H, qq, Hd), 4.66-4.51 (1H, d), 4.78-4.37 (1H, d), 4.01-3.13 (10H,m), 2.5-2.44 (0.4H,m), 2.41-2.25 (0.4H, m), 2.09-1.88(3H, s)).

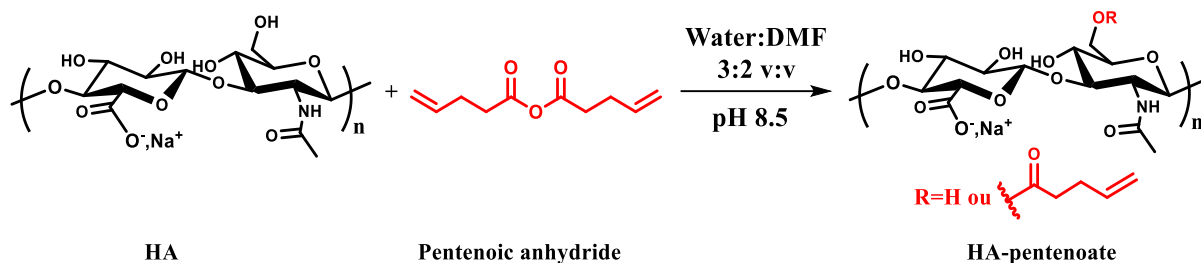


Figure 28. Coupling of pentenoic anhydride with HA.

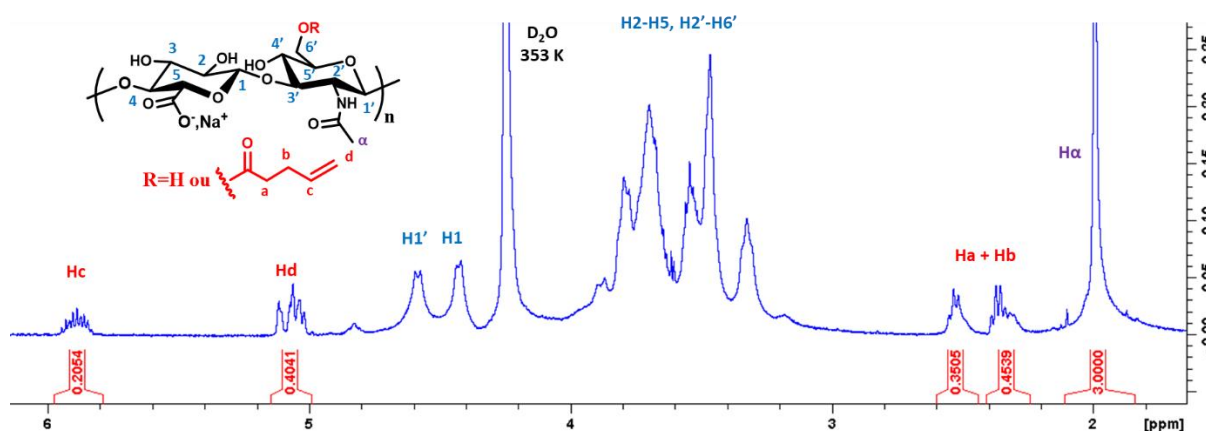


Figure 29. ^1H NMR spectrum of HA-pentenoate, in D_2O at 4 mg/mL at 80 °C.

VII.1.e. Synthesis of N-(2,3-dihydroxypropan)-penten-5-amide

400 μL of 2,3-dihydroxypropylamine (4.89 mmol, 1 equivalent) were dissolved in 50 mL of DMF. 1022 μL of N,N-diisopropylamine (1.2 equivalents) and 1073 μL of pentenoic anhydride (1.2 equivalents) were added and the medium stirred overnight at room temperature. DMF was evaporated, and the residual yellow oil was purified on chromatography column (silica gel; dichloromethane/methanol 95/5 (v/v)) to give N-(2,3-dihydroxypropan)-penten-5-amide with a total yield of 74 % as a yellowish solid (Figure 30, ^1H NMR (CDCl_3) Figure 31: 6.01 (1H, bs), 5.84-5.74 (1H, qq), 5.09-5.00 (2H, m), 5.77-5.71 (1H, p), 3.57-3.49 (2H,m), 3.45-3.33 (2H,m), 2.44 (2H, bs), 2.41-2.88 (4H, m)).

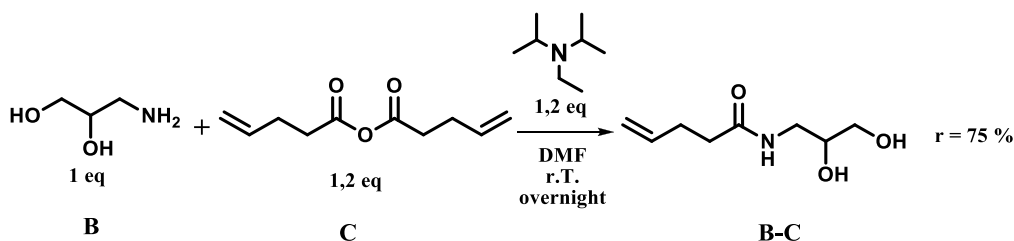


Figure 30. Synthesis of *N*-(2,3-dihydroxypropyl)-penten-5-amide from pentenoic anhydride and 2,3-dihydroxypropylamine.

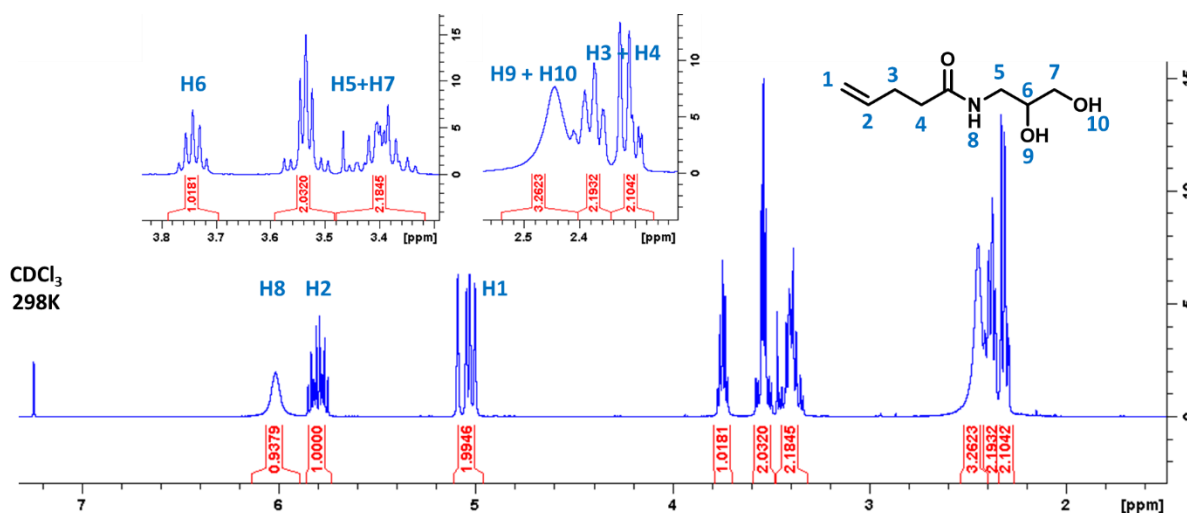


Figure 31. ¹H NMR spectrum of *N*-(2,3-dihydroxypropyl)-penten-5-amide, in CDCl₃ at 5 mg/mL at 25°C.

VII.1.f. Synthesis of methyl-EDOT-pentenoate

100 mg of hydroxymethyl-EDOT (0.581 mmol, 1 equivalent) were dissolved in 6 mL of DMF with 126.7 μ L of *N,N*-diisopropylamine (1.2 equivalents) and 1073 μ L of pentenoic anhydride (1.2 equivalents). The medium was stirred overnight at room temperature. DMF was evaporated, and the residual yellow oil was purified on chromatography column (silica gel; petroleum ether/ethyl acetate 65/35 (v/v)) to give methyl-EDOT-pentenoate as a yellowish oil with a yield of 52.1 % (Figure 32, ¹H NMR (CDCl₃) Figure 33: 6.35-6.32 (2H, q), 5.85-5.75 (1H, m), 5.08-4.98 (2H, qq), 4.38-4.33 (1H, m), 4.30-4.28 (2H, q), 4.22-4.18 (2H, dd), 4.04-3.99 (1H, dd), 4.47-4.33 (2H, t), 2.40-2.36 (2H, t)).

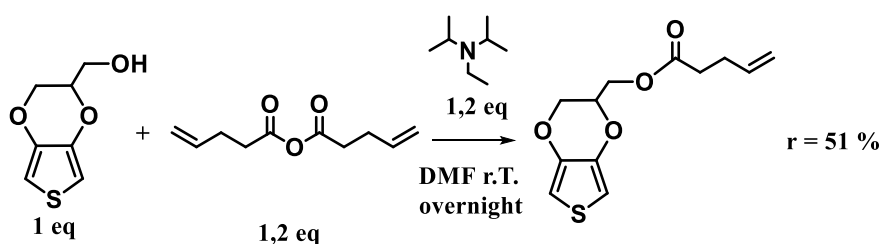
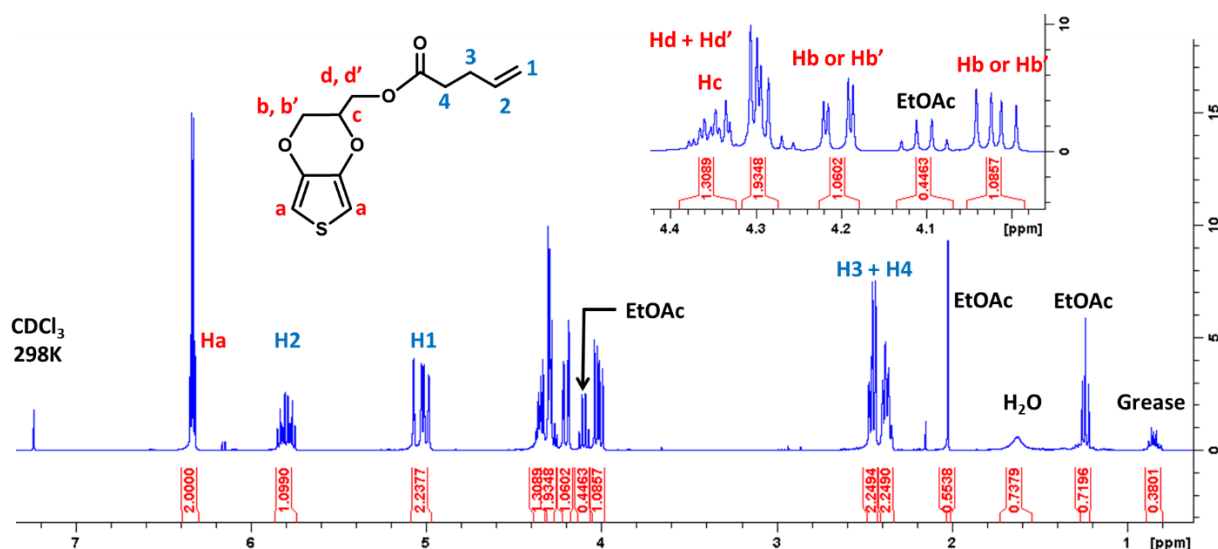


Figure 32. Coupling of hydroxymethyl EDOT with pentenoic anhydride.

Figure 33. ^1H NMR spectrum of *N*-(2,3-dihydroxypropan)-penten-5-amide, in CDCl_3 at 5 mg/mL at 25°C.

VIII.1.g. Synthesis of pent-5-enoxymethyl-EDOT

100 mg of hydroxymethyl-EDOT (0.581 mmol, 1 equivalent) were dissolved in 3 mL of anhydrous THF with 116.10 mg of sodium hydride in mineral oil at 60 % (2.903 mmol of NaH, 1 equivalent), sealed under argon, stirred 20 minutes and then cooled down to 0°C. 137.7 μL of 5-bromopentene (2 equivalents) were added dropwise in 3 minutes. The mixture was stirred for 24 h at 60°C under reflux under argon, then cooled down and filtered. The THF was evaporated and the residual brownish oil was purified on chromatography column (silica gel; hexane/ethoxyethane 80/20 (v/v)) to yield to pent-5-enoxymethyl-EDOT as a yellowish solid (35 % yield, Figure 34, ^1H NMR (CDCl_3) Figure 35: 6.31-6.26 (2H, t), 5.83-5.74 (1H, m), 5.02-4.93 (2H, qq), 4.30-4.20 (2H, m), 4.06-4.01 (1H, q), 3.67-3.65 (1H, dd), 3.60-3.56 (1H, dd), 3.50-3.47 (2H, t), 2.13-2.07 (2H, q), 1.70-1.63 (2H, quint).

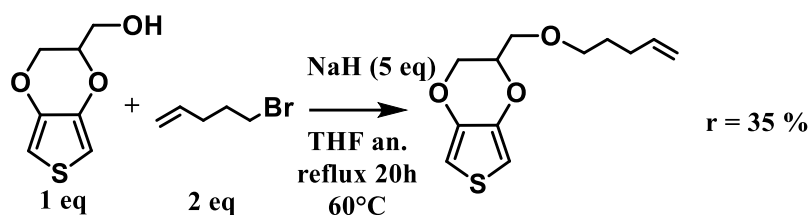
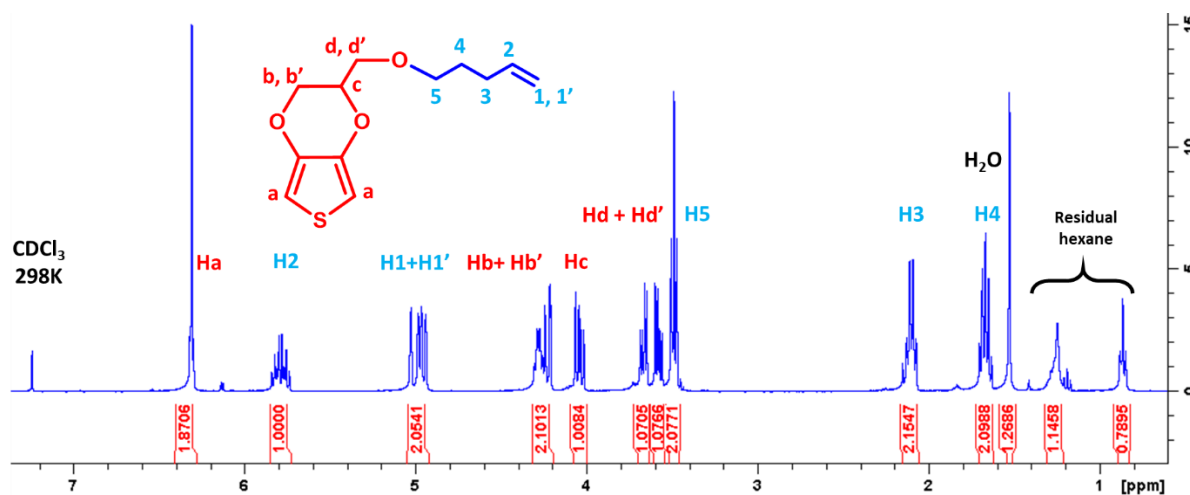


Figure 34. Coupling of hydroxymethyl-EDOT with 5-bromopentene.

Figure 35. ^1H NMR spectrum of pent-5-enoxymethyl-EDOT, in CDCl_3 at 3.6 mg/mL at 25°C.

VII.1.h. Synthesis of PEDOTenex:HAS₄-PBA_{0.3} ink

The following protocol is indicated for a molar fraction EDOT-ene/EDOT $x = 0.5$. 1 g of HAS₄-PBA_{0.30} (1 equivalent) was dissolved into 16 mL of degassed water:MeCN 9:1 v:v. 188 μL (250 mg, 1.5 equivalents) of EDOT and 122 μL (141 mg, 0.5 equivalent) of EDOT-ene **4** (respectively 151 mg of EDOT-ene **3**, 0.5 equivalent) were added (so as $[\text{HAS-PBA} + \text{EDOT} + \text{EDOT-ene}] = 37.5 \text{ g/L}$). The medium was stirred for 2 hours at 4 °C under nitrogen. 9.78 mg of FeSO_4 was added (0.015 equivalent compared to EDOT). 711.6 mg of APS (1.33 equivalent compared to EDOT) was dissolved in 16 mL of degassed and cold water:MeCN 9:1 v:v, then added dropwise in 1h to the medium using a syringe pump. The medium was stirred for 4 hours at 4 °C under nitrogen, then at room temperature until pH was stable below 1.1-1.2. The reaction was quenched adding 32 mL of water, then homogenized at 10,000 rpm for 10 minutes using an IKA Ultra Turrax T-10 basic disperser with a S 10 N-8G dispersing tool (Roth, Karlsruhe, Germany). The medium was dialyzed against osmosed water with a 6-8 kg/mol dialysis membrane (Spectrum Laboratories, CA, USA), changing the bath until water

conductivity was below 8 $\mu\text{S}/\text{cm}$. Then pH was adjusted to 7.4 and PEDOTene_{0.5}:HAS₄-PBA_{0.3} was recovered by freeze-drying as a deep blue powder, with a yield superior to 80%.

VII.1.i. Synthesis of PEGene

PEGene was synthesized in two steps from O-(2-aminoethyl)-O'-[2-(Boc-amino)ethyl] deca(ethylene glycol) (Figure 15).

Reaction of O-(2-aminoethyl)-O'-[2-(Boc-amino)ethyl]deca(ethylene glycol) with pentenoic anhydride

1 g of O-(2-aminoethyl)-O'-[2-(Boc-amino)ethyl]deca(ethylene glycol) was dissolved in 185 mL of DMF with 340 μL of pentenoic anhydride (abridged AP, 1.2 equivalents) and 324 μL of N,N-diisopropylamine (1.2 equivalents). The mixture was stirred overnight at room temperature. DMF was evaporated, and the resulting yellow oil was purified on chromatography column (silica gel; dichloromethane/methanol 95:5 (v/v)) to yield to AP-NH-(PEG)₁₁-NH-Boc as a yellowish oil (90 % yield, ¹H NMR D₂O, 80 °C, Figure 36: 6.00-5.85 (1H, m), 5.17-5.04 (2H, qq), 4.25 (HOD, s), 3.82-3.67 (40H, d), 3.67-3.60 (4H, td), 3.44-3.39 (2H, t), 3.33-3.27 (2H,t), 2.41-2.34 (4H, m), 1.53-1.42 (9H_{boc}, s)).

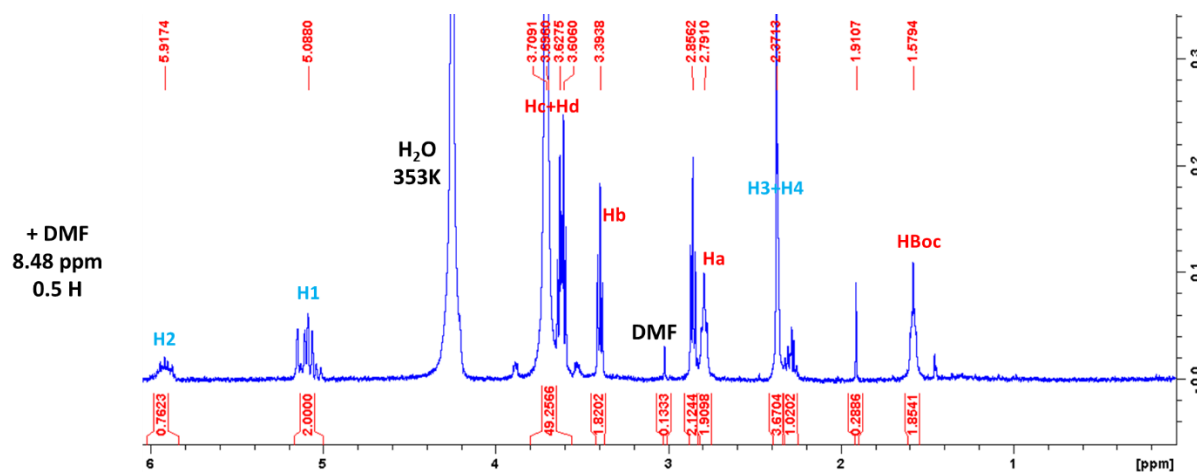


Figure 36. ¹H NMR of AP-NH-(PEG)₁₁-NH-Boc, in D₂O at 4.2 g/L at 80 °C.

Hydrolysis of the tert-butoxycarbonyl (Boc) protective group

7.169 mL of pure trifluoroacetic acid (60 equivalents) were added dropwise to AP-NH-(PEG)₁₁-NH-Boc and stirred strongly for 5 minutes. The mixture was then quickly cooled down on ice and 70 mL of NaOH 1 M were added slowly under strong stirring. The pH was adjusted to 4.5. The mixture was then charged on a column filled with ion exchange resin AG-MP50®

from BioRad (Milan, Italy) and rinsed with 100 mL of water at pH 4.5, then 300 mL of water. The unprotected amine was released from the resin eluting with ammonium hydroxide at 4 v/v%, and isolated by evaporation, yielding to PEGene as a yellow solid with a total yield in two steps of 80.5 % (^1H NMR (D_2O , 25 °C), Figure 37: 5.95-5.82 (1H, m), 5.17-5.04 (2H, qq), 4.80 (HOD, s), 3.82-3.67 (40H, d), 3.67-3.60 (4H, td), 3.44-3.39 (2H, t), 2.93-2.87 (2H,t), 2.42-2.34 (4H, m)).

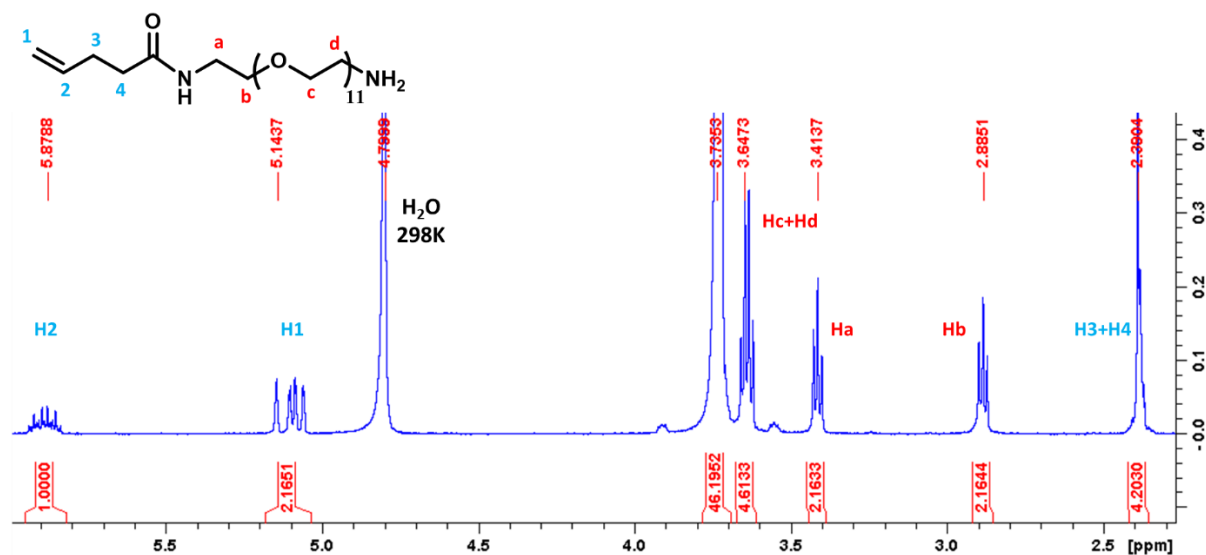


Figure 37. ^1H NMR of PEGene, in D_2O at 4.2 g/L at 25 °C.

VII.1.k. Grafting of PBA and PEGene on HAS

The protocol was adapted from Auzély *et al.*^{43, 44} (Figure 17). 1 g of HAS₄ was dissolved in 292 mL of water. Then 203 mL of DMF were added slowly. 510 mg of DMTMM (1.5 equivalents), 70 mg of 3-APBA (0.3 equivalent) and 460 mg of PEGene (0.6 equivalent) were dissolved separately in 4 mL of water each. DMTMM was added to the reaction medium, then 3-APBA, then PEGene. The pH was adjusted to 6.5 and the medium stirred overnight at room temperature. NaCl was added to obtain a final NaCl concentration of 0.3 M, then the medium was purified by ultrafiltration on a 10 kDa ultra-filtration membrane (Amicon Bioseparations, Millipore, NH, USA), and freeze-dried. HAS-PBA-PEGene was recovered with a yield superior to 90%. PBA and PEGene substitution degrees on the HA backbone, DS_{PBA} and $\text{DS}_{\text{PEGene}}$, were analyzed by ^1H NMR using the integration of HAS acetyl protons as a reference. DS_{PBA} was equal to the sum of the integration of aromatic protons of PBA divided by 4, yielding to $\text{DS}_{\text{PBA}} = 0.3$. $\text{DS}_{\text{PEGene}}$ was equal to the integration of the alkene proton around 5.9 ppm, giving

$DS_{\text{PEGene}} = 0.22$. (^1H NMR (D_2O , 80°C), Figure 16: 7.92-7.81 (0.3Ha, s), 7.70-7.53 (0.6Hb+c, dd), 7.50-7.40 (0.3H,d t), 5.95-5.82 (0.22H, m), 5.23-3.26 (m + HOD peak at 4.25), 2.40-2.33 (0.64H, s), 2.32-1.94 (3H, s)).

VII.1.I. PEDOT:HAS₄-PBA_{0.3}-PEGene_{0.22} ink polymerization protocol

1 g of HAS₄-PBA_{0.30}-PEGene_{0.22} (1 equivalent) was dissolved into 138 mL of degassed water. 440.5 μL (586 mg, 4 equivalents) of EDOT was added (so as [HAS-PBA-PEGene + EDOT] = 10 g/L). 5.7 mg of FeSO_4 were added (0.005 equivalent compared to EDOT) and 1.251 g of APS (1.33 equivalent compared to EDOT) were dissolved in 10 mL of degassed water and added at once to the HAS-PBA solution. Quickly after, the solution was mixed for 10 minutes at 25000 rpm using an Ultra Turrax T-10 basic disperser with a S 10 N-8G dispersing tool (Roth, Karlsruhe, Germany). After mixing, the solution was stirred at room temperature under nitrogen until pH was stable below 1.4-1.5 (18 to 24 h). The medium was dialyzed against osmosed water with a 6-8 kg/mol dialysis membrane (Spectrum Laboratories, CA, USA), changing the bath until water conductivity was below 8 $\mu\text{S}/\text{cm}$. Then pH was adjusted to 7.4. The medium was then filtered successively under 3 μm , 1.2 μm and 0.8 μm if possible, using acetate cellulose filters to remove large aggregates. The PEDOT:HAS₄-PBA_{0.3} was recovered by freeze-drying as a deep blue powder, with a yield superior to 80%.

VII.2. Characterizations

VII.2.a. Rheology

Oscillatory shear experiments of (PEDOT:HAS-PBA + HA-Fru) hydrogels were performed with a cone-plate rheometer (AR 2000 EX from TA Instruments Inc.). The cone had a diameter of 2 cm and an angle of 4° . 300 μL of (PEDOT:HAS-PBA + Ha-Fru) mixture were deposited on the plate, and the cone set 109 μm above. It was controlled during the experiments by maintaining the normal force at 0 ± 0.1 N. To prevent water evaporation, the measuring system was surrounded with a low-viscosity silicon oil (50 mPa·s) carefully added to the edges of the cone. Oscillatory frequency sweep (0.01–10 Hz) experiments were performed within the linear viscoelastic range (strain set at 5%) to determine the frequency

dependence of the storage (G') and loss (G'') moduli. No frequency data beyond 10 Hz are presented because inertial artifacts (raw phase angle $> 150^\circ$) were observed at frequencies higher than 10 Hz^[41,42].

Oscillatory amplitude sweep experiments at 1 Hz were used to determine the linear-viscoelastic range of the hydrogel networks and to derive the yield stress. They were immediately followed by time sweep experiments at 1 Hz and a strain of 5% (linear viscoelastic region) to monitor the recovery of the rheological moduli.

For the measurement of the self-recovery of the hydrogels after four cycles of stress-induced breakdowns, four cycles of a time sweep experiment (Stress at 340 Pa at 1 Hz) with a duration of 2 min, followed by a time sweep experiment (Stress at 50 Pa at 1 Hz) with a duration of 3 min, were performed.

VII.2.b. Photorheometry

An AR2000Ex rheometer (TA Instruments Inc.) fitted with a UV-curing cell ($\lambda = 365$ nm) and an aluminum plate (diameter 20 mm) was used for the in situ measurement of the viscoelastic properties of the hyaluronic-based hydrogels. Following deposition of 400 μ L of a mixture of HA-pentenoate, cross linker (750 g/mol PEG-(SH)₂ or DTT), photoinitiator (LAP), and eventually PEDOT:HAS-PBA ink, the gap between the flat quartz plate and the aluminum plate was set to 1160 μ m. It was controlled during the experiments by maintaining the normal force at 0 ± 0.1 N.

On each hydrogel, oscillatory time sweep and frequency sweep experiments were performed. They were carried out at 25°C with a film of silicone to avoid solvent evaporation. All the dynamic rheological data were checked as a function of strain amplitude to ensure that the measurements were performed in the linear viscoelastic region.

In the oscillatory time sweep experiments, the storage modulus (G') and loss modulus (G'') were measured during a period of 25–30 min at a fixed frequency of 1 Hz and a fixed strain of 3.5%. Typically, after the deposition of the polymer solution in PBS between the plates and equilibration for 1 min, the solution was exposed to light ($\lambda = 365$ nm) for 25–30 min at a fixed light power (20 mW/cm²) leading to gelation.

VII.2.c. Ink film deposition on glass slides

Slides were washed with acetone and ethanol. Lyophilized PEDOT-based ink was dissolved in water at 13 g/L and the suspension was strongly stirred for 10 minutes and sonicated in an ultrasound bath for 30 seconds. 60 μ L of suspension were deposited on a glass slide inside a silicon ring of 1 cm inner diameter. The ink was dried at room temperature, then the silicon ring was removed from the glass substrate.

VII.2.d. Conductivity measurements

Film sheet resistivity R_{sheet} was determined using a 4-point probe from Ossila (Power Cord Type, Sheffield, England), over a wide range of tension and current to certify the ohmic behaviour. Conductivity σ was calculated as $\sigma = 1/R_{sheet} \cdot h \cdot c$ where c was a geometric corrector coefficient determined by the software and h the film thickness measured with a Dektak DXT profilometer (Brüker, Palaiseau, France). Conductivity was measured in several location of the film, then averaged.

For a uniform sheet thickness, sheet resistance is a special case of resistivity. Its unity is $\Omega/\square = \Omega/(m/m)$. The “ \square ” is adimensionnal, but kept to not confuse the sheet resistance from the bulk resistance.

VII.2.e. Functionalization of glass-slides with thiol moieties

Glass slides were rinsed with acetone, then ethanol. Surface silanol functions were generated with O_2 plasma activation using a MVD 100 system manuel (molecular vapor deposition) from Applied MST (San Jose, CA, USA) (450 sccm, 200 W, 500 s), and then immediately immersed in toluene containing 10 mM of 3-mercaptopropyltrimethoxysilane (MPTMS), and heated overnight at 80°C (Figure 38). Thiol functionalized glass slides were then sonicated 10 minutes in acetone, 10 minutes in ethanol, and finally annealed 3h at 110 °C. Thiol functionalized glass slides were stored under argon in the dark. Before use, they were immersed 1 hour in 1,2-dithiothréitol at 0.5 g/L pH 8.3 to reduce oxidise disulfure bridges.

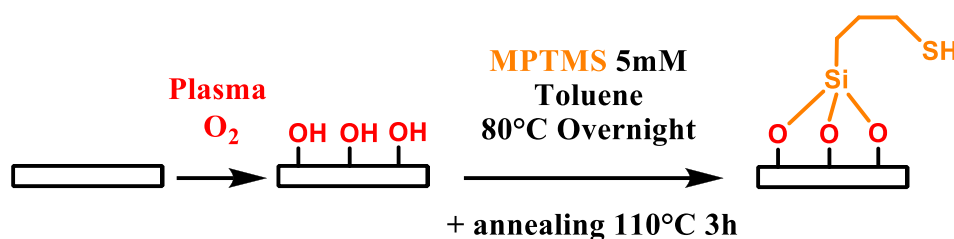


Figure 38. Functionalization of glass slides with thiols functions

VII.2.f. Dynamic Light Scattering (DLS)

DLS measurements were recorded on a Zeta sizer NanoZS from Malvern Instruments Ltd. (Worcestershire, England). For DLS measurements, samples were diluted at 0.05 g/L in water and equilibrated at 25°C. Measurements were made 3 times in a row. The “Zaverage” value was reported. The Zaverage is the intensity weighted mean hydrodynamic size of the ensemble collection of particles measured by DLS.

VII.2.g. Viscosity measurements

Viscosity experiments were performed with an AR 2000 EX cone-plate rheometer (TA Instruments, Eschborn, Germany). The cone has a diameter of 4 cm and an angle of 4°. 1150 µL were deposited on the plate, and the cone set 75 µm above. In a steady-state flow, three shear rate ramps from 0.1 Hz to 700 Hz at 25°C, with 6 points per decade were performed. To prevent water evaporation, the measuring system was surrounded with a low-viscosity silicon oil (50 mPa.s) carefully added to the edges of the cone.

VII.2.h. Surface tension

Surface tensions were measured using a DSA100 drop shape analyzer from Krüss (Hamburg, Germany) using DSA4 software from Krüss. The pending drop technique was used, with a Laplace-Young drop fitting algorithm. The needle used was a NE45 KRÜSS needle with an inner diameter of 1.8 mm (Hamburg, Germany). The density of the gas surrounding phase was set at 0.0012 g/L and the density of the ink was considered as the same of water at 25°C: 0.997 g/L.

VII.2.i. Atomic force microscopy (AFM) analysis

AFM analysis were performed at the Platform for Nano Characterization (PFNC) of CEA-LETI by Denis Mariolle, using a Dimension ICON microscope from Brüker (Palaiseau, France) in scanning spreading resistance microscopy (SSRM) mode using ADAMA AD-2.8-AS and ADAMA AD-40-AS diamond tips from Brüker, and NANOSENSORS CDT-NCHR diamonds tips from Nanosensor (Neuchatel, Switzerland). Data were treated using Nanoscope Analysis V2.0. Data display and roughness analysis were made using Image Metrology SPIP V6.7.2.

VIII. Bibliography

- [1] C. M. Proctor, I. Uguz, A. Slezia, V. Curto, S. Inal, A. Williamson, G. G. Malliaras, *Advanced Biosystems* **2019**, *3*, 1800270.
- [2] P. Leleux, J. Rivnay, T. Lonjaret, J.-M. Badier, C. Bénar, T. Hervé, P. Chauvel, G. G. Malliaras, *Adv. Healthcare Mater.* **2015**, *4*, 142–147.
- [3] P. Leleux, C. Johnson, X. Strakosas, J. Rivnay, T. Hervé, R. M. Owens, G. G. Malliaras, *Adv. Healthcare Mater.* **2014**, *3*, 1377–1380.
- [4] J.-Y. Chiu, C.-M. Yu, M.-J. Yen, L.-C. Chen, *Biosensors and Bioelectronics* **2009**, *24*, 2015–2020.
- [5] J. Oziat, Electrode 3D de PEDOT: PSS Pour La Détection de Métabolites Électrochimiquement Actifs de *Pseudomonas Aeruginosa*, PhD Thesis, Lyon, **2016**.
- [6] A. Håkansson, S. Han, S. Wang, J. Lu, S. Braun, M. Fahlman, M. Berggren, X. Crispin, S. Fabiano, *J. Polym. Sci. Part B: Polym. Phys.* **2017**, *55*, 814–820.
- [7] D. Mantione, I. del Agua, A. Sanchez-Sanchez, D. Mecerreyes, *Polymers* **2017**, *9*, 354.
- [8] I. del Agua, D. Mantione, U. Ismailov, A. Sanchez-Sanchez, N. Aramburu, G. G. Malliaras, D. Mecerreyes, E. Ismailova, *Advanced Materials Technologies* **2018**, *3*, 1700322.
- [9] M. Solazzo, K. Krukiewicz, A. Zhussupbekova, K. Fleischer, M. J. Biggs, M. G. Monaghan, *J. Mater. Chem. B* **2019**, *7*, 4811–4820.
- [10] M. Elmahmoudy, Micro- et Nano-patterning de Polymères Conducteurs pour des Applications Biomédicales, **n.d.**
- [11] S. Inal, A. Hama, M. Ferro, C. Pitsalidis, J. Oziat, D. Iandolo, A.-M. Pappa, M. Hadida, M. Huerta, D. Marchat, P. Mailley, R. M. Owens, *Advanced Biosystems* **2017**, *1*, 1700052.
- [12] T. Figueiredo, J. Jing, I. Jeacomine, J. Olsson, T. Gerfaud, J.-G. Boiteau, C. Rome, C. Harris, R. Auzély-Velty, *Biomacromolecules* **2020**, *21*, 230–239.
- [13] J. Mergy, A. Fournier, E. Hachet, R. Auzély-Velty, *Journal of Polymer Science Part A: Polymer Chemistry* **2012**, *50*, 4019–4028.
- [14] C. E. Hoyle, C. N. Bowman, *Angewandte Chemie International Edition* **2010**, *49*, 1540–1573.
- [15] C. E. Hoyle, T. Y. Lee, T. Roper, *Journal of Polymer Science Part A: Polymer Chemistry* **2004**, *42*, 5301–5338.
- [16] H. C. Kolb, M. G. Finn, K. B. Sharpless, *Angew. Chem. Int. Ed.* **2001**, *18*.
- [17] M. Schuster, C. Turecek, B. Kaiser, J. Stampfl, R. Liska, F. Varga, *Journal of Macromolecular Science, Part A* **2007**, *44*, 547–557.
- [18] A. Urrios, C. Parra-Cabrera, N. Bhattacharjee, A. M. Gonzalez-Suarez, L. G. Rigat-Brugarolas, U. Nallapatti, J. Samitier, C. A. DeForest, F. Posas, J. L. Garcia-Cordero, A. Folch, *Lab Chip* **2016**, *16*, 2287–2294.
- [19] B. D. Fairbanks, M. P. Schwartz, C. N. Bowman, K. S. Anseth, *Biomaterials* **2009**, *30*, 6702–6707.
- [20] S. Paiva, P. Joanne, C. Migdal, E. L. Soler, Y. Hovhannisyan, A. Nicolas, O. Agbulut, *ACS Biomaterials Science & Engineering* **2020**, *6*, 340–351.
- [21] E. Hachet, H. Van Den Berghe, E. Bayma, M. R. Block, R. Auzély-Velty, *Biomacromolecules* **2012**, *13*, 1818–1827.
- [22] D. Mantione, A. V. Marquez, F. Cruciani, C. Brochon, E. Cloutet, G. Hadziioannou, *ACS Macro Lett.* **2019**, *8*, 285–288.
- [23] D. Caras-Quintero, P. Bäuerle, *Chem. Commun.* **2004**, 926–927.
- [24] W. Su, H. T. Nguyen, M. Cho, Y. Son, Y. Lee, *Synthetic Metals* **2010**, *160*, 2471–2475.
- [25] H.-A. Lin, S.-C. Luo, B. Zhu, C. Chen, Y. Yamashita, H. Yu, *Advanced Functional Materials* **2013**, *23*, 3212–3219.
- [26] H. Yuk, B. Lu, S. Lin, K. Qu, J. Xu, J. Luo, X. Zhao, *Nat Commun* **2020**, *11*, 1604.
- [27] L. Ferlauto, P. Vagni, A. Fanelli, E. G. Zollinger, K. Monsorno, R. C. Paolicelli, D. Ghezzi, *Biomaterials* **2021**, *274*, 120889.
- [28] L. D. Garma, L. M. Ferrari, P. Scognamiglio, F. Greco, F. Santoro, *Lab Chip* **2019**, *19*, 3776–3786.

- [29] C. A. Mire, A. Agrawal, G. G. Wallace, P. Calvert, M. in het Panhuis, *Journal of Materials Chemistry* **2011**, 21, 2671.
- [30] K. Wang, L. Tian, T. Wang, Z. Zhang, X. Gao, L. Wu, B. Fu, X. Liu, *Composite Interfaces* **2019**, 26, 27–40.
- [31] H. Zhang, M. Yue, T. Wang, J. Wang, X. Wu, S. Yang, *New J. Chem.* **2021**, 45, 4647–4657.
- [32] D. Mantione, I. del Agua, W. Schaafsma, M. ElMahmoudy, I. Uguz, A. Sanchez-Sanchez, H. Sardon, B. Castro, G. G. Malliaras, D. Mecerreyes, *ACS Appl. Mater. Interfaces* **2017**, 9, 18254–18262.
- [33] Y. Xu, Z. Sui, B. Xu, H. Duan, X. Zhang, *Journal of Materials Chemistry* **2012**, 22, 8579–8584.
- [34] D. Mawad, E. Stewart, D. L. Officer, T. Romeo, P. Wagner, K. Wagner, G. G. Wallace, *Advanced Functional Materials* **2012**, 22, 2692–2699.
- [35] B. Wu, B. Cao, I. M. Taylor, K. Woeppel, X. T. Cui, *Front. Chem.* **2019**, 7, 178.
- [36] M. Sassi, L. Mascheroni, R. Ruffo, M. M. Salamone, G. A. Pagani, C. M. Mari, G. D’Orazio, B. La Ferla, L. Beverina, *Organic Letters* **2013**, 15, 3502–3505.
- [37] B. Wei, L. Ouyang, J. Liu, D. C. Martin, *Journal of Materials Chemistry B* **2015**, 3, 5028–5034.
- [38] D. Alemu, H.-Y. Wei, K.-C. Ho, C.-W. Chu, *Energy Environ. Sci.* **2012**, 5, 9662.
- [39] X. Tang, H. Kwon, H. Ye, J. Y. Kim, J. Lee, Y. J. Jeong, S. H. Kim, *Physical Chemistry Chemical Physics* **2019**, 21, 25690–25699.
- [40] D. Tarus, E. Hachet, L. Messenger, B. Catargi, V. Ravaine, R. Auzély-Velty, *Macromolecular Rapid Communications* **2014**, 35, 2089–2095.
- [41] R. E. Hudson, A. J. Holder, K. M. Hawkins, P. R. Williams, D. J. Curtis, *Physics of Fluids* **2017**, 29, 121602.
- [42] I. M. Krieger, *Journal of Rheology* **1990**, 34, 471–483.

Chapter 4.

Development of pure conductive PEDOT-based hydrogel doped by HAS₄-PBA_{0.3}

I. Introduction.....	196
II. Synthesis of conductive hydrogels in two steps.....	197
II.1. Development of HAS-ArEne	197
II.1.a. Grafting of ArEne on HAS ₄	197
II.1.b Electric properties of PEDOT: HAS ₄ -ArEne _{0.5} ink	198
II.1.c. Synthesis of HAS ₄ -ArEne _{0.5} hydrogels	199
II.2. EDOT polymerization in a preformed hydrogel	201
II.2.a. Two step synthesis of PEDOT:HAS ₄ -ArEne _{0.5} hydrogel	201
II.2.b. Limitation of PEDOT:HAS ₄ -ArEne _{0.5} two steps hydrogels.....	202
II.2.c. Conclusion.....	204
III. Synthesis of conductive hydrogels in one step	205
III.1. Cross-linking of HAS ₄ -PBA _{0.3} by adipic acid dihydrazide without EDOT	205
III.1.a. Influence of solvent and pH during HAS ₄ -PBA _{0.3} cross-linking.	206
III.1.b. Influence of NaCl concentration on cross-linking reaction	208
III.1.c. pH variation during EDOT polymerization	209
III.2. Simultaneous hydrogel cross-linking and EDOT polymerization.....	210
III.2.a. Conductive hydrogel synthesis.....	210
III.2.b. Mechanical properties	212
III.2.c. PEDOT:HAS ₄ -PBA _{0.3} /ADH hydrogels swelling behavior.....	213
III.2.d. PEDOT:HAS ₄ -PBA _{0.3} /ADH hydrogel conductivity	214
III.2.e. Conclusion	216
IV. Electrochemical properties PEDOT:HAS ₄ -PBA _{0.3} / ADH hydrogels	217
IV.1. Properties of interest and experimental setup.....	217
IV.2. Charge storage capacity (CSC).....	218
IV.3. Charge injection capacity	220
IV.4. Electrical impedance spectroscopy.....	222
IV.5. Application: stimulation of mice hippocampus	224
V. Discussion.....	227
V.1. Synthesis of HAS ₄ -ArEne _{0.5}	227
V.2. Two-steps pure conductive hydrogels	227
V.3. One-step pure conductive hydrogel	228
V.3.a. Mechanical and electrochemical properties.....	229
V.3.b. Potential system improvement.....	231
VI. Conclusion.....	233
VII. Materials and methods	234

VII.1. Synthesis	234
VII.1.a. Materials	234
VII.1.b. Synthesis of HAS-ArEne.....	234
VII.1.c. Determination of the degree of substitution of HAS-ArEne by the follow up of the amide coupling reaction.....	235
VII.1.d. Synthesis of conductive HAS ₄ -ArEne _{0.5} hydrogel	236
VII.1.e. Synthesis of conductive PEDOT:HAS ₄ -PBA _{0.3} / ADH one pot hydrogels	237
VII.2. Characterization.....	238
VII.2.a. Photorheometry of HAS ₄ -ArEne _{0.5} hydrogels.....	238
VII.2.b. Rheology.....	239
VII.2.c. Swelling behavior	239
VII.2.d. Uniaxial compression experiments	239
VII.2.e. Cavity electrode preparation	240
VII.2.f. Electrochemical characterization.....	241
VII.2.i. Ex-vivo mice hippocampus stimulation.....	242
VIII. Bibliography	244

I. Introduction

In the previous chapters, the development of a new conductive and resorbable ink was described. PEDOT:HAS₄-PBA_{0.3} which design was detailed in chapter 2 displayed a conductivity around 1.5 S/cm and was cytocompatible. In order to make it insoluble in aqueous medium, different cross-linking strategies were implemented in chapter 3.

A derivative of HAS₄-PBA_{0.3} (Chapter 2, Table 5) with an additional alkene function grafted via a PEG spacer was synthesized (HAS₄-PBA_{0.3}-PEGene_{0.22}, Chapter 3, Table 4b) in order to obtain thiol-ene cross-linkable PEDOT: HAS₄-PBA_{0.3}-PEGene_{0.22} ink (Chapter 3, section III.2.). As EDOT highly absorbs UV photons, only thin films (thickness < 1 mm) could be cross-linked, and such material, suited for the printing electrical tracks, could not be used to design macroscopic hydrogels.

In order to design a conductive thick hydrogel, with homogenous cross-linking throughout all the matrix, a new strategy needs to be implemented. Considering the various strategies reported in the literature and described in chapter 1, and with the condition of conductivity properties in mind, it was first proposed to design a hydrogel in two steps: 1) preforming a hydrogel with PEDOT dopant constituting one of the elements of matrix of the hydrogel; then 2) filling it with the conductive monomer and polymerizing it via chemical polymerization.

This strategy in two steps is described in section II. However as detailed below, it was not fully satisfactory. Therefore another strategy in which matrix cross-linking with PEDOT dopant occurs simultaneously to EDOT polymerization (one-step strategy) was also implemented, and is described in section III. The material obtained in section III was then carefully characterized (section IV). Section V discusses the results in details.

II. Synthesis of conductive hydrogels in two steps

A first strategy to implement the synthesis of thick conductive hydrogels in 2 steps was to form a hydrogel with HAS₄-PBA_{0.3}-PEGene_{0.22} using thiol-ene chemistry, then polymerize EDOT in this hydrogel matrix. HAS₄-PBA_{0.3}-PEGene_{0.22} was dissolved in water at various concentrations with PEG-(SH)₂ (Mn = 3.5 kg/mol, molar ratio $n_{\text{SH}}/n_{\text{alkene}} = 1$), and LAP at 1 g/L as a photo initiator. The mixtures were irradiated for 15 minutes at 40 mW/cm² at 365 nm to cross-link the gel. Hydrogels using HAS₄-PBA_{0.3}-PEGene_{0.22} at 20 and 30 g/L resulted in very soft gels which were not processed any further. Hydrogels using HAS₄-PBA_{0.3}-PEGene_{0.22} at 40 and 50 g/L were slightly more rigid, but still too soft to be used as matrix for the conductive polymer. Pure HAS₄-PBA_{0.3}-PEGene_{0.22} hydrogels appeared to be too soft, almost fluid, and were not suitable for further processing.

II.1. Development of HAS-ArEne

Therefore, a new HAS₄ derivative was required in order to obtain more rigid hydrogels. This new derivative should meet the same requirements as HAS₄-PBA_{0.3}-PEGene_{0.22}: it should be a derivative of HAS₄ with an aromatic group for the conductivity properties, and possess an alkene function through a short spacer arm to avoid steric hindrance after coupling with HAS₄. The PBA moieties were not specifically required, and were suppressed. Additionally, we chose to graft it on the HA carboxylic acid functions via an amidation reaction, similarly to 3APBA.

Since the commercial molecule 4-[(pent-4-en-1-yloxy)methyl]aniline (abridged ArEne) commercialized by Uorsy (Kiev, Ukraine), containing both an aromatic group and an alkene function, filled the structural criteria (Figure 1), it was selected to obtain new HAS₄-ArEne derivatives.

II.1.a. Grafting of ArEne on HAS₄

4-[(pent-4-en-1-yloxy)methyl]aniline (ArEne) was grafted on HAS₄ **8** (Chapter 2, Table 3, M_w = 100 kg/mol) via an amide coupling reaction between the carboxylic acid function of HAS₄ and the amine function of ArEne using 4-(4,6-dimethoxy-1,3,5-triazin-2-yl)-4-

methylmorpholinium chloride (DMTMM) as a coupling agent, at pH 6.5 (Figure 1). The ArEne substitution degree DS_{ArEne} of the HAS₄ was estimated from the reaction kinetics, monitored using the TNBS method (section VII.1.c.), as it could not be determined using ¹H NMR since the ¹H signals of HAS₄ were superimposed with the ¹H signals of ArEne (Figure 21). DS_{ArEne} was found to be 0.5, with a 100% grafting yield.

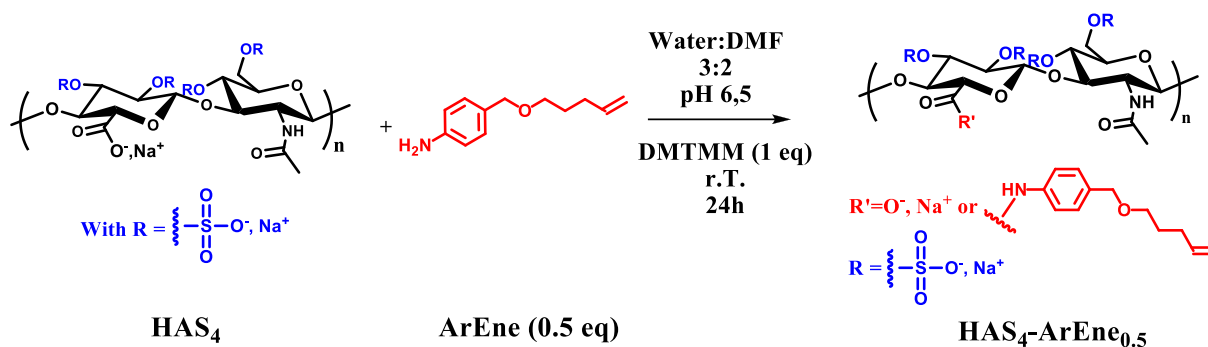


Figure 1. Amide coupling reaction of HAS₄ with ArEne.

II.1.b Electric properties of PEDOT: HAS₄-ArEne_{0.5} ink

In order to assess the capacity of HAS₄-ArEne_{0.5} to dope PEDOT efficiently, PEDOT: HAS₄-ArEne_{0.5} ink was synthesized using the optimized PEDOT polymerization protocol developed in chapter 2 (section III.3.). Briefly, 1 equivalent of HAS₄-ArEne_{0.5} was dissolved at 10 g/L in water with 4 equivalent of EDOT, 0.05 equivalent of FeSO₄ compared to EDOT and 1.33 equivalent of APS compared to EDOT. The mixture was mixed 10 minutes at 25000 rpm and then stirred overnight.

After 18 hours stirring, it was observed that the ink that was not directly in contact with the magnetic stirrer formed a gel in the vial. The dark gel broke easily when manipulated, and dislocated under water addition. To evaluate its conductive properties, this physical hydrogel was dispersed, and purified as usual: dialysis against water, neutralization and freeze drying. It could not be filtered even on 8 μm -pore filters. Finally PEDOT: HAS₄-ArEne_{0.5} ink was dispersed at 13 g/L in water and 60 μL were drop-casted on a glass slide and dried overnight. The film thickness was measured with a mechanical profilometer, and its resistivity, with a 4 point probe, leading to a conductivity of 0.4 S/cm. This conductivity was lower than that of

PEDOT:HAS₄-PBA_{0.3} (≈ 1.5 S/cm). This was attributed to the poor quality of the ink which formed a physical gel during ink polymerization.

Additionally, this ink could be cross-linked with PEG-(SH)₂ ($M_n = 3.5$ kg/mol, molar ratio $n_{SH}/n_{alkene} = 1$) and LAP at 1 g/L, at 365 nm and 40 mW/cm² in 10 minutes, for ink concentrations above 25 g/L. But as for PEDOT:HAS₄-PBA_{0.3}-PEGene_{0.22} inkXL, only thin films could be cross-linked. The need for prior hydrogel cross-linking before EDOT polymerization was again justified.

II.1.c. Synthesis of HAS₄-ArEne_{0.5} hydrogels

As HAS₄-ArEne_{0.5} demonstrated to act adequately as a dopant for PEDOT, its gelation properties were then investigated.

HAS₄-ArEne_{0.5} hydrogels were cross-linked using thiol-ene photochemistry and the hydrogel storage modulus G' were measured. First HAS₄-ArEne_{0.5} was dissolved in water at 20 g/L with PEG-(SH)₂ ($M_n = 3.5$ kg/mol) so that the molar ratio $n_{SH}/n_{alkene} = 0.5$, and LAP = 0.5 g/L. The kinetics of the cross-linking reaction was investigated using an AR2000-Ex rheometer with a UV curing cell (Protocol detailed in section VII.2.). Briefly, the hydrogel precursor mixture was deposited on a cone-plate rheometer, equilibrated for 2 min before being exposed to UV light at 365nm at 20 mW/cm². The elastic and loss modulus G' and G'' were monitored over time. Initially, G'' was larger than G' , which reflected the viscous behavior of the sample. After a short induction period of 2 minutes, the storage and loss moduli increased due to the formation of elastic effective intermolecular cross-links, and G' quickly increased to reach a plateau around 924 Pa in less than five minutes (Figure 2a). The following frequency sweep provided proof of the formation of a chemical hydrogel with $G' \gg G''$ and constant elastic modulus values at all frequencies (Figure 2b). This experiment demonstrated the ability of the new HAS₄-ArEne_{0.5} to form a soft hydrogel ($G' \sim 1$ kPa, in the same range of elastic moduli of brain^[1]) even at relatively low HAS₄-ArEne_{0.5} concentration (20 g/L), and low cross-linking ratio ($n_{SH}/n_{alkene} = 0.5$).

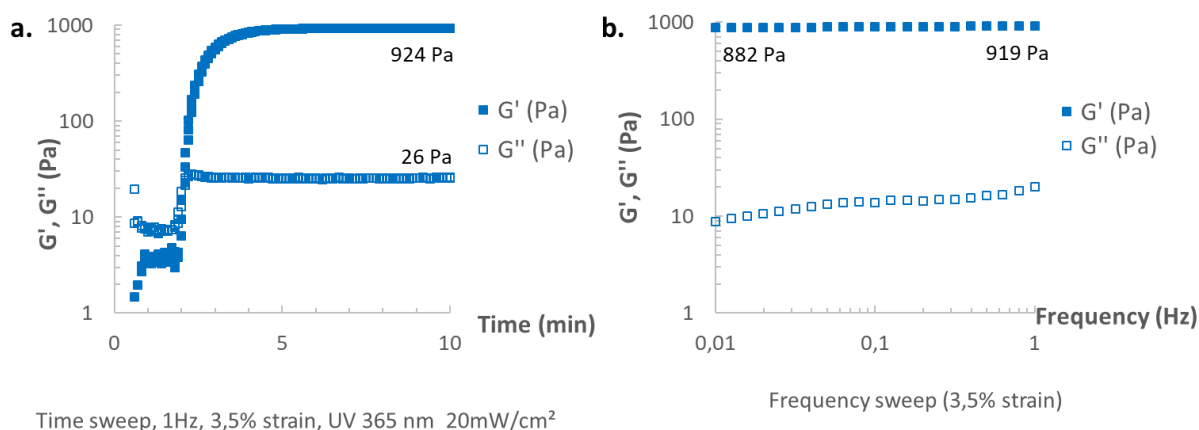
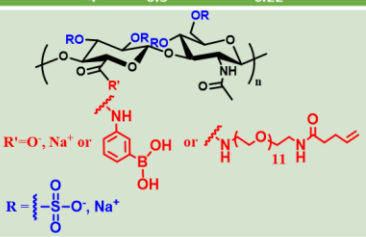
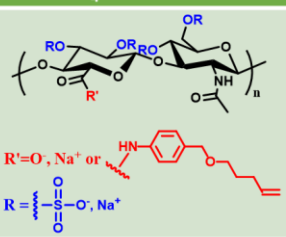


Figure 2. a. Time sweep at 1Hz, 3.5% strain, under UV irradiation (365 nm) at 20 mW/cm². b. Frequency sweep at 3.5% strain after gel cross-linking.

Additional gelation experiments were implemented to investigate other gelation conditions. HAS₄-ArEne_{0.5} was dissolved in water at 40 g/L with PEG-(SH)₂ ($M_n = 3.5$ kg/mol, molar ratio $n_{SH}/n_{alkene} = 1$) and LAP at 1 g/L, and irradiated as described above, leading to a gel with a storage modulus of 117 ± 1 kPa in a few minutes, with a stable viscoelastic behavior (constant G' and G'') over a wide range of frequencies (from 0.01 to 4 Hz). HAS₄-ArEne_{0.5} proved to be a relevant candidate to develop new conductive hydrogels with a storage modulus in the 1 – 100 kPa range, as aimed in this Ph.D. project.

In summary, the newly synthesized HAS₄-ArEne_{0.5} displayed good gelation properties and demonstrated to act adequately as a dopant for PEDOT. Its properties made it a good complement of HAS₄-PBA_{0.3}-PEGene_{0.22} in this project, as this later displayed poor gelation properties, but was a good PEDOT dopant, whereas HAS₄-ArEne_{0.5} displayed great gelation properties, but was a slightly less good PEDOT dopant. HAS₄-PBA_{0.3}-PEGene_{0.22} thus appeared to be adapted to print conductive cross-linked thin tracks, while HAS₄-ArEne_{0.5} seemed to be adapted to the design of bulk conductive hydrogels. Those different properties are summarized in Table 1.

Table 1. Complementary properties of HAS₄-PBA_{0.3}-PEGene_{0.22} and HAS₄-ArEne_{0.5}.

	HAS ₄ -PBA _{0.3} -PEGene _{0.22}	HAS ₄ -ArEne _{0.5}
		
	Low DS _{PEGene} (max 0.2)	High DS _{ArEne} (up to 0.5)
	Long and costly to obtain	Quickly synthesised
Corresponding ink	Form monodisperse particles (300-1000 nm)	Form aggregates
	Cross-linkable at high concentration (>50g/L)	Cross-linkable at medium concentration (>25g/L)
σ (S/cm)	Up to 4	0.3-0.7
Application	Printed cross-linked conductive tracks	Conductive hydrogels

II.2. EDOT polymerization in a preformed hydrogel

II.2.a. Two step synthesis of PEDOT:HAS₄-ArEne_{0.5} hydrogel

HAS₄-ArEne_{0.5} was used to synthesize conductive hydrogels in two steps. The first one relied on hydrogel cross-linking. The second one consisted in hydrogel loading with EDOT and oxidative polymerization of EDOT inside the hydrogel matrix (Figure 3).

HAS₄-ArEne_{0.5} was dissolved in 0.15 M NaCl at 30 g/L with PEG-(SH)₂ ($M_n = 3.5$ kg/mol, $n_{\text{thiol}}/n_{\text{alkene}} = 0.75$), and LAP at 0.75 g/L. 0.15 M of NaCl was added to the solvent and to all ulterior baths to minimize gel swelling through the screening of intra-network electrostatic repulsions. This appeared to be an important parameter to control in order to control EDOT concentration inside the gel. 150 μL of the mixture was poured in a cylindrical mold ($\varnothing_{\text{int}} = 5.8$ mm, $h = 8$ mm) and irradiated 10 min at 40 mW/cm² at 365 nm. The cylindrical mold was then turned upside down and irradiated 5 additional minutes to ensure homogenous cross-linking in all gel height (Figure 3, step 1), then unmold.

The gel was loaded in EDOT by diffusion. The gel was immersed in 4 mL of 0.15 M NaCl : acetonitrile 6:4 v:v containing 67.8 mM of EDOT so as there were 2 equivalents of EDOT compared to HAS₄-ArEne_{0.5} in 150 μL (the hydrogel volume). This immersion was realized one more time to ensure total loading of EDOT in the hydrogel (Figure 3, step 2.1). Acetonitrile was

used as a co-solvent in this step to totally solubilize EDOT in order to ensure its correct diffusion inside the hydrogel matrix

Finally, the gel was immersed in a solution containing both EDOT oxidant (APS), and catalyst (FeSO₄) at different concentrations so as there were 1.33 equivalent of APS and 0.005 equivalent of FeSO₄ compared to EDOT in 150 μ L (volume of the hydrogel). After 24 hours, a dark hydrogel was obtained (Figure 3, step 2.2, Figure 4a), demonstrating EDOT polymerization. The gel was washed by successive baths of PBS to remove EDOT polymerization by-products, and to neutralize it. Noticeably, no PEDOT leached in the washing bath, showing that PEDOT chains were well-trapped inside the hydrogel matrix.

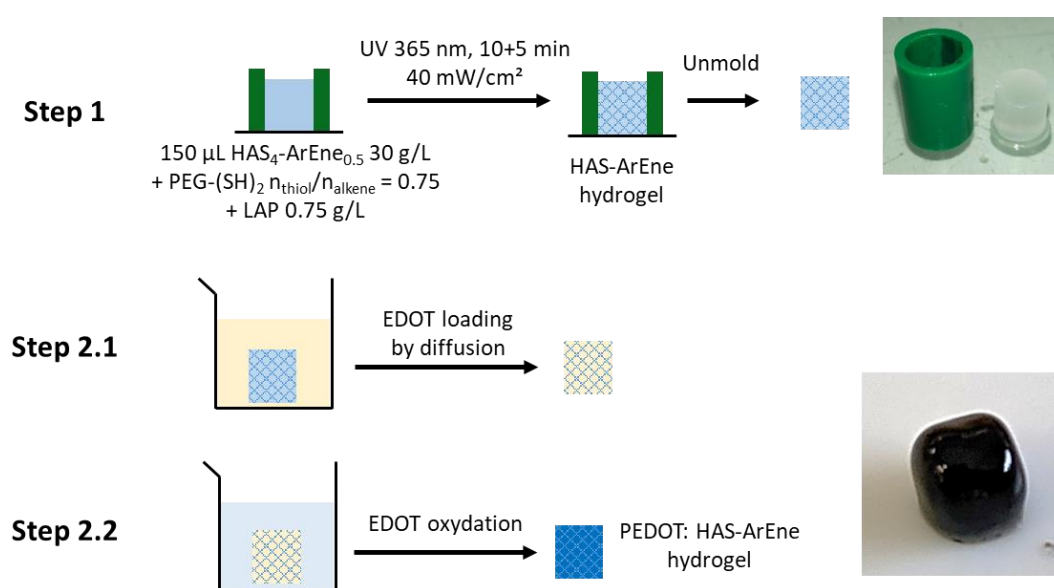


Figure 3. Two step synthesis of PEDOT:HAS₄-ArEne_{0.5} hydrogel.

II.2.b. Limitation of PEDOT:HAS₄-ArEne_{0.5} two steps hydrogels

All PEDOT:HAS₄-ArEne_{0.5} hydrogels synthesized using this protocol displayed two limiting characteristics: first, instead of deep blue, they were dark black (Figure 4a), which is a characteristic color of PEDOT over-oxidation; second they were all partially degraded on the surface after PEDOT oxidation (step 2.2, less sharp hydrogel geometry). These two facts suggested that the amount of APS introduced during PEDOT oxidation was over the necessary quantity. As APS was consumed during PEDOT polymerization, the total amount of APS

diffusing effectively inside the hydrogel was superior to 1.33 equivalent compared to PEDOT, resulting in PEDOT over-oxidation, and matrix degradation by oxidation.

To solve this issue, the concentration of APS and FeSO₄ during step 2.2 were adjusted: [APS] and [FeSO₄] in step 2.2 were chosen so as there were 1.33 equivalent of APS and 0.005 equivalent of FeSO₄ compared to EDOT in all the bath. This strategy resulted in very slow EDOT polymerization in 48 to 72 h, but with final undamaged light blue hydrogels (Figure 4b).

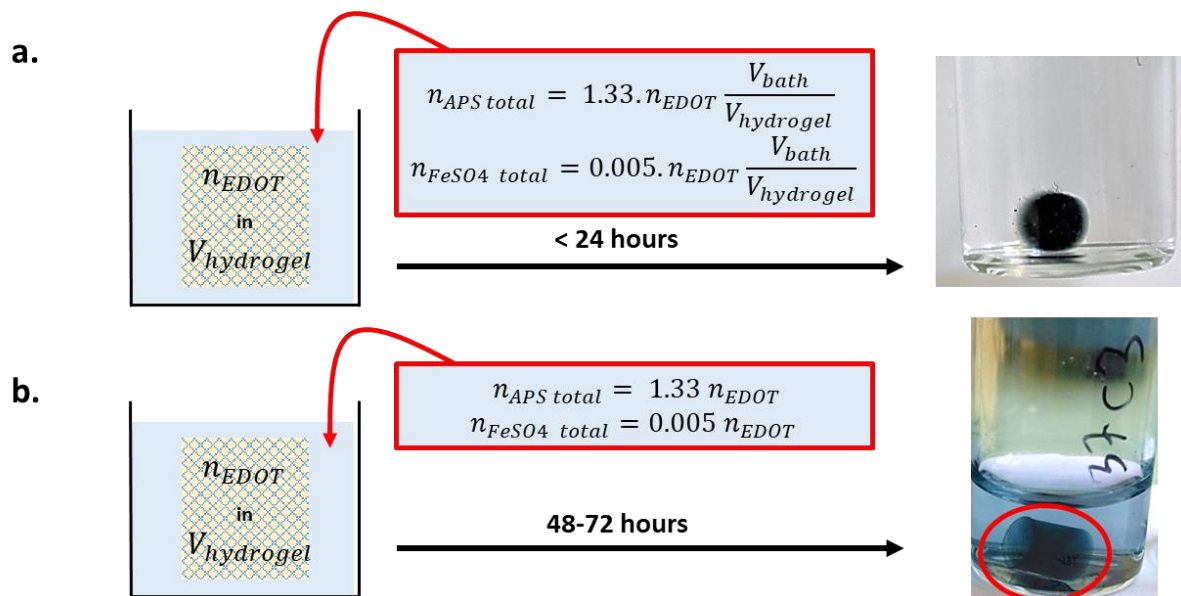


Figure 4. PEDOT:HAS₄-ArEne_{0.5} hydrogels after step 2.2, if (a) [APS] and [FeSO₄] are chosen so as $n_{APS\ in\ hydrogel} = 1.33 \cdot n_{EDOT}$ and $n_{FeSO4\ in\ hydrogel} = 0.005 \cdot n_{EDOT}$, or if (b) [APS] and [FeSO₄] are chosen so as $n_{APS\ total} = 1.33 \cdot n_{EDOT}$ and $n_{FeSO4\ total} = 0.005 \cdot n_{EDOT}$.

Although this second strategy appeared to be suitable to synthesize conductive hydrogels, the slow EDOT polymerization resulted in too low PEDOT concentration inside the hydrogel as EDOT had time to diffuse out of it (blue color of the oxidative bath after step 2.2., Figure 4b). Furthermore, as n_{APS} and n_{FeSO_4} were constant in the oxidative bath, whatever its volume (equation Figure 4b), this strategy was highly dependent on step 2.2 bath size, as larger bath implied even lower APS and FeSO₄ concentrations. Therefore, this protocol was not reproducible with gel of different size, or different glassware, as each new experimental set up would require [APS] and [FeSO₄] optimization.

II.2.c. Conclusion

In summary, either PEDOT was over-oxidized and the hydrogel matrix degraded by the excess of oxidant, or PEDOT was oxidized too slowly, letting it the time to diffuse out of the hydrogel. In both cases, the oxidation of PEDOT loaded in HAS₄-ArEne_{0.5} hydrogel was highly dependent on gel size and geometry, and on bath size, namely on the experimental device. This prevented the precise control of EDOT/HAS₄-ArEne_{0.5} ratio and PEDOT oxidation degree, from one batch to another. As a matter of fact, the mechanical and electro chemical properties of this gel could not be characterized. It was not investigated any further.

Another polymerization protocol was needed, in order to have a precise control on EDOT/HAS₄-ArEne_{0.5} ratio, and PEDOT oxidation degree, from one batch to another.

III. Synthesis of conductive hydrogels in one step

In order to develop rigorously a conductive hydrogel, a protocol which was independent from batch size and where all EDOT polymerization parameters could be controlled was required. To circumvent the problem met with PEDOT:HAS₄-ArEne_{0.5} hydrogels, it was decided to implement a one-step protocol, where both PEDOT polymerization and hydrogel cross-linking would take place simultaneously.

III.1. Cross-linking of HAS₄-PBA_{0.3} by adipic acid dihydrazide without EDOT

As in the previous section, the conductive hydrogel had to include as less non-conductive materials as possible, and composed of HAS₄-PBA_{0.3} (Chapter 2, Table 5), or a similar derivative, in order to maximize its final conductivity. Here, simultaneous EDOT polymerization and hydrogel matrix cross-linking were attempted. However, it had to be taken into account that EDOT color quickly changed during its polymerization, which hindered light propagation, starting from a cloudy emulsion to evolve in a dark blue material. Therefore, contrary to hydrogels based on PEDOT:HAS₄-ArEne_{0.5} described in section II.2, where a transparent hydrogel could be first cross-linked using UV-initiated thiol-ene chemistry, here photo-initiated thiol-ene chemistry could not be employed, as it would have yield heterogeneous cross-linking throughout the hydrogel matrix.

Therefore, it was decided to cross-link HAS₄-PBA_{0.3} through the reaction of its carboxylic acid groups with a bis-hydrazide derivative to form the hydrogel matrix. Adapting the work from Yang *et al.*^[2], HAS₄-PBA_{0.3} was cross-linked using adipic acid dihydrazide (ADH), via an amide coupling reaction using N-(3-Dimethylaminopropyl)-N'-ethylcarbodiimide hydrochloride (EDC) as a coupling agent (Figure 5). ADH is a biocompatible compound, widely used to cross-link water based emulsions^[2] and enabled to design biodegradable hydrogels^[3]. Besides, the low pKa of the hydrazide function (≈ 3.4) enables coupling reactions at low pH, which is mandatory for a reaction carried out simultaneously with EDOT polymerization that releases protons.

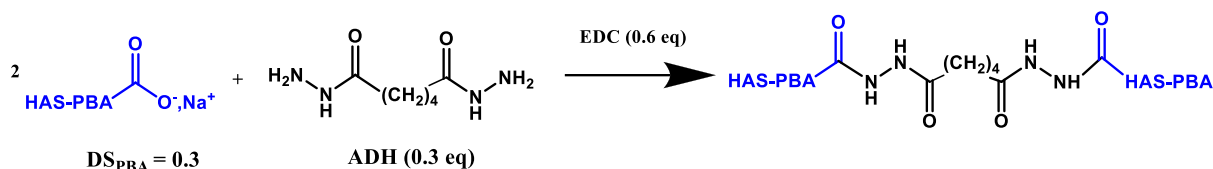


Figure 5. Coupling of HAS₄-PBA_{0.3} with ADH.

In all the following section, HAS₄-PBA_{0.3} synthesized from HAS **8** (Chapter 2, Table 3, Mw ≈ 100 kg/mol) was used. The ADH cross-linking of HAS₄-PBA_{0.3} without EDOT was first investigated to evaluate the potential final storage modulus range and the kinetics of the reaction.

III.1.a. Influence of solvent and pH during HAS₄-PBA_{0.3} cross-linking.

The modification of hyaluronic acid mediated by carbodiimides has been widely investigated in the literature^[4,5]. The extent of the reaction has been determined by the amount of protons available, and thus by the pH of the solution. Buffer salts have often been used as proton sources to control the kinetics of the reaction. The amount of available protons depends on the pH of the mixture and the pKa of the buffer component. Buffer salts enable more controlled gelation and more homogeneous hydrogels as they release protons progressively.

The effect of three buffer salts on the HAS₄-PBA_{0.3} kinetics of cross linking by ADH in the presence of EDC were investigated: 2-(N-morpholino)ethanesulfonic acid (MES), 2-[Bis-(2-hydroxy-ethyl)-amino]-2-hydroxymethyl-propane-1,3-diol (BisTris) and tris(hydroxymethyl)aminomethane (Tris). They display respectively pKa of 6.15, 6.46 and 8.1 at 25°C (Figure 6). As the cross-linking of HAS₄-PBA_{0.3} by ADH was expected to happen simultaneously with EDOT polymerization, the pH was expected to quickly decrease. Therefore, cross-linking reactions without EDOT were realized at three different pH to cover a wide range of experimental conditions: 4.75, 3.45 and 2.1. 4.75 was chosen as it is known to be the optimal pH for coupling using EDC^[4], while 3.45 was selected as it was the pH of the initial reaction in the work of Yang *et al.* that we were trying to adapt^[2]. pH 2.1 allowed us to

study low pH conditions, as expected at the end of EDOT polymerization. Noticeably, all those pH were out of the buffer zone of the three investigated buffer salts. These molecules were thus expected to behave as controlled proton source, but not as buffers.

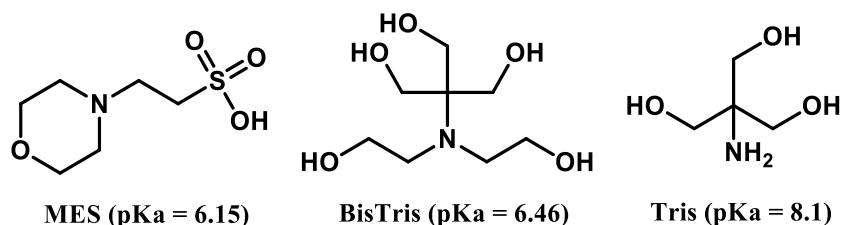


Figure 6. Three investigated buffer salts to monitor HAS₄-PBA_{0.3} cross-linking by ADH.

Briefly, HAS₄-PBA_{0.3} was dissolved at 40.0 g/L in 0.1 M of MES (or BisTris or Tris) and 0.15 M of NaCl, at pH 2.10, (or 3.45 or 4.75), with ADH at 2.2 g/L (molar ratio of $n_{\text{carboxylate}}/n_{\text{hydrazide}} = 0.75$), and EDC at 9.6 g/L (molar ratio of $n_{\text{carboxylate}}/n_{\text{EDC}} = 1$). 0.15 M of NaCl was added to all solutions to increase the ionic strength in order to screen electrostatic repulsions between HAS₄-PBA_{0.3} chains as ADH is a short cross-linker.

The kinetics of the cross-linking reactions were followed using a cone-plate rheometer. The elastic and loss modulus, G' and G'' , were monitored over time (Figure 7). Initially, G'' was larger than G' , which reflected the viscous behavior of the sample. Then, the storage and loss moduli increased due to the formation of intermolecular cross-links. The gelation time was recorded at the crossover of G' and G'' ^[6], and was lower than 3 minutes in all cases. Noticeably, no mixture in Tris 0.1 M formed a gel. Corresponding data are not shown. Tris was not used any longer.

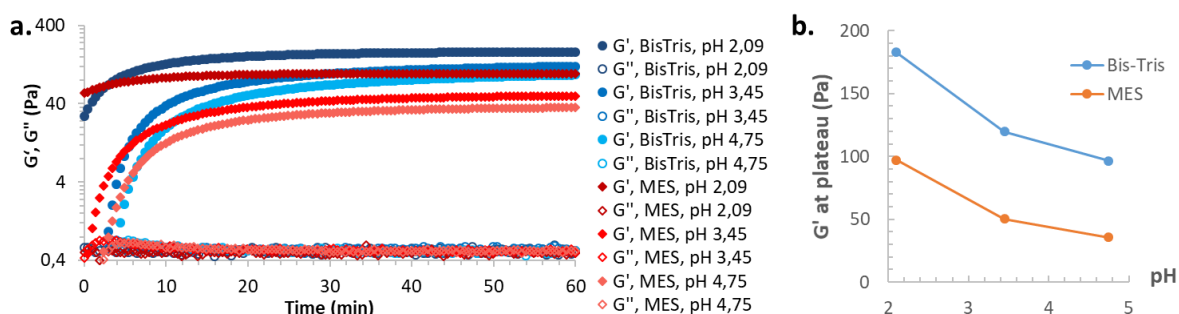


Figure 7. Cross-linking of HAS₄-PBA_{0.3} by ADH in various solvents and pH. a. Kinetics of the reaction. b. Value of the storage modulus G' at the plateau.

As the pH decreased, the cross-linking reactions were quicker and yielded to higher final storage moduli. Interestingly, the hydrogels which were cross-linked in MES were softer than hydrogels cross-linked in BisTris, though the pKa of MES is lower than the one of BisTris (6.15 vs 6.46). MES was expected to release more protons than BisTris at low pH, and thus was expected to yield tougher hydrogels. This phenomenon could be attributed to the numerous hydroxyl groups of BisTris which could stabilize the hydrogel with H bonds, resulting in tougher gels .

Nevertheless, the reached storage moduli were all below 200 Pa, which was too low for the applications targeted in this thesis.

III.1.b. Influence of NaCl concentration on cross-linking reaction

In order to increase the hydrogels storage modulus G' , NaCl concentration of the cross-linking medium was increased.

In the previous experiments, NaCl concentration was set at 0.15 M to ensure the charge screening of HAS₄-PBA_{0.3} to decrease chain repulsions. Indeed, Lalevée *et al.*^[7] demonstrated that the charge screening of hyaluronic acid was achieved for NaCl concentrations above 0.1 M. However, taking into the account the high negative charge density of HAS₄-PBA_{0.3} due to the four sulfates per HA repeating unit (linear charge density parameter $\lambda \sim 3.5$, where $\lambda = l_b/b$, l_b is the Bjerrum length ($l_B = 7.13 \text{ \AA}$ at 25°C in water) and b is the axial distance between successive charges fixed to the polyelectrolyte chain), it can be assumed that a fraction of the Na⁺ counterions condensed onto the HAS₄-PBA_{0.3} backbone to neutralize negative charges, according to the Manning' counterion condensation theory^[8]. Based on this, the density of bound Na⁺ counterions close to the polymer backbone may have prevented the cross-linker to reach the carboxylates groups. In order to alleviate the steric hindrance around the carboxylates, we increased more the ionic strength by increasing the NaCl concentration from 0.15 M to 0.5 M in order to decrease the electrostatic potential around the highly charged HAS₄-PBA_{0.3} backbone and thereby, to reduce the cation charge density around the polyelectrolyte backbone.

HAS₄-PBA_{0.3} was dissolved at 40.0 g/L in 0.1 M of MES (or BisTris) and 0.5 M of NaCl, at pH = 2.10 (or 3.45 or 4.75), with ADH at 2.2 g/L in order to have a molar ratio of

$n_{\text{carboxylate}}/n_{\text{hydrazide}} = 0.75$, and EDC at 9.6 g/L in order to have a molar ratio of $n_{\text{carboxylate}}/n_{\text{EDC}} = 1$. The elastic and loss modulus, G' and G'' , were monitored over time as described before (section III.1.a.), and the value of the final G' values at the plateau were compared with those in 0.15 M NaCl (Figure 8).

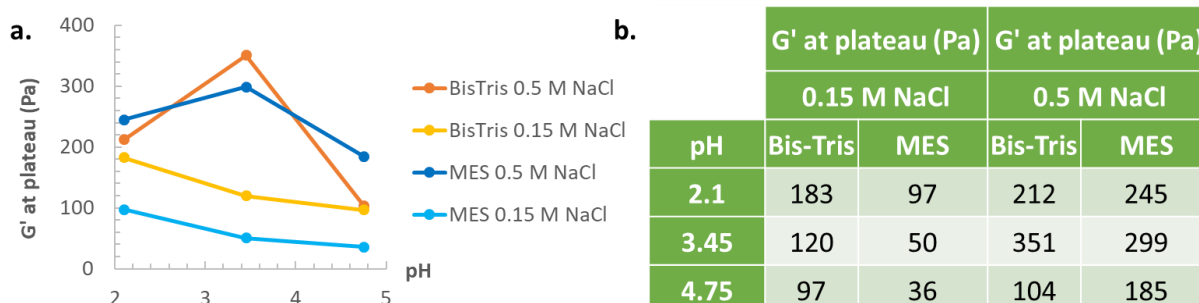


Figure 8. Comparison of HAS₄-PBA_{0.3} / ADH hydrogel storage moduli when cross-linked in MES or BisTris at 0.1 M, at different pH, with NaCl concentration of either 0.15 M or 0.5M.

As expected, all the storage moduli of the hydrogels cross-linked in 0.5 M NaCl were higher than those cross-linked in 0.15 M NaCl. Interestingly, at 0.15 M NaCl, the storage modulus G' increased as the pH decreased, whereas for 0.5 M, a maximum of G' is reached for pH around 3.45. This pH value corresponds to the pK_a of the hydrazide function.

All further experiments were carried out in 0.5 M NaCl to ensure high cross-linking degree.

III.1.c. pH variation during EDOT polymerization

In the previous section, we showed that the cross-linking of HAS₄-PBA_{0.3} by ADH was highly pH dependent. As the pH decreases during EDOT polymerization (Chapter 1, Figure 5), it was important to assess the kinetic of this pH decrease to understand better the potentials interdependency between PEDOT polymerization and HAS₄-PBA_{0.3} cross-linking.

HAS₄-PBA_{0.3} was dissolved at 40 g/L in 0.1 M BisTris at pH 4.75 containing 0.5 M NaCl, ADH at 2.2 g/L (molar ratio of $n_{\text{carboxylate}}/n_{\text{hydrazide}} = 0.75$), EDOT (2 equivalents of EDOT compared to HAS₄-PBA_{0.3}), and APS at 289.5 g/L (molar ratio of $n_{\text{APS}}/n_{\text{EDOT}} = 1.33$). Noticeably, no EDC was added to avoid gelation of the mixture. The mixture was mixed for 2 minutes at 25 000 rpm to form an EDOT emulsion. The pH was measured right after the mixing, and was equal to 1.51. The reaction was stirred for another 72 hours, and the pH, measured again at

1.45. An additional experiment was performed in the same conditions, without APS, to evaluate whether EDOT emulsion is acid, or whether it was the onset of the EDOT polymerization that triggered the decrease of pH. The pH remained stable around 4.75 for 72 hours.

This experiment showed that during EDOT polymerization, the pH quickly decreased below 2, even when starting from pH = 4.75. Therefore, for the subsequent reactions where both HAS₄-PBA_{0.3} cross-linking by ADH and EDOT polymerization occurred simultaneously, the reaction medium was determined as BisTris 0.1 M + NaCl 0.5 M with pH = 4.75, as cross-linking in BisTris demonstrated to result into hydrogel with higher G'.

With these conditions set, the simultaneous hydrogel cross-linking and EDOT polymerization was investigated.

III.2. Simultaneous hydrogel cross-linking and EDOT polymerization

III.2.a. Conductive hydrogel synthesis

HAS₄-PBA_{0.3}, ADH and EDOT were dissolved at various concentrations and ratios (Table 2) in BisTris 0.1 M + NaCl 0.5 M, pH 4.75. At the last moment, APS was added and the mixture was mixed 2 minutes at 25,000 rpm in order to obtain homogenous EDOT emulsion. Then EDC was added to the medium, which was mixed 10 additional seconds at 25 000 rpm, and immediately transferred into different molds for gelation (Figure 9). All synthesized hydrogels are summarized in Table 2.

Noticeably for simultaneous hydrogel cross-linking and EDOT polymerization, the molar ratio $n_{\text{EDC}}/n_{\text{carboxylate}}$ was set at 1.5, while it was set at 1 for hydrogel cross-linking without EDOT. This was done to take into account the fast degradation of EDC at low pH (75% in 25 minutes at pH 2.52), as exhibited by Nakajima *et al.*^[5], since, we observed a quick pH decrease under 1.5 in less than 2 minutes due to EDOT polymerization in section III.1.c.

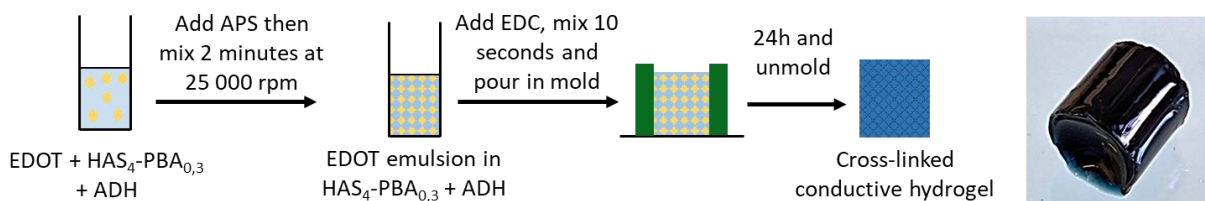


Figure 9. Synthesis of conductive PEDOT:HAS₄-PBA_{0.3} / ADH hydrogels.

Table 2. Synthesized on pot conductive PEDOT:HAS₄-PBA_{0.3} / ADH hydrogels.

Hydrogel #	Hydrogel cross-linking parameters			EDOT polymerization parameters	
	[HAS ₄ -PBA _{0.3}] (g/L)	ratio $n_{\text{hydrazide}}/n_{\text{carboxylate}}$	ratio $n_{\text{EDC}}/n_{\text{carboxylate}}$	Molar ratio $n_{\text{EDOT}}/n_{\text{HAS4-PBA0.3}}$	Molar ratio $n_{\text{APS}}/n_{\text{EDOT}}$
1	40	0.75	1.5	2	1.33
2	40	0.75	1	2	1.33
3	40	0.90	1.5	2	1.33
4	40	0.90	1.5	3	1.33
5	40	0.90	1.5	2	1
6	50	0.75	1.5	2	1.33
7	50	0.90	1.5	2	1.33
8	50	0.90	1.5	3	1.33

Unfortunately, this protocol demonstrated a lack of reproducibility. Some identical hydrogels could gellify in a few minutes as well as several hours, without any explanation for this difference. Besides, the unmolding protocol at the end of the gelation to recover cylindrical hydrogels proved to be delicate to implement, as hydrogels were sticky and often tore apart when unmolded due to adhesion with the mold. The final cylindrical hydrogels used for mechanical properties characterization often contained inside cracks.

Therefore, though 8 different hydrogels were synthesized to investigate the role of the various conductive hydrogels parameters (Table 2), no conclusion could be drawn from this set of experiments as data sets were incomplete or not rigorous. By lack of time, the experimental setup could not be optimized. However, individual characterization enabled to evaluate the final properties of the newly developed PEDOT:HAS₄-PBA_{0.3} / ADH hydrogels.

III.2.b. Mechanical properties

The evolution of the mechanical properties of PEDOT:HAS₄-PBA_{0.3} /ADH hydrogels during gelation could not be investigated using a cone-plate rheometer as for HAS₄-PBA_{0.3} /ADH hydrogels. Indeed, the reaction conditions were too aggressive for the metal of the rheometer plate and the rheometer geometry, which could have been damaged (pH below 1.5, NaCl concentration of 0.5 M favoring pitting corrosion, and oxidative conditions with the persulfates to polymerize EDOT).

To measure their mechanical properties, compression tests were performed. The hydrogel precursor mixtures were poured in a cylindrical mold, ($\varnothing_{\text{int}} = 5.8$ mm, $h = 5$ mm) and after cross-linking (≈ 20 hours), the cylindrical hydrogels were unmold and swollen in PBS to remove reaction by-products and to neutralize their pH. Uniaxial compression tests were performed using a texturometer. Successive compression cycles at 10%, 20%, 30%, 40% and 50% of deformation were performed. The normal stress σ_{nominal} was calculated as the normal force divided by the surface area of the material whereas the displacement data λ were expressed as an extension ratio, $\lambda = (h_0 - \Delta h)/h_0$, where Δh is the displacement data and h_0 the initial height of the hydrogel. The storage modulus G' of the materials could be calculated as the slopes of $\sigma_{\text{nominal}} = f(\lambda - \frac{1}{\lambda^2})$ in the linear response of the gel, as described in the Neo-Hookean model^[9–11] (Figure 10).

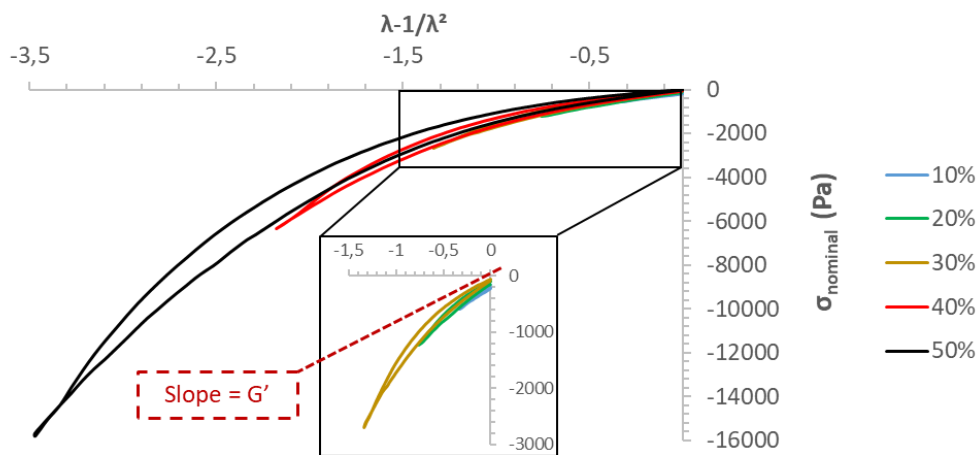


Figure 10. σ_{nominal} according to $\lambda - 1/\lambda^2$ for successive uniaxial compression tests of hydrogel 3.

Among all the synthesized hydrogels, only two cylindrical hydrogels **3** (Table 2) were successfully cross-linked from the same hydrogel precursor mixture and both unmolded without any rupture in the gel due to adherence to the mold inside. Therefore they could be analyzed as described above and compared. The data analysis enabled to obtain the storage modulus G' of both hydrogels **3** for each compression cycle (Table 3). For both hydrogels, G' was relatively constant from one cycle to another, indicating the reversibility of the compression. The two hydrogels **3** displayed an average G' variation of 13.5 %, indicating the reproducibility of the uniaxial compression protocol.

Table 3. Storage modulus G' of hydrogels **3** obtained via successive uniaxial compression tests.

	Hydrogel 3	Hydrogel 3bis
G' cycle 1 10% deformation	1.35×10^3	1.03×10^3
G' cycle 2 20% deformation	1.40×10^3	1.23×10^3
G' cycle 3 30% deformation	1.35×10^3	1.27×10^3
G' cycle 4 40% deformation	1.37×10^3	1.23×10^3
G' cycle 5 50% deformation	1.33×10^3	1.13×10^3
Average storage modulus G'	1.36×10^3	1.18×10^3

Interestingly, those storage modulus values were much higher than those obtained for hydrogels without EDOT (Figure 8b). To investigate rigorously the impact of PEDOT addition inside the hydrogel matrix, an additional hydrogel, similar to hydrogel **3**, except without EDOT or APS, was synthesized and analyzed using a cone-plate rheometer, as described in section III.1. This hydrogel displayed a final storage modulus around 250 Pa, 4.5 times lower than hydrogel **3** which include EDOT.

It appeared that the addition of EDOT in the hydrogel matrix resulted in a large increase of storage modulus G' .

III.2.c. PEDOT:HAS₄-PBA_{0.3} /ADH hydrogels swelling behavior

The swelling ratio of the hydrogels was measured. Briefly, after cross-linking, hydrogels were immersed in PBS to swell until their mass stabilized (2-3 days). The mass swollen in PBS ($m_{\text{swollen PBS}}$) was measured. Then hydrogels were immersed in successive water baths to

remove all PBS salts, freeze-dried, and their dry mass (m_{dry}) measured. The swelling ratio Q was determined as:

$$Q = \frac{m_{swollen\ PBS}}{m_{dry}}$$

Results are summarized in Figure 11. As mentioned before, the cross-linking protocol presented a lack of reproducibility, highlighted by swelling measurements: the relative variation of swelling ratio for a same hydrogel could be higher than 100 %. However, some trends could be observed. Hydrogels **2**, which were prepared with 1 equivalent of EDC (versus 1.5. for all the other hydrogels), displayed the highest swelling ratio of 47 ± 21 . This suggests a lower crosslinking density for them.

Besides hydrogels **8** displayed the second highest swelling ratio of 43 ± 22 , indicating that too much EDOT could result into lower final cross-linking degree.

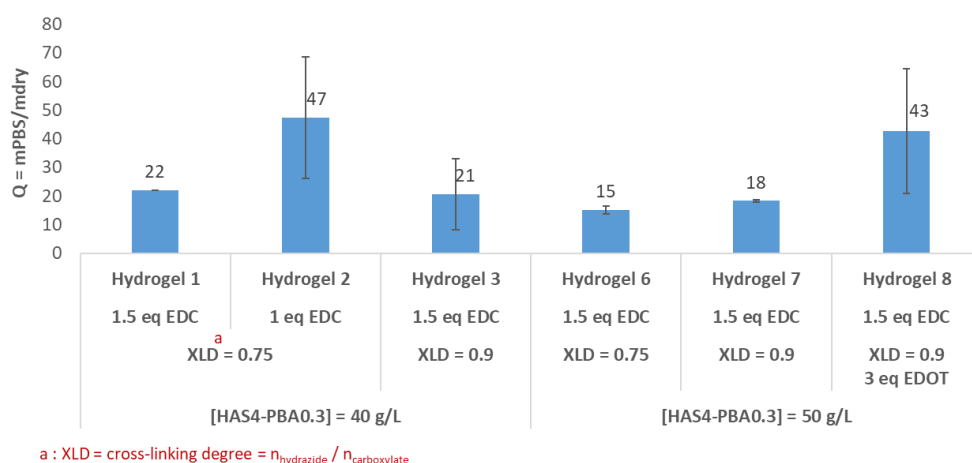


Figure 11. Swelling ratio of hydrogels in PBS (error bars $n=3$).

III.2.d. PEDOT:HAS₄-PBA_{0.3} /ADH hydrogel conductivity

To investigate the conductivity of the PEDOT:HAS₄-PBA_{0.3} /ADH hydrogels, 75 μ L of the hydrogel precursor mixture were poured after mixing in a cylindrical tube of 0.15 mm internal diameter (Figure 12a). After gelation, the conductivity was measured using the transmission line measurements (TLM) technique^[12]. Briefly, this technique enables to determine the conductivity of a film or a bulk material while minimizing the effects of contact resistance between the material and the probe.

The total resistance of a PEDOT:HAS₄-PBA_{0.3} /ADH hydrogel cross-linked in a tube was measured with an ohm-meter, using electrode at each extremity of the tube to make contact with the hydrogel (Figure 12b). The total measured resistance is thus $R = 2R_{\text{contact}} + R_{\text{hydrogel}}$ where $R_{\text{hydrogel}} = L/(\sigma S)$ with L is the hydrogel length between the two probes, σ the hydrogel conductivity and S the section of the tube. By measuring the resistance of hydrogels with different lengths (progressively cutting the tube containing the material) and plotting the total resistance according to the material length, the slope of the curve is proportional to $1/(\sigma S)$. Knowing the tube section, it is possible to determine the material conductivity (Figure 12c).

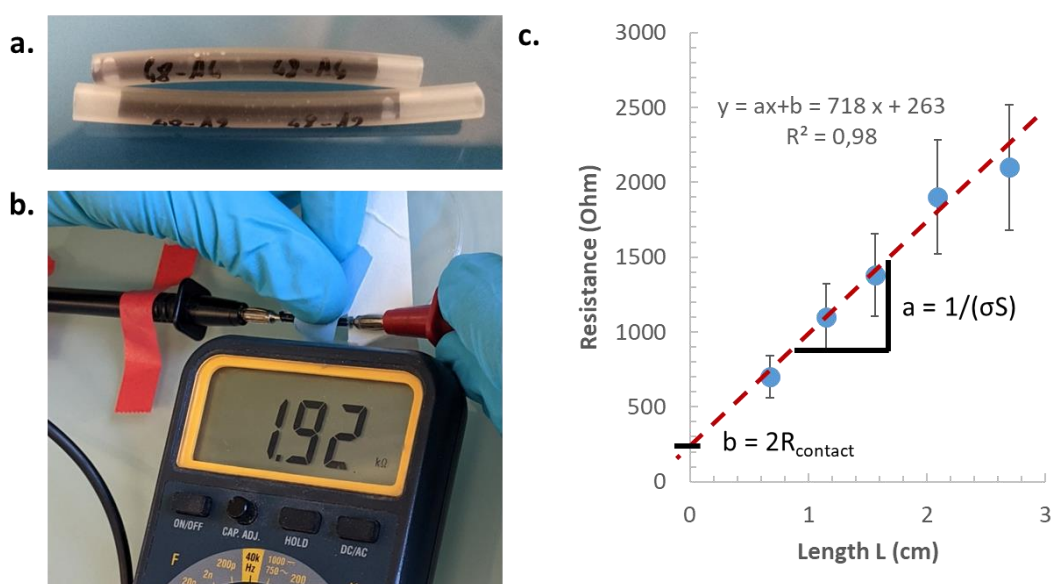


Figure 12. TLM measurements. a. PEDOT:HAS₄-PBA_{0.3} /ADH hydrogel in a tube. b. Ohm-meter electrode in the tube. c. Total resistance according to material length for hydrogel 1.

This method enabled to determine the hydrogel conductivity, but the electrical contact between the ohm-meter planar probes and the hydrogel in the tube was not perfectly reproducible, and led to measurements with high error bars. The uncertainty for all measurements did not enable to study the influence of hydrogel composition and synthesis conditions on final conductivity. However, they all displayed the same conductivity order of magnitude of 10^{-2} S/cm. This conductivity was two orders of magnitude lower than the conductivity of pure PEDOT:HAS₄-PBA_{0.3} inks.

III.2.e. Conclusion

The simultaneous cross-linking of HAS₄-PBA_{0.3} with ADH and EDOT polymerization resulted in conductive hydrogels displaying a storage modulus around 1.3 kPa, 4.5 times higher than HAS₄-PBA_{0.3} / ADH hydrogels without EDOT, and a conductivity around 10⁻² S/cm. However the protocol was not perfectly reproducible and still required optimizations to obtain samples which could be analyzed quantitatively and comparatively to thoroughly optimize the formulation.

Nevertheless, their electro-chemical properties were investigated to assess their potential utilization in bioelectronic medical devices.

IV. Electrochemical properties PEDOT:HAS₄-PBA_{0.3} / ADH hydrogels

IV.1. Properties of interest and experimental setup

The electrochemical properties of the conductive PEDOT:HAS₄-PBA_{0.3} / ADH hydrogels were investigated to assess their potential applications in bioelectronic devices. As described in chapter 1, the three properties of interest are the charge storage capacity (CSC), the charge injection capacity (CIC), and the impedance at 1 kHz. As the developed conductive hydrogels were intended for tissue stimulation and/or monitoring, the targeted electrochemical values are summarized in Table 4. Briefly, charge storage capacity should be at least higher than 1 mC/cm², to be competitive with traditional stimulation recording electrode^[13]; the CIC higher than 100 μ C/cm² to excess the CIC of Pt electrode in-vivo^[14]; and the impedance at 1 kHz should be as low as possible to enhance recording/stimulation quality^[15], with a suitable range between 0.1 and 600 k Ω for recording neural signals^[16].

Table 4. Targeted conductive hydrogel electrochemical properties for tissue stimulation/monitoring.

Property	Targeted value/range	Reference value for a Pt electrode
Charge storage capacity (CSC) (mC/cm ²)	> 1	0.55 ^[13]
Charge injection capacity (CIC) (μ C/cm ²)	> 100	35-54 ^[17]
Impedance Z at 1 kHz (Ω)	as low as possible, < 6x10 ⁵ Ω	1-1000 depending on electrode size ^[15]

Electro-characterizations were performed using a SP-200 potentiostat with a three electrode cell. The reference electrode was Ag/AgCl, and the counter electrode was a platinum foil. To use the hydrogel as a working electrode, 6 μ L of the hydrogel precursor mixture were poured in a small home-made cavity electrode, on a platinum rod of 2 mm diameter, pre-functionalized with electro-polymerised PEDOT:HAS₄-PBA_{0.3} in order to graft the hydrogel covalently to the surface (Figure 13, detailed protocol in section VII.2.e).

Thus, small 6 μ L cylindrical hydrogels grafted on a platinum surface were obtained, and constrained in a cavity, ensuring that the electrochemical characterizations were performed on the bulk hydrogel, and not the water layer at the platinum/hydrogel interface.

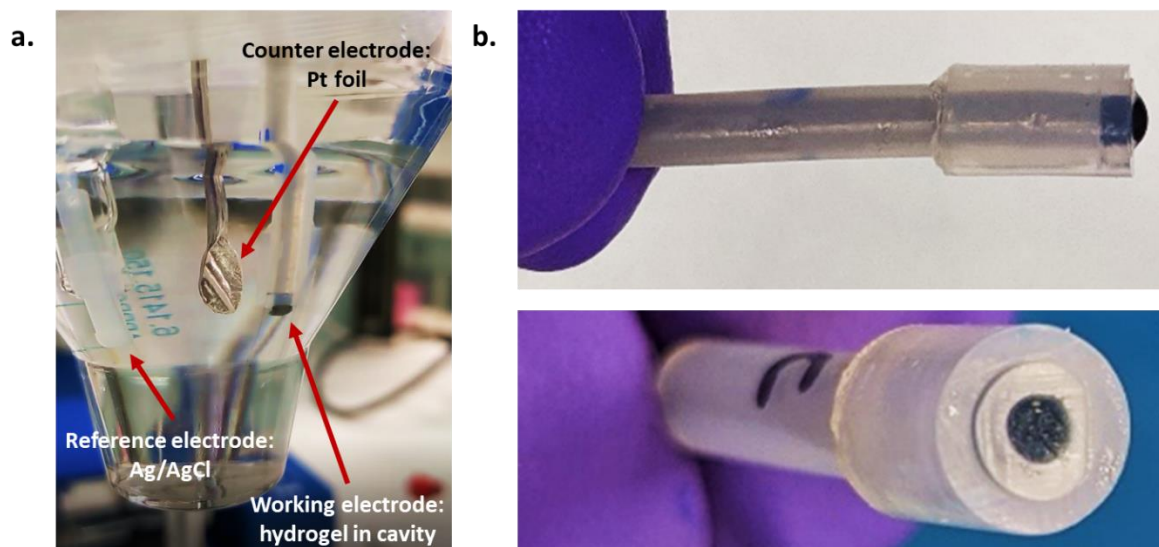


Figure 13. Experimental setup for electrochemical characterizations. a. Three electrode cell. b. Home-made cavity electrode to characterize conductive hydrogels.

The electrochemical properties of the synthesized hydrogels could not be all compared to each other because of the lack of perfectly reproducible results. In the following sections, the characterization of hydrogel **5** (Table 2) will be detailed, as its synthesis proved to be the more repeatable of all.

For all samples, cavity electrode were prepared as detailed in section VI.2.e. The hydrogel volume was identical for all samples and equal to 6 μL .

IV.2. Charge storage capacity (CSC)

The CSC is an index of the electrode charge transfer capabilities of a material^[18] and is useful to estimate the amount of charge an electrode can “store” before being injected in the electrolyte, where redox reactions occur. However, the CSC does not represent the total charge practically available for injection by a short pulse, as in practice, only the most superficial layers of the electrode will actively be involved. Therefore, CSC overestimates the charge available^[18].

In the literature, the CSC is given in mC/cm^2 , as the electro- characterized materials are often considered as bidimensionals. Their active surface is considered as equal to the contact

surface area between the material and the conductive materials. Noticeably, in our system, the electroactive part of the material could not be considered as bidimensional. Therefore the CSC was given in mC/cm³. To compare to the literature, they were also calculated in mC/cm². Depending on whether the surface CSC (CSC_{2D} in mC/cm²) was considered, or the volume CSC (CSC_{3D} in mC/cm³), the following equation were used:

$CSC_{2D} = -\frac{1}{v \cdot S_{electrode}} \int_{i < 0} IdV$ where $S_{electrode}$ was the contact area between the gel and the Pt surface (3.14 mm² in our case).

Or $CSC_{3D} = -\frac{1}{v \cdot V_{Hydrogel}} \int_{i < 0} IdV$ where $V_{Hydrogel}$ was the hydrogel volume (6 μL in our case). In both cases, v were the voltage sweeping rate (50 mV/s).

Briefly, 6 μL of the gel precursor mixture were poured in the pre-functionalized cavity electrode and sealed overnight at room temperature for the gel to cross-link without water evaporation. Then the hydrogels in cavity were rinsed in PBS at least 24h to equilibrate salt concentration and neutralize the matrix pH. Cyclic voltammetry was performed at 50 mV/s from -0.5 V to 0.6 V in degassed PBS. 10 cycles were performed. The signal stabilized around the 8th cycle. To assess the real contribution of the conductive hydrogel **5** to the measured current, the CV of the initial bare platinum electrode, and the CV of the pre-functionalized electrode with electro-polymerized PEDOT:HAS₄-PBA_{0.3} (EP ink) was also recorded. The signal of the conductive hydrogel **5** was deduced by subtracting the signal of the EP ink + Platinum to the hydrogel signal. The 9th cycle is reported in Figure 14.

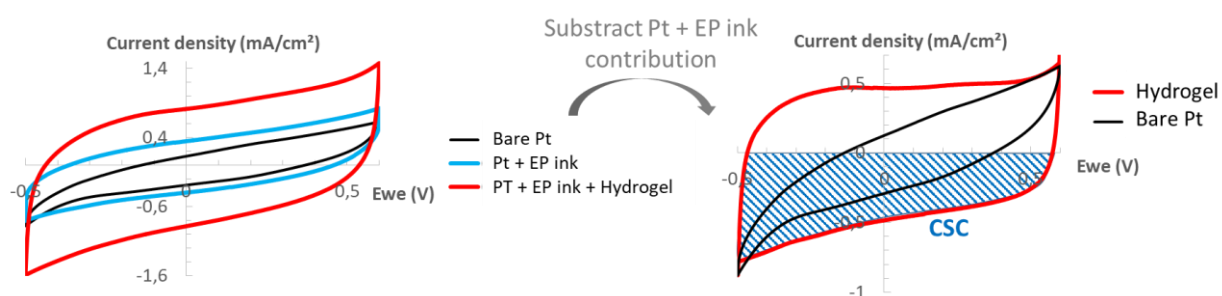


Figure 14. Cyclic voltammograms of the bare platinum surface, of the bare platinum surface functionalized with electro-polymerized PEDOT:HAS₄-PBA_{0.3} (EP ink) and of the final cavity electrode containing the conductive hydrogel on top of the Pt surface and the EP ink.

The CSC_{2D} of hydrogel **5** was estimated to be 9.6 ± 2.6 mC/cm², corresponding to a volumetric CSC_{3D} of 50.2 ± 14.6 mC/cm³ (n=3). The cyclic voltammogram of the conductive

hydrogel **5** displayed after correction almost constant anodic and cathodic current plateau, characteristic of a capacitive behavior.

This CSC value is above the CSC_{2D} reported for other PEDOT-based conductive interpenetrating hydrogels, such as the PEDOT:PSS / alginate hydrogels doped by multiwall carbon nanotubes developed by Wang *et al.*^[19] (CSC_{2D} = 0.5-1.2 mC/cm², Chapter 1 Table 2). Still, they were below the CSC_{2D} of pure conductive PEDOT:PSS hydrogels reported by Lu *et al.*^[20] (CSC_{2D} = 60 mC/cm², physically cross-linked by chain entanglement) and Novikov *et al.*^[21] (CSC_{2D} = 20 mC/cm², physically cross-linked after acidic treatment, Chapter 1 Table 3). Compared to traditional hard electrode, those CSC values are competitive (CSC_{sputtered iridium oxide film} = 23 mC/cm²^[13], CSC_{Platinum} = 0.550 mC/cm²^[14], CSC_{PEDOT-PSS coatings on ITO} = 3.6 mC/cm²^[22]).

IV.3. Charge injection capacity

The charge injection capacity (CIC) of an electrode is defined as the amount of charge that the electrode can inject per unit area without causing irreversible electrochemical reactions or tissue damage^[23]. This value is important in tissue stimulation^[24] as it must never be exceeded. The main risk is to exceed the water hydrolysis potential which could trigger the local formation of gas bubbles, which can be lethal in the case of a bioelectronic device implanted on the brain for instance^[13].

As for CSC, the CIC is given in mC/cm² (noted CIC_{2D}), but with our bulk conductive hydrogels, it was more significant to define volumetric CIC (CIC_{3D} in mC/cm³). While the CSC of a material is determined using cyclic voltammetry, the CIC is determined by current pulse experiment: to assess the CIC of hydrogel **5**, series of successive biphasic current pulse experiments were performed, progressively increasing their amplitude to increase the injected charge. The pulse sequence was composed of a cathodic current pulse of 125 ms followed by a resting time of 30 ms, then by a charge-compensating anodic pulse of 250 ms, followed by a resting time of 1 second. This sequence was repeated 30 times. Working electrode potential was monitored over time. The amplitude of the current pulses $A_{current\ pulse}$ was progressively increased, until an inflexion in the working electrode potential

during the cathodic pulse was observed, indicating the onset of redox reactions (including water splitting reaction, Figure 15). The time between the beginning of the cathodic pulse, and the apparition of the inflexion length was defined as t_{max} . The surfacic and volumic charge injection capacity CIC_{2D} and CIC_{3D} were defined as

$$CIC_{2D} = \frac{t_{max} \cdot A_{current\ pulse}}{S_{hydrogel}} \text{ and } CIC_{3D} = \frac{t_{max} \cdot A_{current\ pulse}}{V_{hydrogel}}$$

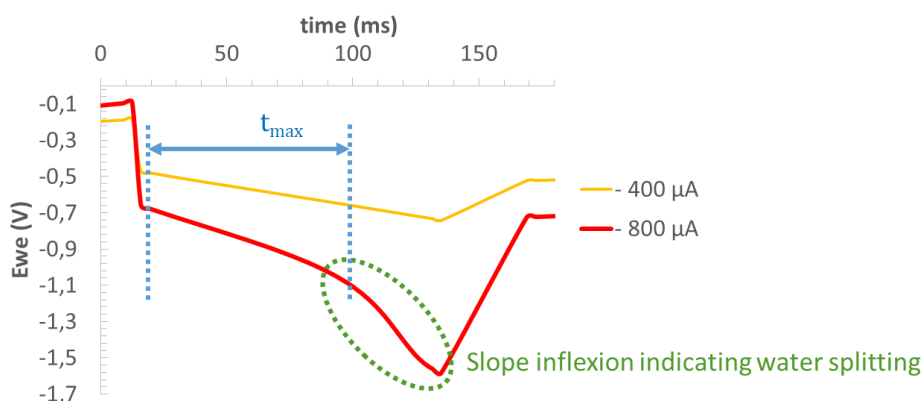


Figure 15. Pulse experiments performed on hydrogels **5** to investigate its CIC. Cathodic pulses on hydrogel **5**, with apparition of a potential inflexion point for a current amplitude of -800 μ A.

Hydrogel **5** displayed CIC_{2D} values of $2.5 \pm 0.2 \text{ mC/cm}^2$ ($CIC_{3D} \approx 13.1 \pm 1.0 \text{ mC/cm}^3$, Table 5). Those CIC_{2D} values were competitive with the CIC_{2D} of a PEDOT:PSS film electropolymerized on an ITO glass slide (3.6 mC/cm^2 [22]), and two orders of magnitude lower than the CIC_{2D} measured for PEDOT:PSS hydrogel, doped by ethylene glycol and cross-linked by GOPS, reported by Fanelli *et al.* [25] ($263.6 \pm 247.5 \text{ mC/cm}^2$). Nevertheless, the hydrogels developed in this project displayed CIC_{2D} higher than those of traditional PtIr or Pt electrode used for tissue stimulation (around $100 \mu\text{C/cm}^2$ [14] or $34\text{-}54 \mu\text{C/cm}^2$ [17] respectively). They could still be useful in tissue stimulation.

Table 5. CIC_{2D} and CIC_{3D} of hydrogel 5 ($n=3$).

Hydrogel #	CIC_{2D} (mC/cm ²)	CIC_{3D} (μC/cm ³)
5	2.5 ± 0.2	13.1 ± 1.0

IV.4. Electrical impedance spectroscopy

Finally, electrical impedance spectroscopy (EIS) experiments were performed to assess the electrical answer of hydrogel **5** to a potential harmonic perturbation, typically a sinusoidal signal, over a wide range of frequencies (mHz-GHz). Comparing the amplitude and phase of the input signal and the amplitude and phase of the output signal, the electrochemical impedance Z of the system can be deduced. For tissue monitoring, low electrode impedance is crucial to acquire *in-vivo* high-quality signals^[26]. Also, it could prevent faradic reactions and increase the signal-to-noise ratio^[27], which should be around five for qualitative measurements^[13]. For tissue stimulation, low impedance are also required to ensure safe reversible charge injection^[28].

In neural recording, the local fields potentials vary at frequencies ranging from 1 to 300 Hz, while actions potentials are fired at 300-3000 Hz^[29]. Therefore the impedance at 1 kHz is generally reported to estimate the recording quality of the electrode as they are mainly meant for the monitoring of precise individual action potentials^[13]. But depending on what is studied, impedance at 1 or 100 Hz could also be relevant.

Before EIS experiments, the open circuit potentials of hydrogel **5** was monitored to ensure the hydrogel had reached its electric potential equilibrium. It was reached in 20 to 40 minutes. For EIS experiments, the applied AC voltage was 0.01 V and measurements were taken at a DC potential corresponding to the open circuit potential against the reference electrode. Bode diagrams was plotted (Figure 16).

Table 6. Impedance properties of hydrogels 5 (n=3).

Sample	$f_{\text{cut-off}}$ (Hz)	$ Z $ at 1 kHz	Phase at 1 kHz
Hydrogel 5	2 ± 1	412 ± 35	-2 ± 1
Bare Pt	NA	222 ± 10	-40 ± 1

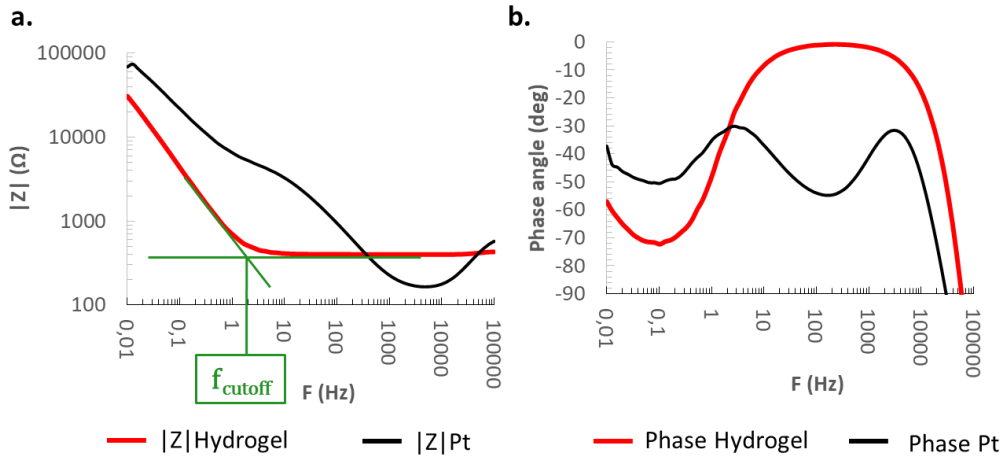


Figure 16. Bode plot of hydrogel 5. a. Impedance of hydrogel 5. b. Phase of hydrogel 5.

Hydrogel 5 displayed an impedance at 1 kHz of $412 \pm 35 \Omega$ with a cut-off frequency $f_{\text{cut-off}}$ of 2 ± 1 Hz (Figure 16a), and a phase from 1 Hz to 1000 Hz close to 0 ($-2 \pm 1^\circ$, $n=3$), which was in agreement with the mean impedance at 1 kHz for conductive PEDOT-based interpenetrating hydrogels reported in the literature (10^3 - $10^5 \Omega$, Chapter 1, Table 2), but above the reported impedance at 1 kHz for pure PEDOT-base conductive hydrogels (80 - 300Ω , Chapter 1, Table 3). In all cases, these impedance could be considered as “low”, as they were in the lowest part of the acceptable impedance range for tissue stimulation/monitoring (section IV.1). These hydrogels were thus promising candidates for tissue stimulation and/or monitoring.

The Nyquist plot of the conductive hydrogel 5 was also recorded (data not shown). Basic fitting was attempted, using the equivalent circuit described in chapter 1, Figure 19b: briefly, the electrolyte/hydrogel electrical interface was considered as a leakage resistance in parallel with a capacitance accounting for the electrical double layer. This equivalent circuit did not enable to fit the data properly. No further fitting of the Nyquist plot were attempted,

as the hydrogel physical structure was not investigated by lack of time. More complex equivalent circuits, with Warburg elements to take into account diffusion process for instance, would not have been relevant as not based on physical analysis.

IV.5. Application: stimulation of mice hippocampus

The previous sections exhibited that hydrogel **5** displayed reasonably low impedance and charge storage capacity suitable for tissue stimulation and monitoring^[13,28]. Therefore, *ex-vivo* mice hippocampus stimulation experiments were realized in cooperation with Fabien Lanté of the Neuroscience Institute of Grenoble (GIN). In these experiments, our hydrogels were interposed between a stimulation electrode and a freshly vivisect mice brain slice with still active neurons in the hippocampal CA1 region, to inject a current pulse to polarize neuron membranes, hoping to trigger action potentials that could be monitored.

Hydrogel **5** was used for these experiments. The hydrogel precursor mixture was prepared as described in section II.2.a., and poured into small PTFE tube that would serve as hydrogel sheath for the experiments (Figure 17a). After PEDOT polymerization and matrix cross-linking, the hydrogel was immersed several days in artificial cerebrospinal fluid (ACSF) buffer. A commercial concentric bipolar electrode was plunged in it (Figure 17b), and hydrogel **5** was put in contact with the hippocampal CA1 region in ACSF buffer, with a counter electrode right aside, to elicit cells, and a reference electrode further away in the buffer (Figure 17c). Biphasic current pulses were generated according to Yuan *et al.*^[30] protocol (detailed protocol in section VII.2.).

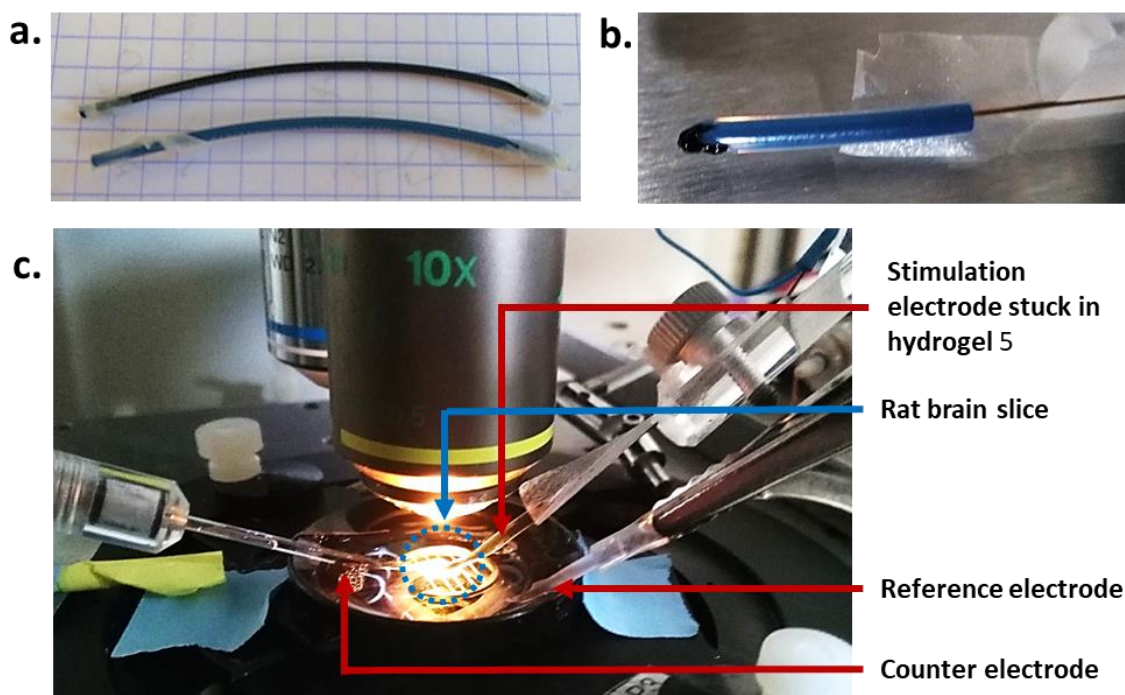


Figure 17. Rat brain slice experimental setup. a. Hydrogel 5 cross-linked in a tube. b. Stimulation electrode plunged into hydrogel 5. c. Experimental bench with a three electrode cell.

When the commercial stimulation electrode was in contact with the neural cell, the current pulse polarized neuron membranes and action potentials were fired (Chapter 1 section III.1.b.), releasing intracellular electrolytes in the medium, changing the medium potential. The difference of potential between the counter electrode and the reference electrode was recorded (Figure 18a). Typically, a first thin and intense signal was recorded, corresponding to the stimulation pulse, followed by the action potential signal, typically of 100 mV intensity for 10 ms. (Figure 18b).

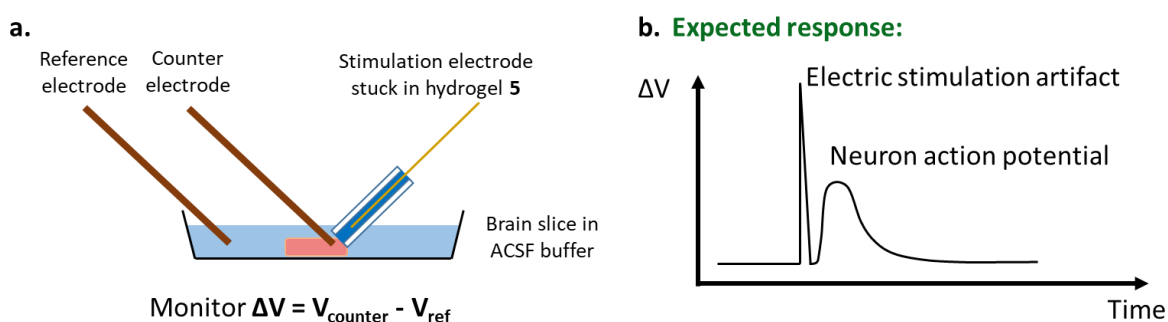


Figure 18. a. Scheme of the experimental setup. b. Expected potential variation according to time.

For our experiment where hydrogel **5** was interposed between the commercial stimulation electrode and the brain slice, the stimulation artifact was observed, but no action potential was observed afterward, not matter the intensity of the stimulation current pulse. This indicated that the stimulation current pulse was actually transmitted to the ACSF buffer, but that it was not enough to elicit neuron action potentials.

V. Discussion

V.1. Synthesis of HAS₄-ArEne_{0.5}

HAS₄-PBA_{0.3}-PEG_{0.22} developed in chapter 2 to obtain photo-cross-linkable inks proved to be not relevant to prepare hydrogels with a “high” storage modulus G' around 1 kPa. The alkene substitution degree might be too low. Therefore, a new HAS₄ derivative was synthesized replacing the PBA moiety by 4-[(pent-4-en-1-yloxy)methyl]aniline (ArEne), including both an aromatic group and an alkene function at the end of an hydrophilic chain.

ArEne was grafted on HAS₄ via an amide coupling, using DMTMM as a coupling agent, as for 3APBA. This molecule displayed high grafting yield (100 %), which can be attributed to the high nucleophilicity of the amine in para position of an oxygen on the aromatic ring^[31].

To assess the capacity of HAS₄-ArEne_{0.5} to dope PEDOT efficiently, a PEDOT:HAS₄-PBA_{0.3} ink was synthesized as described in chapter 2. Though the ink formed a physical gel during polymerization. This hydrogel was very brittle, and a conductivity of 0.4 S/cm could be measured after ink purification and film formation. This synthesis confirmed once more the synergy between the sulfate and the aromatic groups to efficiently dope PEDOT, but also the fact that the aromatic group had to be charged (like PBA), to avoid a physical cross-linking of the ink between PEDOT clusters and HAS₄-(Aromatic groups) chains.

V.2. Two-steps pure conductive hydrogels

PEDOT-based conductive hydrogels were synthesized in two steps, first photocross-linking HAS₄-ArEne_{0.5} by PEG-(SH)₂ ($M_n = 3.5$ kg/mol), then loading EDOT inside the matrix to polymerize it with an oxidant. If EDOT loading in the hydrogel matrix was satisfactory, its oxidative polymerization proved to be more complicated, as no general rules were to be found regarding the concentration of APS and FeSO₄ in the oxidative bath. Either the PEDOT was over-oxidized and the hydrogel matrix slightly degraded by the excess of APS, or the EDOT polymerization was too slow, resulting in its diffusion out of the hydrogel matrix. An optimal could have been found, but it would have depended on the bath size and on the hydrogel

geometry. It would not have been a general principle, and therefore, another synthesis strategy was investigated to control thoroughly all PEDOT polymerization parameters.

Two-step syntheses of PEDOT-based conductive hydrogels have been implemented in the literature. In particular, Ding *et al.*^[32] designed a 3D-printable photo-curable resin including dissolved EDOT, that polymerized when the cross-linked 3D-printed hydrogel was immersed in an oxidative bath of APS containing also PEDOT dopant (FeCl₃). Their final hydrogels displayed conductivity between 0.5 and 1.2 S.cm depending on the EDOT:APS:FeCl₃ ratio. No further information was given on whether this was a mass or molar ratio. Their final material displayed a tensile strength of 8 MPa. Noticeably in this work, the resin composition enabled a complete solubilization of EDOT after 1 hour of stirring under sonication. Interestingly, Wang *et al.*^[33] implemented a different protocol than ours. After cross-linking a chitosan/gelatin hydrogel using EDC/NHS, they loaded it with APS before immersing the hydrogel loaded with oxidant into EDOT dissolved at 0.4 M in hexane. This resulted into an interfacial polymerization of EDOT at the surface of the hydrogel. Their final hydrogels displayed conductivities between 0.034 and 0.17 S/cm, were biocompatible, and biodegradable by lysozymes (50 ± 20 % mass loss in 8 weeks of incubation depending on hydrogel composition). However, this literature report also indicates some limitations associated to the heterogeneous distribution of PEDOT in the biopolymer matrix: PEDOT nanoparticles only polymerized at the surface of the matrix.

V.3. One-step pure conductive hydrogel

Finally, pure conductive hydrogels were synthesized, using HAS₄-PBA_{0.3} as hydrogel matrix. This hydrogel was synthesized in one step by simultaneously cross-linking HAS₄-PBA_{0.3} by ADH, and polymerizing EDOT with an oxidant. This system was complex to handle as the two reactive systems were interconnected: the cross-linking of HAS₄-PBA_{0.3} by a dihydrazide in the presence of a carbodiimide was highly pH-dependent, while EDOT polymerization released protons, lowering quickly the pH of the medium. But the coupling agent (EDC) was quickly hydrolyzed at low pH. Besides, the medium required an emulsion step to disperse homogeneously the EDOT droplets. Finally, it appeared that the coupling reaction between HAS₄-PBA_{0.3} and ADH required a high NaCl concentration (0.5 M at least). This was attributed

to steric hindrance caused by the condensation of a large part of Na⁺ counterions (fractions of condensed counterions: $1-1/\lambda \sim 0.71$) according to the Manning's counterion condensation theory^[8,34] around the highly charged HAS₄-PBA_{0.3} backbone.

Given all those parameters and constraints, the implemented experimental setup was not reproducible, and could not be optimized by lack of time. Therefore, a complete investigation could not have been implemented to optimize the one-pot hydrogel formulation. The main source of variability was thought to be the emulsion step. On-going investigations will soon enable to conclude.

V.3.a. Mechanical and electrochemical properties

Nevertheless, the mechanical and electrochemical properties were investigated (Table 7): one-pot hydrogels displayed a storage modulus G' around 1-1.5 kPa, a conductivity around 10^{-2} S/cm, a charge storage capacity around 10 mC/cm², a charge injection capacity around 2.5 mC/cm², and an impedance at 1 kHz around 400 Ω .

Table 7. Mechanical and electrochemical properties of the one-pot hydrogels.

Property	Targeted value/range	Reference value for a Pt electrode	Values in this work (n=3)
G' (kPa)	≈ 1	$> 10^3$	1-1.5
Conductivity (S/cm)	$> 10^{-3}$	$> 10^5$	10^{-2}
Charge storage capacity (CSC) (mC/cm ²)	> 1	0.55 ^[13]	9.6 ± 2.6
Charge injection capacity (CIC) (mC/cm ²)	> 0.1	0.100 ^[14]	2.5 ± 0.2
Impedance $ Z $ at 1 kHz (Ω)	$10^2 - 6 \times 10^5$	1-1000 depending on electrode size ^[15]	412 ± 35

It appeared that in spite of the lack of reproducibility, the electrochemical properties were still promising for the utilization of these one-pot hydrogels as contact electrode for tissue stimulation, and/or monitoring^[13,15,28]. Indeed, for tissue monitoring, Tringides *et al.*^[35] recently reported a viscoelastic electrode array with conductive hydrogel tracks and contact

electrode, with conductivity of 0.1-0.35 S/cm and CSC around 10 mC/cm², useful to record brain action potentials, or electric signals in various mice organs. The properties of the hydrogel developed in this work are consistent with theirs.

However, *ex-vivo* stimulation experiments on mice hippocampus neurons proved our hydrogel unable to elicit action potentials. This was attributed to the low conductivity of the developed hydrogel: the ohmic drop between the tip of the commercial stimulation electrode and the brain slice was too high, resulting in too low current densities at the surface of the brain slice to elicit the firing of action potentials. Another possibility could also be the electronic discontinuity between the tip of the commercial micro-electrode used, and the conductive hydrogel: all the electric charges of the metal electrode were converted into ions at the metal/hydrogel interface. The resulting pure ionic conductivity was not enough to elicit the firing of action potentials.

Interestingly, it appeared that the CIC of the one-pot hydrogels were lower than their CSC. It was expected, as for traditional metal electrode, or conductive material coated with electro-polymerized conductive polymer (PEDOT:PSS), the CIC is typically 5-20 % lower than the CSC^[13]. This is due to the fact that the CSC is measured in a quasi-static regime (scan rate < 100 mV/s), enabling all the conductive matrix to transfer charges, while the CIC is measured using high frequencies pulse experiments, enabling only the superficial layers of the bulk conductive material to be electro-active^[15]. However, for our volumic conductive hydrogel, the measured difference between the CIC and the CSC was expected to be lower as the porous nature of the hydrogel should have enabled the formation of electrical double layers throughout all the gel structure (Figure 19), resulting in a theoretical lower difference between the CSC and the CIC for a conductive hydrogel. Complementary analysis are required to conclude on this difference. Other characterization protocols will be implemented, as described by Boehler *et al.*^[15] and Schiavone *et al.*^[18].

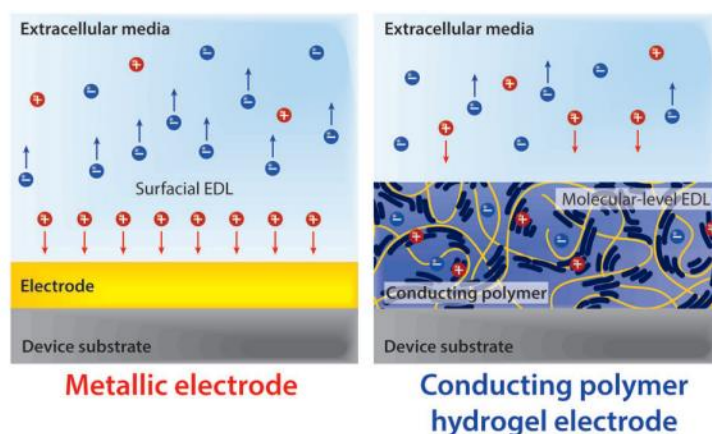


Figure 19. Areal electrical reactivity of a metallic electrode, versus volumetric electrical reactivity of a conductive hydrogel electrode, adapted from Yuk *et al.*^[23].

Hydrogel **5** properties were competitive with the PEDOT/alginate hydrogels of Yang *et al.*^[2] whose work was adapted in this project. They synthesized a conductive alginate porous scaffold by cross-linking alginate with ADH in the presence of EDC and *N*-hydroxysuccinimide, while polymerizing EDOT with APS. After gelation, their hydrogel was washed and freeze-dried to obtain a porous scaffold. Noticeably in this publication, the experimental conditions for synthesis were not investigated. Their scaffolds displayed an impedance $|Z|$ at 1 kHz ranging from 960 to 9000 Ω depending on the EDOT/alginate mass ratio, and conductivities around 10^{-2} S/cm. In this publication, an increase of storage modulus G' was also observed between the pristine hydrogel without PEDOT, and the final conductive hydrogel, increasing from 6.98 kPa at 1Hz to 7.5-100 kPa depending on the EDOT/alginate mass ratio.

This increase of storage modulus G' in this publication and in our work can be attributed to the presence of solid PEDOT clusters in the hydrogel matrix, which harden the hydrogel, while interacting with ADH aliphatic chain, adding a physical cross-linking system.

V.3.b. Potential system improvement

To the best of our knowledge, the simultaneous cross-linking of a hydrogel matrix with conductive polymer polymerization has only been implemented three times in the literature, and only once with PEDOT by Yang *et al.*^[2], as detailed above. Shin *et al.*^[36] synthesized a polypyrrole (PPy) / HA-catechol hydrogel using sodium periodate to both polymerize PPy and cross-link HA-catechol, with the to design human neural stem cells culture platform.

Ravichandran *et al.*^[37] designed an injectable conductive hydrogel relying on the simultaneous quick cross-linking of methacrylated collagen by *N,N'*-methylenebis(acrylamide) and PPy polymerization in the presence of APS and iron^{III} tosylate, in order to design injectable glucose sensors. Noticeably in this last paper, the dopant of the conductive polymer were not the hydrogel matrix but a tosylate salt. The reported values of storage modulus, conductivities and impedance at 1 kHz of those various conductive hydrogels were comparable, and similar to the one obtained in this work.

Interestingly, in the work of Shin *et al.*^[36], both Ppy polymerization and hydrogel cross-linking relied on oxidative reactions by periodates. This was convenient since in this case there was one type of chemistry involved, differently from our protocol where two non-orthogonal chemistries were competing. This paradigm could be adapted to cross-link an HAS₄ derivative, simultaneously with EDOT oxidative polymerization with APS. The HAS₄ derivative should thus include an aromatic group and a chemical moiety sensitive to persulfate for a hypothetical cross-linking reaction. However, such a strategy would not be able to control separately the hydrogel cross-linking degree, and PEDOT oxidation degree. Besides, contrary to Shin *et al.*^[36], the use of catechol should be avoided as it could induce cytotoxicity issues as their slow oxidation kinetics may induce long cells exposure time to free radicals, as evidenced by Sato *et al.*^[38]

Synthesizing pure conductive hydrogel in one pot appears to be a promising strategy as it is convenient, quick, and enables the in-situ formation of hydrogels while controlling all the physico-chemical parameters. The experimental protocol implemented in this project requires further improvements to obtain repeatable hydrogels. Once this goal is achieved, hydrogels with controlled geometry and properties will be synthesized to serve as stimulation electrodes, as they demonstrated low impedance at 1 kHz and high charge storage capacity.

VI. Conclusion

In conclusion, we implemented two different strategies to synthesize pure conductive hydrogel based on PEDOT doped by HAS₄-PBA_{0.3} or one of its derivative.

HAS₄-ArEne_{0.5} proved to be a suitable PEDOT dopant, and a great candidate to form hydrogels with tunable storage modulus. However, the two step loading of EDOT and then polymerization to obtain a conductive hydrogel proved to be not totally satisfactory as it was dependent on the size and geometry of the setup, and did not enable a rigorous control of PEDOT polymerization parameters.

Therefore a one-step protocol was implemented to form an HAS₄-PBA_{0.3} hydrogel cross-linked by ADH, with simultaneous polymerization of EDOT. This protocol lead to hydrogels with satisfactory mechanical and electrochemical properties to be used in stimulation and/or monitoring electrode, but was not totally repeatable, and required further improvements. Besides, biocompatibility and degradability were not investigated by lack of time, and should also be investigated to assess the potential utilization of those pure conductive hydrogels

Pure conductive hydrogels can be used as contact electrode for the stimulation and monitoring of tissues, and the one synthesized in this section proved to be soft enough ($G' \approx 1$ kPa) with low impedance at 1 kHz ($\approx 400 \Omega$) and high charge storage capacity (≈ 10 mC/cm²), to be used in tissue stimulation.

VII. Materials and methods

VII.1. Synthesis

VII.1.a. Materials

HAS₄ and HAS₄-PBA_{0.3} were synthesized and purified as previously described in chapter 2. 3,4-Ethylenedioxythiophene (EDOT), ammonium persulfate (APS), 4-(4,6-Dimethoxy-1,3,5-triazin-2-yl)-4-methylmorpholinium chloride (DMTMM), adipic acid dihydrazide (ADH), N-(3-dimethylaminopropyl)-N'-ethylcarbodiimide hydrochloride (EDC) and sodium hydroxide pellet were obtained from Sigma-Aldrich (Saint-Quentin Fallavier, France). 4-[(pent-4-en-1-yloxy)methyl]aniline (ArEne) was obtained from Uorsy (Kiev, Ukraine). Iron^{II} sulfate heptahydrate was from Alfa Aesar. Hydrochloric acid was from Fischer Scientific. N,N-dimethylformamide (DMF), ethanol 96% (EtOH) and acetonitrile (MeCN) were from VWR International (Fontenay-sous-Bois, France). All reagents were used as received without further purifications.

VII.1.b. Synthesis of HAS-ArEne

The protocol was adapted from Auzély *et al.*^[39,40]. 1 g of HAS₄ was dissolved in 491 mL of water:DMF 3:2 v:v. 342 mg (1 equivalent) of DMTMM was dissolved in 4 mL of water and added to the medium. Then 110.4 μ L (0.5 equivalent, $d_{\text{ArEne}} = 1.17$) of ArEne dissolved in 4 mL of DMF were added. The pH was adjusted to 6.5 with 1 M NaOH and HCl solutions, and the medium stirred overnight at room temperature. NaCl was added to obtain a final NaCl concentration of 0.3 M, then the medium was purified by ultrafiltration on a 10 kDa ultrafiltration membrane (Amicon Bioseparation, Millipore, New Hampshire, USA), and freeze-dried. HAS-ArEne was recovered with a yield superior to 95%. The ArEne substitution degree DS_{ArEne} of the HAS-ArEne was found to be 0.5 estimated from the follow of the amide coupling reaction using the TNBS method, as described below.

VII.1.c. Determination of the degree of substitution of HAS-ArEne by the follow up of the amide coupling reaction

As the superposition of ¹H NMR signals of HAS₄ and grafted ArEne moieties precluded the determination of the DS of HAS-ArEne by ¹H NMR, it was estimated by following up of synthesis, by quantifying the free primary amines in the reaction medium as a function of time. This was based on the reaction of ArEne with 2,4,6-trinitrobenzene sulfonic acid (TNBS), which yields an orange-colored final product (trinitrophenylamine) that absorbs in the UV region, at around 340 nm. The protocol was adapted from Figueiredo *et al.*^[40].

Procedure for the reaction monitoring by quantifying primary amines with TNBS:

Standard curve of ArEne concentration was prepared by diluting 1 mg/mL stock solutions in 0.1 M sodium bicarbonate buffer pH 8.5 at known concentrations of amine (5 to 30 µg/mL). Various volumes of a fresh solution of 0.1 g/L TNBS in the same buffer were added in each solution, in order to get a molar ratio of TNBS/amine of 1, and samples were incubated at 37 °C for 2 h. Then, 150 µL of HCl 1 M were added to the samples, and the product of reaction between the amine and TNBS was analyzed by UV spectroscopy (from 280 to 580 nm, Figure 20a). A standard curve was plotted with the maximal absorbance values (Figure 20b). It is important to note that the wavelength of the maximal absorbance depends on the primary amines (372 nm for ArEne).

The same procedure was used to quantify amines during the amide coupling reactions with HA, by taking 100 µL aliquots of the reaction medium as a function of time (Figure 20c and d). 100 % of conversion was obtained for HAS₄-ArEne within 24 h, which gave values of DS_{ArEne} of 0.5 (Figure 20).

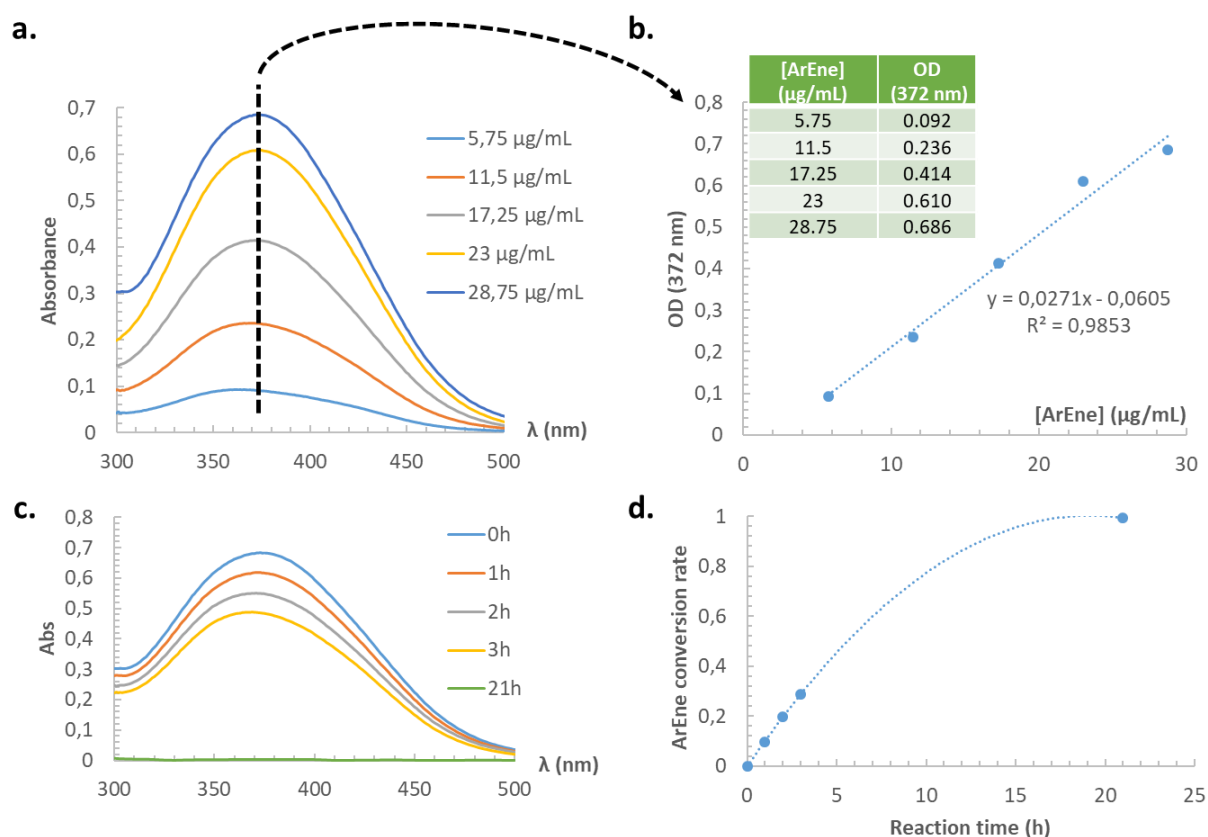


Figure 20. a. Absorbance spectrum of standard ArEnE reacted with TNBS. b. Calibration curve for ArEnE at 372 nm. c. Absorbance spectrum of aliquots of reactional medium at different times, after reaction with TNBS d. Corresponding ArEnE conversion rate using the established calibration curve.

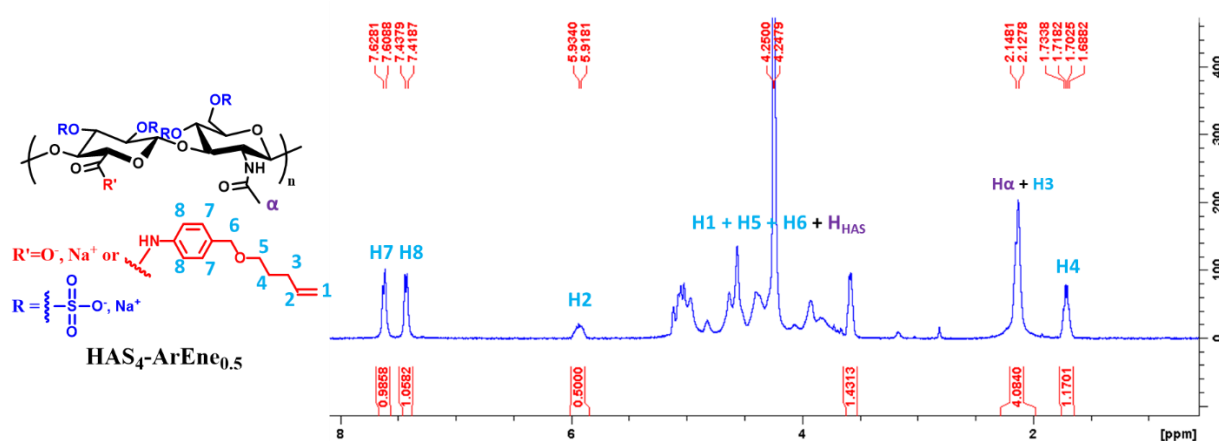


Figure 21. ¹H NMR spectrum of HAS₄-ArEnE_{0.5} at 4 g/L in D₂O at 80°C. DS_{ArEnE} determined by the TNBS method.

VII.1.d. Synthesis of conductive HAS₄-ArEnE_{0.5} hydrogel

Synthesis of HAS-ArEnE hydrogel

HAS₄-ArEnE_{0.5} was dissolved at 30 g/L in 0.15 mM NaCl with PEG-(SH)₂ (M_n = 3.5 kg/mol) such as the molar ratio $n_{\text{thiol}}/n_{\text{alkene}} = 0.75$, and LAP at 0.75 g/L. After vortexing, 150 µL

of the mixture was poured in a cylindrical mold ($\varnothing_{\text{inner}} = 5.8$ mm) and irradiated 10 min at 365 nm at 40 mW/cm², then put upside down and irradiated 10 min at 365 nm at 40 mW/cm² (to ensure homogenous cross-linking in all gel thickness).

EDOT loading of the HAS-ArEne hydrogel

The 150 μ L HAS₄-ArEne_{0.5} hydrogel was immersed 4h in 2 mL of EDOT at [EDOT]_{bath} = 67.8 mM (so as there were 2 equivalents of EDOT compared to HAS₄-ArEne_{0.5} in the 150 μ L of hydrogel) in NaCl 0.15 M : acetonitrile 6:4 v:v. This bath was repeated twice to ensure complete loading of the HAS-ArEne hydrogel in EDOT.

Polymerization of loaded EDOT in the HAS-ArEne hydrogel

The HAS₄-ArEne_{0.5} hydrogel loaded with EDOT was then immersed in 4 mL of oxidant (APS) and catalyst (FeSO₄) at different concentrations:

- Either [APS]_{bath} and [FeSO₄]_{bath} were chosen such as [APS]_{bath} = 1.33 [EDOT]_{bath} and [FeSO₄]_{bath} = 0.015 [EDOT]_{bath}.
- Or [APS]_{bath} and [FeSO₄]_{bath} were chosen such as $n_{\text{tot APS in bath}} = 1.33 n_{\text{tot EDOT in hydrogel}}$ and $n_{\text{tot FeSO}_4 \text{ in bath}} = 0.005 n_{\text{tot EDOT in hydrogel}}$.

After polymerization was completed (hydrogel was deep blue), the conductive hydrogel was washed for 4 hours in a bath of NaCl 0.15 M : acetonitrile 6:4 v: v to remove unreacted EDOT, then 4 hours in 3 successive baths of PBS 1X to remove EDOT polymerization by-products, and to neutralize the gel.

VII.1.e. Synthesis of conductive PEDOT:HAS₄-PBA_{0.3} / ADH one pot hydrogels

The protocol was adapted from Yang *et al.*^[2]. The following protocol is also valid for BisTris and Tris instead of MES.

HAS₄-PBA_{0.3} was dissolved at 40 g/L, in MES 0.1 M + NaCl 0.5 M pH 4.75, with ADH at 2.2 g/L in order to have a molar ratio $n_{\text{hydrazide}}/n_{\text{carboxylate}} = 0.75$, EDOT in order to have 2 equivalents of EDOT compared to HAS₄-PBA_{0.3}, and APS at 289.5 g/L in order to have a molar ratio of $n_{\text{APS}}/n_{\text{EDOT}} = 1.33$. The mixture was mixed at 25,000 rpm using an IKA Ultra Turrax T-10 basic disperser with a S 10 N-8G dispersing tool (Roth, Karlsruhe, Germany). Then, concentrated

EDC was added to the emulsion in order to have a molar ratio $n_{\text{EDC}}/n_{\text{carboxylate}} = 1.5$. The emulsion was mixed 10 additional seconds before pouring it immediately in the desired mold.

For uniaxial compression tests and electrochemical characterizations, PEDOT:HAS₄-PBA_{0.3} / ADH hydrogels were immersed in three successive PBS baths of at least 4 hours to remove reactions by-products, to adjust the salt concentration of the matrix, and to neutralize the hydrogel pH.

VII.2. Characterization

VII.2.a. Photorheometry of HAS₄-ArEne_{0.5} hydrogels

An AR2000Ex rheometer (TA Instruments Inc.) fitted with a UV-curing cell ($\lambda = 365$ nm) and an aluminum plate (diameter 20 mm) was used for the in-situ measurement of the viscoelastic properties of the HAS₄-ArEne_{0.5}-based hydrogels. Following deposition of 400 μL of a mixture of HAS₄-ArEne_{0.5}, cross linker (PEG-(SH)₂ Mn = 3500 g/mol) and photo initiator (LAP), the gap between the flat quartz plate and the aluminum plate was set to 1160 μm . It was controlled during the experiments by maintaining the normal force at 0 ± 0.1 N.

For each hydrogel, oscillatory time sweep and frequency sweep experiments were performed. They were carried out at 25°C with a film of silicone to avoid solvent evaporation. All the dynamic rheological data were checked as a function of strain amplitude to ensure that the measurements were performed in the linear viscoelastic region.

In the oscillatory time sweep experiments, the storage modulus (G') and loss modulus (G'') were measured during a period of 25–30 min at a fixed frequency of 1 Hz and a fixed strain of 3%. Typically, after deposition of the solution of the mixture of polymers in PBS between the plates and equilibration for 1 min, the solution was exposed to light ($\lambda = 365$ nm) for 25–30 min at a fixed light power (20 mW/cm²) leading to gelation.

VII.2.b. Rheology

Oscillatory time sweep experiments of HAS₄-PBA_{0.3} / ADH hydrogels were performed with a cone–plate rheometer (AR 2000 EX from TA Instruments Inc.). The cone has a diameter of 2 cm and an angle of 4°. 155 µL of hydrogel precursor mixture containing HAS₄-PBA_{0.3}, ADH and EDC, were deposited on the plate, and the cone set 109 µm above. It was controlled during the experiments by maintaining the normal force at 0 ± 0.1 N. To prevent water evaporation, the measuring system was surrounded with a low-viscosity silicon oil (50 mPa·s) carefully added to the edges of the cone. In the oscillatory time sweep experiments, the storage modulus (G') and loss modulus (G'') were measured during a period of 3–4 hours at a fixed frequency of 1 Hz and a fixed strain of 3%.

After time sweep experiments, oscillatory frequency sweep (0.01–10 Hz) experiments were performed within the linear viscoelastic range (strain fixed at 3%) to determine the frequency dependence of the storage (G') and loss (G'') moduli. No frequency data beyond 10 Hz are presented because inertial artifacts (raw phase angle $> 150^\circ$) were observed at frequencies higher than 10 Hz^[41,42].

VII.2.c. Swelling behavior

The equilibrium swelling ratio Q of each hydrogel was measured in PBS. Q was determined as follows:

$$Q = \frac{m_{\text{swollen PBS}}}{m_{\text{dry}}}$$

where $m_{\text{swollen PBS}}$ is the gel mass after swelling in PBS and m_{dry} is the dry gel mass measured after removing the PBS salt by successive water baths, and freeze-drying the sample to remove all the water.

VII.2.d. Uniaxial compression experiments

Compression measurements were carried out using an EZ-X Texture Analyzer (Shimadzu, Marne-la-Vallée, France) equipped with a 5 N cell. The hydrogel, in the form of a cylinder (approximately 5 mm diameter and 4 mm initial height), was placed on the texture

analyzer lower plate and put in contact with the upper plate with a pre-loading force of 0.03N. To avoid hydrogel sticking to the plate, a drop of decane was placed between the gel and the upper plate before contact. Measurements were performed at a compression speed of 17 $\mu\text{m/s}$. Compression cycles were performed as follows: the sample was compressed until reaching 10% of deformation, then the upper plate was lifted to the relaxed gel state (0% of deformation). Successive compressions of 20%, 30%, 40% and 50% of deformation then followed on the same sample, each time coming back to the 0% deformation state between each compression. The load and displacement data were collected during each experiment. The normal stress $\sigma_{nominal}$ was calculated as the normal force divided by the surface area of the material whereas the displacement data λ were expressed as an extension ratio, $\lambda = (h_0 - \Delta h)/h_0$, where Δh is the displacement data and h_0 the initial gap. The storage modulus G' of the materials could be calculated as the slopes of $\sigma_{nominal} = f(\lambda - \frac{1}{\lambda^2})$ in the linear response of gel.

VII.2.e. Cavity electrode preparation

Home-made cavity electrode was realized using a 4 cm long platinum rod of 2 mm diameter. The Pt rod was inserted in a 2 mm intern diameter PTFE tube, and the space between the rod and the tube sealed with epoxy resin to avoid water leeching along the tube which would change the reactive surface of the electrode (Figure 22a). The tip of the Pt rod was polished using successive grit, and final polishing was made using a 1 μm diamond paste (RadioSpares). Then, it was rinsed with ultra-purified water, ethanol and sonicated 10 minutes in ethanol.

PEDOT: HAS₄-PBA_{0.3} was then electro-polymerized on the platinum surface, in order to graft the hydrogel to the surface of the platinum during simultaneous hydrogel cross-linking and EDOT polymerization. A solution of EDOT at 5 mM and HAS₄-PBA_{0.3} at 10 mM in DI water was prepared and degassed, and immediately used as medium for cyclic voltammetry of the Pt surface. A three electrode cell was used: the working electrode was the polished Pt rod in a PTFE tube; the reference electrode was classical Ag/AgCl electrode ([KCl] 3M) for aqueous measurements; counter electrode was a platinum foil. PEDOT: HAS₄-PBA_{0.3} was electro-

polymerized by performing 10 potential cycles from -0,6 V to 0,96V at 25mV/s. The resulting functionalized surface was lightly blue (Figure 22b).

Finally, the cavity was stacked upon the functionalized Pt surface, using a 2 mm internal diameter tubing section stuck inside a larger tube. For all electrodes, 6 μ L of the hydrogel precursor mixture were poured in the cavity on the functionalized Pt surface, and sealed for 24h to prevent water evaporation during gelation. Before electro-characterization, PEDOT:HAS₄-PBA_{0.3} / ADH hydrogels were immersed in three successive PBS baths of at least 4h to remove reactions by-products, to adjust the salt concentration of the matrix, and to neutralize the hydrogel pH.

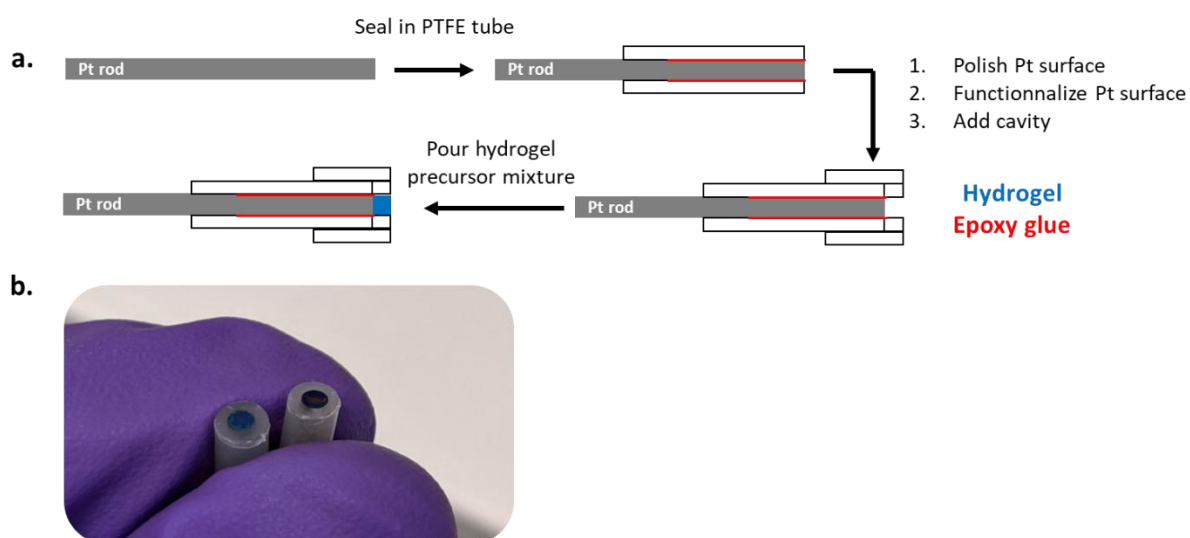


Figure 22. a. Home-made cavity electrode fabrication process. b. Electro-polymerized PEDOT:HAS₄-PBA_{0.3} on the platinum surface.

VII.2.f. Electrochemical characterization

All electrochemical measurements were made with the three-electrode cell previously described. All experiments were performed in freshly prepared and degassed PBS. All electrochemical measurements were performed with a SP-200 potentiostat (BioLogic, Seyssinet-Pariset, France), equipped by EC-Lab[®] V11.31 software.

Cyclovoltametry (CV) experiments were performed at a sweeping rate $\nu = 50$ mV/s from -0.5 to 0.6 V, starting from 0 V compared to open circuit potential (E_{oc}). 10 Cycles were

made. Charge storage capacity was deduced from the cyclic voltammogram using the following equation: $CSC = -\frac{1}{v \cdot S_{electrode}} \int_{i<0} IdV$ where $S_{electrode}$ was the electrode surface.

Impedance spectroscopy (EIS) experiments were realized from 100 kHz to 10 mHz sampling 10 points per decade, using a single sine signal at 0 V versus E_{OC} of 10 mV RMS amplitude. Before EIS acquisition, an open circuit experiment was performed to assess whether the conductive hydrogel potential was stable.

Charge injection capacity was determined by pulse experiments. The pulse sequence was composed of a cathodic current pulse of 125 ms followed by a resting time of 30 ms, then by a charge-compensating anodic pulse of 250 ms, followed by resting time of 1 second. This sequence was repeated 30 times. Working electrode potential was monitored over time. The amplitude of the current pulses $A_{current\ pulse}$ was progressively increased, until an inflexion in the working electrode potential during the cathodic pulse was observed, indicating the onset of water splitting reaction. The time between the beginning of the cathodic pulse, and the apparition of the inflexion length was defined as t_{max} . The volumic charge injection capacity CIC_{3D} was defined as

$$CIC_{3D} = \frac{A_{current\ pulse} \cdot t_{max}}{V_{hydrogel}}$$

VII.2.i. Ex-vivo mice hippocampus stimulation

Ex-vivo rat brain slice stimulation experiments were realized in cooperation with Fabien Lanté of the Neuroscience Institute of Grenoble (GIN).

Three weeks old C57BL/6J mice were sacrificed and their brain removed, and conserved into artificial cerebrospinal fluid (ACSF) buffer, oxygenated bubbling *carbogène* gas (95 % O₂ + 5 % CO₂).

The hydrogel precursor mixture was prepared as described in section II.2.a., and poured into a tube, polymerized, and immersed 2 days into ACSF buffer. An extremity of the tube was cut off to let the gel protrude, and a concentric bipolar electrode from World

Precision Instruments (Friedberg, Germany) was plunged at the other extremity. The electrode was maintained in hydrogel with a piece of tape.

The mice brain was cut in half and maintained into oxygenated ACSF buffer with a small net. The protruding gel was put in contact with the hippocampal CA1 region of the brain. Right aside was positioned a counter electrode, and 2 cm away plunged in the ACSF buffer was positioned an Ag/AgCl reference electrode.

DC monophasic current pulses of 200 μ s with current intensity ranging from 0.01 mA to 1 mA were injected in the hydrogel, and the difference of potential between the counter electrode and the reference electrode was monitored over time.

VIII. Bibliography

- [1] D. Tarus, L. Hamard, F. Caraguel, D. Wion, A. Szarpak-Jankowska, B. van der Sanden, R. Auzély-Velty, *ACS Appl. Mater. Interfaces* **2016**, *8*, 25051–25059.
- [2] B. Yang, F. Yao, L. Ye, T. Hao, Y. Zhang, L. Zhang, D. Dong, W. Fang, Y. Wang, X. Zhang, C. Wang, J. Li, *Biomaterials Science* **2020**, *8*, 3173–3185.
- [3] K. P. Vercruysse, D. M. Marecak, J. F. Marecek, G. D. Prestwich, *Bioconjugate Chem.* **1997**, *8*, 686–694.
- [4] J. W. Kuo, D. A. Swann, G. D. Prestwich, *Bioconjugate Chem.* **1991**, *2*, 232–241.
- [5] N. Nakajima, Y. Ikada, *Bioconjugate Chem.* **1995**, *6*, 123–130.
- [6] E. Hachet, H. Van Den Berghe, E. Bayma, M. R. Block, R. Auzély-Velty, *Biomacromolecules* **2012**, *13*, 1818–1827.
- [7] G. Lalevée, G. Sudre, A. Montembault, J. Meadows, S. Malaise, A. Crépet, L. David, T. Delair, *Carbohydrate Polymers* **2016**, *154*, 86–95.
- [8] D. Stigter, *Biophysical Journal* **1995**, *69*, 380–388.
- [9] M. Mooney, *Journal of Applied Physics* **1940**, *11*, 582–592.
- [10] W.-C. Lin, W. Fan, A. Marcellan, D. Hourdet, C. Creton, *Macromolecules* **2010**, *43*, 2554–2563.
- [11] G. Eda, G. Fanchini, M. Chhowalla, *Nature Nanotechnology* **2008**, *3*, 270–274.
- [12] “t_{lm}_measurements.pdf,” can be found under http://tuttle.merc.iastate.edu/ee432/topics/metals/tlm_measurements.pdf, **n.d.**
- [13] S. F. Cogan, *Annu. Rev. Biomed. Eng.* **2008**, *10*, 275–309.
- [14] S. F. Cogan, P. R. Troyk, J. Ehrlich, T. D. Plante, *IEEE Trans. Biomed. Eng.* **2005**, *52*, 1612–1614.
- [15] C. Boehler, S. Carli, L. Fadiga, T. Stieglitz, M. Asplund, *Nat Protoc* **2020**, *15*, 3557–3578.
- [16] K. Xu, S. Li, S. Dong, S. Zhang, G. Pan, G. Wang, L. Shi, W. Guo, C. Yu, J. Luo, *Adv. Healthcare Mater.* **2019**, *8*, 1801649.
- [17] R. T. Leung, M. N. Shivdasani, D. A. X. Nayagam, R. K. Shepherd, *IEEE Trans. Biomed. Eng.* **2015**, *62*, 849–857.
- [18] G. Schiavone, X. Kang, F. Fallegger, J. Gandar, G. Courtine, S. P. Lacour, *Neuron* **2020**, *108*, 238–258.
- [19] K. Wang, L. Tian, T. Wang, Z. Zhang, X. Gao, L. Wu, B. Fu, X. Liu, *Composite Interfaces* **2019**, *26*, 27–40.
- [20] B. Lu, H. Yuk, S. Lin, N. Jian, K. Qu, J. Xu, X. Zhao, *Nat Commun* **2019**, *10*, 1043.
- [21] A. Novikov, J. Goding, C. Chapman, E. Cuttaz, R. A. Green, *APL Materials* **2020**, *8*, 101105.
- [22] T. Nyberg, A. Shimada, K. Torimitsu, *Journal of Neuroscience Methods* **2007**, *160*, 16–25.
- [23] H. Yuk, B. Lu, X. Zhao, *Chemical Society Reviews* **2019**, *48*, 1642–1667.
- [24] N. Torres-Martinez, D. Ratel, C. Crétallaz, C. Gaude, S. Maubert, J.-L. Divoux, C. Henry, D. Guiraud, F. Sauter-Starace, *J. Neural Eng.* **2019**, *16*, 066047.
- [25] A. Fanelli, L. Ferlauto, E. G. Zollinger, O. Brina, P. Reymond, P. Machi, D. Ghezzi, *Adv. Mater. Technol.* **2021**, 2100176.
- [26] Y. Wang, H. Zhu, H. Yang, A. D. Argall, L. Luan, C. Xie, L. Guo, *Nano Res.* **2018**, *11*, 5065–5106.
- [27] E. Castagnola, A. Ansaldo, E. Maggolini, T. Ius, M. Skrap, D. Ricci, L. Fadiga, *Front. Neuroeng.* **2014**, *7*, 38–43.
- [28] D. R. Merrill, M. Bikson, J. G. R. Jefferys, *Journal of Neuroscience Methods* **2005**, *141*, 171–198.
- [29] Z. J. Du, X. Luo, C. L. Weaver, X. T. Cui, *J. Mater. Chem. C* **2015**, *3*, 6515–6524.
- [30] Y. Yuan, L. Zheng, Z. Feng, G. Yang, *Different Effects of Monophasic Pulses and Biphasic Pulses Applied by a Bipolar Stimulation Electrode in the Rat Hippocampal CA1 Region*, In Review, **2021**.
- [31] M. D’Este, D. Eglin, M. Alini, *Carbohydrate Polymers* **2014**, *108*, 239–246.
- [32] X. Ding, R. Jia, Z. Gan, Y. Du, D. Wang, X. Xu, *Materials Research Express* **2020**, *7*, 055304.
- [33] S. Wang, C. Sun, S. Guan, W. Li, J. Xu, D. Ge, M. Zhuang, T. Liu, X. Ma, *J. Mater. Chem. B* **2017**, *5*, 4774–4788.

- [34] G. S. Manning, *Accounts of Chemical Research* **1979**, *12*, 443–449.
- [35] C. M. Tringides, N. Vachicouras, I. de Lázaro, H. Wang, A. Trouillet, B. R. Seo, A. Elosegui-Artola, F. Fallegger, Y. Shin, C. Casiraghi, K. Kostarelos, S. P. Lacour, D. J. Mooney, *Nat. Nanotechnol.* **2021**, DOI 10.1038/s41565-021-00926-z.
- [36] J. Shin, E. J. Choi, J. H. Cho, A.-N. Cho, Y. Jin, K. Yang, C. Song, S.-W. Cho, *Biomacromolecules* **2017**, *18*, 3060–3072.
- [37] R. Ravichandran, J. G. Martinez, E. W. H. Jager, J. Phopase, A. P. F. Turner, *ACS Appl. Mater. Interfaces* **2018**, *10*, 16244–16249.
- [38] T. Sato, T. Aoyagi, M. Ebara, R. Auzély-Velty, *Polymer Bulletin* **2017**, *74*, 4069–4085.
- [39] D. Tarus, E. Hachet, L. Messenger, B. Catargi, V. Ravaine, R. Auzély-Velty, *Macromolecular Rapid Communications* **2014**, *35*, 2089–2095.
- [40] T. Figueiredo, J. Jing, I. Jeacomine, J. Olsson, T. Gerfaud, J.-G. Boiteau, C. Rome, C. Harris, R. Auzély-Velty, *Biomacromolecules* **2020**, *21*, 230–239.
- [41] R. E. Hudson, A. J. Holder, K. M. Hawkins, P. R. Williams, D. J. Curtis, *Physics of Fluids* **2017**, *29*, 121602.
- [42] I. M. Krieger, *Journal of Rheology* **1990**, *34*, 471–483.
- [43] L. Assaud, N. Massonnet, D. Evrard, H. Vergnes, L. Salvagnac, V. Conédéra, L. Noé, M. Monthieux, P. Gros, P. Temple-Boyer, B. Caussat, *Journal of Electroanalytical Chemistry* **2016**, *771*, 73–79.

General conclusion

This Ph.D. project aimed at the development of new PEDOT-based building blocks for the design of conductive biocompatible transient bioelectronic devices, more specifically, conductive tracks and conductive contact electrodes. The absence of long-term study of the (bio)degradability and cytotoxicity of PEDOT:PSS, led us to develop a new PEDOT dopant based on hyaluronic acid, with the objective to take advantage of the high biocompatibility and biodegradability of this natural ubiquitous glycosaminoglycan. Different HA derivatives were synthesized, and enabled to design conductive cross-linkable PEDOT-based inks, processable via inkjet printing, as well as soft conductive hydrogels for contact electrodes.

The first step of the project was the chemical modification of HA in order to introduce chemical moieties of interest mimicking the structure of PSS that proved to be an efficient PEDOT dopant. HA was first sulfated, which led to the development of a new sulfation protocol, outperforming all those reported in the literature. This optimized sulfation procedure allowed not only to achieve higher final sulfation degrees, but also to minimize chain degradation. The key parameters appeared to be the basic quenching of the sulfation reaction, as well as the low temperature during the sulfation reaction. The sulfated HA (HAS) proved to be insensitive to enzymatic degradation, but was still degraded in a few months due to auto-hydrolysis. Next, aminophenylboronic acid groups (PBA) were grafted on HAS to introduce aromatic groups to enhance the hydrophobic interactions with PEDOT. Finally, various PEDOT:HAS-PBA inks were synthesized, and a synergy between the sulfates and the PBA groups was evidenced, resulting in the design of highly conductive PEDOT:HAS₄-PBA_{0.3} ink with a conductivity up to 1.5 S/cm, two orders of magnitude higher than PEDOT:HA ink conductivity^[1]. The PEDOT:HAS₄-PBA_{0.3} ink proved to be biocompatible and could be inkjet-printed after synthesis optimization and formulation.

Then, different strategies were implemented to cross-link PEDOT:HAS₄-PBA_{0.3} in order to make it insoluble in water, which is mandatory in bioelectronics. Dynamic cross-linking using the ability of PBA moieties to form reversible boronate ester^[2], and photo-activated thiol-ene cross-linking were investigated. The successive protocols highlighted various constraints. First, it appeared that the sulfates groups on HAS₄-PBA_{0.3} backbone were bulky and prevented cross-linking reactions relying on chemical functions too close to the backbone. Then, it appeared that the PEDOT parts of the PEDOT:HAS₄-PBA_{0.3} ink particles were buried inside HAS₄-PBA_{0.3} shells as no PEDOT signal was observed in ¹H NMR spectrum of inks, hence

the use of alkene-functionalized EDOT proved to be ineffective to cross-link PEDOT-based inks, and. Finally, important conductivity decrease and heterogeneous cross-linking were observed when PEDOT:HAS₄-PBA_{0.3} ink was included in a cross-linked matrix, demonstrating that PEDOT-HAS₄-PBA_{0.3} must be part of the cross-linking network, and not embedded in a cross-linked network. For all these reasons, HAS₄-PBA_{0.3} was further modified, by introducing an alkene function through an oligo-EG spacer arm. The resulting HAS₄-PBA_{0.3}-PEGene_{0.22} polyelectrolyte proved to be a great PEDOT dopant (conductivity up to 3.8 S/cm when non cross-linked, and 0.6 S/cm when cross-linked), and final PEDOT:HAS₄-PBA_{0.3}-PEGene_{0.22} inks could be formulated, inkjet-printed and photo-cross-linked, yielding insoluble conductive tracks. These tracks were still conductive when immersed in water, though displaying a reversible 3-fold increase of resistance. Interestingly, the conductivity in a dry state increased after several hydration/drying cycles, starting from 0.6 S/cm up to 4.9 S/cm in 6 cycles, due to film washing and ink particles reorganization, as evidenced by AFM. However, due to PEDOT absorption of UV photons, only thin films could be cross-linked using this methodology.

Finally, pure conductive hydrogels were synthesized to serve as contact electrodes with tissues, as hydrogels match their mechanical properties, and can be highly biocompatible compared to classical electrode materials, due to their high hydration and porosity. A first strategy consisted in loading a pre-formed photocross-linked hydrogel based on a HAS₄ derivative (HAS₄-ArEne_{0.5}) with EDOT, and then polymerizing EDOT in an oxidative bath. However, this two-step protocol proved to be unsatisfactory as it depended on hydrogel size and setup geometry. A one-step protocol was developed as an alternative strategy to prepare conductive hydrogels. This consisted in cross-linking HAS₄-PBA_{0.3} with a dihydrazide, while simultaneously polymerizing EDOT. This protocol was easy to enforce and should have enabled to rigorously control all the final gel mechanical and electrochemical properties. However, a lack of repeatability was observed, which has not been resolved yet because of a lack of time. Nevertheless, final conductive hydrogel properties were investigated: they displayed a storage modulus G' around 1-5 kPa with a conductivity of 10^{-2} S/cm. Their low impedance at 1 kHz ($< 1000 \Omega$), and high storage capacity (1-5 mC/cm²) made them promising candidates for tissue stimulation and monitoring^[3].

Among the initial objectives of this Ph.D. project, the development of an innovative biocompatible and degradable PEDOT dopant was achieved, leading to new biocompatible and

disintegrable PEDOT-based inks that proved to be versatile, processed either by inkjet-printing or cross-linked as hydrogels. However, while the cytotoxicity of PEDOT:HAS₄-PBA_{0.3} was assessed, the cytotoxicity of cross-linked printed tracks and of conductive hydrogels still needs to be characterized. Besides, the (bio)degradability of final one-step conductive PEDOT-based hydrogels could not be investigated because of a lack of time. The most important limitation of the developed PEDOT:HAS₄-PBA_{0.3} ink was its low conductivity, around 1 S/cm, which was however one to two orders of magnitude higher than the conductivity of other PEDOT:glycosaminoglycans inks reported in the literature^[1], but still limited compared to PEDOT:PSS conductivity (10¹-10³ S/cm). However, it should not prevent its utilization in tissue monitoring electrodes, as Tringides *et al.*^[4] recently reported a viscoelastic electrode array with conductive hydrogel tracks with conductivity of 0.1-0.35 S/cm, useful to record brain action potentials, or electric signals in various mice organs. Concerning tissue stimulation, doping PEDOT:HAS₄-PBA_{0.3} with additional materials such as graphene oxide^[5], carbon nanotubes^[4] or metallic nanoparticles^[6] could be a solution to increase its conductivity. Those materials should be preferred to traditional PEDOT:PSS secondary dopant (glycerol, EG, DMSO...) which present a lack of compatibility with HAS₄-PBA_{0.3}.

Nonetheless, the pure conductive hydrogels based on HAS₄-PBA_{0.3} and PEDOT are promising, as they displayed suitable electrochemical properties for tissue stimulation and monitoring^[3] ($Z_{1\text{ kHz}} < 1\text{ k}\Omega$, $\text{CIC} \approx 280\text{ }\mu\text{C}/\text{cm}^2$, $\text{CSC} \approx 2\text{-}5\text{ mC}/\text{cm}^2$). Besides, if their biocompatibility and degradability prove to be comparable to the ones of their constituents, they could also serve as transient conductive culture platforms for electro-sensitive cells, which could be of great interest for organ-on-chips or tissue engineering such as nerve regeneration for instance^[7-9].

Bibliography

- [1] D. Mantione, I. del Agua, W. Schaafsma, J. Diez-Garcia, B. Castro, H. Sardon, D. Mecerreyes, *Macromol. Biosci.* **2016**, *16*, 1227–1238.
- [2] T. V. B. Figueiredo, Hydrogels Injectables et Auto-Réparants à Base de Polysaccharides Réticulés Par Des Liaisons Ester Boronate : Relations Entre Le Mode de Complexation Acide Boronique-Saccharide et Les Propriétés Mécaniques, PhD Thesis, **2018**.
- [3] S. F. Cogan, *Annu. Rev. Biomed. Eng.* **2008**, *10*, 275–309.
- [4] C. M. Tringides, N. Vachicouras, I. de Lázaro, H. Wang, A. Trouillet, B. R. Seo, A. Elosegui-Artola, F. Fallegger, Y. Shin, C. Casiraghi, K. Kostarelos, S. P. Lacour, D. J. Mooney, *Nature Nanotechnology* **2021**, DOI 10.1038/s41565-021-00926-z.
- [5] M. Javadi, Q. Gu, S. Naficy, S. Farajikhah, J. M. Crook, G. G. Wallace, S. Beirne, S. E. Moulton, *Macromol. Biosci.* **2018**, *18*, 1700270.
- [6] Y. Ahn, H. Lee, D. Lee, Y. Lee, *ACS Appl. Mater. Interfaces* **2014**, *6*, 18401–18407.
- [7] V. Guarino, M. A. Alvarez-Perez, A. Borriello, T. Napolitano, L. Ambrosio, *Adv Healthcare Mat* **2013**, *2*, 218–227.
- [8] L. Ghasemi-Mobarakeh, M. P. Prabhakaran, M. Morshed, M. H. Nasr-Esfahani, H. Baharvand, S. Kiani, S. S. Al-Deyab, S. Ramakrishna, *J Tissue Eng Regen Med* **2011**, *5*, e17–e35.
- [9] G. Y. Özgenel, *Microsurg.* **2003**, *23*, 575–581.

Abstract

Research on flexible biocompatible conductive materials has been burgeoning over the last decades due to the huge number of applications in bioelectronics. Recently, conductive bioelectronic devices based on commercial PEDOT:PSS (3,4-poly(ethylenedioxythiophene) : poly(styrene sulfonate)) have been developed, using conductive hydrogels as contact electrodes. The soft and flexible nature of these polymer networks make them suitable candidates for electronics/soft tissue interface. However, those conductive materials display some limitations for *in vivo* implantation due to problems of biocompatibility and biodegradability of PSS. In this work, we aimed to replace PSS by a modified hyaluronic acid (HA) derivative to develop a new biocompatible and degradable PEDOT dopant. This HA derivative enabled to design a new biocompatible, degradable, printable and cross-linkable PEDOT-based ink, and as well, served as an extracellular-matrix-mimicking building block for the construction of pure conductive hydrogels. These properties could enable the design of soft transient electronic devices, which could avoid implant removal surgery.

Keywords: PEDOT, hyaluronic acid, hydrogel, inkjet-printing, transient bioelectronics, degradability

Résumé

Cette dernière décennie, le développement de matériaux conducteurs, biocompatibles et souples a connu un grand engouement en raison du grand nombre d'applications potentielles dans le domaine de la bioélectronique. Récemment des dispositifs médicaux utilisant le PEDOT:PSS (3,4-poly(éthylènedioxythiophène : poly(styrène) sulfonate)) ont été développés, avec des hydrogels conducteurs comme électrodes de contact, qui sont des candidats prometteurs pour l'interfaçage électronique/tissu. Néanmoins, les matériaux employés sont limitant pour des dispositifs implantés *in vivo* en raison du manque de biocompatibilité et de dégradabilité du PSS. Dans cette thèse, nous avons cherché à remplacer le PSS par un dérivé de l'acide hyaluronique pour concevoir un nouveau dopant du PEDOT biocompatible et dégradable. Ce dérivé a permis la conception d'une nouvelle encre biocompatible, dégradable, imprimable et réticulable, et a également servi comme base structurelle pour la conception d'hydrogels conducteurs à base de PEDOT, proche de la structure du milieu extracellulaire. Ces divers atouts pourraient permettre de concevoir des dispositifs électroniques implantables temporaires, qui ne nécessiteraient pas de chirurgies explantatoires.

Mots clés : PEDOT, acide hyaluronique, hydrogel, impression jet d'encre, bioélectronique dégradable